



HAL
open science

Comportement viscoélastique longitudinal du bois vert: diversité et prédiction à long terme

Jana Dlouha

► **To cite this version:**

Jana Dlouha. Comportement viscoélastique longitudinal du bois vert: diversité et prédiction à long terme. Mécanique [physics.med-ph]. Université Montpellier II-Sciences et Techniques du Languedoc, 2009. Français. NNT: . tel-00567065

HAL Id: tel-00567065

<https://theses.hal.science/tel-00567065>

Submitted on 18 Feb 2011

HAL is a multi-disciplinary open access archive for the deposit and dissemination of scientific research documents, whether they are published or not. The documents may come from teaching and research institutions in France or abroad, or from public or private research centers.

L'archive ouverte pluridisciplinaire **HAL**, est destinée au dépôt et à la diffusion de documents scientifiques de niveau recherche, publiés ou non, émanant des établissements d'enseignement et de recherche français ou étrangers, des laboratoires publics ou privés.

**UNIVERSITE MONTPELLIER II
SCIENCES ET TECHNIQUES DU LANGUEDOC**

THESE

pour obtenir le grade de

DOCTEUR DE L'UNIVERSITE MONTPELLIER II

Discipline : Mécanique et Génie Civil

Ecole Doctorale : Information, Structures et Systèmes

présentée et soutenue publiquement

par

JANA DLOUHÁ

le 1^{er} Juillet 2009

**COMPORTEMENT VISCOELASTIQUE LONGITUDINAL DU BOIS
VERT: DIVERSITE ET PREDICTION A LONG TERME**

JURY

Loïc Daridon
Joseph Gril
Petr Horáček
Parviz Navi
Sylvie Castagnet
David Hunt

Président de jury
Directeur de thèse
Directeur de thèse
Rapporteur
Rapporteur
Examineur

Remerciements

Il y a tellement de monde que je voudrais remercier que je vais certainement en oublier quelques uns dans ma maladresse. J'espère quand même ne pas avoir oublié ceux qui ont joué les rôles principaux pendant le déroulement de ma thèse....

D'abord et surtout un grand merci à Joseph de m'avoir accueilli au sein du LMGC, d'avoir suivi mon travail et de m'avoir apporté ses conseils indispensables.

Un grand merci aux responsables de la formation universitaire à l'UMII et à l'IUT de Nîmes de m'avoir accordé les deux demi-postes d'ATER qui m'ont permis de terminer mon travail de thèse dans de bonnes conditions.

Merci à Bruno de m'avoir aidé tout au long de cette course d'endurance autant professionnellement que personnellement.

Un immense merci à Tancrède qui s'est infligé, entre autres, la tâche ingrate de lire et relire mon manuscrit.

Merci à Olivier d'avoir apporté son regard de mécanicien généraliste sur mon travail.

Merci à tous les autres permanents dont les conseils j'ai profité à un moment ou un autre.

Merci à tous les thésards, post-docs et stagiaires d'avoir créé une ambiance conviviale et en particulier de m'avoir supporté pendant la période de la rédaction.

Merci à Willy de m'avoir écouté et soutenu quand j'en avais besoin.

Velký dík patří Petru Horáčkovi za to že mi umožnil pracovat na dizertační práci v rámci spolupráce s francouzskou laboratoří .

A nakonec bych chtěla moc poděkovat svým rodičům za jejich podporu po dobu celého studia.

USED ABBREVIATIONS AND SYMBOLS

ACP	approximated complex plane
a^*	complex formulation $a^* = a' + ia''$ where $a' = E'_{//}/\rho$ and $a''/a' = \tan\delta_{//}$
b^*	complex formulation $b^* = b' + ib''$ where $b' = 4G'_{//}/\rho$ and $b'' = 4G''_{//}/\rho$
β^*	complex formulation $\beta^* = \beta' + i\beta''$ where $\beta' = b'/a'$ and $\beta'' = b''/a''$
a_{ta}	aging time shift factor
a_T	temperature shift factor
C_{xx}	elements of the stiffness matrix
CP	complex plane
E	Young's modulus
E^*	complex formulation of the Young's modulus $E^* = E' + iE''$
E/ρ	specific Young's modulus along the grain
$E_{//}/\rho$	specific Young's modulus along the microfibrils
θ	microfibril angle
G^*	complex formulation of the shear modulus $G^* = G' + iG''$
h	thickness
f	resonance frequency
J^*	complex compliance
J'	storage compliance (real part of the complex compliance)
J''	loss compliance (imaginary part of the complex compliance)
J_0	initial compliance
J_i	instantaneous compliance
$J(t)$	time-dependent compliance
J - T effect	assumption stating the temperature effect on the initial compliance
k	power parameter
$\lambda(T)$	softening parameter
l	length of the specimen
LRT	directions: longitudinal – radial – tangential
m	constant depending on the vibration mode
MFA	microfibril angle
μ	aging rate
P	porosity
ρ_b	basic density, further denoted only ρ
ρ_{cw}	density of the cell wall
$\rho_{sat100\%}$	totally saturated specific gravity
$\rho_{satX\%}$	partially saturated specific gravity
R	universal gas constant
RH	relative humidity
rms	root mean square
SE	standard error
SD	standard deviation
S_L	saturation level
τ	characteristic/doubling time
T	temperature
T_0	reference temperature
t_a	aging time
t_c	creep time, further denoted only t

$\tan \delta$	damping coefficient ($\tan \delta = E''/E'$)
$\tan \delta_{//}$	damping coefficient along the microfibrils
T_g	temperature of glass transition
t_L	loading time
t_{stab}	stabilisation time
TTAE	time-aging time equivalency
TTE	time-temperature equivalency
W	activation energy
W_0	activation energy deduced from visually generated master curve without J-T effect.

COMPORTEMENT VISCOELASTIQUE LONGITUDINAL DU BOIS VERT: DIVERSITE ET PREDICTION A LONG TERME

Le but de l'étude consistait à prédire le comportement viscoélastique longitudinal du bois vert dans la période correspondant à la vie d'un arbre et d'explorer la diversité de ces propriétés. Le travail s'est déroulé en deux temps. Une analyse exploratoire des propriétés vibratoires a été effectuée sur un large échantillon incluant divers types de bois, y compris des bois de réaction, issus de dix espèces tropicales. Dans un deuxième temps, une sélection restreinte des échantillons a été utilisée pour une étude approfondie du comportement en fluage à long terme. Par ailleurs, la relation avec les paramètres structuraux tels que densité, angle des microfibrilles et pourcentage des éléments anatomiques a été étudiée.

Une procédure d'évaluation du fluage à long terme a été mise au point à partir d'essais à différentes températures. L'occurrence du vieillissement physique suite au refroidissement consécutif au chauffage au dessus de la température de transition vitreuse du bois a été mise en évidence. L'applicabilité du principe d'équivalence temps-température a été remise en question par l'analyse des résultats dans le plan complexe approché (PCA). L'hypothèse supplémentaire de la dépendance de la complaisance initiale à la température, similaire à l'élasticité entropique des polymères amorphes, a été proposée et appliquée, permettant de prédire avec succès le comportement à long terme à partir d'essais courts. Le fluage thermoactivé, ainsi que le phénomène de vieillissement physique, ont été décrits par un modèle de Maxwell parabolique identifié à partir de la représentation des résultats dans le PCA. Le comportement en fluage est apparu non corrélé au coefficient d'amortissement mesuré lors des essais vibratoires, suggérant une dissociation entre les mécanismes rhéologiques qui contrôlent le comportement viscoélastiques aux échelles de temps acoustiques (quelques centaines de Hertz) et biologiques (plusieurs années). Enfin, l'hypothèse d'un effet prépondérant de la lamelle mitoyenne sur le processus de fluage a été suggérée pour expliquer les faibles corrélations observées entre le fluage relatif et la structure des parois cellulaires.

VISCOELASTIC BEHAVIOUR OF GREEN WOOD ALONG FIBRES: DIVERSITY AND LONG-TERM PREDICTION

The aim of the study was to predict the long-term creep behaviour of green wood in the longitudinal direction for a period corresponding to the life of a tree and to explore the variability of this behaviour. The study took place in two steps commencing with a screening of vibration properties on a large sample of ten tropical species including different wood types, the reaction wood included. Next, a small subsample was used for an in depth analysis of the long-term creep properties. Further, the relation of viscoelastic properties with structural parameters such as basic density, microfibril angle and percentage of anatomical elements was investigated.

A testing procedure was developed to assess the long-term viscoelastic properties based on short-term creep tests performed at different temperatures. Occurrence of physical aging subsequent to a quench from a temperature above the glassy transition was evidenced. Direct applicability of the time-temperature equivalency was questioned by discrepancies observed in the approximated complex plane (ACP). Additional assumption of a temperature-dependent initial compliance, similar to the entropic elasticity in amorphous polymers, was suggested and successfully applied to obtain reliable long-term creep predictions. Thermo-activated creep behaviour along with physical aging was described by a parabolic Maxwell model identified from the representation of experimental data in the ACP. The creep behaviour was revealed not to be related to the damping coefficient measured by the vibration method, indicating that different rheological mechanisms govern the viscoelastic behaviour at acoustic time scales (hundreds of Hz) and biologic scales (several years). In conclusion, the hypothesis of the middle lamella playing a key role in the long-term creep was proposed to explain the weakness of the correlations observed between the amount of relative creep and the structure of the cell wall.

DISCIPLINE : MECANIQUE ET GENIE CIVIL

MOTS-CLES : VISCOELASTICITE – MODELE PARABOLIQUE - BOIS VERT – BOIS TROPICAUX

LABORATOIRE DE MECANIQUE ET GENIE CIVIL - 860, Route de St Priest – 34090 - Montpellier

SUMMARY TABLE

SUMMARY TABLE	1
GENERAL INTRODUCTION	5
LITERATURE OVERVIEW	7
1) WOOD STRUCTURE	7
1.1 Microstructure	7
1.2 Cell wall structure	7
1.3 Constitutive polymers	8
1.4 Distribution of the main polymers in the cell wall	9
1.5 Properties of cell wall components and their interactions	10
2) MECHANICAL CONSEQUENCES OF THE BIOLOGICAL SYNTHESIS OF WOOD	11
2.1 Origin of pre-stresses	11
2.2 Biological consequences of pre-stresses	12
2.2.a Increase of the stem bending resistance	12
2.2.b Interactive shape regulation	12
2.3 Reaction wood	13
2.4 Consequences on the measurement of viscoelastic properties	14
3) LINEAR VISCOELASTICITY	15
3.1 Physical sources of viscoelastic behaviour	15
3.1.a Energetic and entropic elasticity	15
3.1.b Glass-rubber transition	16
3.2 Transition regions in wood	17
3.3 Experimental observations	18
3.3.a Creep tests	18
3.4 Phenomenological framework	22
3.4.a Statement of the Boltzmann superposition principle	22
3.4.b Effect of temperature	22
3.5 Mechanical models	28
3.5.a Spring-dashpot models with single relaxation time	28
3.5.b Models with distribution of retardation times	29
3.5.c Multi-transition models	31
3.5.d Representation in complex plane	31
4) STRUCTURE/PROPERTY RELATIONS	33
4.1 Density and MFA	33
4.2 Density and MFA as a predictor of longitudinal wood stiffness	33
4.3 Determinants of vibration properties	35
4.4 Determinants of creep properties	37
4.4.a MFA	37
4.4.b Effect of constitutive polymers	39
5) ROLE OF THE VISCOELASTICITY IN THE LIVING TREE	40
A) EXPLORING THE DIVERSITY OF VIBRATION PROPERTIES OF TROPICAL WOODS	41
1) INTRODUCTION	41
2) STUDIED WOOD MATERIAL/SAMPLING	42
2.1 Sample selection	42
2.2 Repartition of specimens for different studies	43
2.3 Specimens preparation	47
3) METHODOLOGY	47
3.1 Growth stress measurements	47
3.2 Vibration measurements	48
3.2.a Comparison of damping measurement methods	49
3.2.b Repeatability of the vibration measurement	50
3.3 Investigation of the effect of storage conditions	51
3.4 MFA measurements	51
3.5 Anatomical structure	52
3.6 Simple model predicting specific modulus and damping coefficient of the cell wall material	53
3.6.a Simplified model based on Hooke's law of angle lamina	53
3.6.b Complex formulation	54

3.6.c	Expression of the specific modulus and damping coefficient in the local coordinate system	55
4)	EFFECT OF STORAGE PROCEDURE	56
4.1	Long-term storage in water at low temperature	56
4.2	Effect of soaking in 40% ethanol.....	58
4.3	Effect of air drying.....	59
4.4	Conclusion about storage	60
5)	OTHER INVESTIGATED EFFECTS	61
5.1	Effect of hygrothermal recovery.....	61
5.2	Difference between air dried and oven dried state.....	61
5.3	Comparison of empirical relations between damping and specific modulus in air dry and green state.....	63
5.4	Conclusion.....	63
6)	BASIC STRUCTURE – PROPERTY RELATIONS	64
6.1	Green density – Basic density	64
6.2	MFA – Basic density.....	65
6.3	Structural determinants of elastic modulus	67
6.4	Structural determinants of specific modulus	68
6.5	Structural determinants of damping coefficient.....	71
6.6	Conclusion.....	74
7)	PREDICTING CELL WALL PROPERTIES FROM THE WOOD PROPERTIES AND MICROFIBRIL ANGLE.....	75
7.1	Capacity of the model to describe observed behaviour	75
7.2	Variability of the properties between wood specimens from straight growing trees and wood specimens from tilted trees	75
7.3	Cell wall properties along microfibrils.....	77
8)	INTERSPECIFIC AND INTRASPECIFIC VARIABILITY OF VIBRATION PROPERTIES.....	77
8.1	Screening of intraspecific variability by species.....	77
8.2	Anatomical structure as a possible determinant of vibration properties.....	81
8.3	Conclusion.....	82
B)	LONGITUDINAL CREEP OF GREEN WOOD.....	83
1)	DEVELOPMENT OF THE CREEP DEVICE AND TESTING PROCEDURE	83
1.1	Tensile creep device.....	83
1.2	Creep specimens.....	84
1.3	Development of the experimental procedure	86
1.3.a	Instantaneous deformation.....	86
1.3.b	Particular case of curved specimens	86
1.3.c	Duration of the procedure	87
1.3.d	Stability of gage output	87
1.4	Some verifications	88
1.4.a	Repeatability	88
1.4.b	Tests of linearity and recovery	88
1.4.c	Correction of the creep signal	89
1.5	Data processing and analysis.....	90
2)	EVIDENCE AND MODELLING OF PHYSICAL AGING.....	92
2.1	Introduction.....	92
2.2	Material and methods	93
2.3	Results and discussion	94
2.3.a	Suitability of experimental procedure and evidence of aging phenomenon	94
2.3.b	Identification of a rheological model.....	95
2.3.c	Optimisation of model parameters	96
2.3.d	Application to the analysis of Nakano's data.....	99
2.3.e	Discussion on the physical processes involved	99
2.4	Conclusion.....	100
3)	APPLICABILITY OF THE TIME-TEMPERATURE EQUIVALENCY	102
3.1	Introduction.....	102
3.2	Material and methods	103
3.2.a	Characteristics of selected specimens.....	103
3.2.b	Experimental procedure	104
3.2.c	Correction of strain data.....	104
3.3	Results and discussion	104
3.3.a	Building of the master curve using log time shifts	104
3.3.b	Examination of experimental data in the complex plane	105

3.3.c	Identification of the rheological model.....	108
3.3.d	Variation of model parameters issued from different fitting methods	109
3.3.e	Simplified predictions of the long-term creep based on reduced number of creep tests	112
3.4	<i>Conclusion</i>	114
4)	RELATIONSHIP BETWEEN STRUCTURAL PARAMETERS, VIBRATION PROPERTIES AND CREEP PROPERTIES.....	115
4.1	<i>Relation between creep and vibration data</i>	116
4.2	<i>Variability of the creep response</i>	117
4.3	<i>Structural determinants of viscoelastic behaviour</i>	118
4.4	<i>Conclusion</i>	120
5)	CONCLUSION.....	121
C)	CONCLUSIONS AND PERSPECTIVES.....	123
1)	METHODOLOGICAL ADVANCES	123
1.1	<i>Storage of green specimens</i>	123
1.2	<i>Correction of the creep signal obtained during tests at elevated temperature and suggested experimental procedure</i>	123
1.3	<i>Simplified experimental procedure for satisfactory long-term predictions of the creep behaviour</i>	124
2)	INTERPRETATION OF CREEP DATA	124
2.1	<i>Assessment of physical hypothesis using ACP</i>	125
2.2	<i>Identification of a parametric rheological model</i>	125
3)	STRUCTURAL DETERMINANTS OF VISCOELASTIC PROPERTIES	125
3.1	<i>Relationships between vibration properties and structural parameters</i>	125
3.2	<i>Determinants of the creep behaviour</i>	126
4)	VISCOELASTIC PROPERTIES OF WOOD AT DIFFERENT STRUCTURAL SCALES.....	127
4.1	<i>Simplified representation of the hierarchical wood structure</i>	127
4.2	<i>Contribution of middle lamella and fibres at macroscopic scale</i>	129
4.3	<i>Processes involved at the tree scale</i>	129
5)	PERSPECTIVES	130
	REFERENCES	131
	FIGURE LIST	141
	TABLE LIST	147
	APPENDIX	149

GENERAL INTRODUCTION

This work is an integral part of an ANR research project called «Woodiversity» (ANR-05-BDIV-012-04) which focused on the variability of structures and properties of trees growing in the tropical rainforest. Tropical rainforests are highly competitive environments characterised by high density of stems, closed forest canopy and limited light availability. Severe growing conditions are at the origin of the diversity of structures and properties of tropical species. Numerous strategies have been developed by trees to optimise their performance and survive in the forest until their reproductive maturity. The aim of the ANR project was to analyse the biological significance of the diversity of wood structure and mechanical properties. The role of the *Tree and Wood Mechanics research team* in LMGC was to advance methodologies for characterisation of mechanical properties of green wood. The present work focuses in particular on viscoelastic properties of green wood in the longitudinal direction.

The context of the ANR project is plant biomechanics. It means that throughout all the study, wood is not considered as a material to be used for man-made structures, but as a building material designed to ensure living functions of a tree. That's why it was essential to study wood in a state that is as representative as possible of its native state in the living tree. For this purpose, wood samples had to be kept in water, sometimes for long durations, and the effect of different storage conditions on mechanical properties of wood has been investigated. The aim of the PhD project was to develop an experimental device and appropriate procedure to assess the viscoelastic behaviour of green wood and explore its variability along with their structural determinants.

Data were collected in view of biomechanical applications such as models dealing with the tree reorientation process or bending resistance. Thus, time scales in which we were interested corresponded to decades of years. To predict behaviour at these time scales, we need to set up a precise experimental procedure. Because this procedure required a long experimental time, it was hindering to the second objective: to investigate the diversity of viscoelastic behaviour. Therefore, the first screening of viscoelastic properties was performed on a large sample of tropical species using a rapid vibration method. Afterwards, an in depth study of viscoelastic behaviour was performed on a limited selection of specimens exhibiting contrasted properties. The aim was to assess general features of the viscoelastic behaviour. To gain an insight into the origin of viscoelastic properties, some structural parameters such as basic density and microfibril angle were measured on the sample. These parameters are known to be the determinants of elastic properties. In this study, the pertinence of the latter parameters for viscoelastic considerations was investigated.

The manuscript is organised in two parts according to our objectives. The first part deals with the diversity of viscoelastic response measured at short observation times and the relation between viscoelastic and structural parameters. The second part focused in greater detail on the validity of some assumptions generally used for predictions of the long-term viscoelastic behaviour from short-term experimental data. Structural complexity of natural materials such as wood makes it difficult for the direct application of experimental procedures and theoretical principles often borrowed from other fields, such as polymer science, and many precautions have to be taken. We have tried in this work to gain an insight into the current understanding of the viscoelastic properties of wood in the green condition, the variability of the viscoelastic response and the role of the temperature in the acceleration of viscoelastic processes.

LITERATURE OVERVIEW

The following chapter introduces wood structure and properties as well as general concepts for investigating viscoelastic properties. The specificity of wood behaviour originating from its biological synthesis and present state of knowledge on the contribution of wood components to the viscoelastic behaviour is presented. Some specific points will be however introduced in the introduction of corresponding chapters.

1) Wood structure

Wood with its inherent strength is a product of growing trees. The primary function of the woody trunk of the living tree is to provide support for the photosynthetic energy factory *i.e.* leaves at the top and to provide transport of water and nutrients moving up to those leaves. The photosynthetic sugars produced by the leaves mostly move down the stem via the bark tissues. Woody tissues, interior to the bark, are organised in concentric anisotropic bands made up of cells with specific functions.

1.1 Microstructure

Three main features characterize the microstructure:

- highly elongated cells called tracheids in softwood and fibres in hardwoods constituting the bulk of the wood;
- parenchyma cells oriented in radial or in axial direction;
- large diameter cells with large pore spaces and thin cell walls called vessels.

While vessels ensure the transport function in hardwood, mechanical function is provided mainly by tracheids and fibres. Tracheids average about 3.5 mm in length and 0.035 mm in diameter while fibres are generally shorter (1–1.5 mm) and smaller in diameter (0.015 mm). Parenchyma cells function as a means of either longitudinal or radial nutrient transport/storage. However, Burgert *et al.* (1999) stated recently that in addition to their storage and transport function ray cells have also a mechanical function. Reiterer *et al.* (2002) have also reported the importance of the radial reinforcement of the wood structure by rays. Excepting radial parenchyma, all cells are aligned along the longitudinal axis of the stem so that wood can be represented as a cellular solid as illustrated in Figure 0-1a. This is particularly true in softwoods where tracheids represent up to ~95% of the bulk of the wood. In hardwoods there is wide variation in the proportion of cell types. We can encounter large percentage of vessels ~ 21.4% in *Betula lutea* or of parenchyma totals ~ 28% in *Carya ovata* (Kollmann and Côté 1968). Accordingly to its microscopic structure, wood is highly anisotropic. Its anisotropy can be reduced to an orthotropic behaviour with stem planes of symmetry defining three directions – longitudinal, radial and tangential (L – R – T). Mechanical properties are mainly determined by the fibre fraction and cell wall thickness. Accordingly to fibre orientation, mechanical performances of wood in L direction are higher than in transverse directions.

1.2 Cell wall structure

Cell wall of wood fibres can be represented as a multi-layer fibre-reinforced composite (Figure 0-1b). Each cell wall layer is made up of ‘fibres’ of crystalline cellulose called microfibrils embedded in a matrix of amorphous hemicelluloses and lignin.

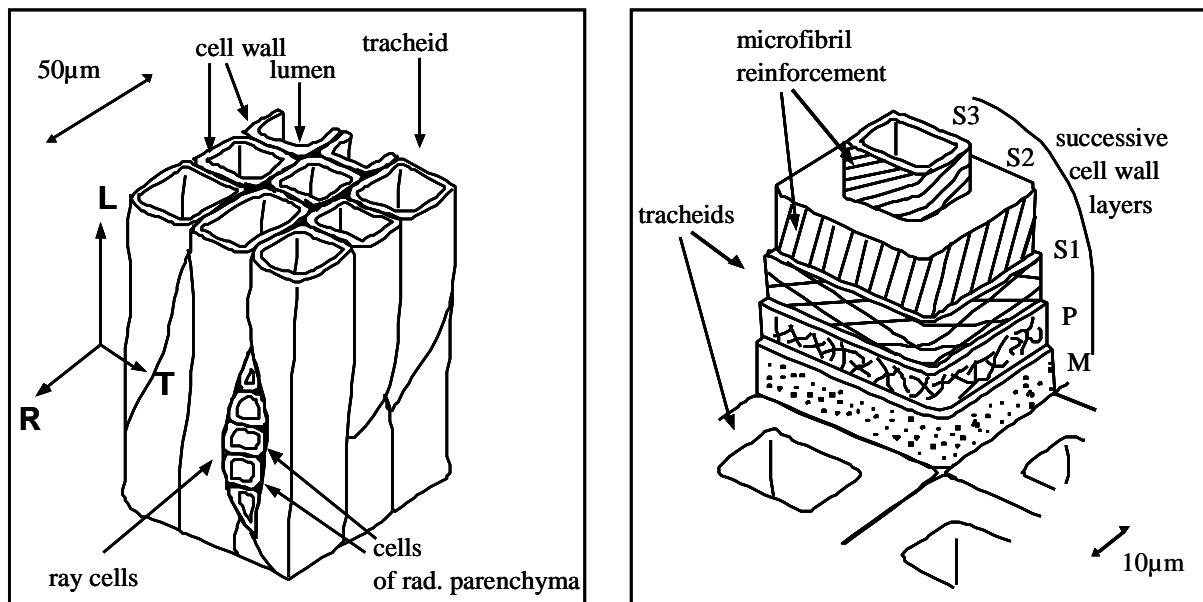


Figure 0-1: (a) Honeycomb-like structure of wood at microscopic scale. (b) Multi-layered structure of the cell wall. From (Norimoto and Gril 1989).

Between individual cells there is a thin layer called middle lamella which glues the cells together to form the tissue and is mainly composed by pectin and lignin. In the primary wall the cellulose fibrils are arranged in thin randomly oriented layers. As the primary wall is the first layer deposited during the development of a cell, this system allows for an expansion of the young cell driven by the softening of the interfibril matrix. It is difficult to distinguish the primary wall from the middle lamella using microscopy so that the term compound middle lamella is often applied to both regions. Contrary to the primary layer, the secondary layers are characterised by a high degree of parallelism of microfibrils. Typical secondary cell wall is divided into three different layers, S1, S2, and S3. The S1 layer is about 0.1-0.3 μm thick and exhibits gentle helical slope of the fibrils. The S2 layer, usually 1-5 μm in thickness, accounts for 75% to 85% of the total thickness of the cell wall. The S2 layer contains from 30 to 150 lamellae, all exhibiting microfibrils spiralling in a right-hand running a steep angle (10° to 30°) to the fibre axis further denoted microfibril angle (MFA). Orientation of microfibrils in S2 layer affects significantly many properties of wood material along with their anisotropic character. The innermost layer of the secondary cell wall, the S3 layer, is again very thin (~0.1 μm) with MFA of 60° to 90° with regard to the cell axis (Fengel and Wegener 1984).

1.3 Constitutive polymers

The main wood components are cellulose, hemicelluloses and lignin. Nearly 50% of the wood material is made up of cellulose. Cellulose occurs in wood in the form of slender filaments or chains, these having been built up within the cell wall from the glucose monomer. Whilst the degree of polymerisation can vary considerably from one species to another, it is considered to range from 8000 to 10 000 units on average. Successive units in the chain are rotated through 180° and covalent bonding by β-1-4 linkage gives rise to a straight chains. Supramolecular structure is cellulose is characterised by highly ordered arrangement with densely packed molecules, building up a fibrous-like rod structure called a microfibril. This structure is based on the alignment of the cellulose chains parallel to each other and connected between them by intra and intermolecular hydrogen bonds. However, microfibrils are not totally crystalline and regions with less ordered arrangement of the cellulose molecules occur. In wood it is estimated that about 70% of the cellulose is crystalline (Fengel and Wegener 1984).

Hemicelluloses are in close association with cellulose in the cell wall. The molecular chains are much shorter than those of cellulose, they have side-groups and are branched in some cases. The third macromolecular wood component, lignin, is present in roughly equal proportions to the hemicelluloses. The molecules of lignin are built up differently from those of the polysaccharides, consisting of an aromatic system composed of phenylpropane units. From a morphological point of view, lignin is an amorphous substance located in the compound middle lamella as well as in the secondary walls. During the development of the cells lignin is incorporated as the last component into the cell walls, interpenetrating the fibrils and so strengthening the cell walls (Fengel and Wegener 1984). Most cellulosic plants do not contain lignin and it is the inclusion of this component which imparts much of the stiffness to wood cell walls. Recent works have reported that lignin structure is not completely amorphous. Akerholm and Salmén (2003) have shown that there is a preferred orientation of the phenyl-propane units of lignin along the fibre axis in spruce tracheids. This implies there is an ordered structure of lignin in the secondary wall of tracheids analogous to that of the cell-wall polysaccharides. The dynamic IR-spectra also indicated that lignin exhibits a much more viscoelastic behaviour than do the carbohydrates.

In addition to main constitutive polymers of wood – cellulose, hemicelluloses, lignin – wood contains the so-called extractives. The extractives cover a wide range of chemical compounds though they generally represent only a small part of wood. They can be extracted from wood by means of polar and non-polar solvents. As a rule, extractives represent a small proportion of wood, fewer than 5%, but relatively high amounts of extractives are found in some tropical and subtropical woods (up to 30% according to CIRAD¹ database). Extractives affect the wood density estimates (Singleton *et al.* 2003) and some of them are known to considerably affect the damping coefficient (for details see §4.3) and some other properties such as shrinkage (Choong and Achmadi 1991) or durability.

1.4 Distribution of the main polymers in the cell wall

Cell wall layers differ not only by structural arrangement but also by the chemical composition as pictured in Figure 0-2. The middle lamella and primary wall are mostly composed by lignin (8.4% of the total weight), pectin, protein and xyloglucane (1.4%) included in the picture label hemicelluloses and very little cellulose (0.7%). The S1 layer consists of cellulose (6.1%), hemicelluloses (3.7%), and lignin (10.5%). The S2 layer is the thickest layer and has the highest carbohydrate content which is the mostly cellulose (32.7%) with lesser quantities of hemicelluloses (18.4%) and lignin (9.1%). The S3 layer, the innermost layer, consists of cellulose (0.8%), hemicelluloses (5.2%), and very little lignin. It is interesting to note that although the relative lignin ratio is low within the S2 layer, the same amount of lignin as in the middle lamella exists within this layer because of its large overall mass (Winandy and Rowell 2005).

¹ Centre de coopération internationale en recherche agronomique pour le développement (French Agricultural Research Centre for International Development)

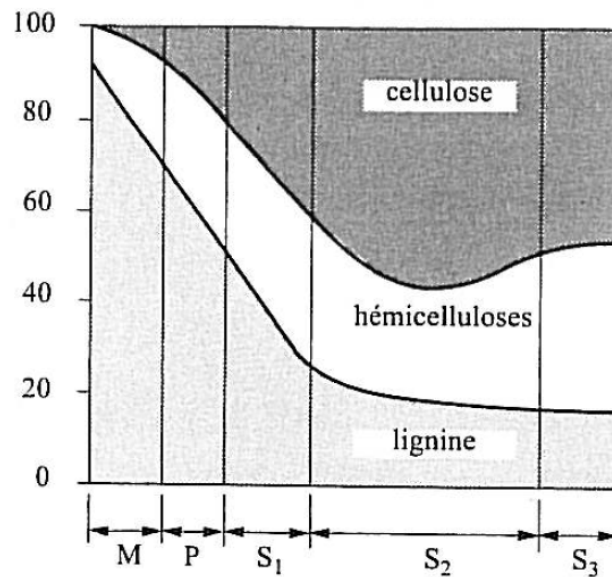


Figure 0-2: Distribution of main wood components in different layers of the cell wall according to Panshin and de Zeuw [cited by (Navi and Heger 2005)].

1.5 Properties of cell wall components and their interactions

An extensive overview of current knowledge about the cell wall component properties was recently done by Salmén and Burgert (2009). The following statements are extracted from this paper. The crystalline stiffness of cellulose is around 134 GPa, regardless of some discussion about the absolute number. However, the variability of the crystalline regions and the stiffness variations along the cellulose aggregates still need an in-depth consideration. The effective stiffness value of the cellulose in the cell wall structure is still not clear. Mechanical data for hemicelluloses and lignin are scarce; with only the old data of Cousins (1978; 1976) being available. Cousins estimated the Young's modulus of isolated Klason lignin to 2.3GPa at 12% moisture content (Cousins 1978) and that of hemicelluloses to 0.01GPa in saturated state (Cousins 1976). However, these values may only be taken as approximations and as indirect evidence, as both the molecular structure and the spatial arrangement of these polymers differ substantially in isolated form and within the in situ polymer matrix. At first glance, it seems that the overall contribution of the soft matrix polymers to the stiffness of the cell wall is of less importance, in particular, in the case of small cellulose MFAs. However, the importance of the mechanical properties of the matrix polymers cannot be neglected in particular for viscoelastic behaviour that is governed mainly by amorphous constituents. Further, sensitivity of wood to water is a good example on the necessity to consider also the hemicelluloses contribution to wood behaviour.

Besides the properties of individual polymers, their interactions greatly affect the performance of the cell wall assembly. The specific bonding pattern at their interfaces plays an essential role in this regard. The bonding of hemicelluloses to the cellulose fibril surfaces is not based on covalent bonds but mainly on hydrogen bonds. This results in a strong but also flexible connection of both polymers, as hydrogen bonds can easily be opened and reformed (Altaner and Jarvis 2008). Lignin is not bound directly to cellulose, but it is covalently bound to hemicelluloses. Hence, the amphiphilic hemicelluloses play an essential role in the maintenance of the cell wall assembly while lignin reacts as a bulking agent preventing buckling of microfibrils. The interactions between the constituents of the cell wall occur on an extremely intermixed level. This explains to some extent the fact that properties of the cell wall do not generally reveal strong dependencies of one component to another. It is also still not clear whether and how crosslinks exist within cellulose aggregates between

hemicelluloses and cellulose microfibrils. In other words, a network structure within the secondary cell wall is not clarified and we do not know how strong such a network could be.

2) Mechanical consequences of the biological synthesis of wood

2.1 Origin of pre-stresses

During its life, a tree experiences incremental diameter growth together with an increase of external forces, mainly because of the self loading of the tree. In addition, newly formed wood cells are pre-stressed during the maturation process. Immediately after cell birth, the newly developed cells undergo a several day long maturation period, during which two mechanisms take place in the cell wall; lignification and cellulose crystallization. As lignin is deposited, the amorphous cellulose matrix swells transversely and when cellulose crystallization occurs, microfibrils shrink longitudinally (Okuyama *et al.* 1994). Under the combined effect of these two mechanisms, single cell tends to shrink longitudinally and expand transversally as illustrated in Figure 0-3. However, the maturing wood cells are attached to older, already lignified and thereby much stiffer cells which prevent the tendency of maturing cells to shrink. Hence, these maturing cells are held in a state of longitudinal tensile stress, and it is only on cutting the wood, that these “maturation stresses” can be released in the form of residual strains along the longitudinal axis (Archer 1986; Kubler 1987). The wood cells at the surface of a tree are therefore stretched longitudinally and compressed tangentially and can be said to be held in tension. However, as more and more wood is added to the tree surface, the wood cells inside the trunk are slowly compressed, until they are completely held in compression, toward the centre of the trunk. This gradient of mechanical stress in a trunk, whereby the outside is held in tension, and the centre in compression, is called growth stress, and can be highly detrimental to wood quality, resulting in warping and twisting of boards and planks.

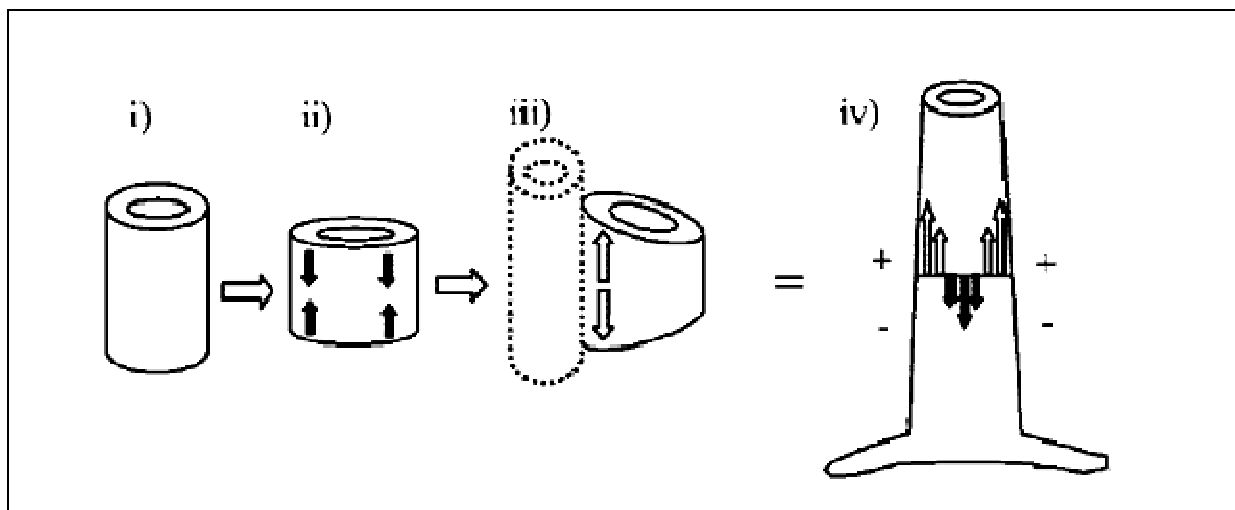


Figure 0-3: Maturation process and origin of growth stresses as pictured by (Plomion *et al.* 2001). As the newly developed wood cell (i) begins to differentiate (ii), the deposition of lignin and cellulose in the secondary cell wall tends to stretch the cell laterally and cause it to shrink longitudinally (black arrows). However, as the differentiating wood cell is attached to older wood (iii), it cannot deform completely, thereby setting up a mechanical stress in the cell wall (empty arrows). In normal wood (NW), this translates into a tensile stress, therefore, the wood in the outer surface of a tree (iv) is usually held in tension (+ and empty arrows). However, accumulation of peripheral maturation tensile stresses must be balanced by internal compression of the stem (- and full arrows).

2.2 Biological consequences of pre-stresses

2.2.a Increase of the stem bending resistance

One of important consequences of pre-stresses for the tree is to improve the instantaneous bending resistance of stems. As vital functions of a tree such as cell differentiation or sap conduction are concentrated at the periphery of the stem, it is essential to prevent surface damage when a tree is submitted to bending loads. The impact of pre-stresses on the radial distribution of internal stresses inside a tree under bending loads is nicely explained by Gordon (1978) in Figure 0-4a. When submitted to axial stress wood is more resistant in tension than in compression. Rupture in tension of a fibrous material, like wood, requires a considerable energy because of the complex organisation of the cell walls that makes them resistant to delamination. In compression, due to the porous honeycomb-like microstructure, the occurrence of localised buckling results in a lower resistance. The opposite is observed across the fibre: fragile rupture in tension and considerable plastic deformation in compression. Wood layers located near stem periphery are pre-strained by longitudinal tension and tangential compression at the expense of less vital internal layers subjected by compensation to longitudinal compression and transverse tension. This improves stem strength and flexibility and tends to prevent breaking or surface damage under bending loads as pictured in Figure 0-4 b.

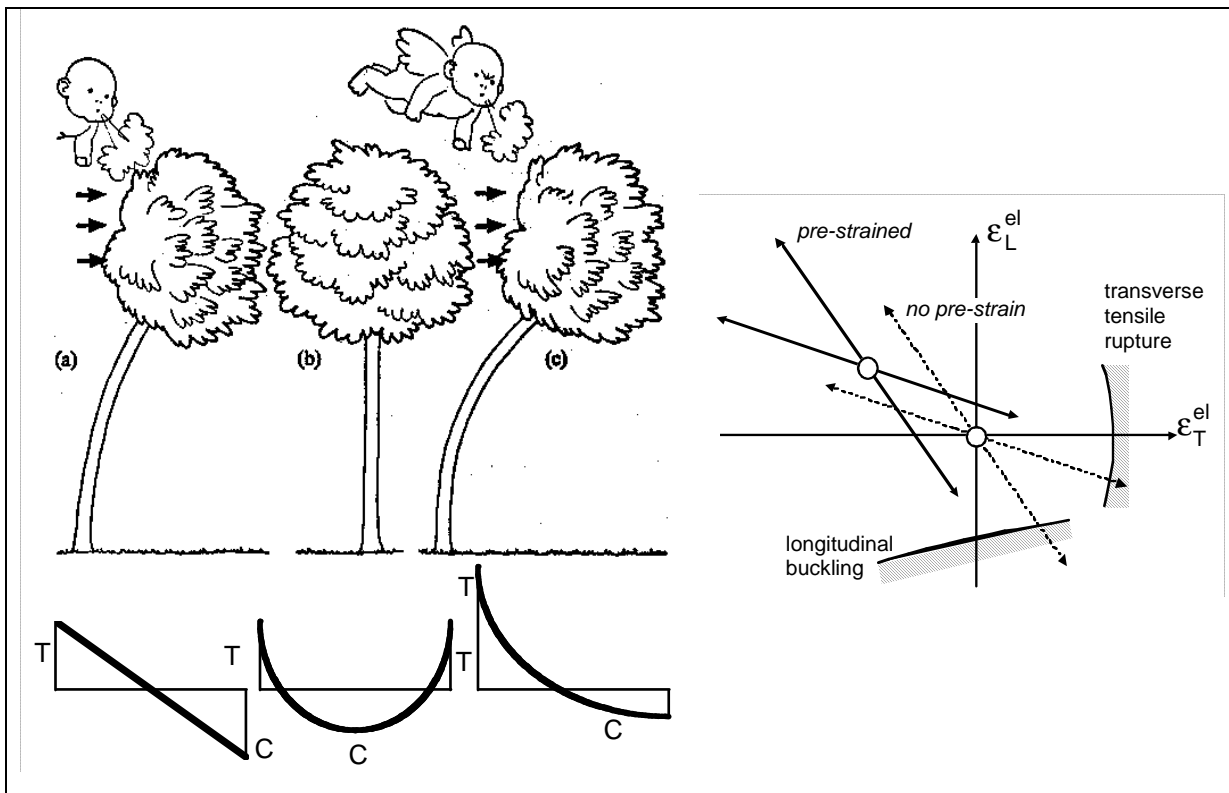


Figure 0-4: Left figure: Pre-stress and bending strength of tree trunks. (a) Tree bent by the wind without considering the field of pre-stresses due to the maturation process. Stress distribution across the trunk is linear and maximum tension and compression are equal. (b) Field of internal stresses resulting from the maturation process. The outside is in tension all around, the inside is in compression. (c) Pre-stressed tree in a strong wind. Compression stress is halved and this tree can bend twice as far as the one in (a). From Gordon (1978). Right figure: The positive effect of growth stresses on stem flexibility.

2.2.b Interactive shape regulation

Tree stems are slender structures that are never perfectly symmetric. Thus, the increase in tree mass due to their growth induces inevitably more or less important bending movements. Given the mechanical design of trees, integration of these movements over time

would ultimately lead to a weeping habit. However, a gravitropic correction is achieved by asymmetric distribution of maturation stresses that balance the bending moment due to asymmetric increase of weight (Alméras and Fournier 2009). Pre-stresses are used by a tree also to control the shape of its branches or possible non-verticality of the stem due to some external loading like wind. Actually, circumferential distribution of longitudinal growth strains is very often asymmetric (Fournier *et al.* 1994). Resulting difference of tensile stresses induced on the upper and lower side of a tree stem or a branch induces a bending moment. Thus, growth stresses allow stem reorientation since the most tensile side pulls the other one. Although cell maturation is very short compared to the subsequent duration of wood existence as a supporting part of the stem, it is of the utmost importance both for the tree stem and for the wood, because of its mechanically active nature (Wilson and Archer 1979). Peripheral variations of initial growth stress provide the stems with the only mechanism of secondary reorientation compatible with their thickness and rigidity, because the amount of maturation strain can be adjusted during the formation of the secondary wall under the action of growth regulators.

2.3 Reaction wood

Investigating the maturation strains on the periphery of a leaning tree, it has been found that maturation strains are systematically different from the usual ones within an angular sector located in correspondence to the leaning direction. This clearly relates to the existence of a specific type of material, called reaction wood unlike normal wood produced *a priori* by straight growing trees. According to measured maturation strains, reaction wood in softwoods is named compression wood and in hardwoods tension wood. Wood tissues produced on the opposite side of the stem are called opposite wood. Occurrence of reaction tissues increases considerably the intraspecific variability of wood structures and properties. Reaction tissues represent in fact a sort of adaptation limit to the growth conditions. Variations appear at three levels: variations of cell shape and cell wall thickness, of cell wall architecture and of chemical composition of polymers constituting the middle lamella.

Compression wood in conifers is more lignified with higher MFA in the cell wall, resulting in a specific longitudinal modulus of elasticity much lower than that of normal wood (Timell 1986). On the contrary, the tension wood of hardwoods is less lignified with lower MFA and has in consequence higher specific longitudinal modulus of elasticity. Tension wood is characterised in many species by the occurrence of fibres with a particular morphology and chemical composition due to the development of so-called G-layer (Scurfield 1973). G-layer was for a long time described as essentially cellulosic highly crystalline layer. Recently, Bowling and Vaughn (2008) have reported the occurrence of arabinogalactan proteins and pectin molecules bound to the G-layer. Moreover, Clair *et al.* (2008) have identified a gel structure in the cell wall of the tension wood explaining its large longitudinal shrinkage. However, G-layer is not always present in tension wood of hardwoods. Among 122 species of Dicotyledonous representing 45 families for the most of tropical origin, only 56 species presented the G-layer in the tension wood (Fisher and Stevenson 1981). A similar observation was also made by Clair *et al.* (2006). The great diversity of reaction woods observed among the different species proves that nature owns a large set of solutions to solve its mechanical problems.

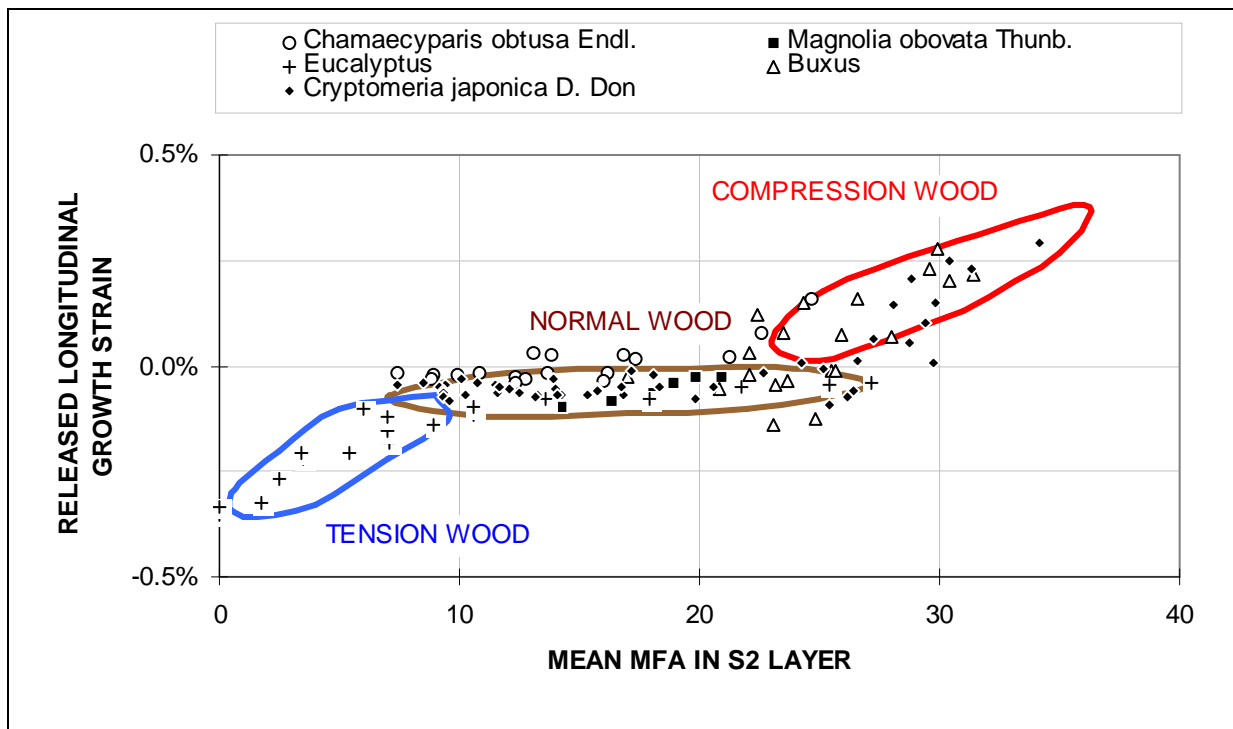


Figure 0-5: Released longitudinal growth strain against mean MFA in S2 layer from (Sassus 1998).

The amount of pre-stress was found to be correlated to the microfibril angle as illustrated in Figure 0-5 where values of released longitudinal growth strain are plotted against the mean MFA (Sassus 1998). The classical division between normal wood and reaction wood is given here a mechanical interpretation. Normal wood produces maturation strains ranging from -0.1% to 0% , and corresponds to a MFA of 7 to about 25° . Tension wood produces highly negative strains, down to -0.35% , with a MFA approaching zero. Compression wood produces positive strains, up to 0.3% , with a MFA exceeding $20\text{--}30^\circ$. Taking into account cell wall architecture and physico-mechanical properties of individual wood constituents, numerical models allow to estimate important properties as elastic compliance, maturation strains, hygrothermal expansion (Gril *et al.* 1999; Yamamoto *et al.* 2002). Both, variations of MFA and of chemical composition have to be taken into account to fit with experimental observations.

Due to differences in wood structure and chemical composition, reaction tissues exhibit different physical and mechanical properties. While similar characteristics (wider ring width, higher specific gravity, lower specific modulus) have been reported for different compression woods (Timell 1986; Gindl 2002), mechanical properties of tension wood seem to be variable. Some studies reported considerably higher elastic modulus in tension wood compared to opposite wood (Coutand *et al.* 2004) or a significant tendency between released growth strains and elastic modulus (Clair *et al.* 2003; Fang *et al.* 2008) while others have not detected any tendency between released growth strains and elastic modulus (Sassus 1998). Opposite trend, *i.e.* higher specific modulus in opposite wood compared to tension wood, was observed in two tropical species (Ruelle *et al.* 2007).

2.4 Consequences on the measurement of viscoelastic properties

Growth stress can be understood as the loading history applied to the material before tree felling. Locked-in strains are partially released by cutting specimens from the tree. However, some residual strains are still locked in the wood material and can be released by heating the piece of wood in a green state beyond the softening point of lignin (see §3.4.b for details). This phenomenon is known as hygrothermal recovery of locked-in strains (Yokota and Tarkow 1962). Heating of green wood therefore involves a complex set of deformation

processes. In addition to the reversible thermal strain characterised by negative expansion coefficient below the softening temperature of lignin, the material recovers locked-in strains resulting from the maturation process. The release of locked-in strains was observed by Yokota and Tarkow (1962) beyond $\sim 35^{\circ}\text{C}$. Gril *et al.*(1993) reported that release of strains becomes visible when the temperature of water exceeds $40\text{-}50^{\circ}\text{C}$. Such a deformation complicates the measurement of thermally activated viscoelastic properties because released strains overlap with the creep strain due to the loading.

3) Linear viscoelasticity

Viscoelastic response is often used as a probe in polymer science, since it is sensitive to the material's chemistry and microstructure. While not all polymers are purely viscoelastic to any important practical extent, and even fewer are linearly viscoelastic, the theory of linear viscoelasticity provides a usable approximation for many applications. Even in cases requiring more elaborate treatments, the linear viscoelastic theory is a useful starting point. Following outline of some important aspects of the linear viscoelasticity is widely inspired by some of basic works in this field (McCrum 1967; Nowick and Berry 1972; Ferry 1980; Bodig and Jayne 1982).

3.1 Physical sources of viscoelastic behaviour

3.1.a Energetic and entropic elasticity

When subjected to an applied stress, polymers may deform by either one or both of two fundamentally different atomistic mechanisms named respectively energetic and entropic or rubber elasticity. At first, the lengths and angles of the chemical bonds connecting the atoms may distort, moving the atoms to new positions of greater internal energy. This small motion occurs very quickly, requiring only $\sim 10\text{-}12$ seconds and is called energetic elasticity. Moreover, if the polymer has sufficient molecular mobility, larger-scale rearrangements of the atoms may also be possible. For instance, the relatively easy rotation around backbone carbon-carbon single bonds can produce large changes in the conformation of the molecule. Depending on the mobility, a polymer molecule can extend itself in the direction of the applied stress, which decreases its conformational entropy. In the absence of deforming forces, a polymer will take on a shape that maximizes its randomness and minimizes its free energy. With the application of the load the molecule will partially straighten to a new length $\ell + u_{de}$, as shown in Figure 0-6. The change of the molecular shape is accompanied by a modification of molecular forces throughout the network, resulting in delayed elastic behaviour. If the load is removed the polymer will return to a random, low-energy state. However, the return is delayed by newly formed secondary bonds and entanglement with other molecules. The longer the involved segments the slower these time-dependent phenomena. Elastomers — rubber — respond almost wholly by this so-called entropic mechanism, with little distortion of their covalent bonds or change in their internal energy.

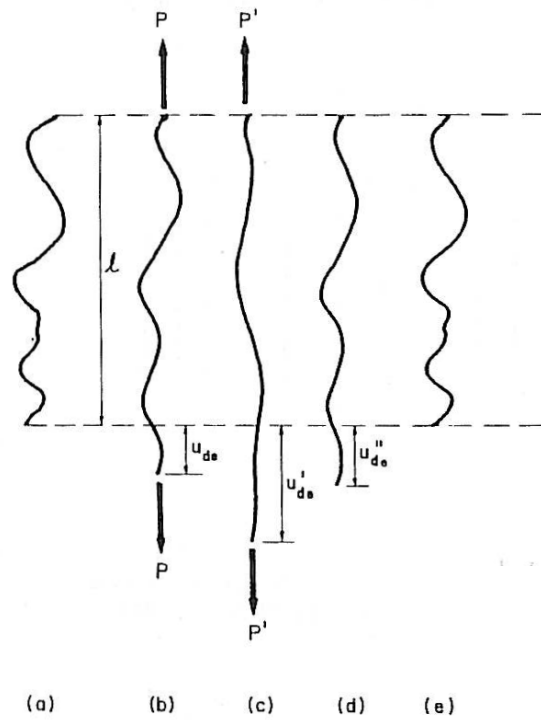


Figure 0-6: Schematic representation of delayed elastic deformation of a polymer chain: (a) original shape, (b) early stage of deformation, (c) final stages of elongation, (d) early stages of recovery, (e) recovered shape. (Bodig and Jayne 1982)

3.1.b Glass-rubber transition

In contrast to the instantaneous nature of the energetically controlled elasticity, the conformational or entropic changes are processes whose rates are sensitive to the local molecular mobility. This mobility is influenced by a variety of physical and chemical factors, such as molecular architecture, temperature or the presence of absorbed fluids which may swell and/or plasticize the polymer.

Often, a simple mental picture of the free volume, roughly defined as the space available for molecular segments to act cooperatively so as to carry out the motion or reaction in question, is useful in intuiting these mobility rates. These rates of conformational change can often be described with reasonable accuracy by Arrhenius-type expressions of the form:

$$\text{rate} \sim e^{-W/RT} \quad \text{Eq. 0-1}$$

where W is an apparent activation energy of the process and R is the (ideal) gas constant. At temperatures much above the glass transition temperature (T_g), the rates are so fast that they are essentially instantaneous, and the polymer acts in a rubbery manner in which it exhibits large, instantaneous, and fully reversible strains in response to an applied stress.

Conversely, at temperatures much less than T_g , the rates are so slow as to be negligible. Here the molecules chain uncoiling process is essentially frozen out, so the polymer is able to respond only by bond stretching. It now responds in a glassy manner, responding instantaneously and reversibly but being unable to be strained beyond a few percent before a brittle fracture occurs.

In the range near T_g , the material is midway between the glassy and rubbery regimes. Its response is a combination of viscous fluidity and elastic solidity, and this region is termed leathery, or, more technically, viscoelastic. The value of T_g is an important parameter of polymer thermomechanical response, and is a fundamental measure of the ability of the

material's molecules for mobility. Factors that enhance mobility, such as absorbed diluents, expansive stress states, and lack of bulky molecular groups, all tend to produce lower values of T_g .

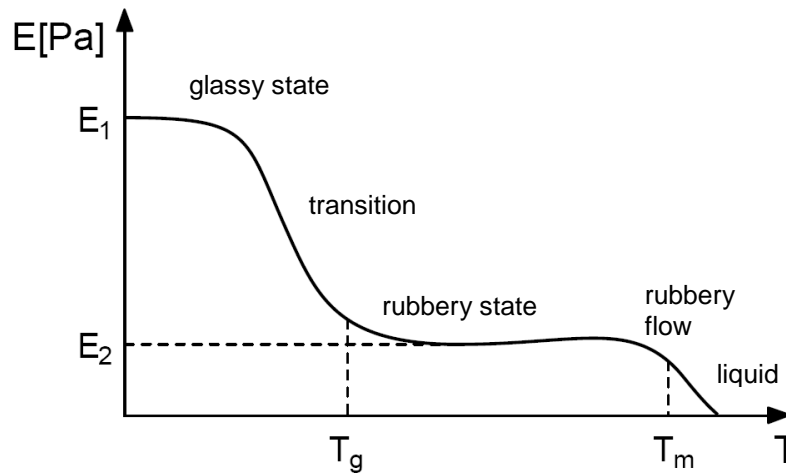


Figure 0-7: Plot of Young's modulus against temperature. T_g stands for the temperature of glassy transition and T_m for the melting point.

3.2 Transition regions in wood

Most polymers exhibit more than one relaxation, or transition region. In order to identify and compare these regions for different polymers, they are often labelled with the letters α , β , γ , etc. α corresponds to the relaxation observed at the highest temperature (at a given frequency) or the lowest frequency (at a given temperature). The β and γ symbols then apply to the other relaxation regions in order of decreasing temperature or increasing frequency. Each transition is associated with corresponding activation energy, and change in the storage modulus and mainly in the loss angle (dissipation) as observed in spruce and maple at 10% moisture content in Figure 0-8 borrowed from (Kelley *et al.* 1987). Analysis was performed on the water swollen wood by DMTA measurements. A peak in the loss angle spectrum is observed at each transition.

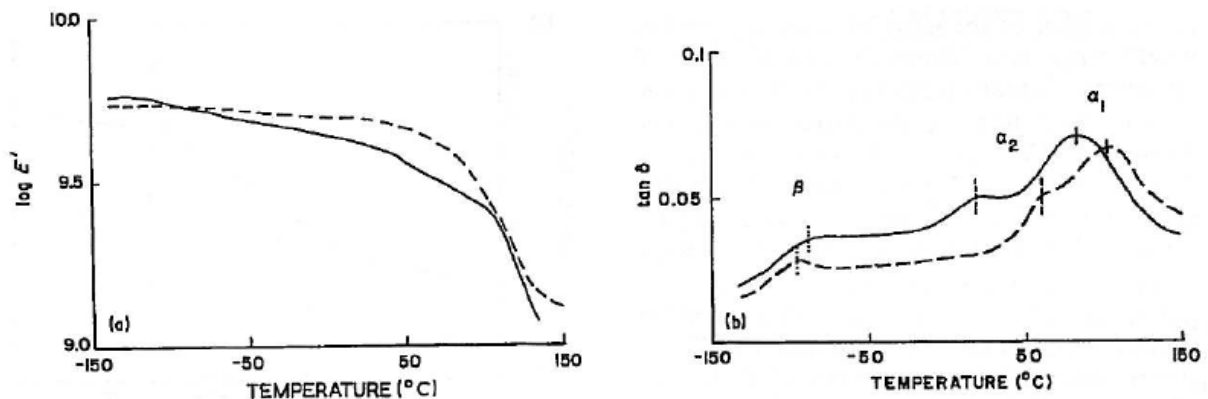


Figure 0-8: Storage modulus E' and loss angle $\tan \delta$ (damping or dissipation) as a function of the temperature measured in spruce (—) and maple (---) at 10% moisture content by (Kelley *et al.* 1987).

No substantial loss in storage modulus was evident over the temperature range of the β dispersion. However, a dramatic decrease in storage modulus is associated with the high temperature α_1 transition. The behaviour of the β transition is characteristic of secondary dispersion involving only small-scale molecular motion while the storage modulus decrease at the α transitions implies large-scale segmental motion which is characteristic of a glassy

transition. Transition α_1 was ascribed to lignin glassy transition whose activation energy is around 350kJ/mol^{-1} . Transition α_2 was associated with hemicelluloses but insufficient resolution in the measurement prevented the calculation of the corresponding activation energy. The β dispersion has an activation energy of 102kJ/mol^{-1} . A relaxation peak with similarly low activation energy has been noted for a variety of hydrophilic polymers, including carbohydrates, under high humidity conditions.

3.3 Experimental observations

In the case of viscoelastic materials, mechanical characterization often consists of performing tests similar to those used for elastic solids, but modified to enable observation of the time dependency of the material response. The most commonly used tests encounter creep, stress relaxation and dynamic loading. In the following, investigation of thermally activated creep properties and underlying principles will be outlined. Vibration measurements used to determine the damping coefficient will be introduced in the chapter A-3.2.

3.3.a Creep tests

Theoretical creep curve

The creep test consists in measuring the time dependent strain resulting from the application of a steady uniaxial stress. In principle, creep curves can be determined over the whole period of prediction. In fact, measurements can only be made between say 1s and approximately 10^5s (*i.e.*, ~ 1 day; $10^6\text{s} \sim 12$ days; $10^7\text{s} \sim 4$ months). The shorter time is limited by the inertia of the creep apparatus and the longer time by the patience of the observer and the ability of doing such a test in good and constant condition during a long time. The creep curve is often represented against the logarithm of time. Note that the logarithmic form of the plot changes the shape of the curve drastically by stretching out the short-time portion of the response and compressing the long-time region.

A theoretical creep curve based on the idea of simple rubber-glass transition is represented in Figure 0-9. Material is supposed to exhibit two limiting compliances. It strains initially to the glassy compliance, which represents its energetic elastic deformation. In time, the compliance rises to an equilibrium or rubbery compliance, corresponding to the entropic elasticity. The value along the abscissa labelled $\log \tau$ marks the inflection from rising to falling slope, and τ is called the characteristic time of the creep process.

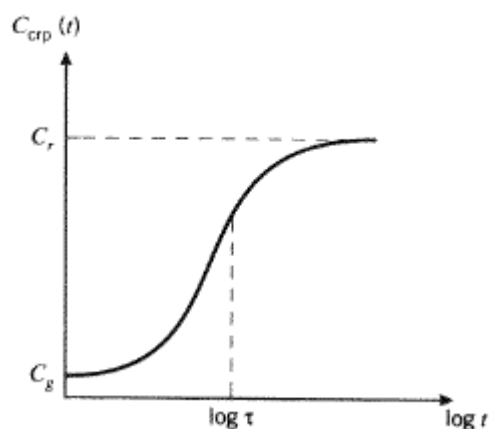


Figure 0-9: Theoretical creep curve representing two limiting compliances: C_g standing for the glassy compliance and C_r standing for the rubbery one.

Short-term and long-term creep curves in wood

A typical curve obtained during short-term creep tests performed on wood specimens is presented in Figure 0-10. Van der Put [cited by (Hunt 2004)] proposed to divide the creep into two processes based on the deformation kinetics. The primary part is completed within one or two days, while the secondary part follows a straight line on a plot of creep against the logarithm of time. A similar observation was done by Hunt (2004) as illustrated in Figure 0-10. Hunt has also examined in his paper experimental results obtained by Gressel originally published in 1984. Gressel has performed eight-year creep tests on beech, pine and spruce in a constant environment of 65% and 20°C. As we can observe from Figure 0-11, the creep curve plotted against the log of time follows essentially a straight line. No inflexion point or progressive slowdown of the creep process can be observed. Thus, it is not possible to confirm whether the secondary creep is likely to follow a straight line indefinitely, or whether the rate decreases eventually towards a viscoelastic creep limit. It is tempting to predict the long-term behaviour by extrapolating such creep curves. An example of a result obtained by Hunt based on one or two weeks tests into the eight years period is given in Figure 0-11. Hunt also found the estimated relative creep after 50years to be dependant on wood quality, quantified by specific modulus, and relative humidity.

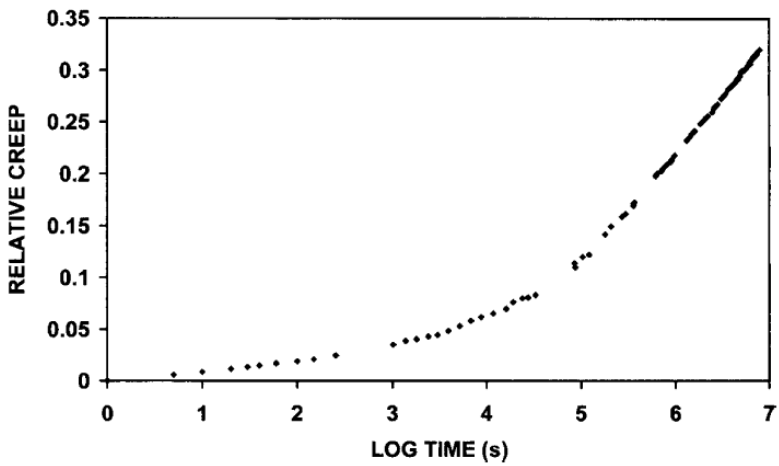


Figure 0-10: Creep data plotted as relative creep against log of time. From (Hunt 2004)

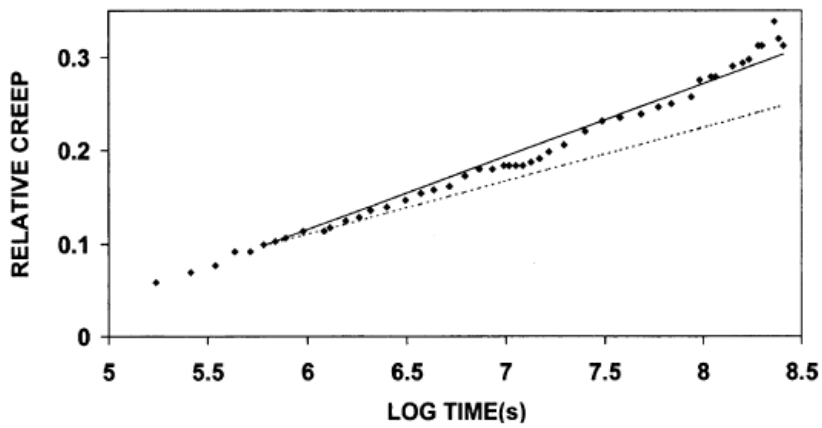


Figure 0-11: Gressel’s eight-year creep data for beech, compared with various method of prediction from short-term data: continuation of slope between 1-2 weeks is represented by the solid line and prediction based on the normalised logarithmic creep rate of the creep after 1 week by the dashed line. From (Hunt 2004).

Domain of linearity in wood

Linearity in this context means that doubling the stress will result in doubling the strain of studied material at any point in its history. In linear elastic material, it is the strain immediately after loading that is proportional to applied stress. In viscoelastic material, the linearity of the behaviour means that the strain at any given time after loading is proportional to the applied stress. Linearity is a condition required for the use of Boltzmann's superposition principle (see §3.4.a) so that it is essential to know the extent of domain of linearity in wood.

If the strain-stress relation is linear, the strain ε resulting from a stress $n\sigma$, where n is a constant, is just n times the strain resulting from single σ . Mathematically, it means that:

$$\varepsilon(n\sigma) = n\varepsilon(\sigma). \quad \text{Eq. 0-2}$$

For linear materials, the family of strain histories $\varepsilon(t)$ obtained at various constant stresses may be superimposed by normalizing them by the applied stress. The linearity property is illustrated in Figure 0-12.

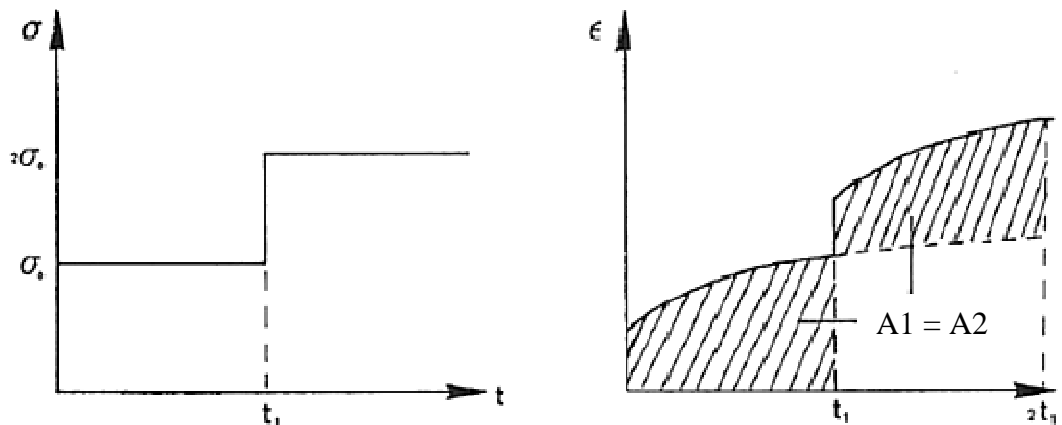


Figure 0-12: Representation of linear viscoelastic behaviour. Left: applied stress, right: resulting strain. From (Le Govic 1988).

A number of studies were interested in the domain of linearity in wood, mostly focused on the limit of linearity in bending and compression. The onset of non-linearity in bending was associated with the behaviour of the compression face of the test piece. The estimated value of the limit of linearity, in general expressed as percentage of ultimate stress, varies considerably from one author to another (Hunt 1988; Le Govic 1988; Navi and Heger 2005). It appears to depend on the type of loading, temperature and moisture content. However it is difficult to compare estimates between them because the ultimate stress can vary by a factor up to three according to the moisture content and type of loading. For this reason, strain might be a more suitable parameter as proposed by Hunt (1989). Hunt has also analysed the onset of non-linearity during mechano-sorptive creep of Baltic redwood (*Pinus Sylvestris*) specimens. His experiments showed that compression test pieces departed from linearity at a total strain around 1400 to 1500 $\mu\text{m}/\text{m}$ and bending test pieces at 1600 $\mu\text{m}/\text{m}$ while the tensile pieces were linear up to 1800 $\mu\text{m}/\text{m}$.

Effect of loading mode

Vittecoq [cited by Genevaux (1989)] has evidenced different behaviour of the stretched and compressed side of a synthetic composite (IM6-914) submitted to bending stress. Difference between Young's modulus measured on both sides was significant as

shown in Figure 0-13. Decrease in the compression modulus with increase of stress can be explained by microscopic buckling of fibres. Elastic bending strain is a superposition of the behaviour in compression and tension and so is for the delayed strain. This can result in repeated apparition of the same relaxation mechanism during the measurement of creep in bending if the latter one is dependent on the stress level. Interpretation of such a signal is not straightforward.

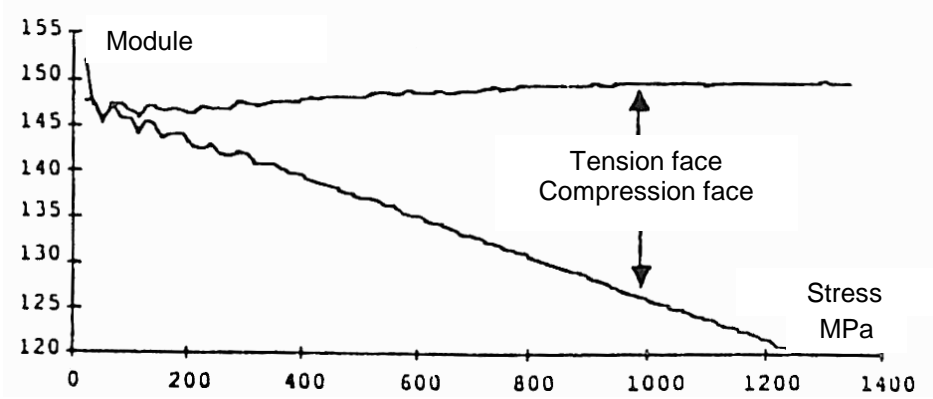
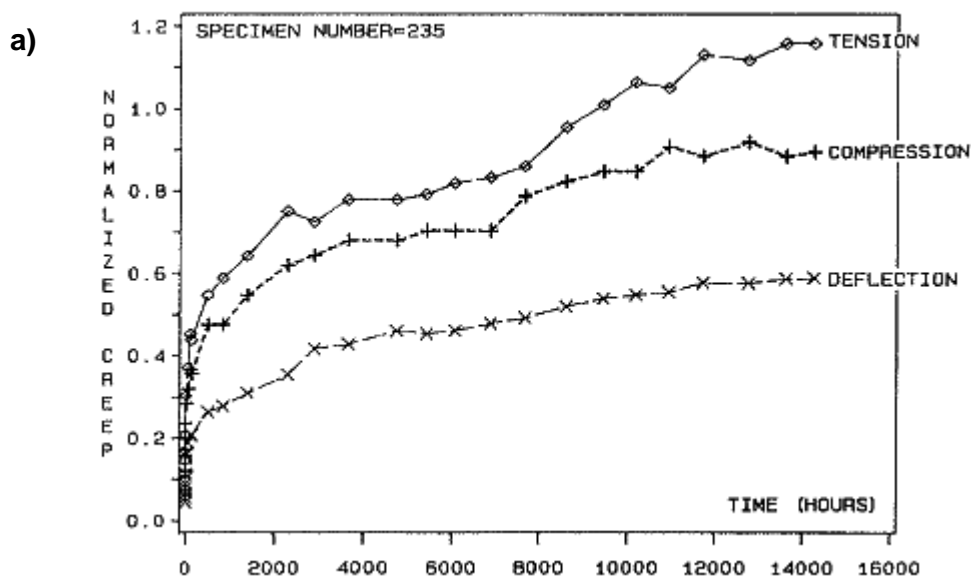


Figure 0-13: Compression and tension modulus of IM6-914 according to Vittecoq [cited in (Genevaux 1989)].

Considering the creep behaviour under different loading mode in wood, Hoffmeyer (1990) investigated the creep under compression, tension and bending for specimens with different moisture content. He reported higher relative creep under tensile and compression loading compared to bending one. According to Navi and Heger (2005), this may be due to the measurement of the strain. While bending creep is typically measured for the entire length (beam deflection), compressive and tensile creeps are measured more locally and are more sensitive to possible defect. At low moisture contents, the relative creep strain in compression and tension are of the same order of magnitude. Conversely, a large difference can be observed at higher moisture content as shown in Figure 0-14b where creep in compression is nearly two times higher than in tension. However, these conclusions have to be taken with precautions because the proportional limit might have been exceeded during these tests as high loads (70% of the instantaneous strength) were applied.



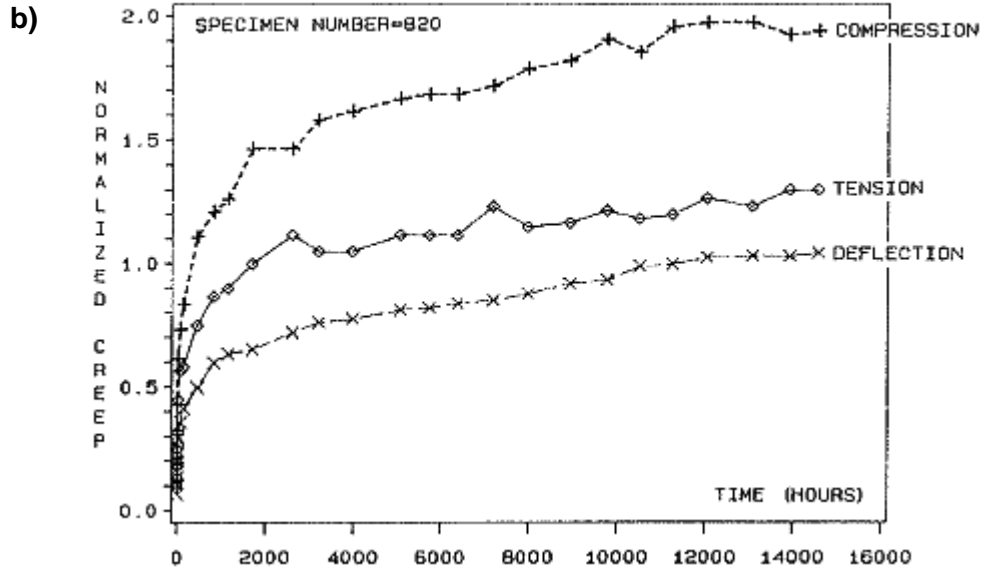


Figure 0-14: Relative creep strains in compression, tension and bending. Moisture content of specimens was of ~11% for the figure (a) and 20% for the figure (b). Borrowed from (Hoffmeyer 1990).

Permanent deformation

Very few references were found about the reversibility of strains developed during the creep tests under constant conditions. Hayashi *et al.* (1993) reported that the time-dependent strain induced by load level up to 58% of the ultimate strength, and applied during 4 to 10 days, is largely recoverable. On the other hand, some irrecoverable components of deformation appear to exist in compression wood resulting in earlier departure from linearity. The level of non-recovered strain seems to be higher after creep tests comparing to relaxation tests (Grossman and Kingston 1954).

3.4 Phenomenological framework

3.4.a Statement of the Boltzmann superposition principle

According to this principle, "if a series of stresses are applied to a material at different times, each contributes to the deformation as if it alone were acting". Mathematically, if the stress due to a strain $\epsilon_1(t)$ is $\sigma(\epsilon_1)$ and that due to a different strain $\epsilon_2(t)$ is $\sigma(\epsilon_2)$, then the stress due to both strains is $\sigma(\epsilon_1 + \epsilon_2) = \sigma(\epsilon_1) + \sigma(\epsilon_2)$. Combining this with the condition for multiplicative scaling used earlier (Eq. 0-2), we have as a general statement of linear viscoelasticity:

$$\sigma(n_1\epsilon_1 + n_2\epsilon_2) = n_1\sigma(\epsilon_1) + n_2\sigma(\epsilon_2). \quad \text{Eq. 0-3}$$

Validity of this hypothesis is required for the use of mechanical models described in the section 3.5.

3.4.b Effect of temperature

Under water saturated conditions, hemicelluloses are already softened at room temperature (Cousins 1978). Consequently, the properties of lignin exert a particularly great influence upon wood properties. Furuta *et al.* (1997) showed that the relaxation around -40 °C was associated with the micro-Brownian motion of hemicelluloses and that around 80 °C with that of lignin. This softening of lignin results in a major reduction in the elastic modulus of the wood, particularly in the direction across the fibres. Salmén (1984) has investigated the

glass transition of wet wood in both, the longitudinal and transverse directions on spruce. He reported a glass transition temperature of 72 °C at low frequencies. The softening along and across the fibre direction were of different amplitude but have shown to be due to the same phenomenon. Directional difference illustrated in Figure 0-15 is merely a reflection of the high degree of anisotropy of the microfibrils within the wood fibres. Similar results are reported also in his following paper (Salmén 1988).

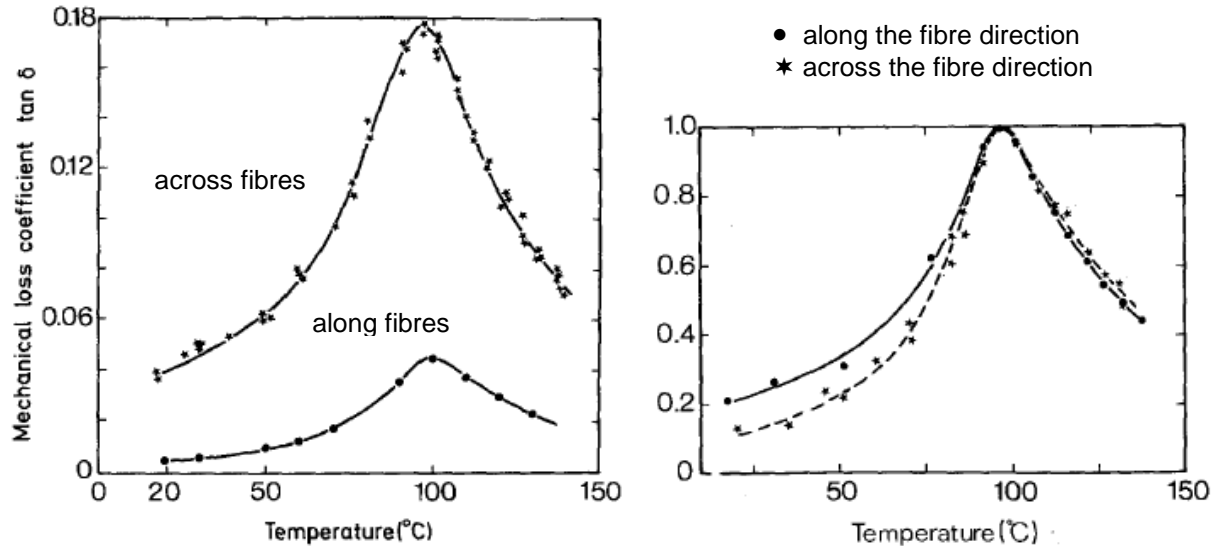


Figure 0-15: (a) Damping coefficient as function of temperature for water saturated wood samples at 10 Hz. (b) Relative damping coefficient. From (Salmén 1984).

Temperature of glassy transition is known to differ between softwoods and hardwoods as well as between species. Hamdan *et al.* (2000) have investigated the effect of temperature on wood constituents of several Japanese softwoods and hardwoods subjected to heat or steam treatment during large radial compression between 0 °C and 200 °C. Two well-defined softening regions were observed. Both groups showed the glass transition T_g of lignin at ~ 90 °C and ~ 60 °C for softwood and hardwood respectively and a second transition region at ~ 160 °C. The softening behaviour between the first and second transition in softwood contrasted with the softening behaviour of hardwood. This difference was ascribed to the difference in chemical structure of lignin between softwood and hardwood. The effect of lignin composition on the T_g of several temperate hardwood and softwood species were investigated in greater detail by Olsson and Salmén (1997). Increased content of methoxyl groups in the lignin was found to correlate with decreased softening temperature of wet wood. This indicates that methoxyl groups in lignin, as a side group occupying a bonding site and hindering the creation of covalent bonds, reduces the crosslink density in the lignin structure thus increasing its mobility.

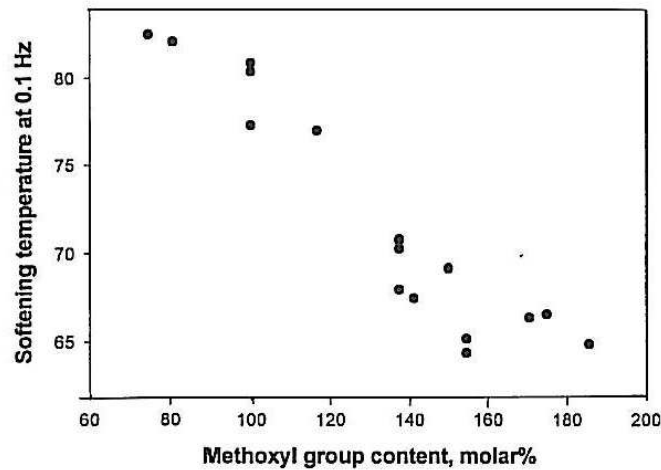


Figure 0-16: Softening temperature of wet wood at a stress frequency of 0.1 Hz against the methoxyl group content of the lignin. From (Olsson and Salmén 1997).

Bardet *et al.* (2003) studied the influence of temperature on transverse mechanical properties of 10 tropical species in the green condition, two of them being also used in the present study (*D. guaianensis* and *V. surinamensis* that is of same genus as *V. michelii*). They reported a transition temperature attributed to the softening of lignin between 51 and 69 °C, depending on the species. Detailed analysis of the apparent modulus in radial compression suggested that complex relaxation phenomena occur around 10 °C.

Time-temperature equivalency

Leaderman 1943 [cited by (McCrum 1967)] was the first to recognize the consequences of the similarity between creep curves measured at closely separated temperatures. It was found that this striking similarity between viscoelastic parameters when measured at closely spaced temperatures is a common occurrence and is not confined to a few relaxations. The procedure of superposing curves at different times and temperatures has come to be known as time-temperature superposition and the obtained curve as a master curve. The principle of the superposition is illustrated in Figure 0-17. Colder temperatures are expected to correspond to shorter times and warmer temperatures to longer times.

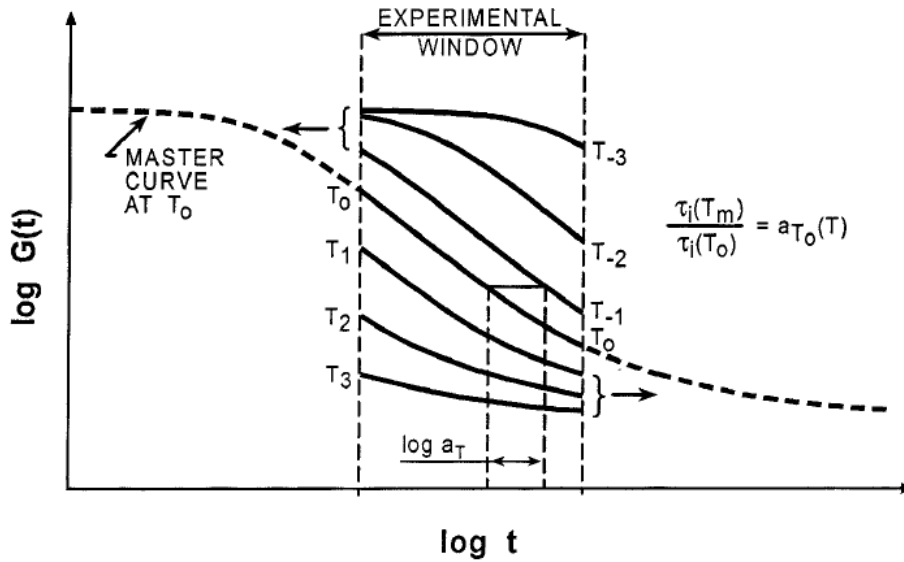


Figure 0-17: Principle of the time-temperature equivalency as pictured by Tschoegl (1997). T stands for temperature, $\log a_T$ for shifts along the $\log t$ axis, τ for the characteristic time.

The time-temperature equivalency assumption is very useful to extend the experimental window and predict long-term behaviour based on short-term tests. The assumption required for the validity of this principle is that all retardation times in the distribution are displaced along the $\ln \tau$ axis by $\ln a_T$ when the temperature is changed from T_0 to T as shown in Figure 0-18. This can be mathematically expressed as:

$$\phi_J^T(\ln \tau) = \phi_J^{T_0}(\ln \tau/a_T), \tag{Eq. 0-4}$$

where $\phi_J^T(\ln \tau)$ is the distribution of retardation times.

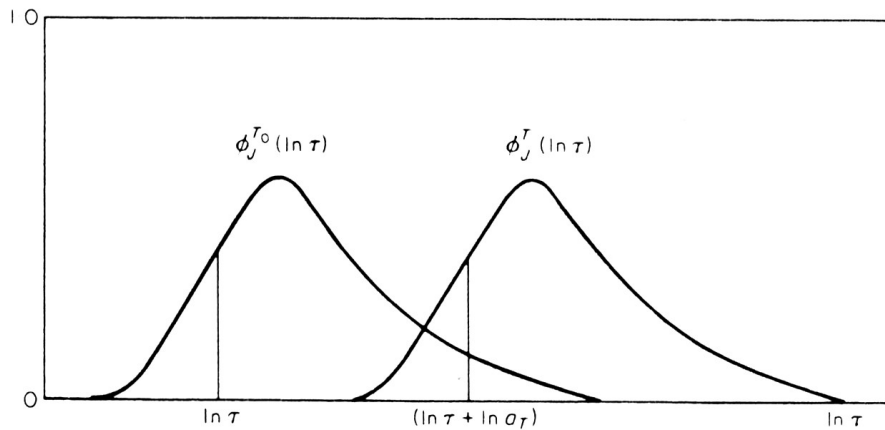


Figure 0-18: Graphical representation of the hypothesis that the retardation spectra at T and T_0 are displaced by $\ln a_T$ but are identical in shape (Alfrey 1948).

Polymers obeying to this law are considered as thermo-rheologically simple materials. It is found that for the great majority of relaxations $\ln a_T$ is a simple function of temperature being given by the Arrhenius equation:

$$\ln a_T = \frac{W}{R} \left(\frac{1}{T} - \frac{1}{T_0} \right) \tag{Eq. 0-5}$$

or the equation of Williams, Landel and Ferry called WLF (Ferry 1980):

$$\ln a_T = -\frac{C_1(T - T_0)}{C_2 + (T - T_0)} \quad \text{Eq. 0-6}$$

where W is the activation energy, R the gas constant and C_1 and C_2 constants. WLF is nearly always applicable to the glass-rubber relaxation. The Arrhenius law is usually applicable to secondary relaxation in amorphous and crystalline polymers.

WLF and Arrhenius equations account for the effect of temperature on the kinetics of the relaxation. It is sometimes necessary to account for the temperature induced changes in limiting moduli as stated by McCrum and Morris (1964). The implications of this correction are described graphically in Figure 0-19.

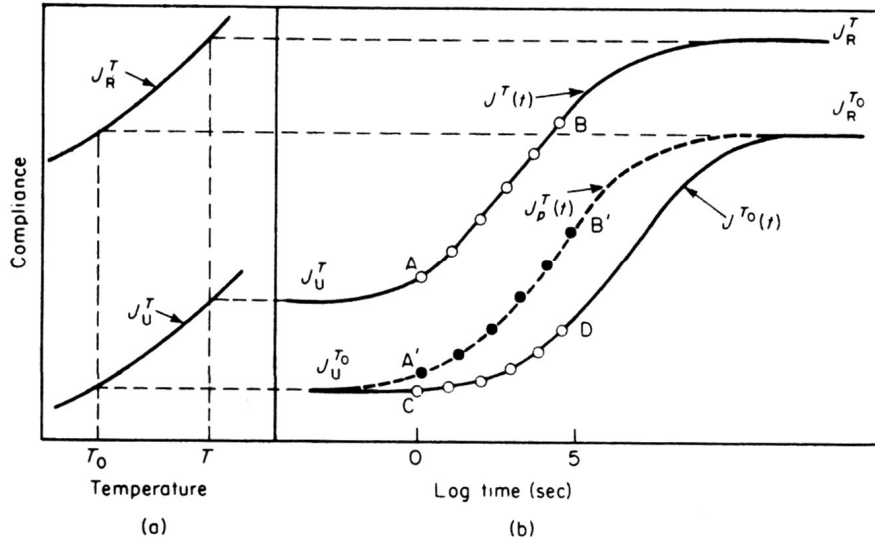


Figure 0-19: Idealized diagram showing effect of the temperature dependencies of limiting compliances denoted here as J_U and J_R on the creep compliance. (a) Plot of J_U and J_R against temperature. (b) Dependence of J^T and J^{T_0} on log time. AB and CD represent the measurable portions of the curve (i.e. for times between ca. 1 and 10^5 s). A'B' represents AB after reduction.

The curves J^{T_0} and J^T for temperatures T_0 and T are plotted by full lines. J^T can not be superposed by a horizontal shift on J^{T_0} if the limiting compliances, labelled in the Figure 0-19 as J_U and J_R , are affected by temperature. To enable the superposition, a multiplicative factor has to account for this temperature effect on the limiting compliance. In particular in regions where the viscoelastic function is flat, the need of this factor is more important to obtain satisfactory matching of creep curves (Ferry 1980). In the case of wood, the applicability of such a correction is not straightforward because of its complex structure (Salmén 1984).

Validity of the time-temperature equivalency in wood

Salmén (1984) reported the applicability of the time-temperature equivalency in wood for temperatures above the glass transition of lignin. This author has also confirmed the validity of the Arrhenius law. Many other authors predicted the long-term behaviour of wood in the hygroscopic region based on this concept (Le Govic *et al.* 1987; Genevaux 1989). However, these considerations relied mostly on visual assessment of the smoothness of the master curve. While investigating the experimental data in the complex plane, Bardet (2001) reported on some discrepancy of the time-temperature equivalency as described by the Arrhenius law. On the other hand, the time-temperature equivalency assumption held the examination in the complex plane in the case the torsion behaviour of green poplar (Vincent 2006). Finally, Placet *et al.* (2007) found that time-temperature equivalency could not be applied to the whole viscoelastic range but seems to be valid within each transition state.

Physical aging

The phenomenon of physical aging is very common and is encountered in thermoplastic mouldings that have been cooled rapidly from an elevated temperature during the shaping operation. In the case of amorphous polymers, the material is still cooling rapidly when the temperature drops below the glass transition temperature T_g . Once below T_g the rate of molecular relaxation is too slow to keep pace with the changes required if the material is to remain at thermodynamic equilibrium. As a result, when the material reaches the thermal equilibrium with the surroundings it is not at thermodynamic equilibrium. Consequently, it will undergo volumetric relaxation, gradually increasing density during an extended aging period. The rate of densification will depend on the aging temperature T_a and the difference between T_a and T_g . Aging may be quite rapid at first if T_a is not too far below T_g but the approach to equilibrium will slow down and aging effects may sometimes still be apparent after many years. If T_g is far below T_g the thermodynamic driving force will be large because the property (e.g. density) will be far from the thermodynamic equilibrium value and will favour change but kinetics are determined by the difference between T_a and T_g , and this will limit the rate of change (White 2006).

Aging of amorphous material was studied extensively by Struik and his book (Struik 1978), published more than a quarter of century ago remains the principle reference on physical aging of polymers. He proposed an experimental protocol to investigate the effect of aging time on small-strain creep properties by performing a set of short time creep tests at different aging times. Short time test means that the testing time must be much shorter than the age of the specimen at the onset of the test. This is called the snapshot assumption because a test performed during such a short time ($t_c = t_a/3$ or even better $t_c = t_a/10$) will exhibit negligible effects of aging. He presumes that individual creep curves can be horizontally shifted to form a master curve and the superimposability of the curves proves that aging does not influence the shape of the creep curve. Struik explained this by the fact that an increase in aging time changes all relaxation times by exactly the same factor and suggests the use of time-aging time superposition principle. Similarly to the time-temperature equivalency principle, this one can be written as follows:

$$\mu = -d(\log \tau)/d(\log t_a) = -d(\log a_{ta})/d(\log t_a), \quad (\text{Eq. 0-7})$$

where μ is the aging shift rate where parameter a_{ta} represents the horizontal shift used in Struik's procedure to form a master curve from creep curves measured at different aging times.

McCrum (1992) claims that there is a paradox between this interpretation and received knowledge in the fields on DMTA (dynamic mechanical thermal analysis) and DETA (dielectric thermal analysis). According to McCrum the existence of large shifts of retardation time (several decades) produced isothermally by aging is not in accord with DMTA or DETA spectroscopy measurements. Thus, he suggests the interpretation of physical aging in creep from sequential aging theory. In a sequential aging mechanism, only viscoelastic elements with retardation times of the order of the aging time are transforming. Elements with retardation time shorter than t_a are already at their equilibrium positions and long retardation time have not yet begun their move to equilibrium. That is to say, the elements age in sequence and the shift factors depends on t_a and also on the retardation time.

Physical aging has been already observed in wood. A number of arguments for its occurrence were given for wood in the hygroscopic range (Hunt and Gril 1996). The effects of a quench (rapid cooling) on wet wood properties was studied by Nakano (2005) who reported a temporary change in viscoelastic properties with a new equilibrium state definitely reached at the end of 10 hours. Free volume creation has been ascribed to the freezing of molecular chains of wood components, most likely lignin, during the quench. On the other

hand, Ishimaru (2003) has investigated the effect of quenching rate on wood creep properties and observed that the effect of cooling had not completely disappeared after 40 days. However, Ishimaru did not examine the aging phenomenon in more detail.

3.5 Mechanical models

3.5.a Spring-dashpot models with single relaxation time

The time dependence of viscoelastic response is analogous to the time dependence of reactive electrical circuits, and both can be described by mechanical models using springs and dashpots. Such models are able to reproduce the instantaneous and delayed strain or stress as well as time-temperature equivalency. These mechanical analogies use Hookean springs, depicted in Figure 0-20 and described by:

$$\rho = k\varepsilon = E\varepsilon \quad \text{Eq. 0-8}$$

where ρ and ε are analogous to the spring force and displacement, and the spring constant k is analogous to the Young's modulus E . The spring models the instantaneous bond deformation of the material, and its magnitude will be related to the fraction of mechanical energy stored reversibly as strain energy.

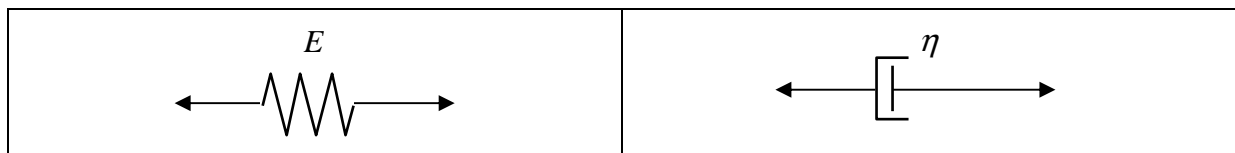


Figure 0-20: Hookean spring (left) and Newtonian dashpot (right).

The entropic uncoiling process is fluid like in nature, and can be modelled by a Newtonian dashpot also shown in Figure 0-20, in which the stress is proportional to a strain rate:

$$\rho = \eta \dot{\varepsilon}, \quad \text{Eq. 0-9}$$

where the over dot denotes time differentiation and η is a viscosity. In many of the relations to follow, it will be convenient to employ the ratio of viscosity to stiffness:

$$\tau = \frac{\eta}{E}. \quad \text{Eq. 0-10}$$

The unit of τ is time, and it will be seen that this ratio is a useful measure of the response time of the material's viscoelastic response.

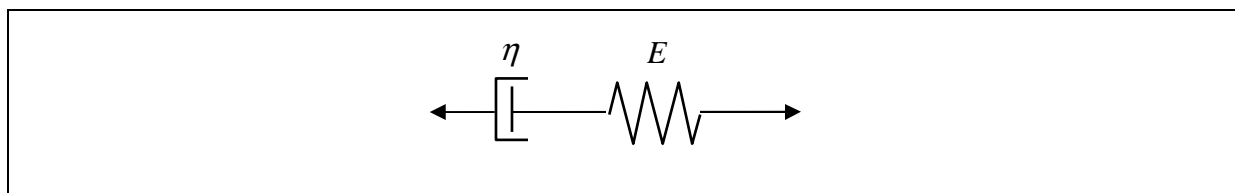


Figure 0-21: The Maxwell model.

The viscoelastic behaviour of polymers can be often described by a combination of springs and a dashpot such as the Maxwell or Zener model. The Maxwell solid, shown in Figure 0-21, is a mechanical model in which a Hookean spring and a Newtonian dashpot are connected in series. The spring should be visualized as representing the elastic or energetic component of the response, while the dashpot represents the conformational or entropic component. In a series connection such as the Maxwell model, the stress on each element is the same and equal to the imposed stress, while the total strain is the sum of the strain in each element. The delayed compliance of such a model is described by:

$$J(t) = J_0 \left(1 + \frac{t}{\tau} \right), \quad \text{Eq. 0-11}$$

where J_0 is the instantaneous compliance and τ the doubling time.

The Maxwell model is valid for a very limited set of materials. For more typical polymers whose conformational change is eventually limited by the network of entanglements or other types of junction points, more elaborate spring-dashpot models can be used effectively. Placing a spring in parallel with the dashpot gives a very useful model known as the Zener model or standard anelastic solid shown in Figure 0-22. The body formed by a spring and dashpot in parallel is called Kelvin body.

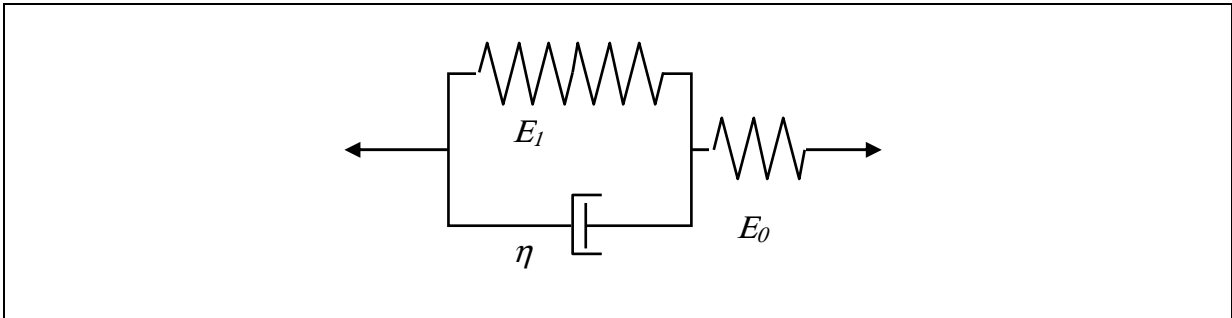


Figure 0-22: The Zener model.

The spring placed in parallel to the dashpot leads to a limited creep. Constitutive law of such a model yields:

$$J(t) = J_0 + J_1 \left(1 - e^{-\frac{t}{\tau}} \right), \quad \text{Eq. 0-12}$$

where τ is the characteristic time.

3.5.b Models with distribution of retardation times

Generalised Kelvin model

A real polymer does not relax with a single relaxation time as predicted by the previous models. Molecular segments of various lengths contribute to the relaxation, with the simpler and shorter segments relaxing much more quickly than the long ones. This leads to a distribution of relaxation times, which in turn produces a relaxation spread over a much longer time than can be modelled accurately with a single relaxation time. To introduce the notion of the distribution of relaxation respectively retardation times, generalised models are used, having as many elementary models in series or parallel as are needed to approximate the distribution satisfactorily.

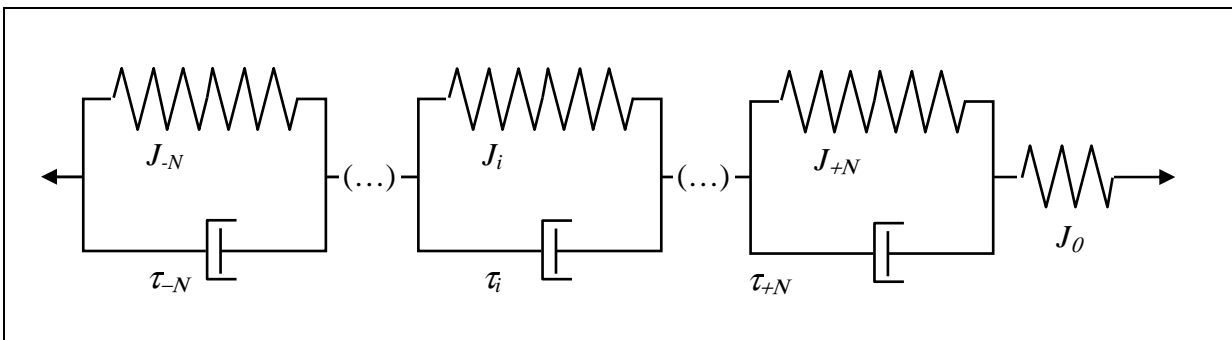


Figure 0-23: Generalised Kelvin model.

The constitutive law of generalised Kelvin model can be written as follows:

$$J(t) = J_0 + \sum_{-N}^N J_i (1 - e^{-\frac{t}{\tau_i}}). \quad \text{Eq. 0-13}$$

This type of model consisting of four Kelvin elements in series was used by Genevaux and Guitard (1988) to describe the creep behaviour of air dry poplar in L, T and R directions observed during creep tests at continuously increasing temperature. Later, it was applied on the green wood behaviour of oak and spruce in T direction (Perré and Aguiar 1999).

Parabolic models

In parabolic models, Newtonian dashpot is replaced by a parabolic one and the kernel t/τ becomes $(t/\tau)^k$. Constitutive law of a Maxwell model containing a parabolic dashpot yields therefore a power law:

$$J(t) = J_0 \left(1 + \left(\frac{t}{\tau} \right)^k \right); \quad \text{Eq. 0-14}$$

where k is the power parameter or also the kinetic parameter whose value can range from 0 to 1. For $k = 1$, we obtain a simple Maxwell model. Small values of k correspond to a broad viscoelastic spectrum. In polymers, values of k around 0.3 are commonly encountered (Tomlins 1996). The applicability of parabolic models to wood was suggested by Huet (1988) and used by his co-workers in CTBA² (Le Govic *et al.* 1988). Its validity was also verified for air-dry wood creep in longitudinal direction (Gril *et al.* 2004). Further, the parabolic model was applied to the green wood relaxation transversally to the fibres (Bardet and Gril 2002) and torsion behaviour of green poplar specimens (Vincent *et al.* 2006). The value of k was in the range 0.1 ~ 0.5 in these cases.

Equivalent creep spectrum

However, parabolic models are more difficult to handle than conventional rheological models. It has been shown (Bardet and Gril 2002; Gril and Hunt 2002) that viscoelastic spectrum corresponding to a parabolic model can be approximated by a generalised Gaussian law. Actually, it is practically equivalent to having a series of Kelvin elements (1...N) with characteristic times τ_i uniformly distributed in a logarithmic scale, and corresponding compliance J_i following:

$$J_k = J_1 \frac{e^{-\frac{1}{2} \left| \frac{\ln \tau_k - \ln \tau_1}{d} \right|^g}}{\sum_{k=-N}^{k=+N} 2^{-\left| \frac{\ln \tau_k - \ln \tau_1}{d} \right|^g}}, \quad \text{Eq. 0-15}$$

where J_1 stands for the sum of J_k , d is the spectrum width relative to the $\ln(t)$, g a parameter that allows us to adjust the spectrum sharpness and τ_1 is the central value. Values of d and g can be calculated for any values of the kinetic parameter k of the parabolic model. The correspondence between generalised Kelvin model and a parabolic Zener model when represented in the complex plane is illustrated in Figure 0-25. Details about the representation of viscoelastic results in the complex plane are given in the 3.5.d.

² Centre Technique du Bois et de l'Ameublement (French Technical Centre for Wood and Furniture)

3.5.c Multi-transition models

Due to its complex polymeric structure, wood does not exhibit thermo-rheologically simple behaviour. Different experimental results (Poliszko 1984; Salmén 1984; Genevaux and Guitard 1988) demonstrated that thermo-viscoelasticity of wood may involve several second order transitions.

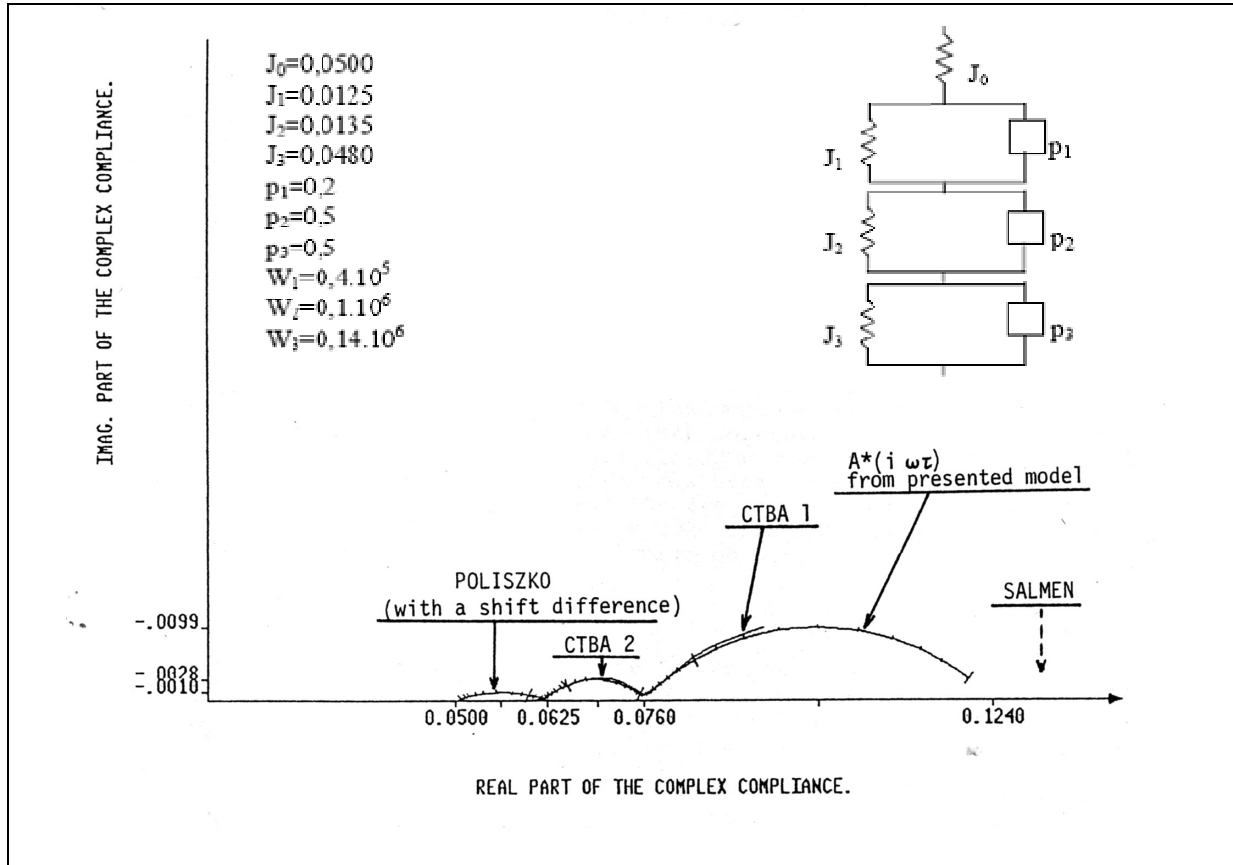


Figure 0-24: Graphical adjustment of the numerical results of the multi-parabolic multi-transition model on the experimental creep results obtained in CTBA and results of dynamic tests at low temperature (Poliszko 1984) and high temperature (Salmén 1984). J stands for the compliance, W for the activation energy and p for the kinetic parameter. From (Huet and Navi 1990).

The existence of more than one relaxation process requires the use of a multi-parabolic model made of several of the generalised Kelvin models in series. Navi and Huet (1990) have shown that a series of four links consisting of parabolic Kelvin elements, one of them being reduced to a spring, represent correctly the actual behaviour of wood over a large experimental window. Their multi-parabolic multi-transition model accounted for experimental results apparently in contradiction to each others. The method proposed relies on the use of complex plots representing the components of complex modulus or, in the case of creep data, an approximation of the complex modulus derived from phase diagrams.

3.5.d Representation in complex plane

Information about the compliance or modulus functions of viscoelastic materials are often obtained through dynamic measurements in the sinusoidal regime. These are most conveniently expressed by the complex compliance J^* :

$$J^*(i\omega, T) = J'(i\omega, T) + iJ''(i\omega, T),$$

where the real J' and imaginary J'' parts are positive functions of the circular frequency ω and of the temperature T . When the frequency-temperature equivalency

(analogous to the time-temperature equivalency) holds, the set of two variables (ω, T) reduces to one variable $\omega\tau$ where $\tau(T)$ is the only parameter affected by temperature. In that case, the complex compliance of the mono-transition power law, corresponding to a parabolic Maxwell model, reads:

$$J^*(i\omega, T) = J_0 \left[1 + (i\omega\tau)^{-k} \right],$$

where J_0 is the initial compliance. When the imaginary part is plotted against the real part in the so called complex plane, the complex compliance is represented by a straight line making an angle $k\pi/2$ with the real axis, which is intersected in J_0 . Complex compliance of the parabolic Kelvin model appears in form of an arc of circle. Thus, for the purpose of model identification, the representation of experimental data in a complex plane is very useful.

For representing results of static tests in the complex plane, an approximation of the storage J' and loss compliances J'' has to be used. Accordingly to Alfrey (1948) we can write:

$$J' \approx J(\log t); \tag{Eq. 0-16}$$

$$J'' \approx \frac{\pi}{2} \cdot \frac{1}{\ln(10)} \frac{dJ(\log t)}{d \log t}; \tag{Eq. 0-17}$$

where t is the creep time. Alfrey's approximation is valid for small J''/J' ratios and broad viscoelastic spectra, which is usually the case in wood and can be verified *a posteriori* in the complex plots.

If the time-temperature equivalency holds, individual creep curves are superposed into one continuous curve in the ACP, as this would ensure that not only the values of the $J(\log t)$ functions match, but also the slope. If other parameters than the characteristic or doubling time are affected by the temperature, we can observe discontinuities between individual creep curves. Thus, ACP does not allow only identification of the mathematical form of the constitutive law without any preconceived idea about the underlying physical phenomenon but it also allows verification of the validity of time-temperature equivalency assumption.

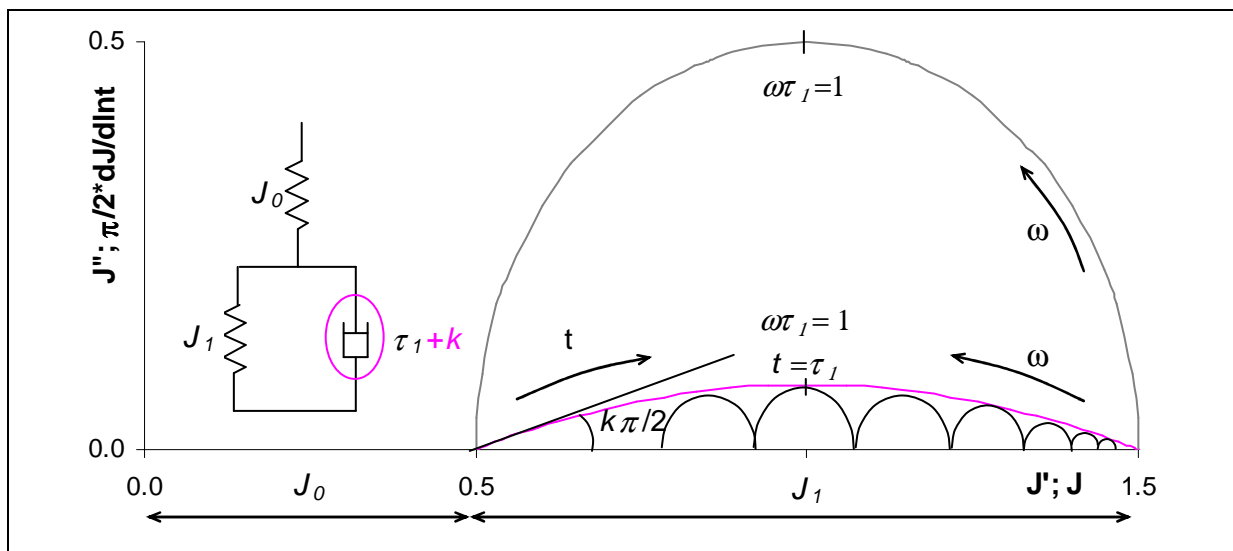


Figure 0-25: Representation of the Zener models containing Newtonian (half circle) or parabolic (arc of circle) dashpot in the complex plane. Approximation of the parabolic model by a series of Kelvin models is also displayed. Axes account for both, representation of dynamic and static data.

4) Structure/property relations

4.1 Density and MFA

MFA shows variable relationship with wood density. In some cases MFA and wood density are correlated, while in other cases they are not as we can observe in Figure 0-26 from (Yang and Evans 2003). Some studies compared MFA with cell wall thickness that is the main determinant of density. Observed relationships, if significant, were attributed to decrease of S2 layer and so larger effect of other layers on the mean MFA or were correlated to the amount of latewood in the ring decreasing the MFA. Thus, it seems likely that any relationship between these properties is entirely coincidental (Donaldson 2008).

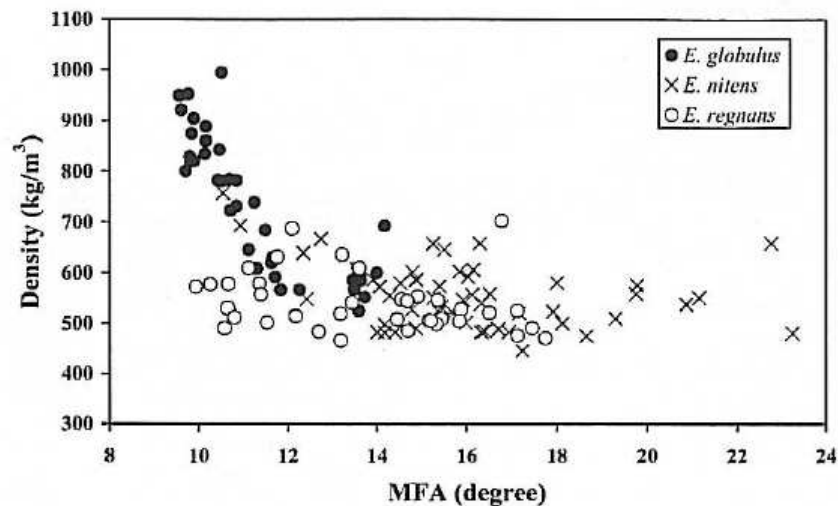


Figure 0-26: Relation between MFA and density for plantation-grown *E. globulus*, *E. nitens* and *E. regnans* between 15 and 33 years of age. From (Yang and Evans 2003).

4.2 Density and MFA as a predictor of longitudinal wood stiffness

Longitudinal stiffness of the cell wall is known to be strongly related to MFA. Numerous models predicting the cell wall stiffness from the properties of cell wall constituents and MFA were proposed and successfully used to describe experimental data (Persson 2000; Salmén 2004). An example of the prediction obtained by Salmén is shown in Figure 0-27. Different physical assumptions used for modelling the cell wall properties based on MFA were reviewed by Xu and Liu (2004).

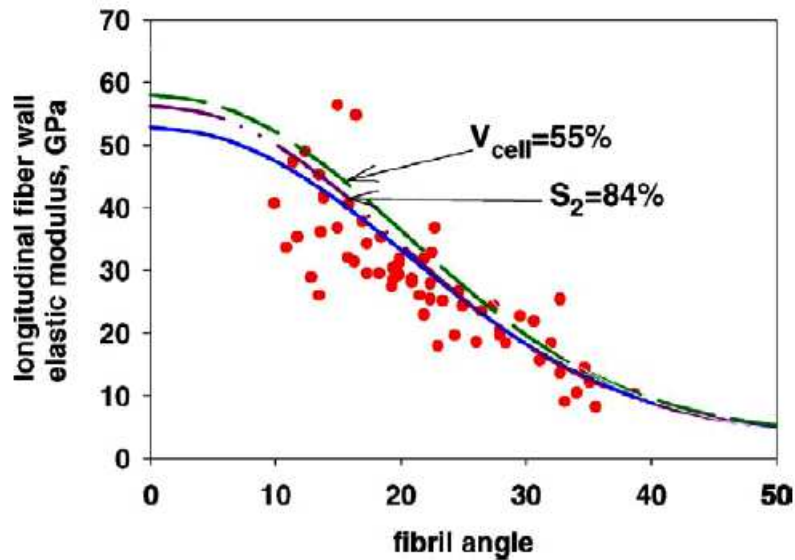


Figure 0-27: The elastic modulus of the fibre wall of wood in the longitudinal direction as a function of fibril angle in the S2-wall as affected by different factors; cellulose content in the S2-wall and proportion of S2-wall compared to measurements by Cave (1969). Reference values: cellulose content in S2-wall 50%, proportion of S2-wall 79%. From (Salmén 2004).

The longitudinal stiffness of the cell wall determined by MFA is in turn related to the longitudinal Young's modulus of a piece of wood by the amount of cell wall per unit volume, usually measured as basic density. This is a direct consequence of the arrangement of wood elements exhibiting honeycomb structure. Considering wood as a cellular solid, we can write according to Gibson and Ashby (1997):

$$\frac{E}{\rho} = \frac{E_{cw}}{\rho_{cw}}; \quad (\text{Eq. 0-18})$$

where ρ is the density and E the Young's modulus of wood and index cw denotes the cell wall properties. The density of the cell wall is very similar for all species, varying from 1.497 to 1.517 for hardwoods (Kellogg and Wangaard 1969). Based on this relation, we can easily predict the Young's modulus of wood from the cell wall modulus and density. This approach is justified for the longitudinal direction. In transverse directions, it is not straightforward to apply because if a piece of wood is submitted to transverse tensile stress, locally the cell walls are submitted to bending and in addition to tensile stress.

Many monospecific studies investigating the relation between MFA, basic density and longitudinal Young's modulus were carried out on commercial species such as *Pinus* or *Eucalyptus* (Butterfield 1998; Yang and Evans 2003). While the Young's modulus-density relationship can be easily verified on a large sample containing different species as shown in Figure 0-28, no verification was found in the literature for the interspecific validity of MFA – specific modulus relationship.

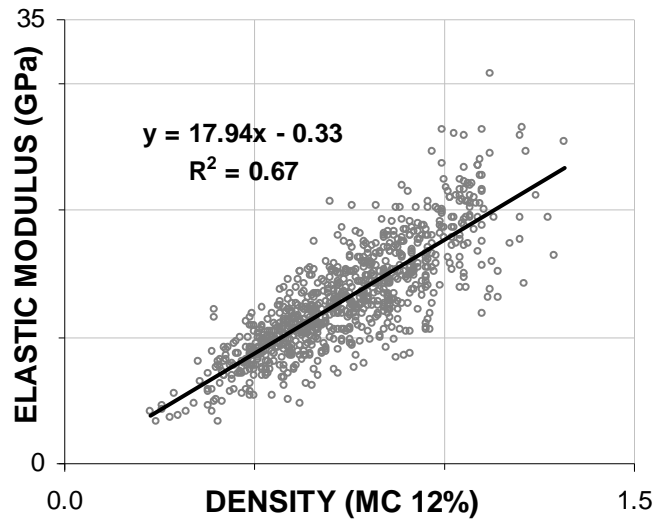


Figure 0-28: Relation between density and elastic modulus on data issued from CIRAD database. Each point represents a mean value by species; altogether ~1000 species are represented.

4.3 Determinants of vibration properties

In the previous section we have seen that the specific modulus was strongly related to MFA. Damping coefficient is known to be well correlated to specific modulus. This relation was established empirically by Ono and Norimoto (1984) on a large sample of hardwoods and softwoods. Regression between both parameters was described by a power law and often presented in double logarithmic scale as shown in Figure 0-29 a. Very strong correlation was also observed between damping coefficient and MFA on hinoki wood by Norimoto *et al.* (1986). They have also proposed a cell wall model that showed a very good agreement with experimental data as shown in Figure 0-29 b.

However, non standard behaviour was observed for some species commonly used for manufacture of musical instruments and was ascribed to the extractive content. Effect of extractives was studied by many authors (Yano 1994; Yano *et al.* 1995; Matsunaga *et al.* 1999; Brémaud *et al.* 2004; Brémaud *et al.* 2004) that have reported considerably lower damping compared to the model established by Ono and Norimoto. The opposite effect, i.e. increase of damping along with increase of specific modulus due to extractives was reported in sugar cane (Obataya *et al.* 1999).

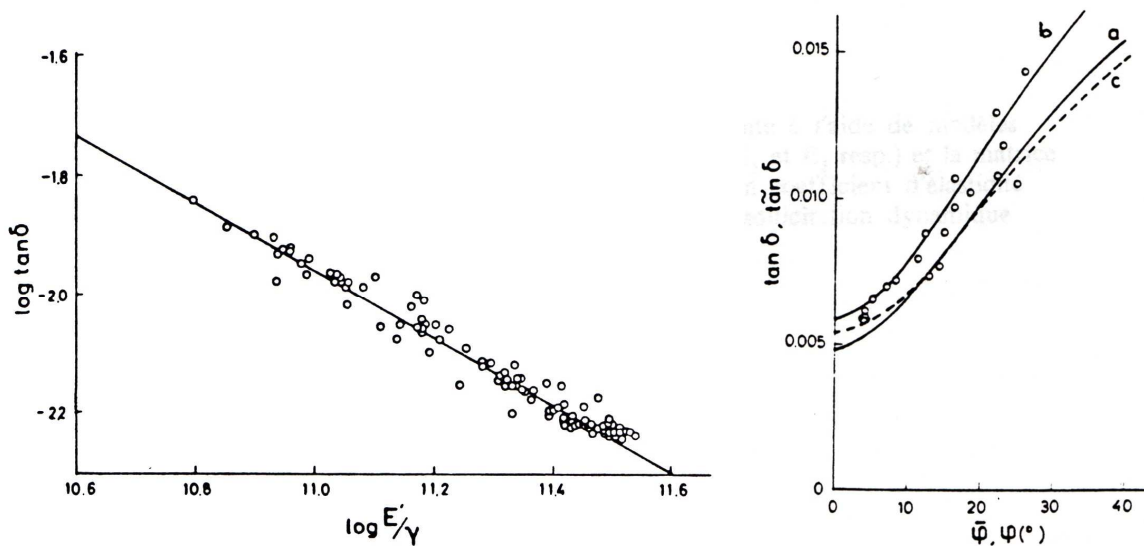


Figure 0-29: (a) Relation between damping coefficient and specific modulus in double logarithmic scale. (b) Relation between damping coefficient and MFA.

Brémaud (2006) has also studied the vibration properties of several softwoods including their compression wood. The relationship between specific modulus, damping and MFA of opposite, intermediate and compression wood is shown in Figure 0-30. The term intermediate was used to denote the wood coming from angular position shifted by 90° relative to compression wood side. We can observe a strong correlation of both mechanical parameters on MFA.

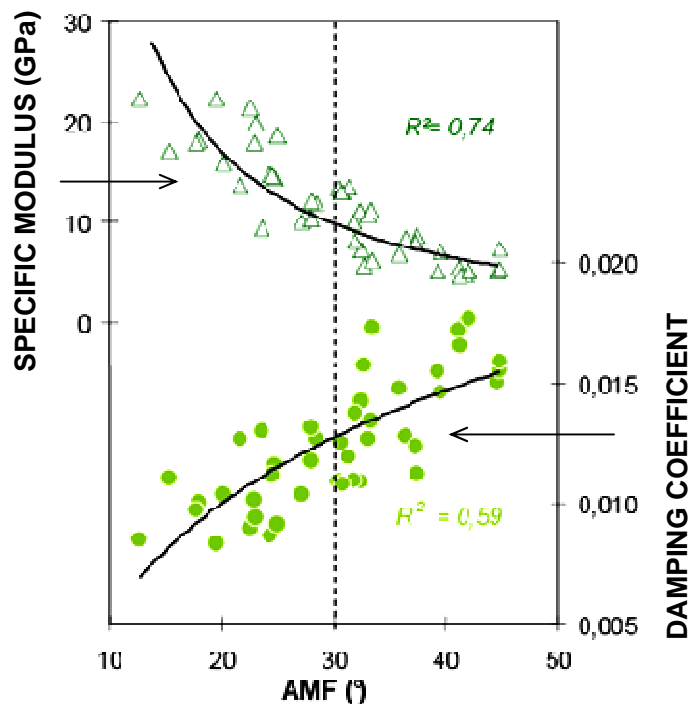


Figure 0-30: Relation between specific modulus, damping coefficient and microfibril angle on a selection of three softwoods including compression wood. From (Brémaud 2006).

A deeper analysis has shown that compression wood has a lower specific modulus and a higher damping coefficient than corresponding normal wood. However, compression wood exhibited a lower damping coefficient than predicted by the Ono and Norimoto model. Compression wood is known for its high lignin content and low cellulose content, so that one

may expect rather high damping coefficient. Relation between damping and specific modulus for each wood type along with the empiric regression by Ono and Norimoto is represented in Figure 0-30. It was suggested that specific modulus may be underestimated because of different percentage of main wood components (more lignin which is lighter than cellulose). But this effect is not sufficient to explain the observed differences.

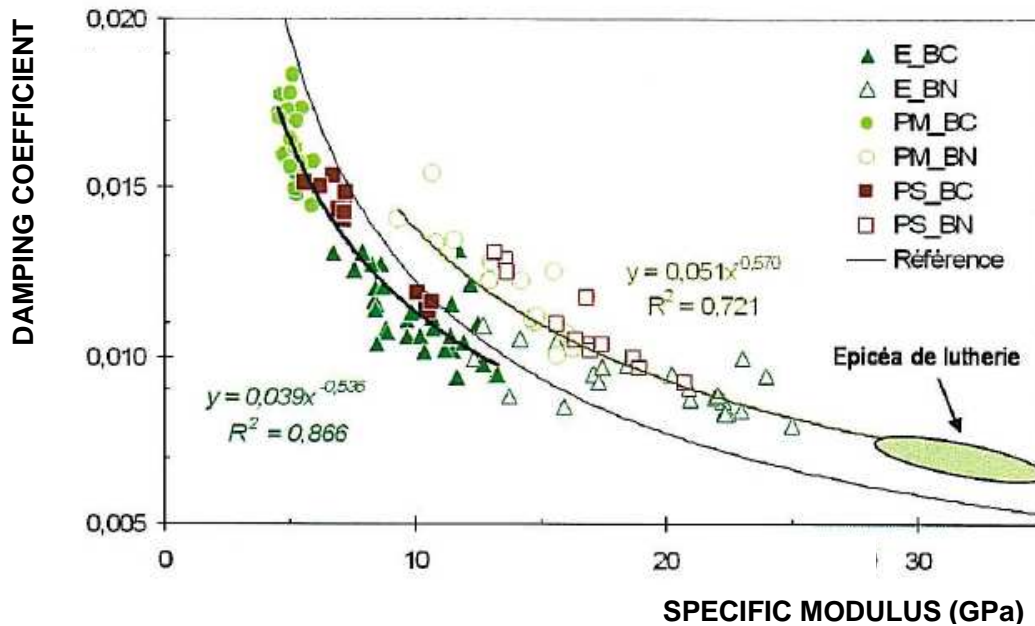


Figure 0-31: Relation between damping coefficient and specific modulus for compression wood (BC), intermediate wood (between BC and BN) and normal wood (BN); E: *Picea abies*; PM: *Pinus pinaster*; PS: *Pinus sylvestris*. From (Brémaud 2006)

4.4 Determinants of creep properties

4.4.a MFA

Several authors reported the dependency of creep response on MFA. El-Osta and Wellwood (1972) investigated the relationship between short-term creep response and MFA of three softwoods. They found a positive linear relationship between MFA and total creep as displayed in Figure 0-32. We can however notice that douglas fir compression wood exhibits considerably higher creep than normal wood. Significant differences were also observed between species. Interpretation of these results is a little bit misled by the use of mean values of MFA for several specimens. However even if only mean valued of total creep are considered, both parameters are still significantly related (Figure 0-32b). On the same sample, El-Osta and Wellwood have also reported a significant negative correlation between the relative cell-wall crystallinity and the amount of short-term creep (El-Osta and Wellwood 1972).

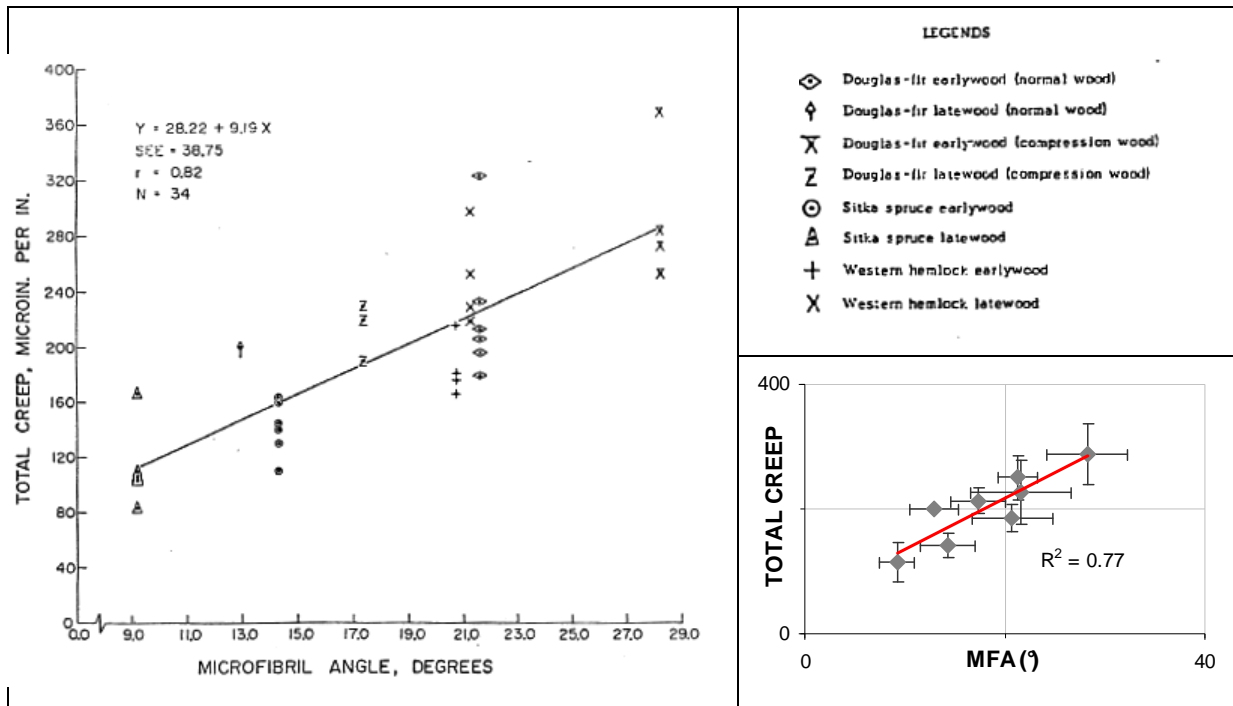


Figure 0-32: (a) Relationship between total creep and microfibril angle as measured by (El-Osta and Wellwood 1972) at 0.03% strain level. (b) Same data when only mean values of total creep by species are considered.

Kojima and Yamamoto (2004) have carried out tensile creep tests on sugi specimens in the green state. Further, observed behaviour was described by a Zener model whose parameters were found to be related to the MFA. However, we consider these results difficult to interpret. To begin, the same load corresponding to the proportional limit of normal wood was applied for all specimens; however, sample contained juvenile wood and these were therefore probably tested beyond their proportional limit. Further, the obtained relationships are not so straightforward to interpret because of uneven repartition of specimens with different MFA. An example of the viscosity parameter of the dashpot plotted against MFA is given in Figure 0-33.

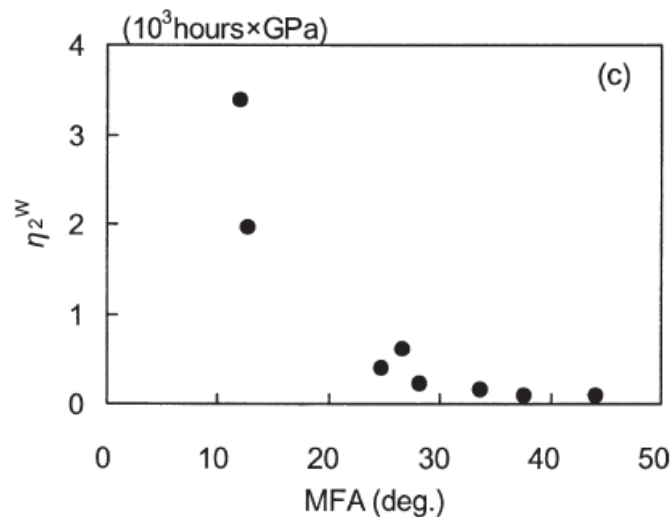


Figure 0-33: Dependency between the adjusted viscosity parameter of Zener model and MFA. From (Kojima and Yamamoto 2004)

Results to the contrary were reported by Gril *et al.* (2004). In this paper, longitudinal creep tests were performed on spruce specimens exhibiting various MFA. When complex rigidities are computed and represented in the ACP, curves exhibited a similar shape but they

are shifted along the coordinate axis representing the real part of Young's modulus. If a reference curve is chosen and other curves shifted along the coordinate axis, all curves form one single curve as we can see in Figure 0-34. The amount of the shift factor was correlated with MFA. This suggests that in a relaxation test, only the elastic response would be affected by MFA but not the relaxation part.

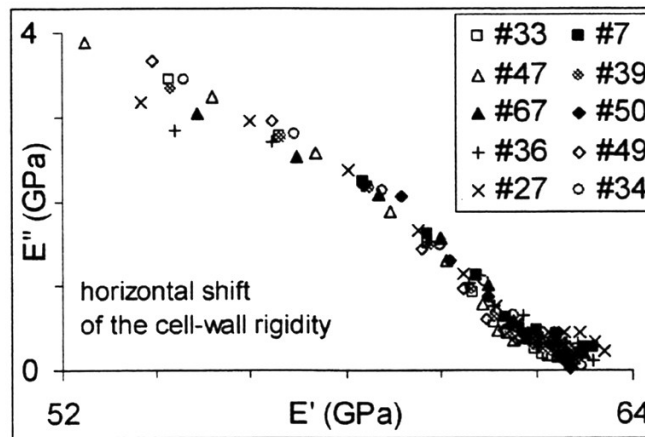


Figure 0-34: PCA plot after horizontal shift along E' axis. Specimen 34 was taken as a reference. From (Gril *et al.* 2004).

4.4.b Effect of constitutive polymers

Salmén *et al.* (2006) investigated the creep of mechanically separated single wood and pulp fibres. During delignification of pulp fibres also 45% of hemicelluloses were removed. Final composition of pulp fibres yielded 80% of cellulose and 20% of hemicelluloses. Pulp fibres exhibited nearly two times lower creep than wood fibres.

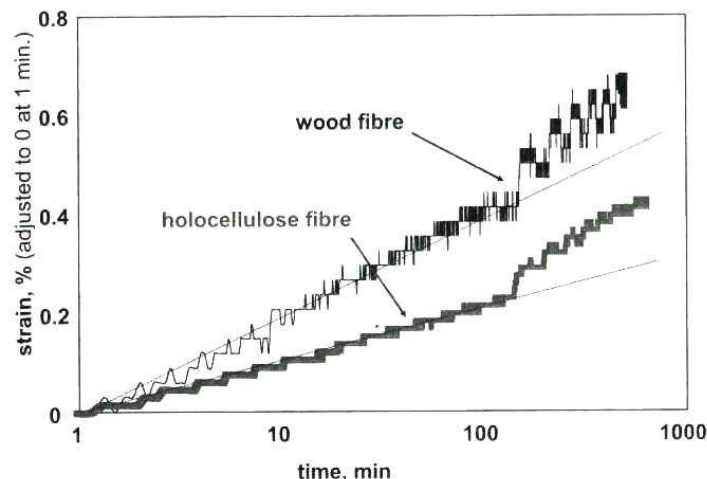


Figure 0-35: Creep of a single wood fibre and of a single pulp fibre, holocellulose. Fibres were tested at 30°C (strain adjusted at zero at one minute after loading). The first creep from 0 to 120 minutes occurred at constant humidity of 80%RH. The second phase from 120 to 615 minutes involved periods at 30 and 80%RH.

Fioravanti *et al.* (2006) investigated the effect of hemicelluloses on the time-dependent behaviour. Tensile creep tests were performed on non-treated spruce and spruce samples after hemicellulose removal. Wood specimens without hemicelluloses exhibited two times less creep compared to equivalent untreated wood. This shows that both components of the amorphous matrix, lignin and the hemicelluloses, are involved in the creep process at room temperature. However, these observations are also affected by the lower moisture equilibrium content of wood with completely or partially removed hemicelluloses.

5) Role of the viscoelasticity in the living tree

Viscoelastic properties of wood as reported above have been mainly studied in view of the use of wood as a building material in man-made structures or to assess the wood behaviour during the transformation processes. Both cases are not relevant when searching for viscoelastic data for biomechanical uses. In the first case, wood behaviour in the hygroscopic region is investigated while in a living tree, cell walls are fully saturated. Transformation processes such as veneer cutting or some of wood shaping are performed in the green state, but rheological properties transversally to the fibre direction are mainly involved. For biomechanical uses only the viscoelastic properties along fibres measured in the green state are relevant.

During the tree growth, large stresses appear inside wood, due to the increasing load of the crown and the process of wood maturation as we have seen in §2. It is well known that the distribution and magnitude of these growth stresses depends on the relative speed of loading and of secondary wood formation. However, the viscoelastic nature of wood introduces an additional time-dependence through the differential relaxation of various tissues. Some previous works focused on modelling of a growing structure submitted to external loads and maturation stresses (Fournier *et al.* 1991; 1991). However, only few works accounted for the viscoelastic nature of wood tissues (Gril and Fournier 1993), probably introducing a considerable bias in the biomechanical models used for tree assessment or growth description.

The viscoelastic behaviour of wood may have a biomechanical impact at various time scales. The dynamic response of a branching system to short-term loads such as wind is modified through the damping coefficient. Stress relaxation in wood tissues affects the effective Young's modulus against permanent loads and thus influences the tree stability and the efficiency of its reorientation process. Finally at a long time scale, the distribution of growth stress is modified due to the partial relaxation of residual stresses during the ageing of the tree, reducing the risk of internal wood failure.

During a preliminary study, the effect of viscoelasticity on biomechanical performances of a tree in reorientation process was investigated numerically by calculating the up-righting efficiency and residual deformability (flexibility) of a titled stem (Dlouhá *et al.* 2008). Due to high levels of pre-stresses accumulated during the reorientation process in the central part of a tree stem its flexibility drops dramatically. In addition to the distribution and magnitude of maturation strains, two factors affect biomechanical performances of a tree in reorientation process: the production of juvenile wood in earlier stages of its life and the viscoelastic properties of wood tissues. Juvenile wood increases the flexibility of the stem for both softwoods and hardwoods. In the case of softwoods, viscoelasticity was shown to have only a minor influence on the stem flexibility. By contrast, it had an important positive impact on the flexibility of hardwoods and thus allowed having an efficient reorientation process while keeping safe against instantaneous bending loading. The trade-off between stem flexibility and the efficiency of its reorientation may imply a biological limit on the magnitude of maturation strains. However, these conclusions have to be taken with precaution because simulations are based on estimated data.

The objective of the present work was to characterize the viscoelastic behaviour of different types of wood having a variety of micro-structural, anatomical and functional features (normal wood, reaction wood and opposite wood) and try to predict the long-term behaviour from short-term tests in order to better understand the impact of viscoelasticity on the biomechanical performance of trees.

A) EXPLORING THE DIVERSITY OF VIBRATION PROPERTIES OF TROPICAL WOODS

1) Introduction

Tropical rainforests represent highly competitive environments characterised by a high density of stems, closed forest canopy and limited understorey light availability. Numerous strategies have been developed by trees to survive in the forest until their reproductive maturity. We can distinguish different growth dynamics from the opportunist pioneer species to the patient shade tolerant species waiting for years in the under storey for the occasion to reach the light. Different growth dynamics result in different mechanical requirements during each stage of the tree life. Consequently, wood of tropical species represents a great variety of structural features and mechanical properties compared to temperate species. Studying tropical diversity is a good opportunity to bring some new highlights on the relation between wood properties and structures and investigate a possibility of trade-offs between different functions to be performed during a tree life as well as the relation to ecological strategies.

In this study, we focused on the diversity and variability of structures and properties of wood from trees in juvenile stage (saplings) where competition for height growth is a critical constraint. Diversity is present at several levels; interspecific diversity comes from the choice of representative examples of different growth strategies while intraspecific diversity from differences in site conditions and growth history. Radial variability of wood properties inside a single tree results from likely juvenile transition (it is difficult to know the age of trees in a tropical canopy and decide about the juvenility of such trees) and circumferential variability from occurrence of reaction tissues. Leaning trees, included in the study, represent very interesting material to investigate the limits of tree performances as well as limits of wood acclimation. To describe the variability of wood properties and structures and search for a connection with the growth strategy or site conditions is the first step of the study.

While collecting data for biomechanical models, one may wonder if wood characteristics measured on a piece of wood after machining and storage is still representative of properties of native wood tissues inside a living tree. We know that wood tissues inside a living tree are pre-stressed. To estimate the mechanical state of wood in native conditions, longitudinal growth strains were measured at the periphery of each tree. Second potential problem is the degradation or change of wood properties due to attack of biological agents or washing of extractives during the storage. The simplest way to prevent wood from biological degradation is drying; however, we know that drying induces some irreversible changes (Kifetew *et al.* 1998; Thuvander *et al.* 2002). Thus, the use of drying in the biomechanical context is questionable. Storage in water saturated condition with moisture content above the fibre saturation point (FSP) is therefore preferable. In the “green” or never-dried state, cell walls are completely saturated, so mechanical properties are not expected to differ between the native state and green state because water in cell cavities is generally considered without effect on mechanical properties. In the present study, impact of different storage procedures on vibration properties of wood was investigated. Effect of some other treatments such as hygrothermal recovery or oven drying was also studied in order to make a relation with rheological models presented in the following chapter.

In the second part of the chapter, we have investigated the validity of some structure – properties relations commonly used to model wood properties. Usually, structure-properties relations are applied either to large sample of species with reduced intraspecific variability or to investigate intraspecific variability of some reduced number of commercial species. Studies including both types of variability, interspecific as well as intraspecific are scarce. Therefore, it can be interesting to investigate the general validity of these relations. Further, a simple

model has been developed to predict mechanical properties of the cell wall material based on wood properties and microfibril angle. Microfibril angle is expected to control the variability of the properties at cell wall level. The goal was to assess its capacity to explain the variability of the cell wall properties of our sample exhibiting high diversity of properties. Finally, percentage of different wood elements was measured for a reduced selection of specimens in order to see how the anatomical structure affects the viscoelastic properties.

2) Studied wood material/Sampling

2.1 Sample selection

Wood material was collected in Paracou Experimental Research Station (5°18' N, 52°55' W) in French Guyana in September 2006 and September 2007 during the training period of ENGREF³ students. Ten tropical species were selected among common species of the tropical rainforest in French Guyana. Except for *D. guyanensis*, they are not of important commercial use. Species were chosen in function of their growth strategy according to the Favrichon's ranking based on the species shade tolerance (Favrichon 1994). To maximise interspecific variability, selection covered a wide range of basic densities inside each growth strategy group as illustrated in Figure A-1. We can however notice that heliophilic and hemi-tolerant species are in average less dense than shade tolerant and understory species as it is reported in another study (Alvarez-Clare and Kitajima 2007).

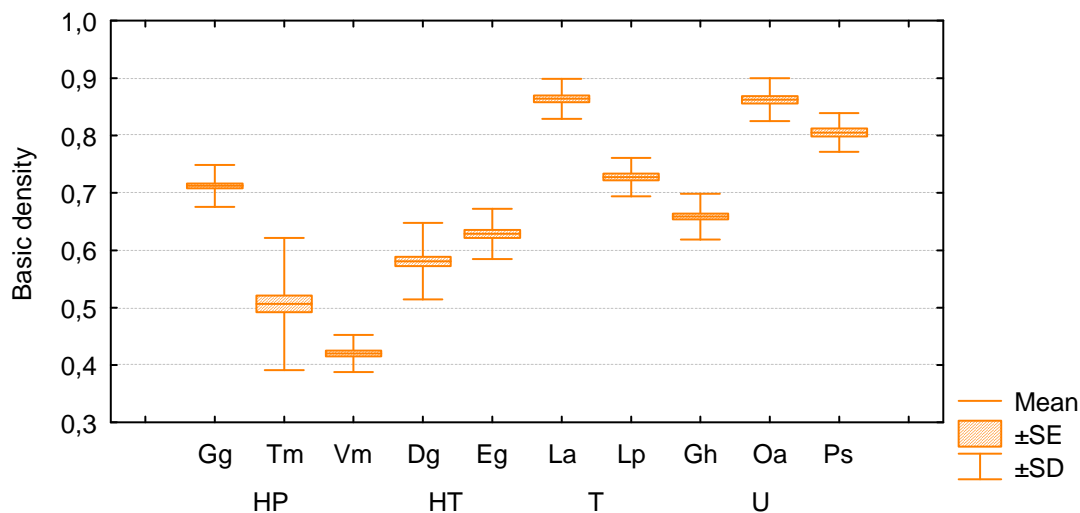


Figure A-1: Distribution and variability of specific gravities between species and growth strategy groups. For key see Table A-1.

Concerning intraspecific variability, the aim was to cover all types of wood tissues; normal wood as well as reaction and opposite wood. Diameter of saplings at the breast height ranged between 4 and 7 cm so that we are likely in the juvenile transition zone. Further, some tilted trees with expected occurrence of reaction wood were collected for each species. Checking for occurrence of tension wood by anatomical observation was impossible considering the number of specimens (550) and also the fact that in some species as for example *V. michelii*, anatomical features of tension wood do not exhibit any apparent difference relative to the normal wood (Chang *et al.* 2009). Therefore, we have used the biomechanical definition considering tension wood as tissues characterised by high level of stress induced during maturation process.

Released longitudinal growth strains were measured on standing trees to assess the mechanical state of wood at the periphery of each tree (for details refer to 3.1). Distribution of

³ Ecole nationale du génie rural, des eaux et des forêts

average values and gradient of growth strains along estimated axis of tension-opposite wood were investigated. Figure A-2 shows distribution of these parameters for tilted and straight growing trees. Average values were similar but the gradient of growth strains was significantly higher in tilted trees compared to straight growing trees, indicating active up-righting reaction of a tree. Gradient of growth strains, expected to be related to the circumferential variability of wood properties, is represented for each species in Figure A-3. We can observe that the level of reactivity differs between species. The most reactive are *L. persistens* and *E. grandiflora* whose congeneric species, *E. falcata*, is known for generation of high levels of growth stresses (Chardin and Sales 1983).

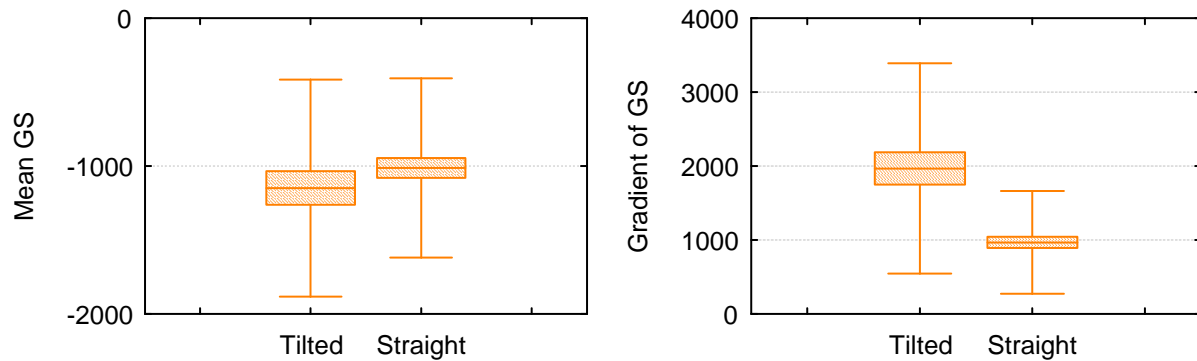


Figure A-2: (a) Average value of released longitudinal growth strain for tilted and straight growing trees. (b) Gradient of growth strains for tilted and straight growing trees.

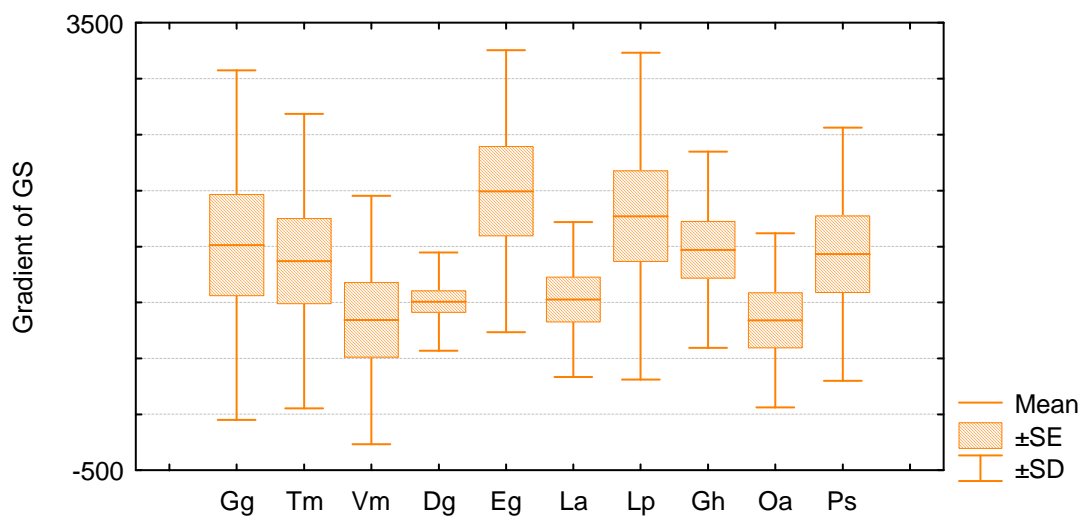


Figure A-3: Interspecific variability of gradients of growth strains. For the species names see Table A-1.

2.2 Repartition of specimens for different studies

In September 2006 more than a hundred trees of ten tropical species were felled. However, wood of only six species could be finally used due to poor quality of green wood sample preparation. Taking advantage of a similar opportunity in September 2007, four more species were added to the selection. Basic information about the species are summarised in Table A-1. Examples of anatomical sections performed by master students from the Wood Science department at MZLU in Brno (Czech Republic) are represented in Figure A-4.

The sample material was used for three studies: screening of mechanical properties by the vibration method, investigation of the storage/heating/drying effect on vibration properties, and creep tests across a range of temperatures. The screening of properties was performed on the whole sample. This material contains:

- Sample 1: 2 heights / 4 trees by species for the selection of six species made in September 2006 (300 specimens);
- Sample 2: 4 complementary species presented in the lower part of Table A-1 used only for the study of interspecific diversity of mechanical properties in green state (250 specimens).

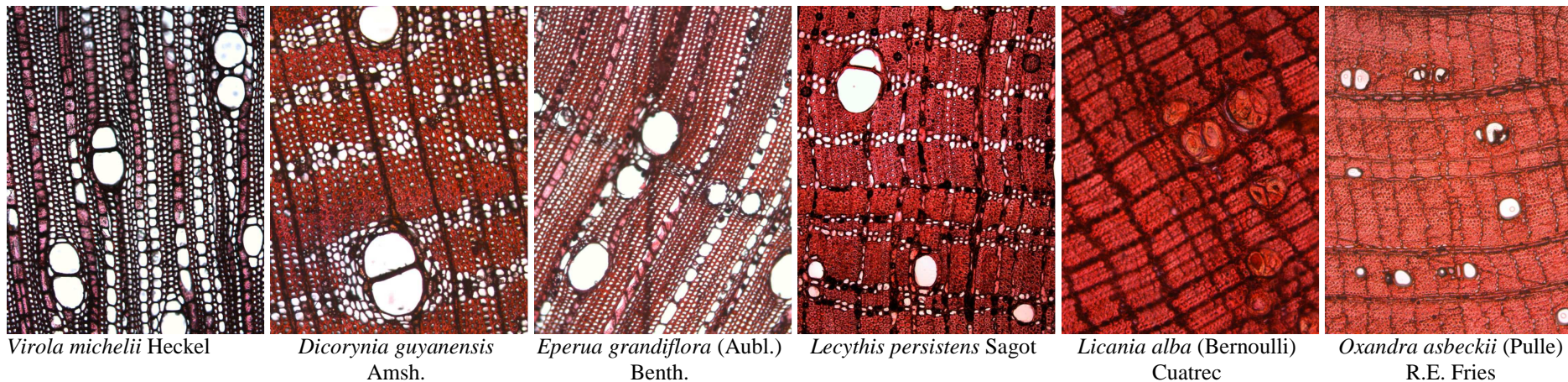
Sample 1 was then broken down into two groups – the first was used for the creep study (G1) and the second one for the storage study (G2; see Figure A-5). Selection for creep tests represented initially one half of Sample 1 containing one tilted and one straight growing tree per species. However as the set up of the creep device and testing procedure was very time consuming, only one part of the G1 could be tested and the remaining part was used to test the effect of air drying (G2-b).

Table A-1: Summary table of some basic information about studied species

Scientific name	Common name	Abr.	Growth strategy	Abr.	Specific gravity	Elastic modulus (Pa)	Lignin %	Cell. %	Hemic. %	AB %	E %
<i>Virola michelii</i> Heckel	Yayamadou montagne	<i>Vm</i>	Heliophilic	HP	0.57	10 072	25.3	46.2	22.6	1.6	2.6
<i>Dicorynia guyanensis</i> Amsh.	Angélique	<i>Dg</i>	Hemi tolerant	HT	0.79	14 799	35.5	42.9	16.1	2.3	2.4
<i>Eperua grandiflora</i> (Aubl.) Benth.	Wapa-courbaril	<i>Eg</i>	Hemi tolerant	HT	0.92	16 824	31.1	36.7	14.4	12.8	4.5
<i>Lecythis persistens</i> Sagot	Maho rouge	<i>Lp</i>	Tolerant	Tol	0.72	12 361	38.2	40.6	15.5	2.0	3.1
<i>Licania alba</i> (Bernoulli) Cuatrec.	Gaulette blanche	<i>La</i>	Tolerant	Tol	1.06		32.3	46.1	17.3	1.0	1.3
<i>Oxandra asbeckii</i> (Pulle) R.E. Fries	Mouamba	<i>Oa</i>	Understorey	U	0.9						
<i>Goupia glabra</i> Aubl.	Goupi	<i>Gg</i>	Heliophilic	HP	0.84	14 670	31.0	41.4	17.3	6.7	3.1
<i>Tachigali melinonii</i> (Harms) Barneby	Diagidia	<i>Tm</i>	Heliophilic	HP			27.8	47.3	16.8	5.8	1.9
<i>Gustavia hexapetala</i> (Aubl.) J.E. Smith	Mantapouhoupa	<i>Gh</i>	Understorey	U	0.78						
<i>Pogonophora schomburgkiana</i> Miers ex Benth.	Guelli koko	<i>Ps</i>	Understorey	U	1.05						

Common name is the most commonly used name in French Guyana; Abr.: abbreviation used in all figures; HP: heliophilic; HT: hemi tolerant; Tol: tolerant; U: uderstorey; Elastic modulus is measured at 12% of moisture content. AB: Alcool-benzen extract. E: Water extract. Data are issued from the CIRAD data base.

Figure A-4: Anatomical structure of studied species



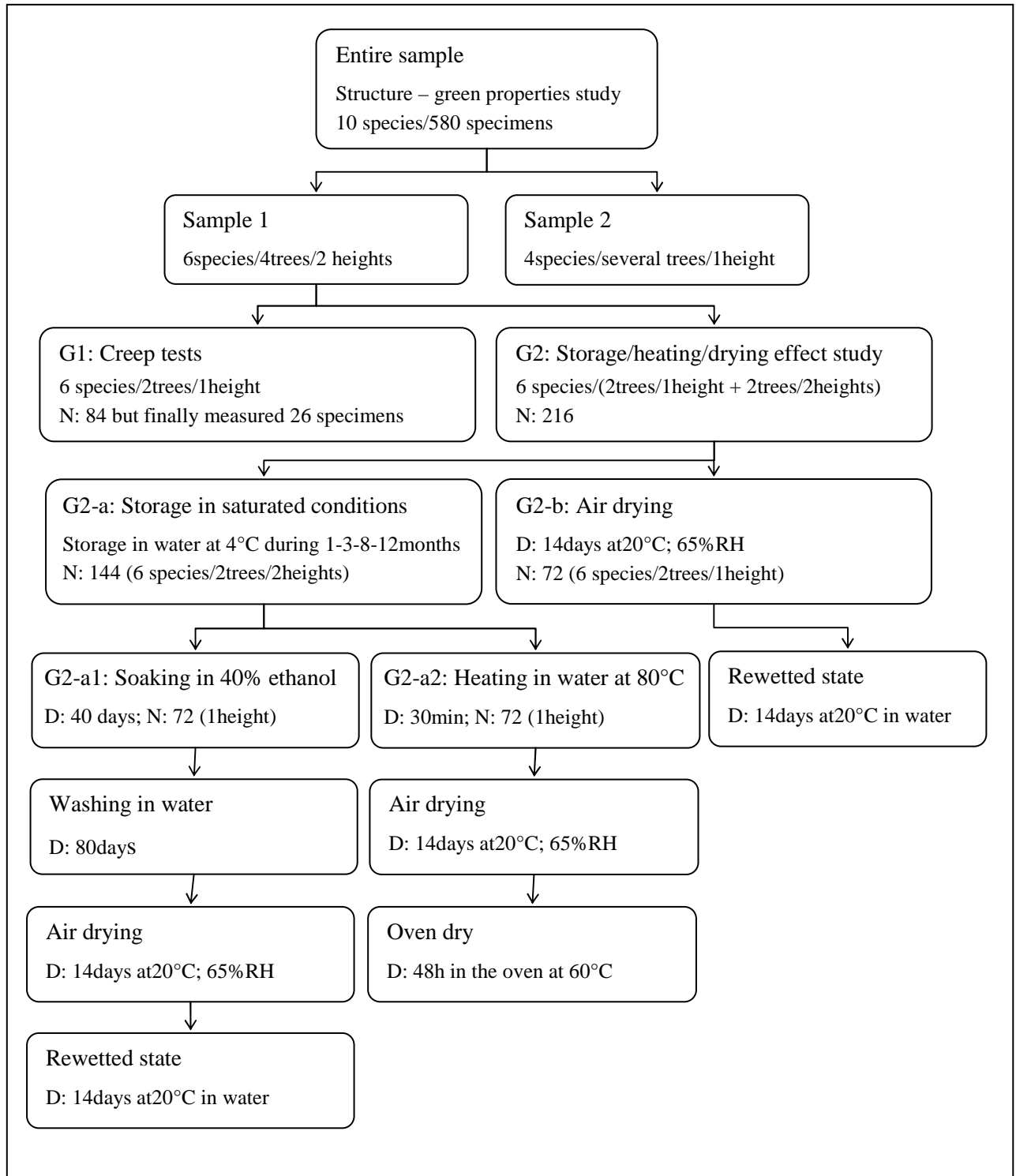


Figure A-5: Repartition of the sample for different tests and treatments. G1 and G2: subsets of sample 1; G2-R and G2-S: subsets of sample G2; N: number of specimens; D: duration of the treatment.

2.3 Specimens preparation

Specimens for vibration measurements were cut along the fibre direction (150 x 12 x 2mm, L x R x T) at three heights following the procedure outlined in Figure A-6. Specimens were prepared along the estimated opposite-tension wood axis. Unfortunately, an important part of marking made in the forest (see §3.1) was partly erased during the transport of wet logs and the estimated direction of tension wood was often lost. Consequently, it was often impossible to link the growth strain measurements to mechanical properties and clearly separate TW from NW. However, we have information about the average level of growth strains inside a tree as well as their gradient. During machining and storage, specimens were kept in the water saturated condition.

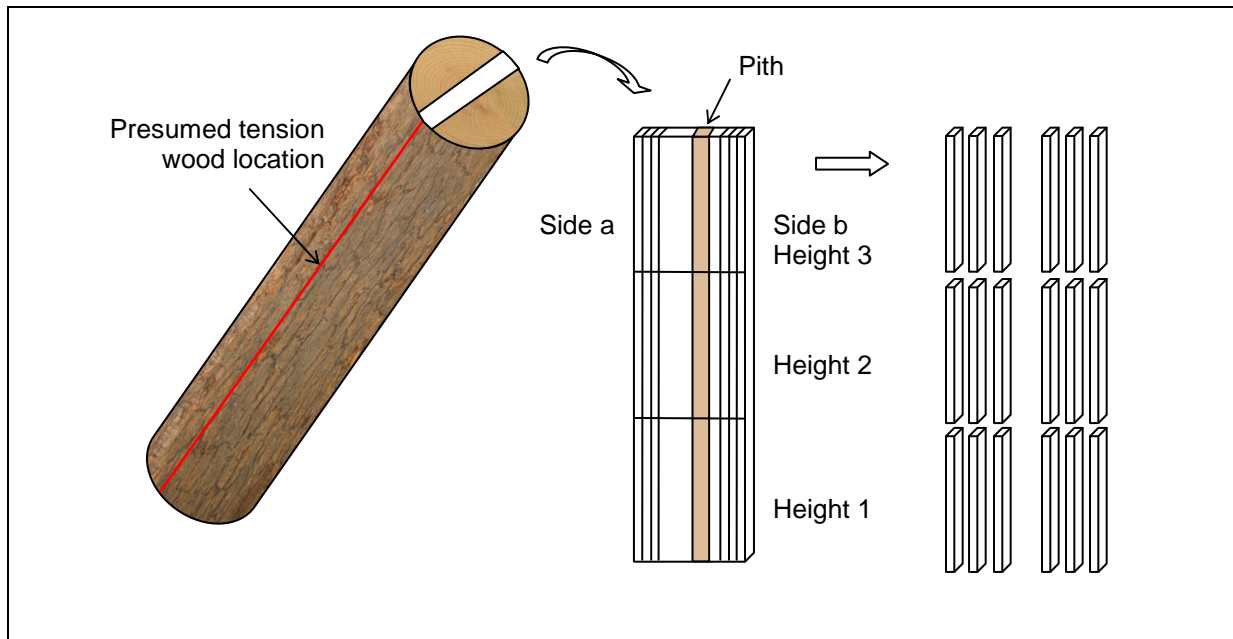


Figure A-6: Preparation of damping specimens from the log collected in the forest.

3) Methodology

3.1 Growth stress measurements

Before felling the tree, we measured its geometry (diameter, stem inclination and tree height). Direction of the largest local inclination between 0.25 m and 0.75 m height was marked on the stem, indicating presumed circumferential location of the tension wood. Afterwards, four strain gages were placed at the periphery of the stem in order to measure the growth strains. Radial position 1 corresponded to opposite wood and radial position 3 to supposed tension wood (Figure A-7). Growth strain measurement was performed in two steps. First the upper part of the stem including the crown was cut at approximately 1.75m height to estimate the support strains. Afterwards, residual part of maturation strains was measured by two grooves method (Yoshida and Okuyama 2002): two grooves were made horizontally at 5 mm above and below each gage (Kyowa KFG-5-120-C1-11L1M2R), the depth of the groove were about 5 mm. Longitudinal strain released by cutting during each phase was recorded on a Wheatstone bridge (Kyowa PCD-300). The part of the log near the strain gage measurement was used for sample preparation.

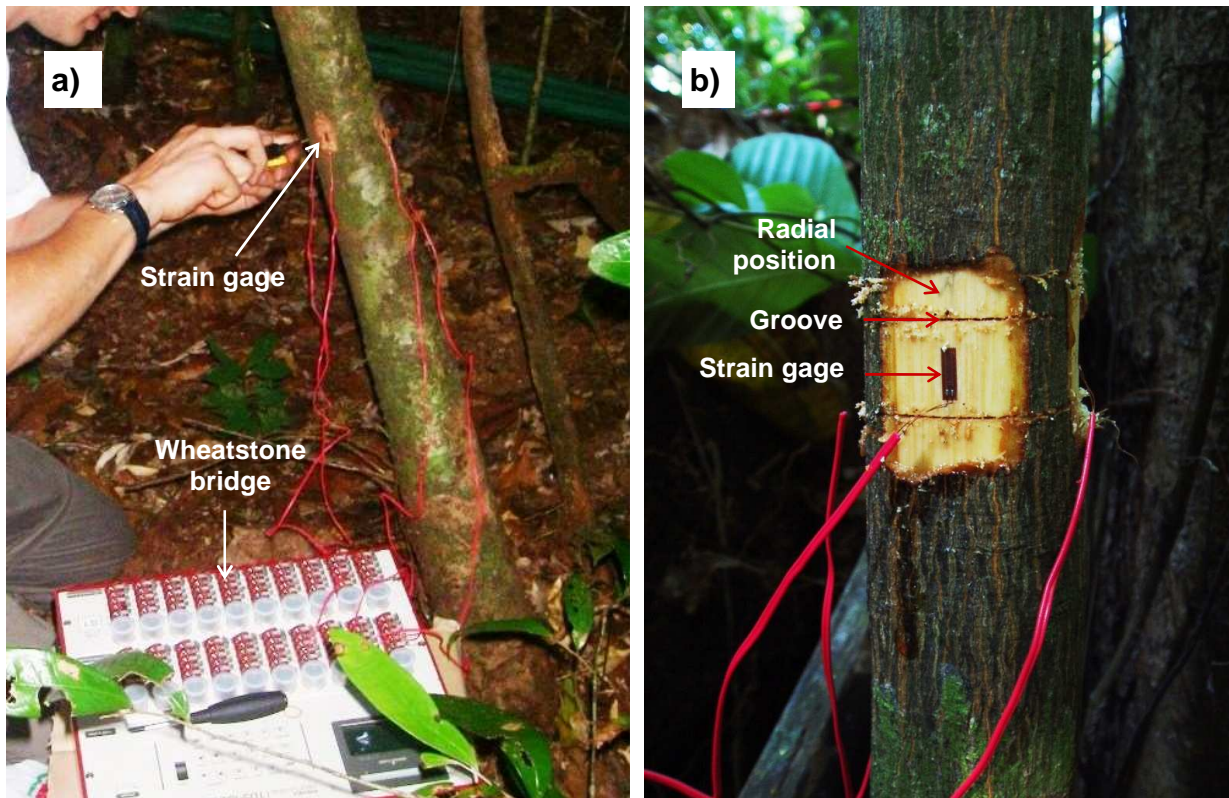


Figure A-7: In-situ growth strain measurement. (a) Instrumentation by strain gages and recording of the strain signal by Wheatstone bridge. (b): Two grooves method and radial position marking.

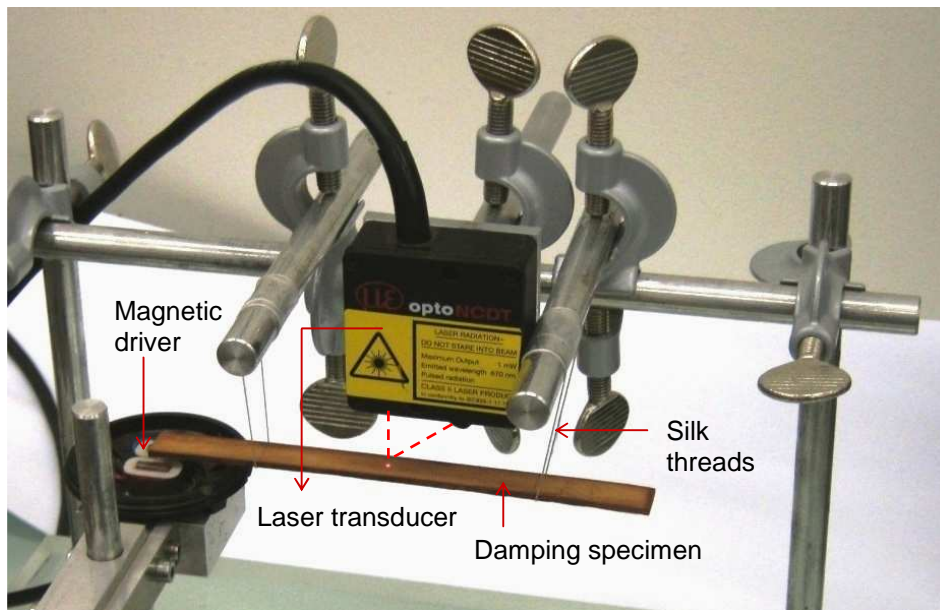


Figure A-8: Experimental device for vibration tests.

3.2 Vibration measurements

Dynamic Young's modulus and damping coefficient in the longitudinal direction were determined by the free-free flexural vibration method at the resonance frequency corresponding to the first vibration mode. Resonance frequency ranged from 200 to 650Hz. During the measurement, the specimen was hung by silk threads and driven by a magnetic driver (a thin iron foil was glued on one end of the specimen). Displacement was recorded by a laser transducer focused on the midpoint of the specimen. A frequency sweep was performed to determine the resonance frequency. Based on the resonance frequency and geometry of the specimen, the specific Young's modulus (E/ρ) was determined as follows:

$$\frac{E}{\rho} = \frac{(4\sqrt{3}\pi)^2 l^4 f^2}{m^4 h^2} \times 10^3 \approx \frac{946.4l^4 f^2}{h^2} \quad \text{Eq. A-1}$$

where l is the length of the specimen, f the resonance frequency, h the thickness of the specimen and m a constant depending on the vibration mode ($m = 4.73$ for the first mode). The damping coefficient was determined by two methods:

- half bandwidth method of the resonance frequency peak (damping 1);
- logarithmic decrement of the signal after stopping excitation (damping 2).

The experimental device used is shown in Figure A-8 and extensively described in (Brémaud 2006). In this work, some details will be given regarding the correspondence of damping estimates obtained by both methods, the repeatability of the measurements and limits of accuracy.

3.2.a Comparison of damping measurement methods

Comparing both methods, we can note that there is a very good agreement between the damping estimates (Figure A-9). However, we can observe a systematic underestimation of the damping 2 estimates of approximately 3.8%. During the measurements it was also noted that method using the logarithmic decrement (Damping 2) was more sensitive to accurate positioning of the specimen and other parameters such as the occurrence of cross-grain.

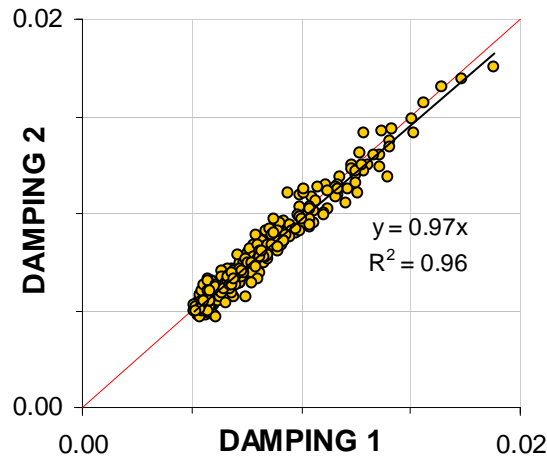


Figure A-9: Comparison of damping results obtained by two different methods: Damping 1: half-band method; Damping 2: logarithmic decrement. Red line represents the relation $y = x$.

This is partially due to the signal treatment as it is done in the current version of the acquisition software. Actually, only a one-sided fit of the logarithmic curve on the acquired waveform is used as shown in Figure A-10. Thus, any minor asymmetry of the output signal considerably affects the obtained result. It is suggested to also use the opposite peaks for the logarithmic fit was made to improve the accuracy of the measurement by logarithmic decrement but was not applied for the presented measurements.

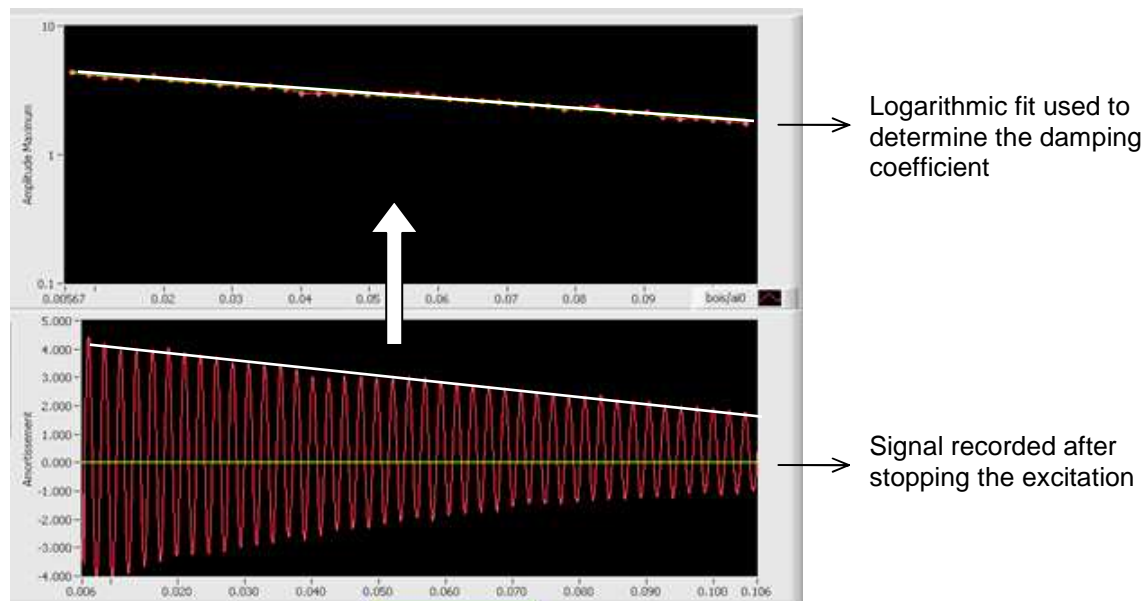


Figure A-10: Measurement of the damping coefficient by logarithmic decrement.

3.2.b Repeatability of the vibration measurement

Three species covering a wide range of elastic moduli and damping coefficients were used for the repetition measurements as shown in Table A-2. Ten repetitions were performed on each specimen. Tests were conducted in air dry conditions to avoid any variation in weight. Results are summarised in Table A-2. Experimental standard deviation (SD) of the resonance frequency estimate was very low, yielding a maximum SD of 0.66 % for the Young's modulus estimate. The repeatability of damping 1 estimate was considerably higher than the repeatability of the damping 2 measurement. Therefore, in the following analysis only damping 1 will be considered and denoted further as damping.

Table A-2: Experimental standard deviations of vibration measurements in air dry conditions.

Species	SD of f estimation	E (GPa)	Induced SD of E	Damping 1 estimate	SD of Damping 1	SD of Damping 2
<i>D. guyanensis</i>	0.06%	8.33	0.12%	8.31E-03	2.95%	12.48%
<i>V. michelii</i>	0.33%	10.68	0.66%	7.74E-03	1.33%	10.25%
<i>O. asbeckii</i>	0.02%	25.63	0.04%	5.48E-03	2.96%	10.76%

Legend: SD: experimental standard deviation; f: resonance frequency; E : Young's modulus; Damping 1: damping coefficient by half bandwidth method; Damping 2: damping coefficient by logarithmic decrement.

The estimation of Young's modulus is actually more affected by the uncertainty of dimension estimates, and in particular thickness. The thickness of our specimens is of approximately 2 mm. It is not easy to obtain a specimen with consistent thickness of 2 mm all along the length ($l = 150$ mm), particularly when machining is done in green state. Occurrence of tension wood makes finishing the surface of the sample by sanding, for example, impossible. The imperfection of the obtained surface may induce some error of the thickness measurements. An error of 2.5% for the thickness measurement yields SD of the modulus estimate equal to 4.82%.

When investigating the Figure A-9, or better Figure A-39, we can observe high concentration of low damping values close to 0.005. It is possible that this was due to the accuracy limit of the experimental device. Therefore, vibration measurements were performed on an aluminium specimen exhibiting a low damping coefficient. Estimated Young's modulus

(71.73 GPa) as well as the damping coefficient (1.33E-03) were close to the data from the CES Selector material database (75GPa; 1.05E-03).

3.3 Investigation of the effect of storage conditions

The aim of the study on storage conditions was to assess the change in properties due to sample storage relative to the green state. Therefore, mechanical properties of specimens in the green condition and in rehydrated state after storage in different conditions were compared. Measurements were performed on the group of specimens denoted G2 which was further divided in two subgroups: G2-a and G2-b (for details see §2.2).

Specimens of group G2-a were used to assess the effect of long-term storage in water at low temperatures ($T = 4 \pm 0.1^\circ\text{C}$). Young's modulus and damping coefficient were measured after 1, 3, 8 and 12 months of storage on the set of 144 specimens (6 species / 2 trees / 2 heights). Then, the G2-a1 subgroup (1 height) was used to investigate the effect of soaking in ethanol. Specimens were measured after 40-day soaking in 40% ethanol solution; after washing in water; in air dry state and in re-saturated state. In parallel, the matched group G2-a2 (second height) was heated in the water at 80°C for 30 minutes. The effect of heating above the temperature of glassy transition was studied for its relation with the second part of the present work dealing with thermally activated viscoelastic properties. G2-a2 specimens were also measured in air dry and oven dry states. Subgroup G2-b was tested in the air dry condition and after resaturation. This enabled us to see if the effect of ethanol and heating above the temperature of glassy transition in green state affects vibration properties in the long-term. Details about the procedure are shown in Figure A-5.

Variations in measured properties were assessed through two parameters: bias and error. Bias is the mean relative change in properties calculated as follows:

$$\varepsilon_b = \frac{\sum \frac{X_{i1} - X_{i0}}{X_{i0}}}{n - 1}, \quad \text{Eq. A-2}$$

where ε_b represents the bias, X_{i0} the property measured in the initial state, X_{i1} the property measured after a given storage period and n the number of tested specimens. Error describes the relative dispersion of values (mean quadratic error) and is given by:

$$\varepsilon_r = \sqrt{\frac{\sum \left(\frac{X_{i1} - X_{i0}}{X_{i0}} \right)^2}{n - 1}}, \quad \text{Eq. A-3}$$

where ε_r is the mean quadratic error.

3.4 MFA measurements

Microfibril angle has been measured by X-Ray diffraction (XRD) on all of the samples. As the specimens are not thick, we could measure directly the damping specimens and the middle part of the bone-shaped creep specimens after removing the heads as shown in Figure A-11. A 4-circle diffractometer (Oxford Diffraction Gemini S) equipped with a 1024x1024 CCD camera was used for the measurements. CuK_α radiation was generated by an X-ray generator operating at 50kV, 25mA. Images were integrated between $2\theta = 21.5$ and 23.5 along the whole 360° azimuthal interval to plot the intensity diagram of the (200) plane. An automatic procedure allowed the detection of the (200) peaks and their inflexion points. The T parameter as used by Cave (1966), was measured as the half distance between intersections of tangents at inflexion points with the baseline. The average MFA of each

specimen was estimated by the “improved Cave’s method” (Yamamoto *et al.* 1993). The results are given as the mean of values obtained for the two (200) peaks.

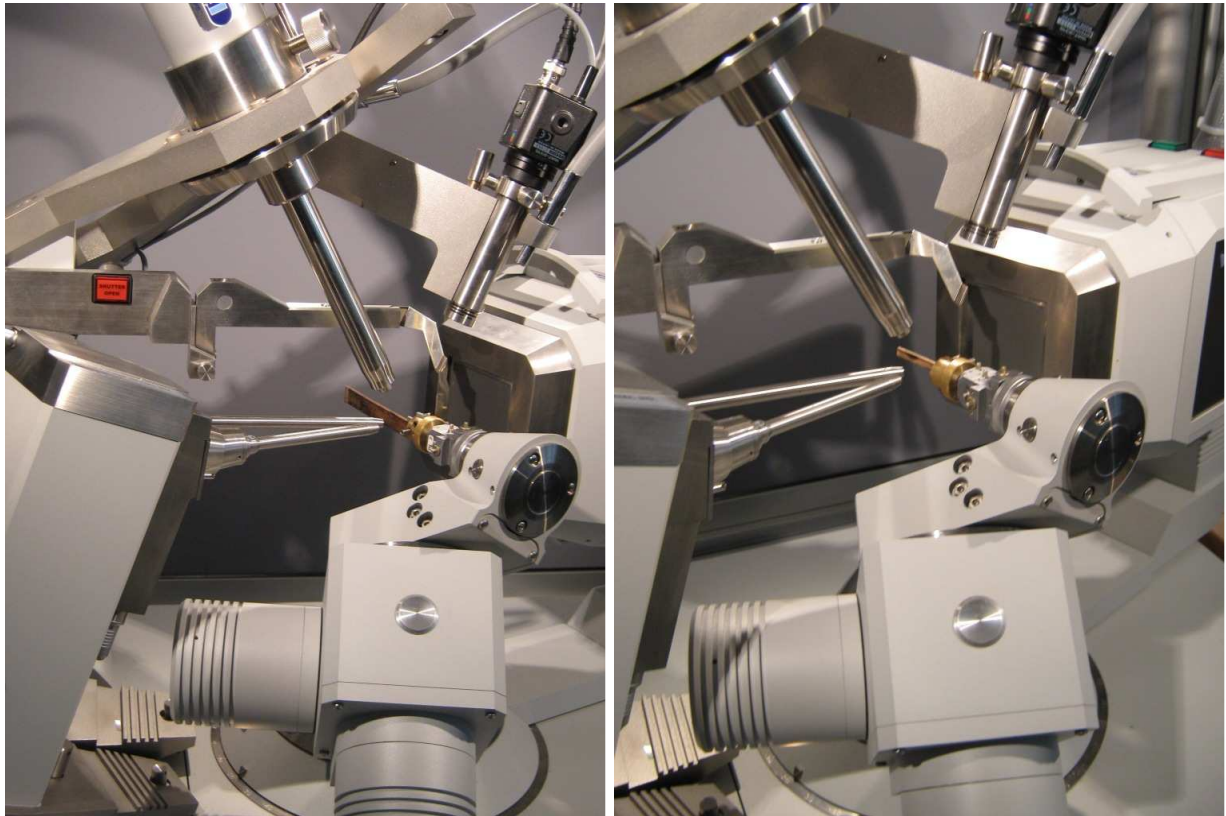


Figure A-11: Measuring the MFA on (a): damping specimen. (b): central part of the creep specimen.

3.5 Anatomical structure

Percentage of different wood elements (vessels, fibres, axial and radial parenchyma) was measured for some specimens from the G1 group used for creep tests. The aim was to see if a creep properties are affected by some particular anatomical structures such as for example high percentage of axial parenchyma in *D. guyanensis* for example. Analysis of anatomical structure was performed on 64 specimens.

During the preparation of the creep specimen, the extremity of the damping specimen was removed (see Figure B-1.22.b). This part was used for anatomical analysis. Transverse sections were prepared from each end of the residual part of the specimen. The sectioning was difficult for some species because of their hardness and occurrence of silica crystals. Hence, prior to cutting the specimens were kept in a softening solution (glycerol: ethanol: water; 1:1:2) and, if necessary, boiled during 4-7days in a solution of glycerol and water (2:1) using the Soxhlet apparatus (Vavřík and Gryc 2004). After softening, transverse sections (25- μm thick) were prepared on a Leica SM2000R microtome and stained by safranin. Five pictures were captured from each section. A Leica DM LS optical microscope equipped by a Leica DFC270 camera directly connected to the computer was used for observations and capturing of pictures. Percentage of wood tissues was measured on a picture using ImageJ software. Anatomical measurements were performed by master students (Markéta Fučíková, Jan Baar and Martin Greško) from MZLU in Brno (Czech Republic).

3.6 Simple model predicting specific modulus and damping coefficient of the cell wall material

Since wood is a cellular material made of cells elongated along the grain direction, we can easily deduce the elastic properties of the wood cell wall from the properties of solid wood in the longitudinal direction as follows:

$$E/\rho_b = E_{cw}/\rho_{cw}, \quad \text{Eq. A-4}$$

where E is the Young's modulus of solid wood, ρ_b is the basic density, E_{cw} is the Young's modulus of the cell wall and ρ_{cw} is the density of the cell wall substance. This approach, however, does not account for the internal organisation of the cell wall. At the cell wall level, wood substance can be represented as a two-phase composite made up of crystalline microfibrils embedded in an amorphous matrix. Crystalline microfibrils are disposed in parallel and inclined at angle θ to the grain direction of the wood called microfibril angle (MFA). Simplified representation of the cell wall is pictured in Figure A-12.

3.6.a Simplified model based on Hooke's law of angle lamina

To apply Hooke's law of angle lamina (Jones 1975), a global coordinate system (L, T) is used for the cell wall and a local coordinate system (1, 2) for the microfibril as represented in Figure A-12. (L, T) and (1, 2) stand for longitudinal and tangential direction in the cell and the microfibril coordinate system, respectively.

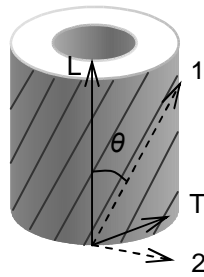


Figure A-12: Simplified representation of a cell wall. LT stand for axes of global coordinate system and 12 for axes of a local coordinate system of the microfibril. θ denotes the microfibril angle.

Assuming $E_L \approx C_{LL}$, the elastic modulus parallel to the cell axis can be written in function of the microfibril angle using the standard formulae of tensor rotation as follows:

$$E_L = C_{11} \cdot \cos^4 \theta + 2 \cdot (2 \cdot C_{66} + C_{12}) \cdot \sin^2 \theta \cos^2 \theta + C_{22} \sin^4 \theta, \quad \text{Eq. A-5}$$

where C_{11} , C_{12} , C_{22} and C_{66} are the elements of the stiffness matrix. The direction denoted as 6 corresponds to the 12 plane.

The relative importance of individual terms on obtained prediction of the Young's modulus was investigated for the range of MFA up to 35° . Values of the elements of the stiffness matrix used for this investigation are shown in Table A-3. The values were outputs from a model simulating the cell wall properties based on the properties of cell wall constituents developed in LMGC (Almeras *et al.* 2005). Simplified predictions of the Young's modulus along fibres neglecting progressively the terms starting from the right side of Eq. A-5 are shown in the Figure A-13. Neglecting of terms containing C_{22} and C_{12} elements does not markedly affect resulting predictions. On the other hand, neglecting the term with shear modulus (C_{66}) has a stronger effect, although the approximation is still good for the investigated range of MFA. Thus, formulation containing two first terms of Eq. A-5 will be used in further development:

$$E_L = C_{11} \cdot \cos^4 \theta + 4 \cdot C_{66} \cdot \sin^2 \theta \cos^2 \theta \quad \text{Eq. A-6}$$

Table A-3: Elements of the stiffness matrix used for testing of the simplified calculus of the elastic modulus along fibres

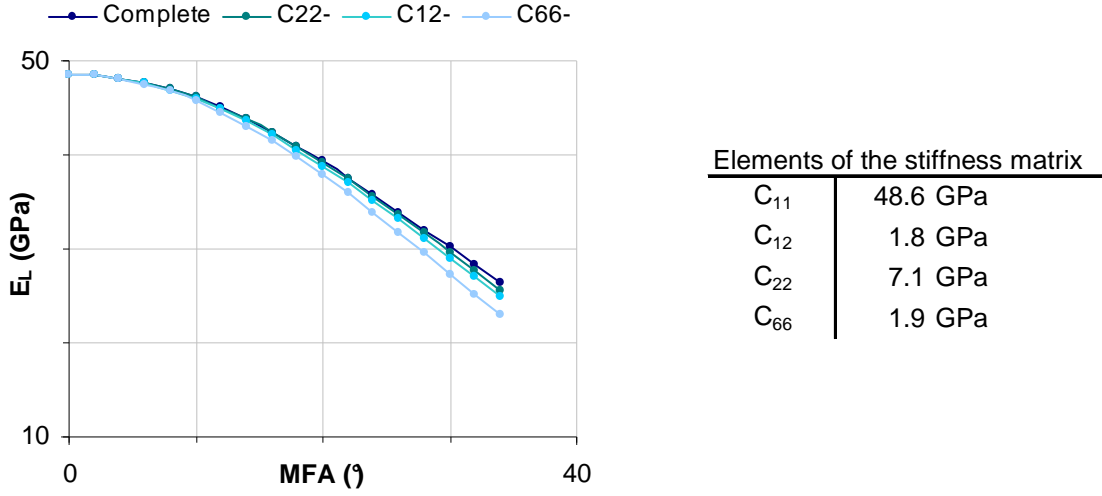


Figure A-13: Prediction of the Young's modulus of the cell wall based on Eq. A-5.

3.6.b Complex formulation

Let us now write the rotation formula in a parametric way:

$$\frac{E_L}{\rho} = a \cdot \cos^4 \theta + b \cdot \sin^2 \theta \cos^2 \theta, \quad \text{Eq. A-7}$$

where a stand for C_{11}/ρ , b for $4 \cdot C_{66}/\rho$ and E_L/ρ is the specific modulus in the L direction. For investigation of viscoelastic properties, it is useful to replace elastic formulation by the complex one:

$$\frac{E_L^*}{\rho} = a^* \cdot \cos^4 \theta + b^* \cdot \sin^2 \theta \cos^2 \theta. \quad \text{Eq. A-8}$$

Thus, we can easily obtain the storage and loss specific modulus by separating the real and imaginary parts as follows:

$$\frac{E_L'}{\rho} = a' \cdot \cos^4 \theta + b' \cdot \sin^2 \theta \cos^2 \theta, \quad \text{Eq. A-9}$$

$$\frac{E_L''}{\rho} = a'' \cdot \cos^4 \theta + b'' \cdot \sin^2 \theta \cos^2 \theta, \quad \text{Eq. A-10}$$

where E_L'/ρ is the storage specific modulus and E_L''/ρ the loss specific modulus. The next step consists in introducing in the current formulation parameters having a physical meaning. Thus, we will note C_{11}/ρ and $\tan \delta_{//}$ the properties of the cell wall substance along the microfibrils. Assuming $a' = C_{11}/\rho$, $a''/a' = \tan \delta_{//}$, $b'/a' = \beta'$ and $b''/a'' = \beta''$, we finally obtain:

$$\frac{E_L'}{\rho} = \frac{C_{11}}{\rho} \cdot \cos^4 \theta \cdot (1 + \beta' \cdot \tan^2 \theta), \quad \text{Eq. A-11}$$

$$\frac{E_L''}{\rho} = a'' \cdot \cos^4 \theta \cdot (1 + \beta'' \cdot \tan^2 \theta), \quad \text{Eq. A-12}$$

$$\tan \delta = \tan \delta_{//} \cdot \frac{(1 + \beta'' \cdot \tan^2 \theta)}{(1 + \beta' \cdot \tan^2 \theta)}, \quad \text{Eq. A-13}$$

where C_{11}/ρ and $\tan \delta_{//}$ represent the properties of the cell wall substance along the microfibrils. Assuming that terms with Poisson's ratio are negligible in the calculation of C_{11} , we can directly write $a = E_{//}/\rho$ and $b = 4 \cdot G_{12}/\rho$. $E_{//}/\rho$ stands for the specific modulus of the cell wall along the microfibrils. Parameter β' represents the ratio of the real parts of shear modulus and storage modulus while β'' stands for the ratio of its imaginary parts.

3.6.c Expression of the specific modulus and damping coefficient in the local coordinate system

Based on Eq. A-11 and A-13 and assumptions mentioned above, we can easily obtain the expression of the properties in the local coordinate system:

$$\frac{E_{//}}{\rho} = \frac{E_L'}{\cos^4 \theta \cdot (1 + \beta' \cdot \tan^2 \theta)}, \quad \text{Eq. A-14}$$

$$\tan \delta_{//} = \tan \delta \cdot \frac{(1 + \beta' \cdot \tan^2 \theta)}{(1 + \beta'' \cdot \tan^2 \theta)}. \quad \text{Eq. A-15}$$

Thus, using the mean values of parameters β' and β'' an estimation of the specific Young's modulus and damping coefficient of the wood substance can be obtained for each specimen.

4) Effect of storage procedure

4.1 Long-term storage in water at low temperature

Young's modulus and damping coefficient were measured on the G2-a sample subset after 1, 3, 8 and 12 months of storage in water at low temperatures. For computation of Young's modulus from vibration data, dimensions were considered to be stable while variations of the weight were taken into account. We observed a slight increase of the weight ($2.19 \pm 2.80\%$) after three months of storage but during following measurements, variations of the weight were negligible. We considered if the increase in weight could be attributed to the increase of saturation level. For this purpose, the theoretical saturation level was computed based on following relations.

The basic density and saturated density as a function of the porosity can be written as follows:

$$\rho_b = (1-P) \cdot \rho_{cw}, \quad \text{Eq. A-16}$$

$$\rho_{sat100\%} = P \cdot \rho_w + \rho_b \quad \text{Eq. A-17}$$

where ρ_b is the basic density, $\rho_{sat100\%}$ the totally saturated density, P the porosity, ρ_w the density of water and ρ_{cw} the density of the cell wall material. Basic density is the ratio of dried cell wall mass to saturated volume often used to investigate properties of the cell wall. The density of the cell wall material is very similar between species and will be further considered equal to 1.5g/cm^3 . Since water has a density of 1 g/cm^3 , the density at a given saturation level is given by:

$$\rho_{satX\%} = P \cdot S_L + \rho_b, \quad \text{Eq. A-18}$$

where S_L represents the relative saturation level. Relative saturation level of the specimens in initial state and after a given period of storage is shown in Figure A-14. We can note the initial saturation were very low for some species. This is probably due to partial water evaporation during the machining of specimens. Saturation level after three months of storage and more is very similar between species. For some specimens, we can observe that the estimation of relative saturation is higher than 1. However, the calculation, explained above, gives only a rough estimation of the porosity. Another effect that is not considered here is the occurrence of extractives. Extractives may induce an increase of the density that results in a lower estimated porosity. However, those extractives located in the cell wall would not affect the porosity.

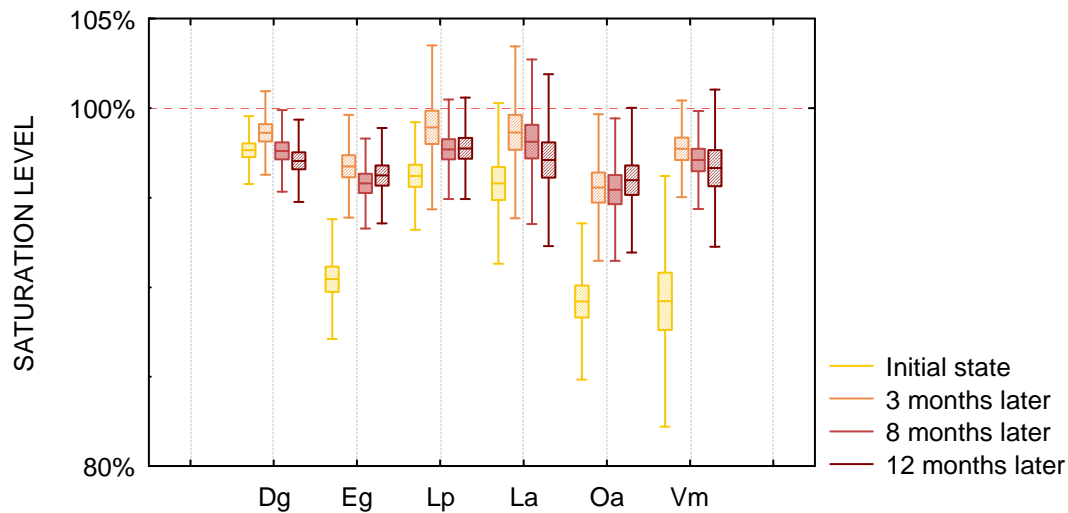


Figure A-14: Saturation level of specimens in initial state and after different storage durations.

Change in Young’s modulus after given storage period is represented in Figure A-15. We can observe slight decrease of the modulus and very good agreement between both measurements. Long-term storage in water at low temperatures does not affect significantly Young’s modulus.

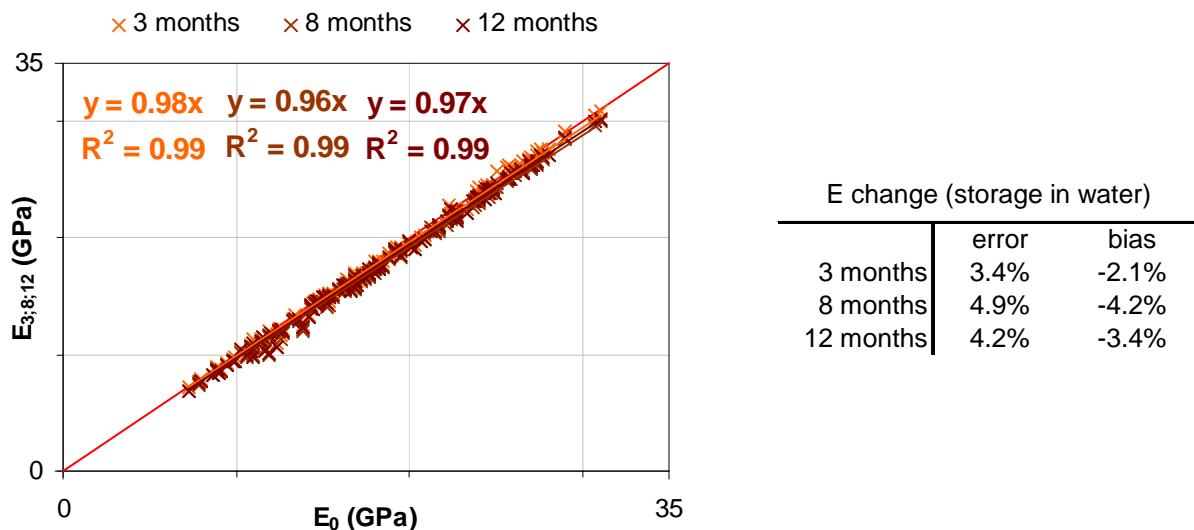
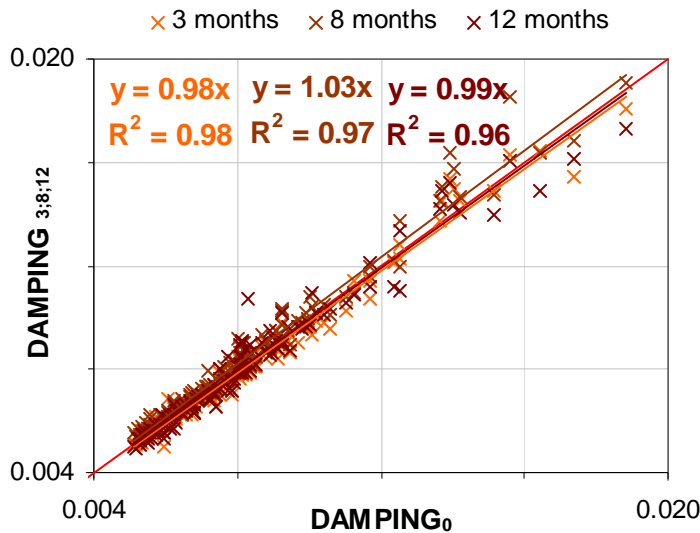


Figure A-15: Variations of Young modulus measured by vibration method in initial state (E_0) and after 3, 8 and 12 months of storage in water at low temperature ($4 \pm 0.1^\circ\text{C}$). The red line represents the relation $y = x$.

Variations of damping coefficient are shown in Figure A-16. We can observe slight variations of damping coefficient, in particular after 8 months storage period. Higher damping measured after 8 months storage may be only an artefact of experimental conditions because it was done during the summer period. Higher ambient temperature could be responsible for the observed increase of the damping coefficient. Results obtained after 3 and 12 months show that storage in water induces slight variations of damping, but with very low systematic error.

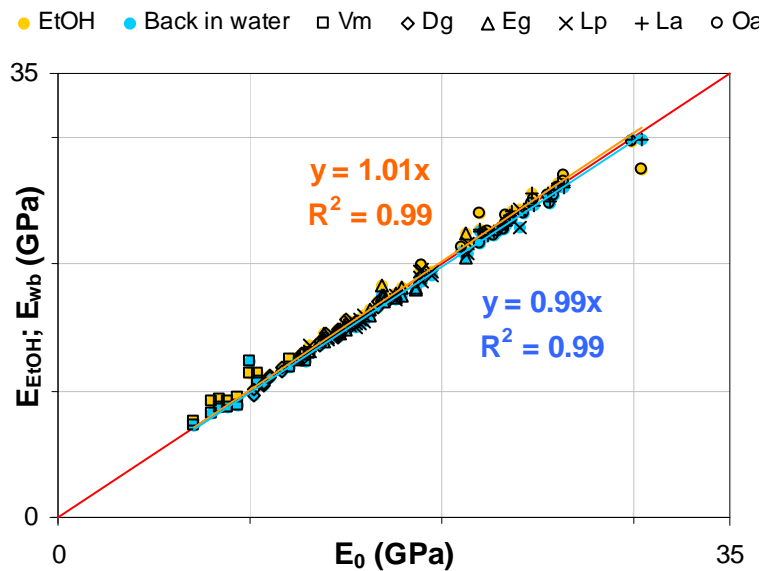


Tand change (storage in water)		
	error	bias
3 months	4.4%	-1.4%
8 months	5.4%	2.8%
12 months	5.4%	-0.7%

Figure A-16: Variations of damping coefficient measured by vibration method after 3, 8 and 12 months of storage in water at low temperature ($4 \pm 0.1^\circ\text{C}$). The red line represents the relation $y = x$.

4.2 Effect of soaking in 40% ethanol

Storage in ethanol is proposed as a way to prevent wet wood from biological degradation in particular during field experiments with no possibility of storage at low temperatures. The effect of soaking in ethanol on vibration properties is shown in following figures. While Young's modulus was only slightly affected by soaking in ethanol (Figure A-17), the damping coefficient has significantly increased (Figure A-18). After washing in water, Young's modulus was slightly decreased whereas damping coefficient estimates were higher than initial values ($6.22 \pm 4.24\%$).



E change (soaking in EtOH)		
	error	bias
EtOH	4.0%	1.8%
Water back	3.5%	-0.9%

Figure A-17: Effects of soaking in 40% ethanol and its residuals after washing in water on Young modulus. The red line represents the relation $y = x$.

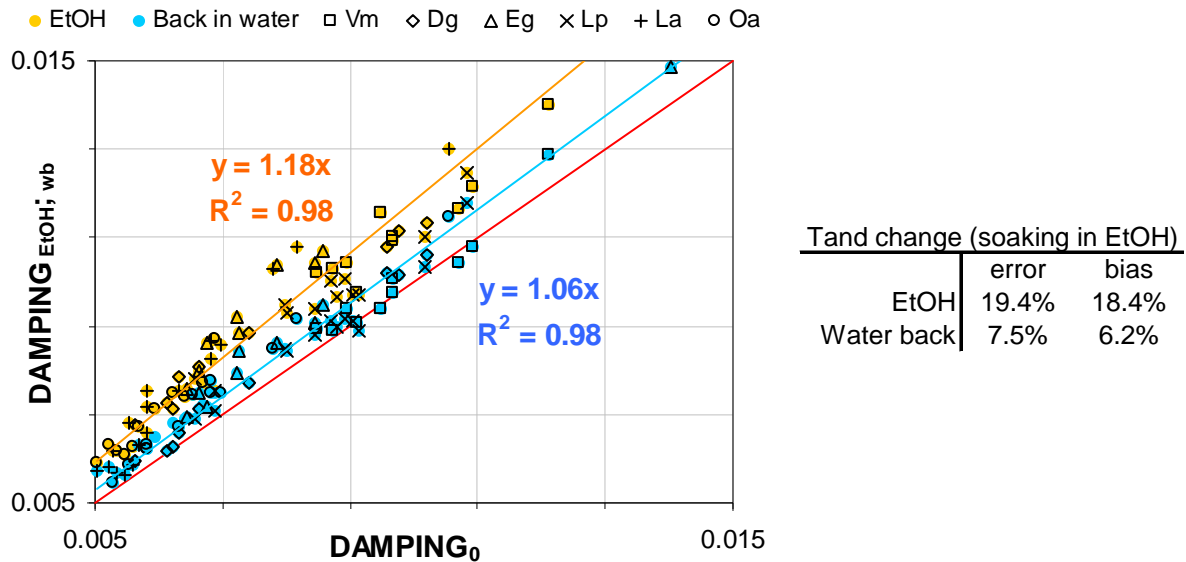


Figure A-18: Effects of soaking in 40% ethanol and its residuals after washing in water on damping coefficient. The red line represents the relation $y = x$.

Soaking in ethanol was accompanied by variations in the weight of specimens (accounted for in E calculations). Slight weight decrease ($-1.49 \pm 0.51\%$) was attributed to lower density of ethanol (0.78 g.cm^{-3}) compared to water. Residual weight decrease after washing in water ($-0.21 \pm 0.33\%$) may indicate only partial removal of ethanol and/or removal of some extractives. No correlation between weight variations and changes in mechanical properties has been observed. That supports the hypothesis about the residual ethanol content. It is also interesting to note that the exchange between water and ethanol-water solution is not complete – in fact only 25% of the water was replaced by the ethanol-water solution (from the calculations of the theoretical weight loss).

4.3 Effect of air drying

In the following section, properties of green wood are compared with the properties of air dried wood and properties of rehydrated specimens after their storage in the air dry condition. Drying of green specimens at room temperature has significantly increased the Young's modulus as shown in Figure A-19. Observed change (+11.6%) is lower than previously reported by Kollmann and Côté (1968): +29% increase of Young modulus, measured by vibration method on oak or by Obataya *et al.* (1998) on spruce: 21.5% and 25.5% respectively for the increase of Young's modulus and decrease of damping coefficient measured by vibration method. However, these studies compared the air dry state with the rehydrated, saturated state and therefore the comparison is not the same as in the current study. After the resaturation Young's modulus is lower than in green state. Thus, the relative difference with air dry state is higher.

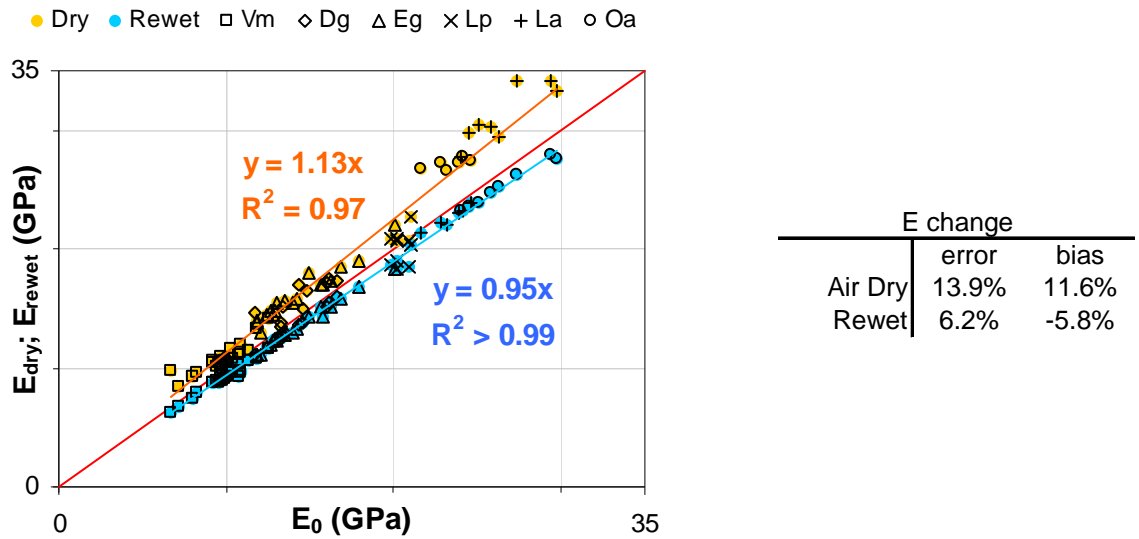


Figure A-19: Effect of air drying and resaturation on Young modulus. E_0 is the never-dry value. The red line represents the relation $y = x$.

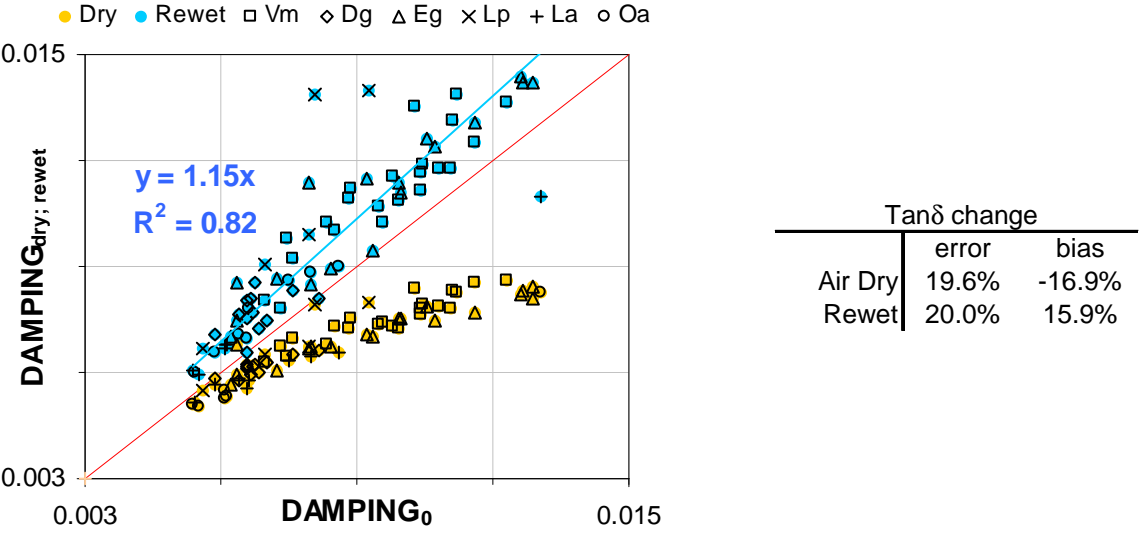


Figure A-20: Effect of air drying and resaturation on damping coefficient. The red line represents the relation $y = x$.

Air drying has induced significant decrease of the damping coefficient as shown in (Figure A-20). We can note that this change is not linear. In rehydrated state, specimens exhibit significantly higher damping coefficient than in green state. This indicates that the effect of air drying affects permanently the damping properties. A likely hypothesis to explain the observed phenomenon is the formation of micro cracks during the drying process which might be a source of increase of internal friction and the more dissipative behaviour of wood. Moreover, high dispersion of damping estimates in rehydrated state compared to previous treatments in ethanol or water shows that effect of drying was variable between specimens. In conclusion, we cannot recommend preventing of biological degradation of green specimens through the drying process for vibration measurements of damping characteristics.

4.4 Conclusion about storage

Storage in water at low temperatures can be advised as the most appropriate way to preserve vibration properties of wood specimens in the green state. The effect of ethanol on viscoelastic properties seems to be only transient but its use is questionable as some doubtful

and undesirable processes may be involved in the transient state (Chang *et al.* 2008). Air drying can be used to preserve specimens against biological attack while elastic properties only are required but is not appropriate for viscoelastic studies.

5) Other investigated effects

5.1 Effect of hygrothermal recovery

Heating above the temperature of glassy transition was investigated for its possible link with part B of the manuscript which focuses on thermally activated viscoelastic properties. To study the effect of hygrothermal recovery, specimens were heated in water at 80°C during 30 minutes and measured after cooling to ambient temperature on the vibration device few hours later. Relative changes of Young modulus and damping coefficient are displayed in Figure A-21. Heating slightly decreased Young modulus ($-2.9\pm 1.8\%$) and markedly increased damping coefficient ($21.2\pm 8.2\%$).

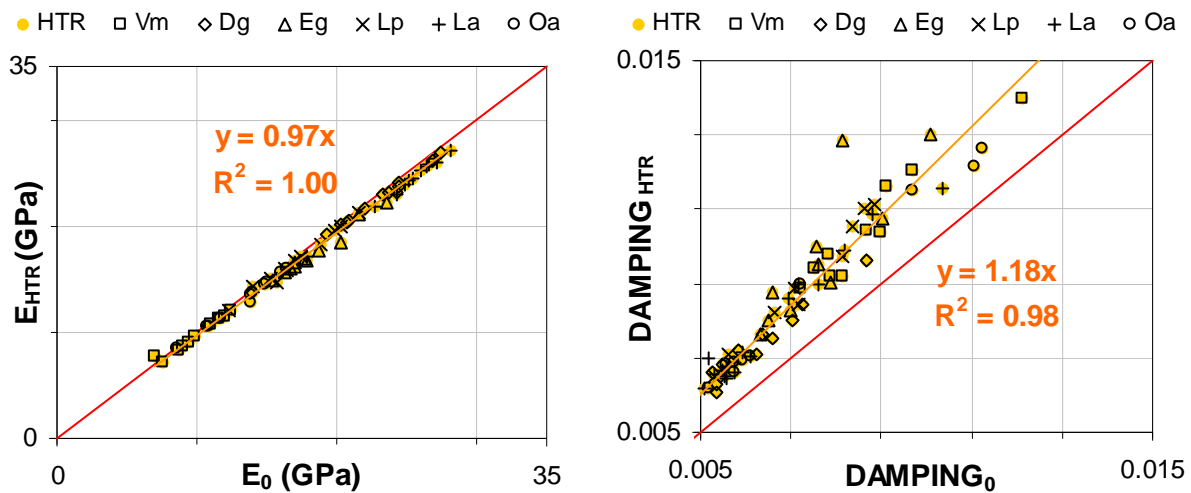


Figure A-21: Effect of heating on Young modulus and damping coefficient.

The simultaneous effect on Young modulus and damping coefficient may be interpreted as a “rejuvenation” effect. When a polymer is heated above T_g , it is in a state of thermodynamic equilibrium. During the cooling to a temperature below T_g , the rate of molecular relaxation is too slow to keep pace with the changes required if the material is to remain at thermodynamic equilibrium. As a result, when the material reaches the thermal equilibrium with the surroundings it is still far from its thermodynamic equilibrium resulting in increased fluidity of the material (see B-2).

5.2 Difference between air dried and oven dried state

Specimens of the sample G2-a2 were further tested in air dry and oven dry state. The aim was to assess the effect of oven drying. Results are represented in Figure A-22. In comparison with air dry state, oven drying has only slightly increased the Young’s modulus. On the other hand, a more significant increase of damping coefficient has been observed upon oven drying.

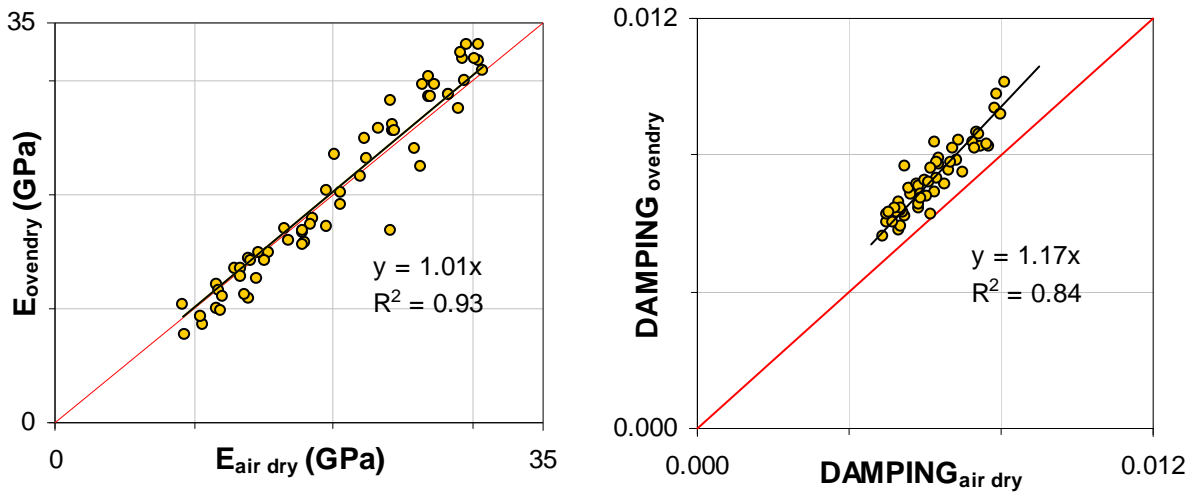


Figure A-22: Effect of oven drying on Young's modulus and damping coefficient. The red line represents the relation $y = x$.

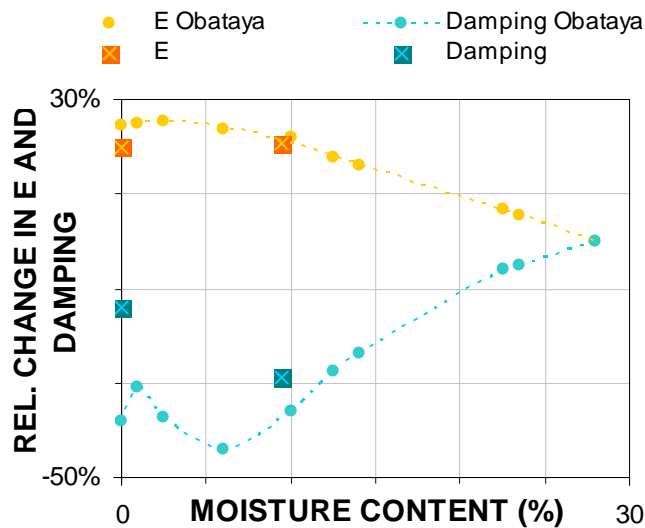


Figure A-23: Effect of moisture content on vibration properties. The lines represent experimental data reported by (Obataya *et al.* 1998) and the squares measurements from the current study.

Similar observations have been previously reported by Obataya *et al.* (1998). Obataya *et al.* studied the influence of absorbed water on vibration properties. We have reproduced their results in Figure A-23 plotting our measurements in the same graph. We can see that measured effect of the moisture content on the elastic modulus is in agreement with Obataya *et al.*'s observations while the effect on damping coefficient was considerably higher in our case. Obataya *et al.* have observed a loss peak around 1% of moisture content. This effect was ascribed to the relaxation related to the motion of absorbed water. Due to the testing time necessary for vibration measurements, it is possible that our specimens have absorbed some humidity during the measurement and so the moisture content could arise to 1%. A slight horizontal shift of damping values could therefore partly explain the observed difference. It was also hypothesised that oven drying could induce micro-cracks in the cell wall layers as suggested by Kifetew *et al.* (1998) based on observations of fracture surfaces of green wood and wood in swollen state after drying. Such micro-cracks would dissipate more energy during the excitation of the specimen thus leading to higher damping coefficient.

5.3 Comparison of empirical relations between damping and specific modulus in air dry and green state

Double logarithmic plots are often used to represent the relation between damping and specific modulus (Ono and Norimoto 1984). Figure A-24 represents the comparison of the empirical regression from the literature with our experimental data. We can see that the relationship between both parameters in air dry and oven dry states is very close to the empirical equation represented by the red line and described by the equation in the box. Green wood properties exhibit completely different behaviour. Equation for the regression between both parameters in green condition is also displayed. We can also note a significant difference between the regression for green specimens and rehydrated specimens. Specific variability of the relation between both parameters will be discussed in §6.5

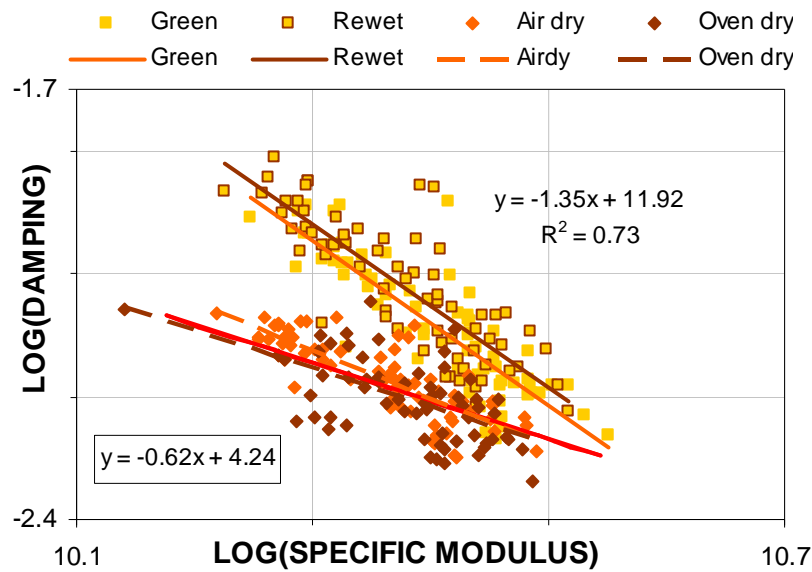


Figure A-24: Double logarithmic relation between damping coefficient and specific modulus in green, rehydrated and air dry state. The red line and the equation in the box represent empirical equation proposed by Ono and Norimoto (1984).

5.4 Conclusion

This section contains some complementary results that are useful for researchers that will work on similar topic. We have quantified the effect of hygrothermal recovery on vibration properties. Significant increase of damping coefficient together with a slight decrease of Young's modulus was attributed to a rejuvenation effect of heating above the temperature of glassy transition. This means that similar effect might be observed on the viscoelastic properties at different time scales, for example creep properties. The topic will be investigated in greater detail in chapter B-2). Next, vibration properties in oven dry state were compared with the properties in air dry state. A considerable increase of damping coefficient in oven dry state compared to air dry state was observed while only slight increase was observed for Young's modulus. We hypothesised that it could be a result of micro cracks due to the oven drying that is more destructive than the air drying. Finally, empirical regression between damping and specific modulus in green state was proposed similarly to the regression previously established for air dry wood. The relation between damping and specific modulus will be investigated in the following chapter.

6) Basic structure – property relations

In this section, diversity of vibration properties measured on ten tropical species including reaction tissues is presented. Basic density and MFA are often considered as structural parameters explaining the diversity of wood vibration properties. However, the effect of MFA was determined mainly based on mono-specific studies. Moreover, reaction wood was not often considered. In the following section, we will investigate if these relationships hold when applied on the highly diversified sample. Commonly measured structural parameters are green density, basic density and MFA. We will first analyse relations between these parameters before examining their relations with mechanical properties. Mean specific values and variability of measured parameters are summarised in the Appendix 1.

6.1 Green density – Basic density

In the context of tree mechanics, first measured property is in general green or saturated density. First question was therefore if green density can be used as a reliable predictor of basic density and so mechanical properties. Based on Eq. A-16 and A-17 given in §4.1, we can obtain a theoretical relation between the saturated density and basic density:

$$\rho_{sat100\%} = 1 + \rho_b/3, \quad \text{Eq. A-19}$$

where $\rho_{sat100\%}$ stands for the completely saturated density and ρ_b for the basic density. Relation between the green and basic density is represented in Figure A-25. The red line represents a theoretical dependency (Eq. A-19). First observation is that experimental regression line is vertically shifted down indicating incomplete saturation of green specimens. This problem was already mentioned in the 4.1. We have seen that the saturation level was different between species. In particular *T. melinonii* specimens exhibit low saturation level (~78%, not shown). Thus, it seems difficult to use the green density as a reliable predictor of basic density and mechanical properties. It may be only used as a rough estimator of interspecific variability of the basic density as shown in Figure A-26.

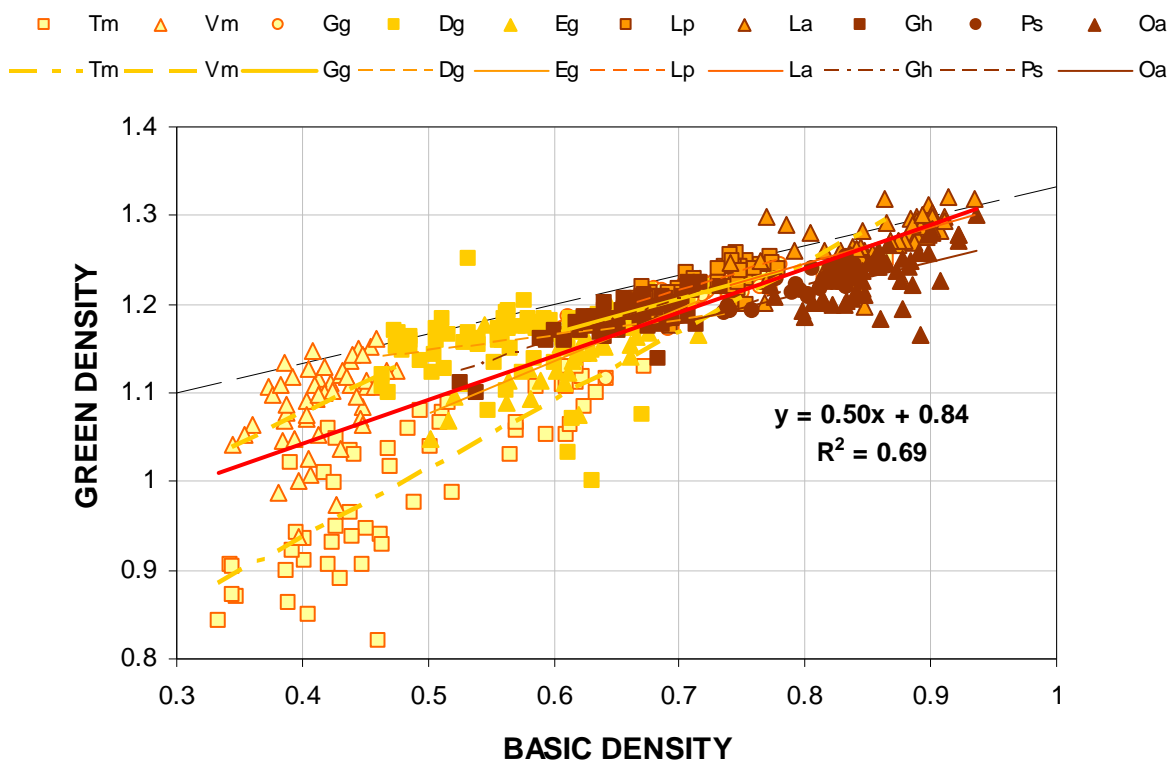


Figure A-25: Relation between green and basic density. Red line represents the regression line on the entire sample and dashed line the theoretical relationship between both parameters. The gradient of colours represents the growth strategy going from the yellow heliophilic to the brown understorey species. The same key is used for all figures of chapter 6.

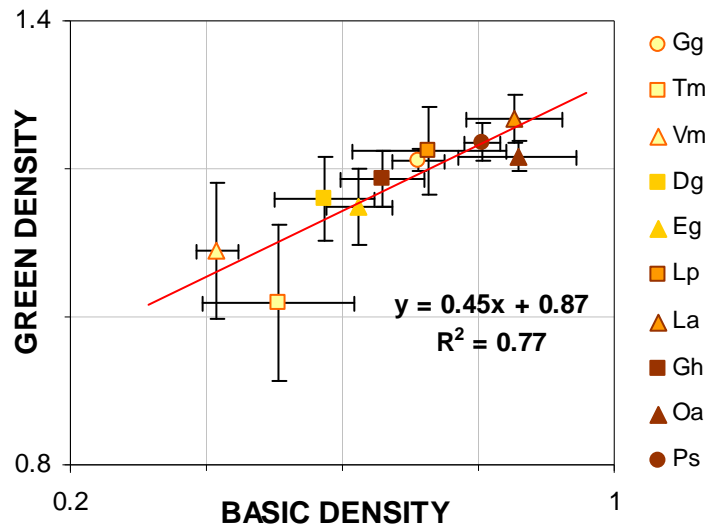


Figure A-26: Relationship between green density and basic density on specific mean values. See Figure A-25 for the caption.

6.2 MFA – Basic density

As we have seen in the 0-4.1, both structural parameters are considered to be independent. Figure A-27 shows that both parameters are indeed not related within species. However, when individual measurements for all species are considered, a slight negative correlation can be detected.

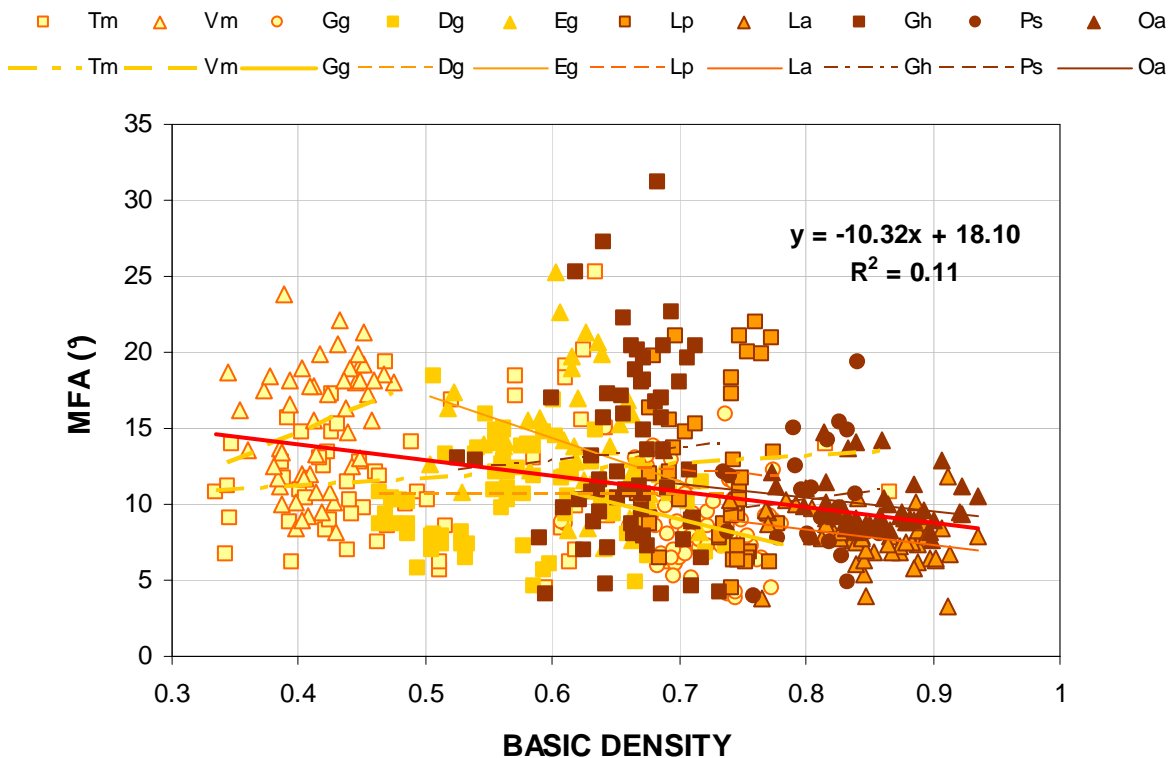


Figure A-27: Correlation between MFA estimates accounting for Yamamoto correction for density and basic density. Red line represents the regression line on the entire sample.

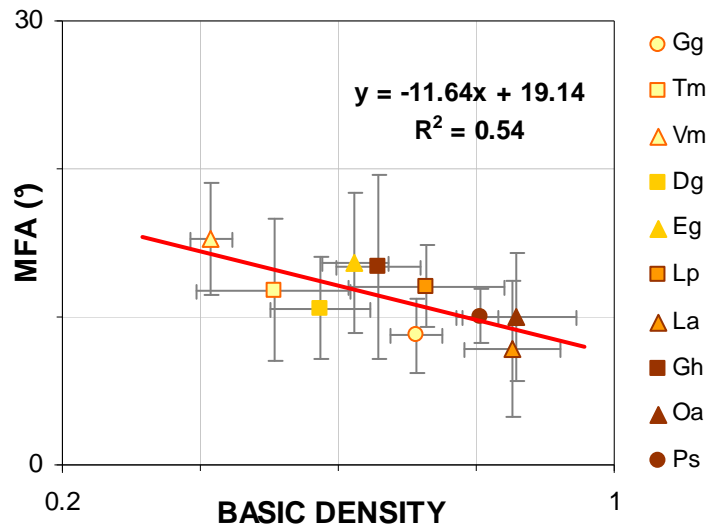


Figure A-28: Correlation between MFA-Yam and basic density on average specific values.

The analysis of the mean value of each species displayed in Figure A-28 shows that specific MFA and basic density are negatively correlated. However, results of Boiffin (2008) support the hypothesis of coincidental nature of the observed relationship. Boiffin (2008) has studied a larger sample of tropical species including seven of ten species used in the present study. Relationship between MFA and basic density obtained on this sample is represented in Figure A-29 and confirms that both parameters are not related.

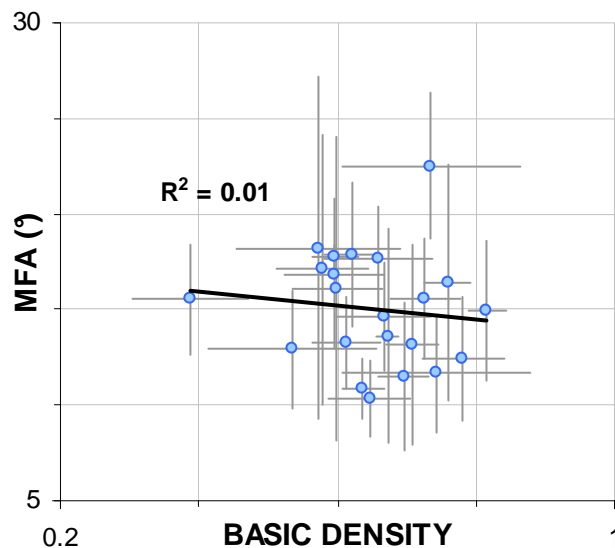


Figure A-29: Correlation between MFA estimates and density on a selection of 22 tropical species (Boiffin 2008).

The relation observed on our sample may be due to the fact that both selected high density species have also low MFA and the lightest species considerably higher MFA than others. Another parameter explaining this result could be the accuracy of MFA estimates. The use of X-ray method tends indeed to underestimate MFA of denser wood (Ruelle *et al.* 2007).

6.3 Structural determinants of elastic modulus

Young's modulus of a cellular solid is expected to be strongly related to its density. We have tried to verify this assumption on our sample. First, the green density was used to predict the Young's modulus. Obtained correlation is not very high as we can see from Figure A-30. This can be ascribed to different levels of saturation between species as explained in §6.1. Removing *T. melinonii* specimens, exhibiting particularly low saturation level, improves the correlation coefficient ($R^2 = 0.54$) however the use of green density to predict mechanical properties remains questionable. Conversely, basic density can be used as more reliable predictor of the Young's modulus despite the high variability of our sample (Figure A-31). We can also notice that the intercept of the regression line is close to zero as it should be the case for a cellular solid.

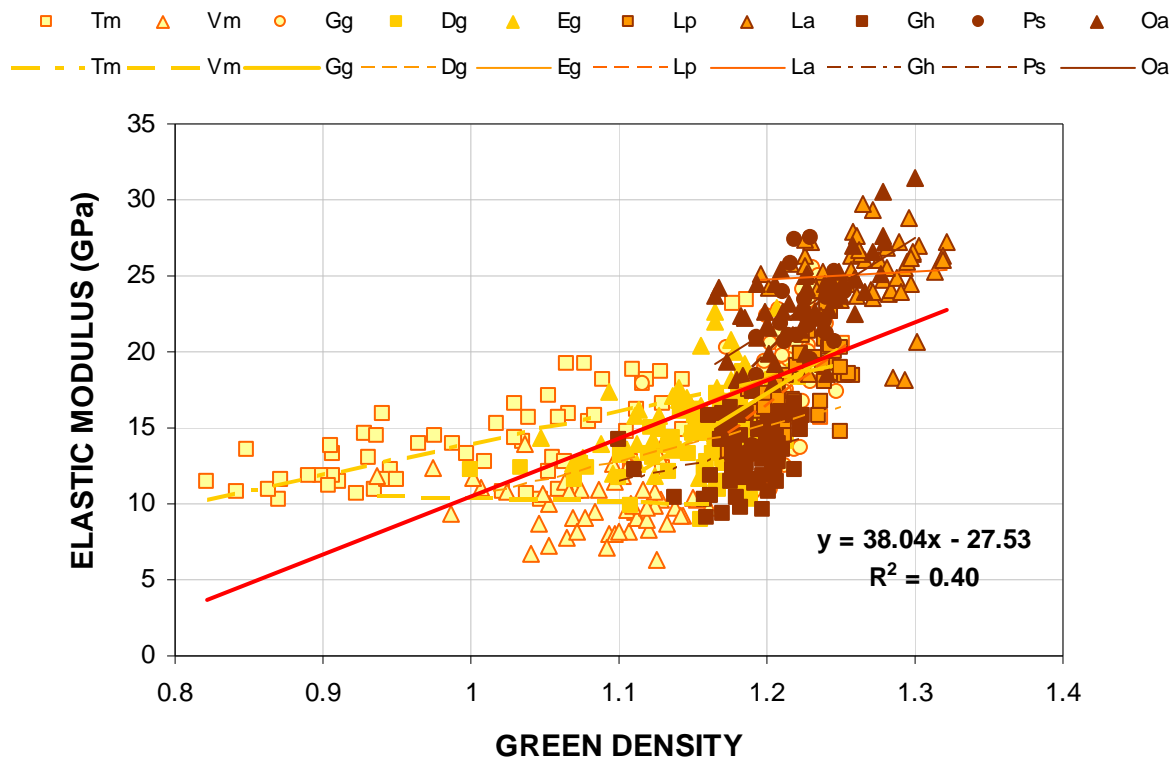


Figure A-30: Relationship between elastic modulus and green density. Red line represents the regression line on the entire sample. Red line represents the regression line on the entire sample.

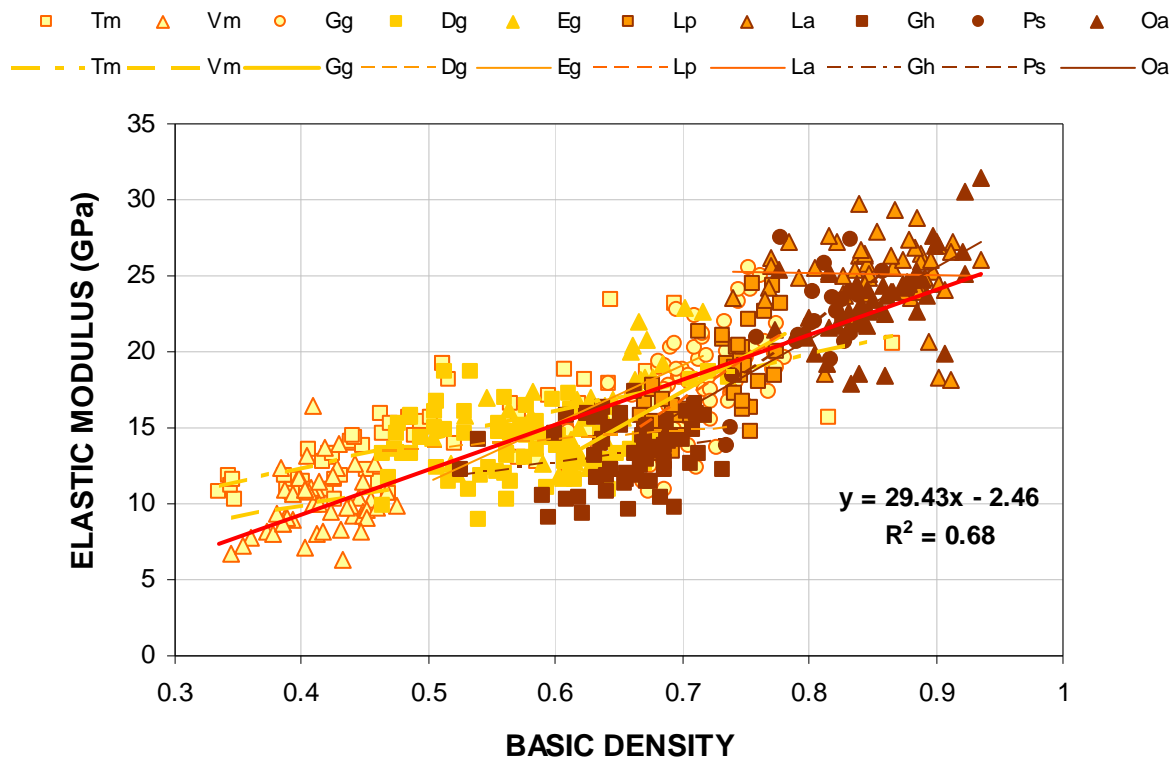


Figure A-31: Basic density as a predictor of the green Young's modulus.

We have shown that basic density can explain 68% of the variation of the stiffness over a wide range of inter and intraspecific diversity in wood quality. However, an important part of the elastic modulus variability remains unexplained.

6.4 Structural determinants of specific modulus

Whereas Young modulus of the wood is proportional to the density, the stiffness of the cell wall itself is independent of the amount of the cell wall. Specific modulus is mainly governed by microfibrils orientation as these represent the stiffest component of the cell wall material. These two assumptions can be verified on following figures (Figure A-32 and Figure A-33). No dependency can be detected between the specific modulus and density. On the other hand, the specific modulus is related to the MFA but the correlation coefficient is not very high. Large scatter of the specific modulus values is observed in particular for low MFAs. The observed scatter is probably related to the occurrence of tension wood specimens that could exhibit, apart of lower MFA, also different chemical composition. However, no case with high MFA and high specific modulus was observed indicating the validity of a relationship between the specific modulus and MFA. If mean specific values are considered, correlation coefficient is higher as we can see from Figure A-34. We can also notice different level of intraspecific variability between species comparing the error bars on the Figure A-34.

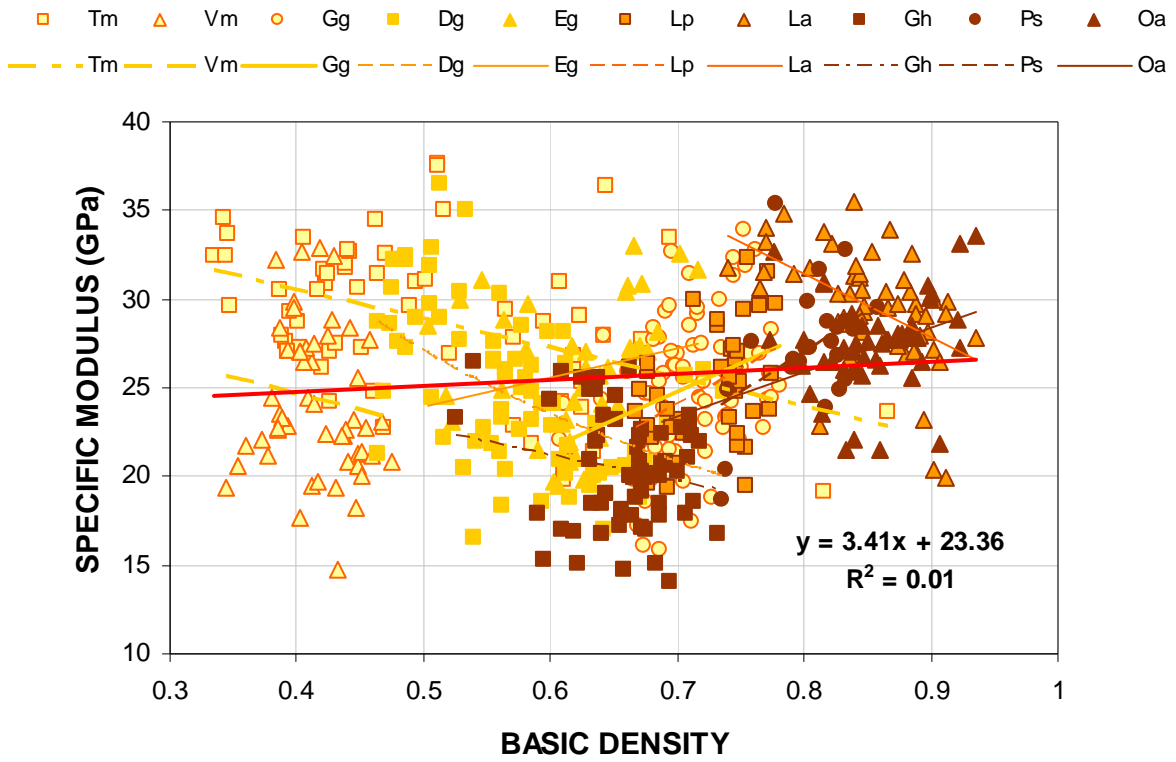


Figure A-32: Relation between the specific modulus and basic density.

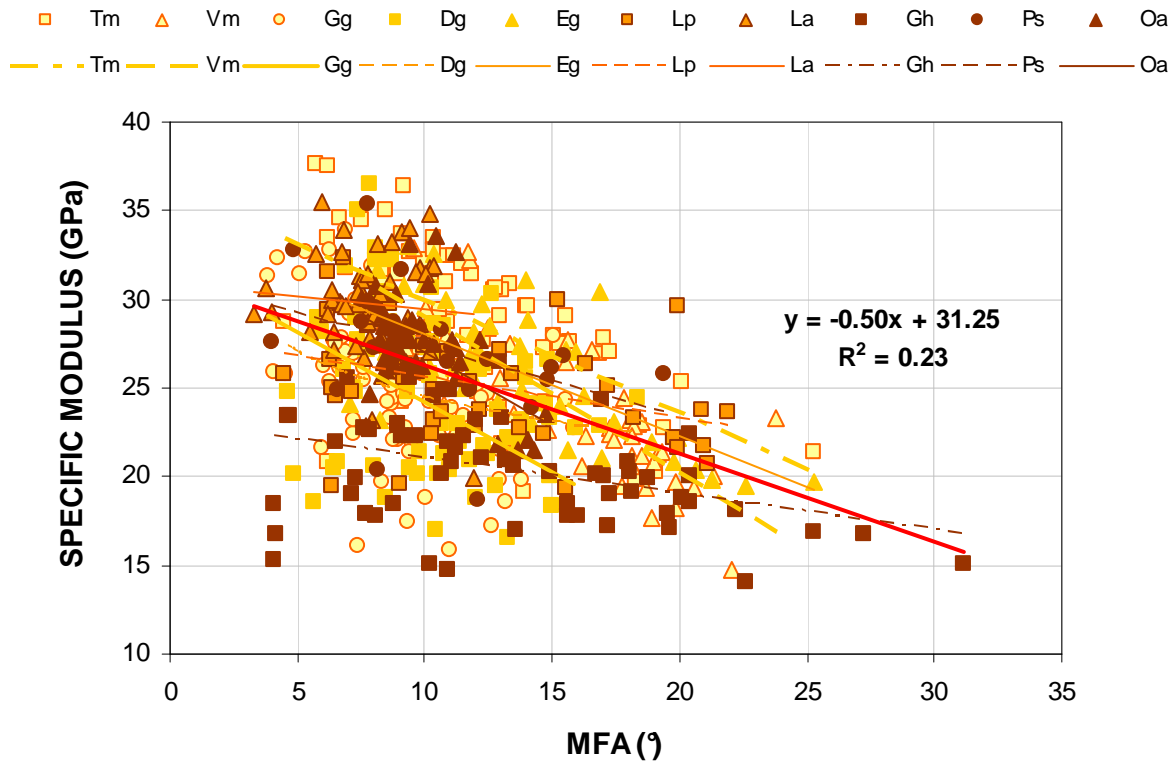


Figure A-33: Relationship between the specific modulus and microfibril angle.

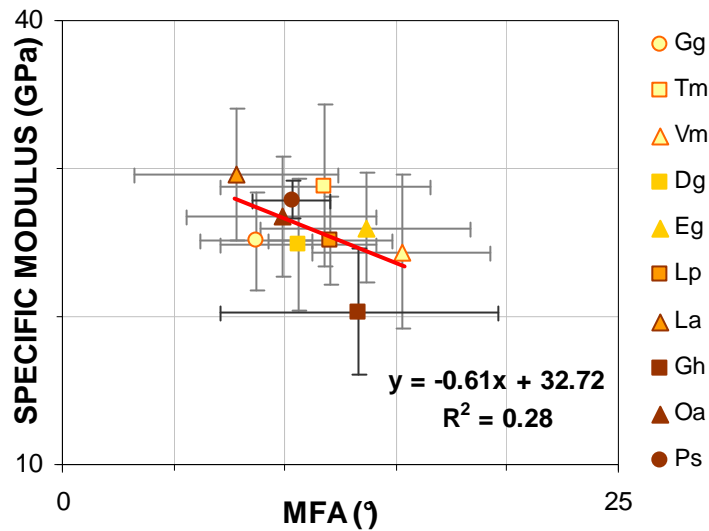


Figure A-34: Relationship between specific modulus and microfibril angle on mean specific values.

Based on assumptions detailed in §3.6.a, specific Young’s modulus is expected to be related to the cosine of MFA raised to the power four. Thus, we can obtain a rough estimation of the specific cell wall modulus along microfibrils computing $E/\rho/(\cos\theta)^4$ denoted further $E/\rho//$. Relationship between the specific modulus along microfibrils and MFA is shown in Figure A-35. No residual dependency of the specific cell wall modulus along microfibrils on the MFA can be observed supporting the validity of the simplification of the rotation formulae as tested in §3.6.a. The mean value of the specific cell wall modulus along microfibrils is about 29 GPa. However, there is a large scatter between the $E/\rho//$ values indicating that MFA is not the only parameter affecting the stiffness of the cell wall. The relationship between the cell wall specific modulus, its dependency on MFA and variability will be investigated in greater detail in §7).

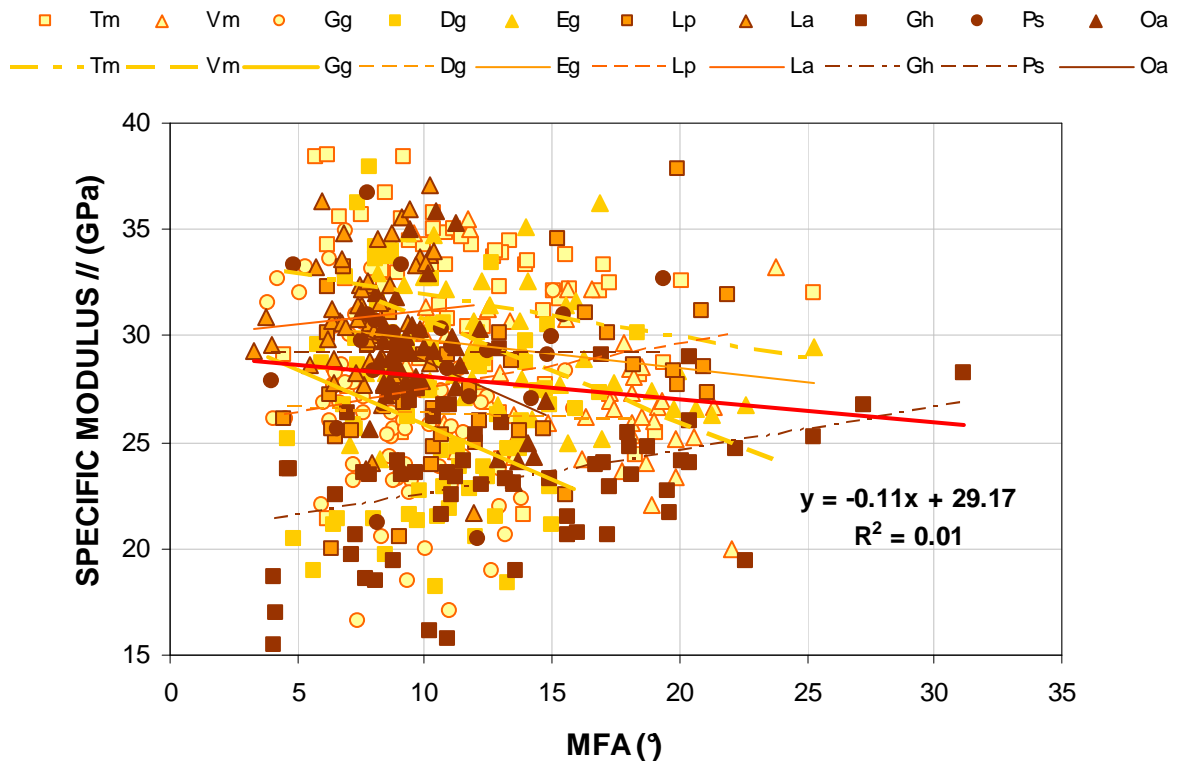


Figure A-35: Relation between the approximation of the specific cell wall modulus along microfibrils and MFA.

6.5 Structural determinants of damping coefficient

From its definition (damping = E''/E'), damping coefficient is independent of density. Conversely, a strong relation with MFA is expected as follows from the formulation of the mechanical model described in §3.6.b. Figure A-36 shows that damping coefficient is not related to basic density. However, no relationship has been detected between damping coefficient and MFA (Figure A-37) which was unexpected. This is mainly due to the large scatter of damping values. This can be affected, as already mentioned above, by the occurrence of tension wood specimens. Effect of the intraspecific diversity on the relationship between damping coefficient and MFA will be further discussed in 7.2.

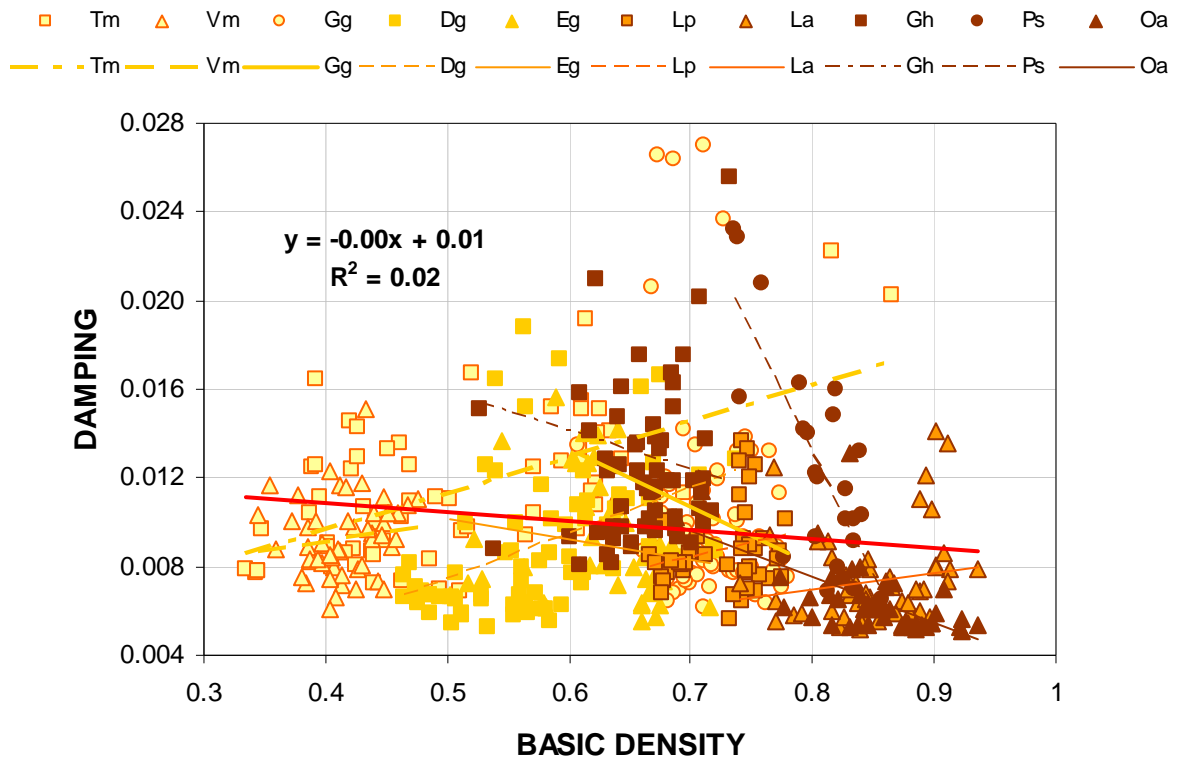


Figure A-36: Relationship between damping coefficient and basic density.

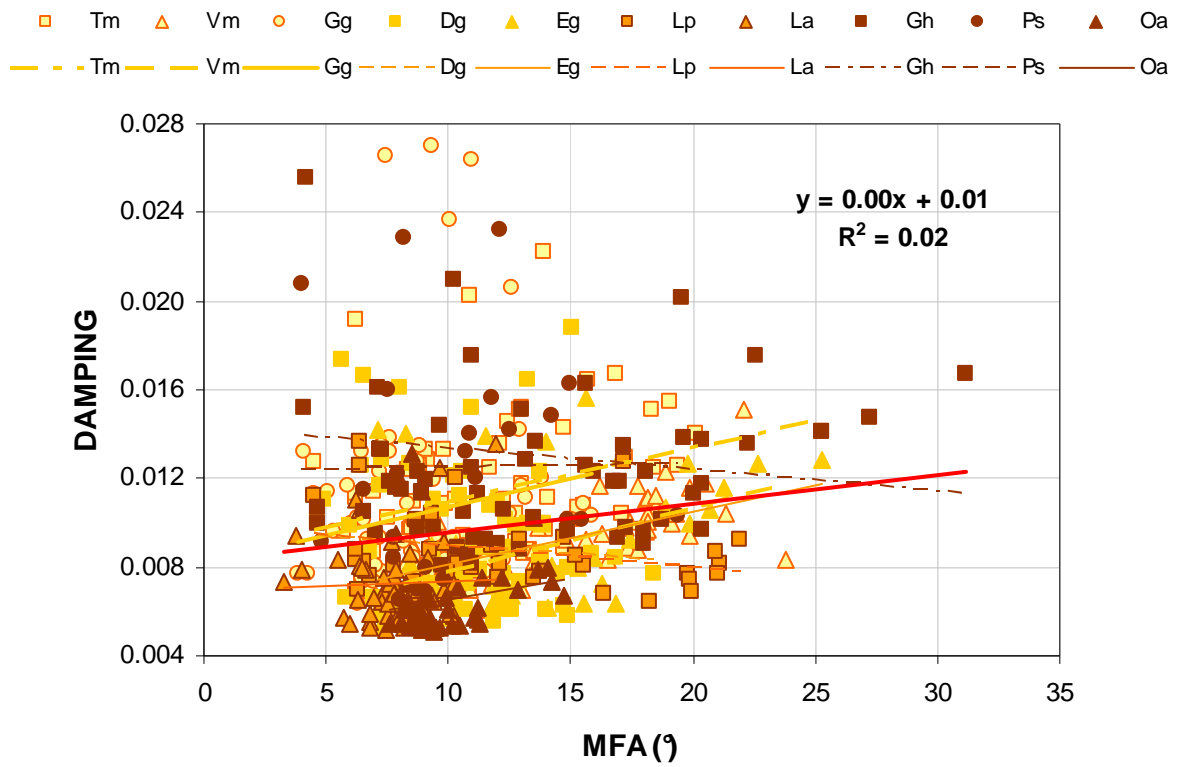


Figure A-37: Relationship between damping coefficient and microfibril angle.

In the previous paragraph, we have observed large residual variability of the specific cell wall modulus along microfibrils unexplained by the MFA effect. In order to investigate if this variability is related to the variability of the damping coefficient, we have plotted both parameters one against another (Figure A-38). No improvement of the correlation or decrease of the scatter was observed compared to the relation between damping coefficient and specific modulus along the fibre direction (Figure A-39). This supports the assumption that parameters affecting the second order variability of the specific modulus (once the MFA effect removed) and the variability of damping coefficient are not the same. The possible sources of the variability of damping coefficient will be analysed in the following chapter.

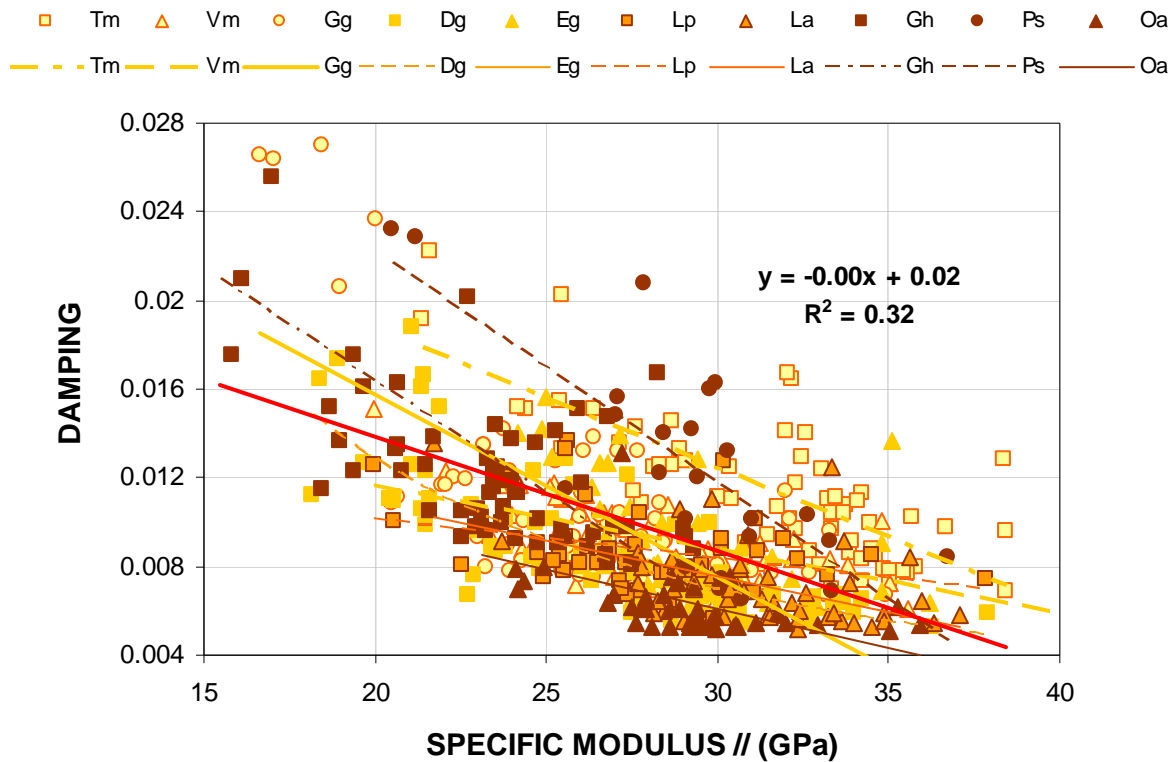


Figure A-38: Damping coefficient versus approximation of specific cell wall modulus along microfibrils.

Some previous works reported significant empirical correlation between damping coefficient and specific modulus (Ono and Norimoto 1984). This empirical relation was not linear but in the form of power law. Relation between both parameters along with the power law regression is represented in Figure A-39. We can observe a significant correlation between both parameters on the entire sample. Excepting *L. persistens* specimens, all intraspecific correlations are significant. This clearly indicates that there is a relation between the stiffness of the cell wall and damping coefficient. Thus, we face a paradox: specific modulus and damping coefficient are strongly related and at the same time the variability of the specific modulus is only partially explained by MFA and the variability of damping coefficient is totally independent of MFA. This result clearly indicates that other parameters than MFA exist and that affect at the same time the specific modulus and damping coefficient.

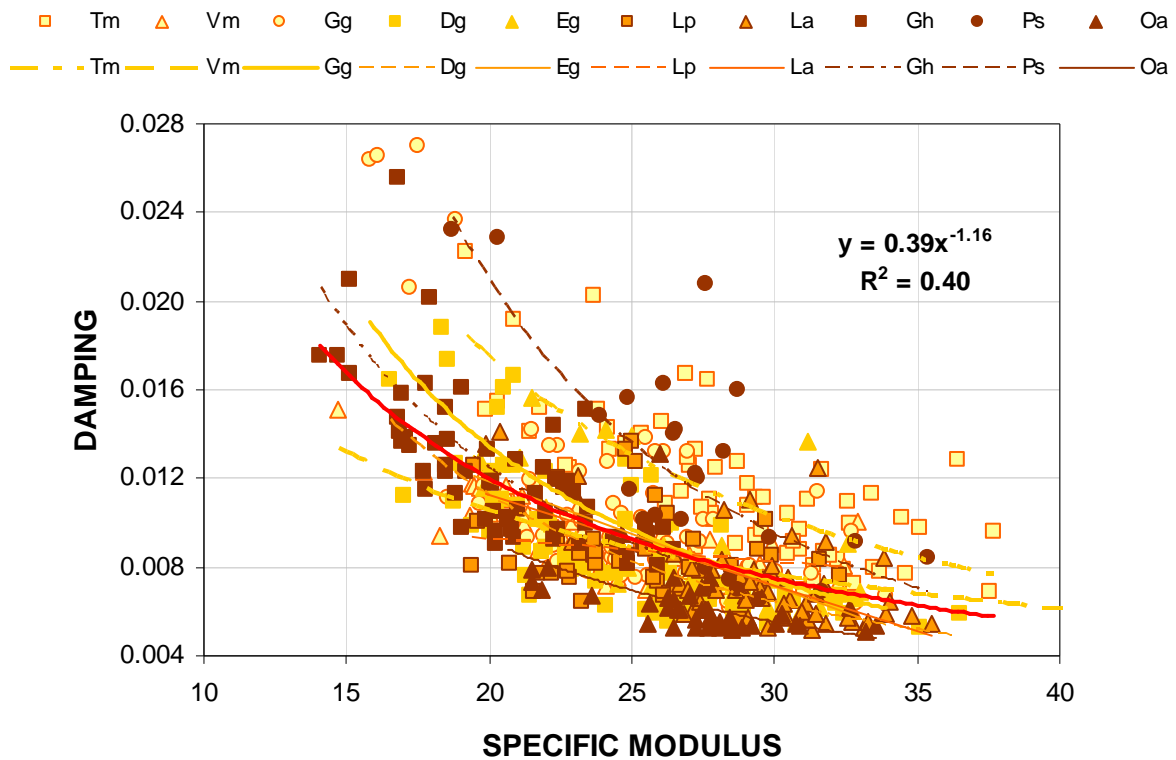


Figure A-39: Relationship between damping coefficient and specific modulus.

6.6 Conclusion

In this chapter, we have assessed the validity of some structure/property relations commonly used to predict the wood behaviour. The use of green density to predict the wood stiffness was rejected because of variable saturation level exhibited by specimens in the green state. On the other hand, basic density was well correlated with the Young's modulus despite the high variability of our sample. The specific modulus proved to be related to the MFA but for the specimens with low MFAs, a large scatter of specific modulus values was observed. This was ascribed to the occurrence of tension wood specimens exhibiting different structural features compared to normal wood. Once the effect of MFA was accounted based on a theoretical relation, the specific modulus along the microfibril was no more related to the MFA. Damping coefficient was independent of density as expected but proved also to be independent of the microfibril angle contradicting some previous reports (Norimoto *et al.* 1986; Brémaud 2006). This may indicate that the damping coefficient is affected by many other parameters such as chemical composition etc. and the MFA effect is of second order. Comparison of the residual variability of the specific cell wall modulus along microfibrils and the variability of the damping coefficient let think that the determinants of this variability are not the same in both cases.

7) Predicting cell wall properties from the wood properties and microfibril angle

After having studied statistical relationships between structural and mechanical properties and compared them to bibliographic data, we will now investigate the applicability of a mechanical model presented in §3.6. The main difference between these two sections is that adjusted model parameters have a physical meaning.

7.1 Capacity of the model to describe observed behaviour

Simple model developed to predict the properties of the cell wall from the properties of solid wood and microfibril angle was presented in §3.6. In the following, the capacity of the model to describe observed relationships is presented. Based on Eq. A-11, parameters a' and β' are adjusted by the least-square method to obtain the best fit with the experimental relationship observed between specific modulus and MFA. Obtained results together with adjusted parameters are shown in Figure A-40. We recall that parameter a' represents the real part of the Young's modulus, β' and β'' the ratios between the real and imaginary parts of shear and Young's moduli respectively and a''/a' stands for the damping coefficient of the cell wall material. Fitting of the parameters a' and β' has given the parameter β' equal to zero. This was attributed to the small effect of cell wall material shear modulus on the estimation of the wood Young's modulus as numerically tested in §3.6.a. In the next step, parameters a''/a' and β'' were adjusted to fit the relationship between damping and MFA. Obtained estimation of the damping coefficient of the cell wall material is reasonable however modelled relationship does not fit well with experimental data. This is due to the large scatter of damping values in particular for low MFA values. In the following, we will try to search for the sources of this variability.

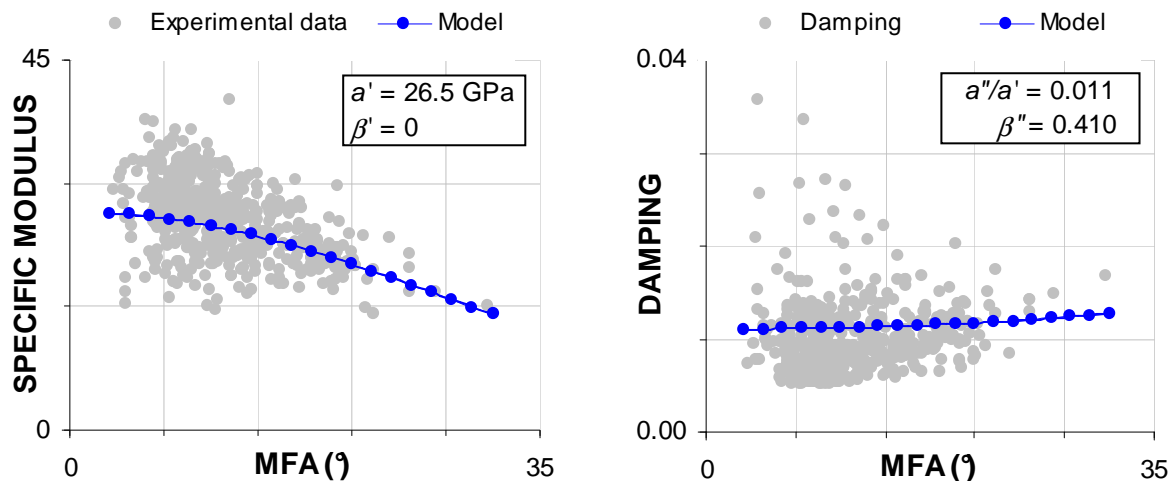


Figure A-40: Correspondence between experimental and modelled values of specific modulus and damping coefficient.

7.2 Variability of the properties between wood specimens from straight growing trees and wood specimens from tilted trees

As already mentioned, the occurrence of reaction wood may be responsible for the high variability of damping values. Therefore, we have split the sample in two groups separating specimens coming from straight growing and specimens from tilted trees. Specimens from tilted trees are supposed to be more variable because of the occurrence of tension wood. The results of the specific modulus fitting for both groups are displayed in

Figure A-41. We can note that dispersion of the specific modulus values is slightly higher for the specimens coming from tilted trees but adjusted model parameters are very close.

The situation is different for the damping – MFA relationship. First, we can note large scatter of damping values of the specimens from tilted trees compared to the specimens from straight growing trees. For specimens from straight trees, there is a significant relation between the damping coefficient and MFA which is reasonably well described by the model. For specimens from tilted trees, there is no relationship between the damping coefficient and MFA. Consequently, optimisation of model parameters yields a straight line. If the parameter β'' is not constrained to be positive, a negative valued is obtained by fitting. This has no physical meaning and proves that experimental data do not obey to the proposed mechanical model. It is interesting to note that the value of the parameter β'' obtained for normal wood is high showing a significant effect of the shear modulus on the damping coefficient conversely to its poor contribution to the Young’s modulus estimation.

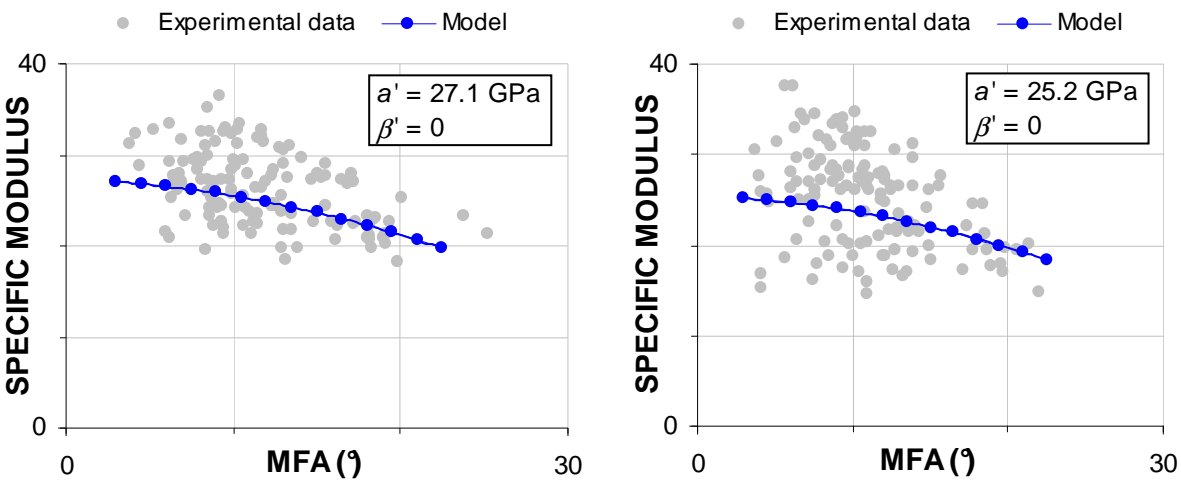


Figure A-41: Prediction of the specific modulus for wood coming from (a) straight growing and (b) tilted trees.

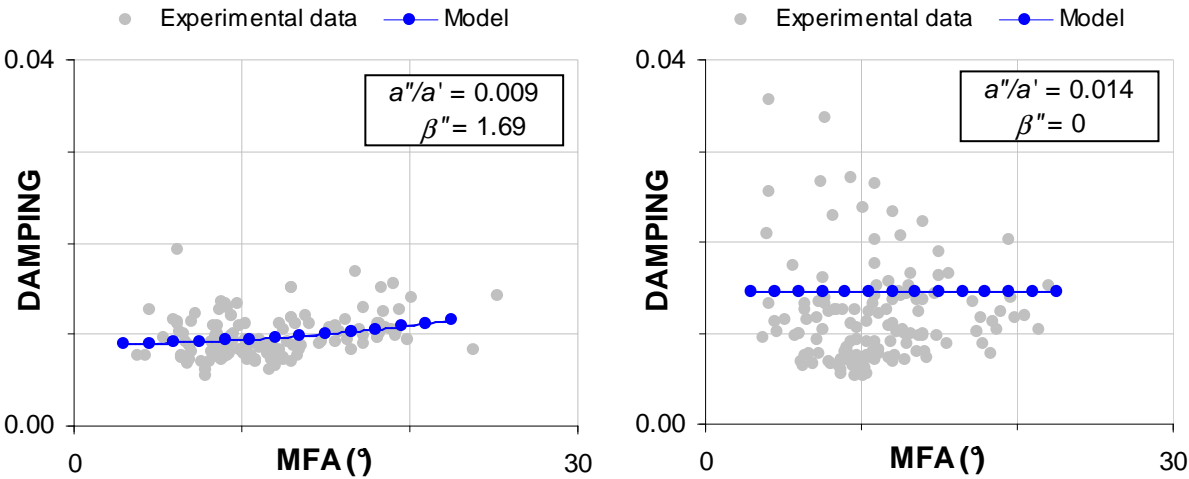


Figure A-42: Prediction of the damping coefficient for wood coming from (a) straight growing and (b) tilted trees.

Separate analysis of wood specimens coming from straight growing and tilted trees has evidenced that the intraspecific variability of damping coefficient is higher than the interspecific one. Proposed model was able to describe correctly the properties of normal wood of all ten species while the occurrence of tension and opposite wood, responsible for the

high variability of studied parameters makes it difficult for the prediction based on the MFA. This clearly shows that besides the variation of MFA, other parameters change significantly in tension and also in opposite wood and that affect the viscoelastic response, at least at short observation times.

7.3 Cell wall properties along microfibrils

Based on Eq. A-14 and A-15, we have predicted the cell wall properties of each specimen using mean values of parameters β' and β'' for each group (straight and tilted trees). The aim was to see if there is a significant difference in the cell wall properties along microfibrils in function of wood types. Specific modulus and damping coefficient of the cell wall along microfibrils for both groups are shown in Figure A-43. It confirms that the variability of specimens with occurrence of tension wood is significantly higher but also the mean values seem to be different. Surprisingly, the mix of opposite and tension wood exhibits in average lower specific modulus and higher damping coefficient.

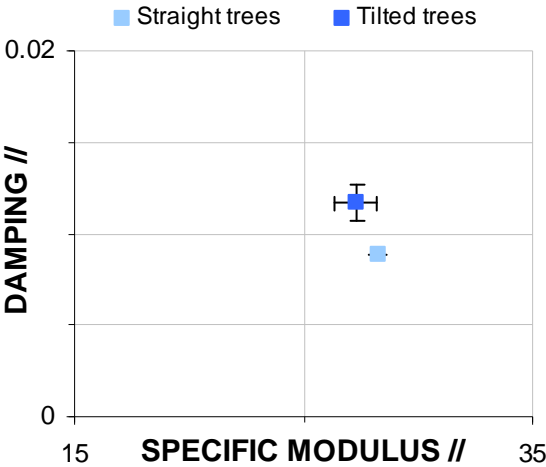


Figure A-43: Specific cell wall modulus and damping coefficient of the cell wall along microfibrils for wood coming from straight growing and tilted trees. Error bars represent the confidence interval for the mean estimation with 95% probability level.

8) Interspecific and intraspecific variability of vibration properties

In the previous chapter, we have seen that wood coming from tilted trees exhibited markedly higher variability than wood coming from straight growing trees. In the following section, we will investigate the differences between studied parameters in function of the wood type *i.e.* normal wood, tension wood and opposite wood. As explained in §2.3, for some species we are not sure about the designation of tension and opposite wood. The following species are concerned: *Eg, La, Oa, Vm*. For this reason, raised conclusions have to be taken with precautions.

8.1 Screening of intraspecific variability by species

Wood types differ essentially by the level of pre-stresses resulting from different growth conditions of a tree. Pre-stresses in normal wood help a straight growing tree to support the weight of its crown and increase the bending resistance of the stem. Opposite and tension wood tissues are usually produced by tilted trees. Thus, they represent a sort of reaction or traumatic tissues. Tension wood is formed on the upper side of leaning trees or branches. High tensile stresses induced during the maturation process tend to up-right the stem to the vertical position. On the opposite side, the level of pre-stresses is very low, in general slightly lower compared to normal wood. Based on mechanical definition using the

level of pre-stresses to differentiate the wood types, we may expect a gradient of mechanical properties and structural features going from the opposite through the normal to the tension wood.

Figure A-44 shows the interspecific and intraspecific variability of basic density. Error bars in the following graphs correspond to the confidence interval (95% probability level). We can note that intraspecific variability is negligible relative to the interspecific one.

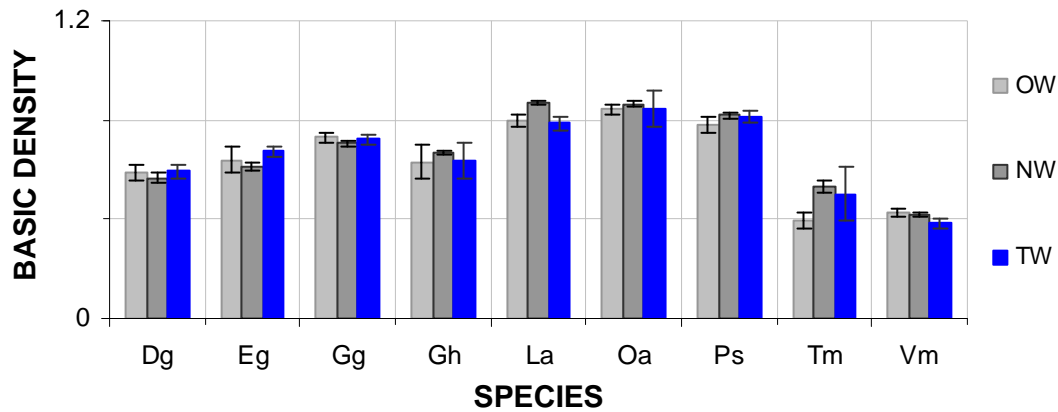


Figure A-44: Variability of basic density in function of species and wood type.

Second parameter investigated is the elastic modulus. Essentially, we can make the same observation as for the basic density: the interspecific variability is predominant. Further, no systematic effect of the wood type can be detected.

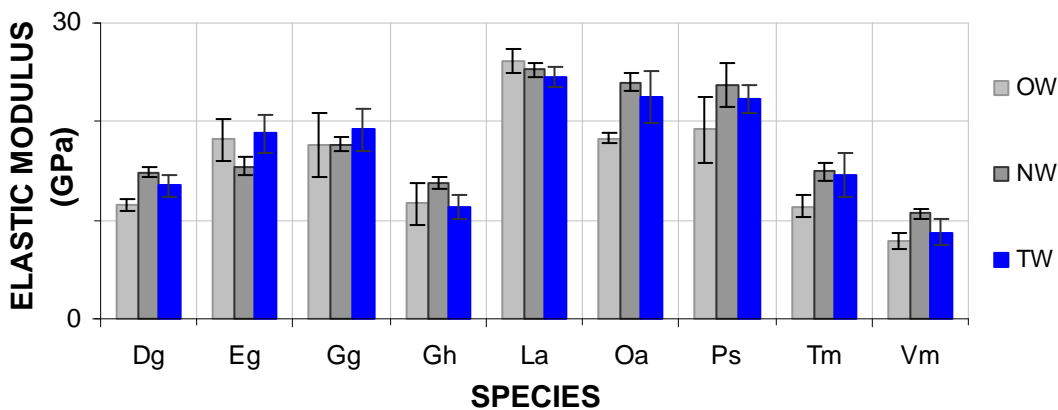


Figure A-45: Variability of elastic modulus in function of species and wood type.

Removing the effect of density results in reduced interspecific variability of mechanical properties as shown in Figure A-46. Conversely, the intraspecific variability has not been affected.

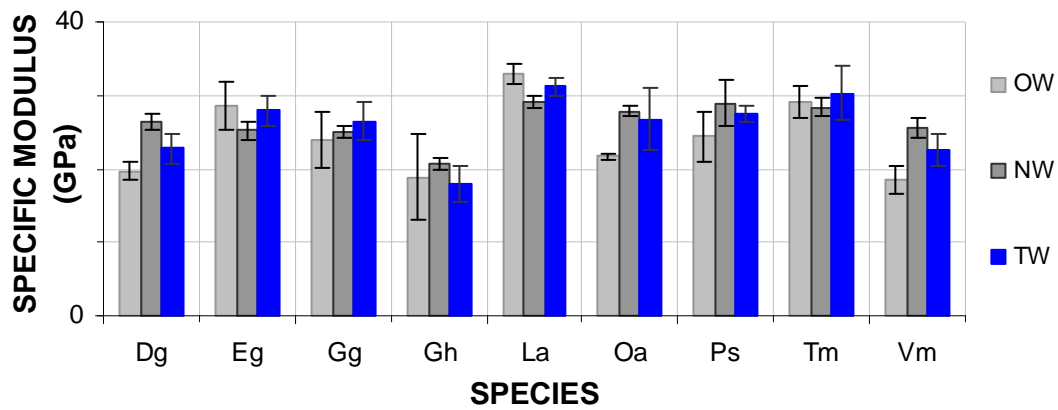


Figure A-46: Variability of specific modulus in function of species and wood type.

Specific modulus represents the stiffness of the cell wall which is expected to be strongly related to the microfibril angle. Thus, the variability of MFA should exhibit inverse variations compared to the specific modulus. Comparing Figure A-46 and Figure A-47, we can observe that such a correlation is verified for the interspecific variations. This was already shown in Figure A-33. Intraspecific variability of the specific modulus does not follow systematically the MFA one. Moreover, tension wood exhibits systematically lower MFA than opposite wood however the relation with normal wood specimens is not straightforward.

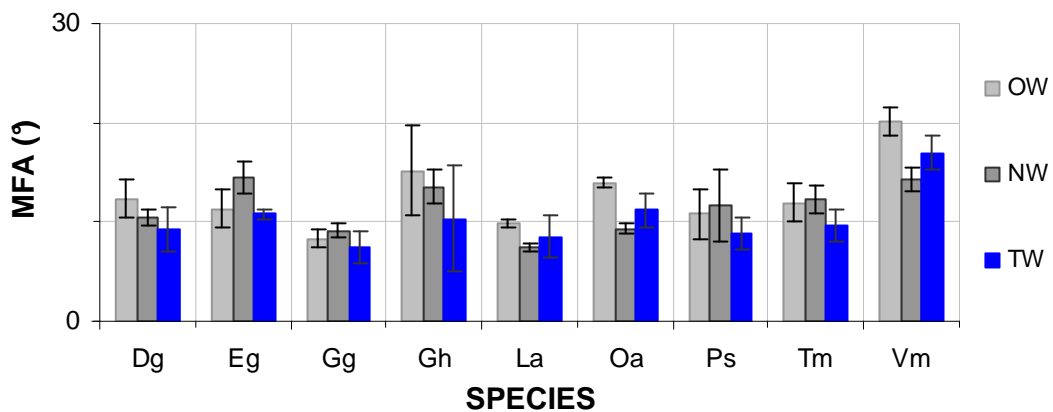


Figure A-47: Variability of microfibril angle in function of species and wood type.

Variability of the damping coefficient is shown in Figure A-48. For the most, damping coefficient of opposite and tension wood is higher than that of normal wood.

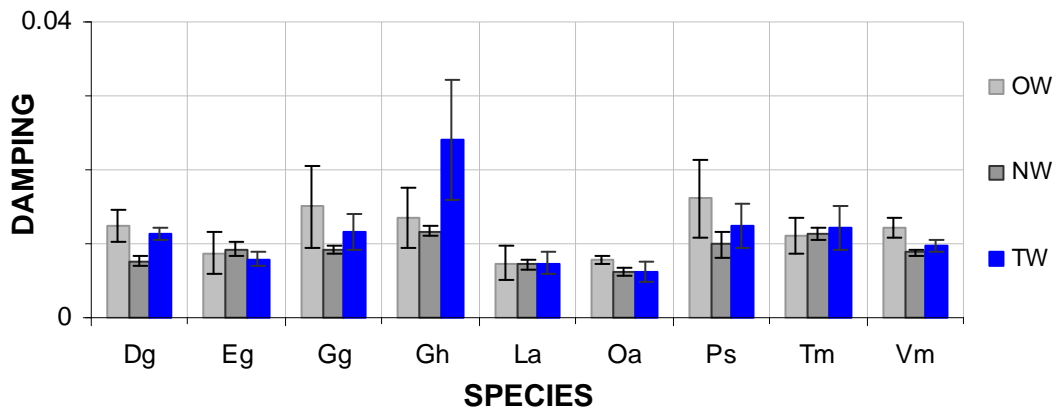


Figure A-48: Variability of damping coefficient in function of species and wood type.

From mechanical point of view, damping coefficient is expected to be related to the microfibril angle. In the §7.2 we have seen that for wood specimens coming from tilted trees, this relation was not verified. Thus, we have plotted the mean damping coefficient against the mean MFA in function of the wood type. As we can see from Figure A-49a, intraspecific variability of the damping coefficient can not be explained by the microfibril angle variations because tension and opposite wood clearly exhibit the same damping coefficient regardless different MFA.

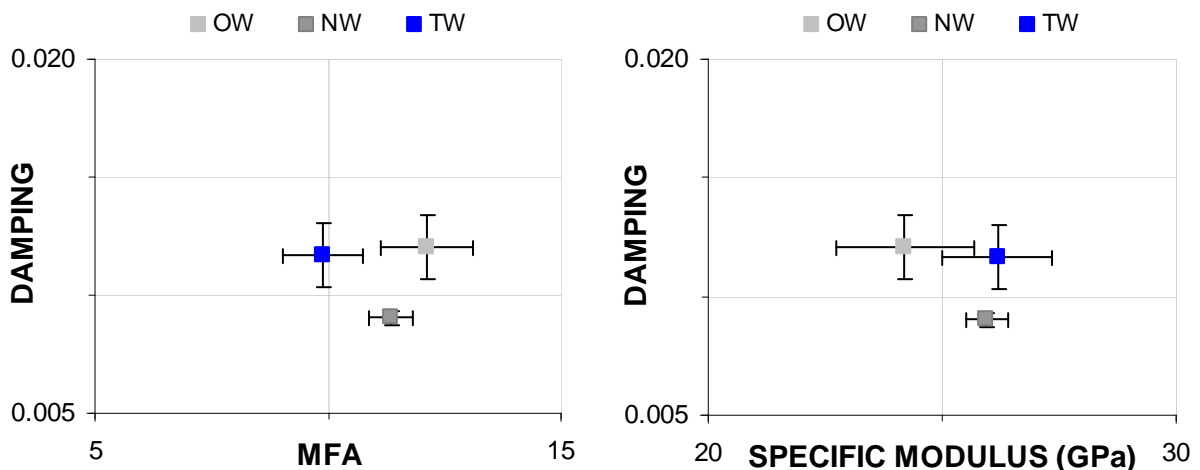


Figure A-49: (a) Relationship between damping coefficient and MFA depending on the wood type. Error bars represent the confidential interval for the probability level of 95%. (b) Relationship between damping coefficient and specific modulus in function of the wood type.

Figure A-49b shows the relation between damping coefficient and specific modulus in function of the wood type. First observation is that the variability of both reaction tissues (opposite and tension wood) is considerably higher compared to normal wood. Opposite wood and tension wood exhibit the same damping coefficient despite different specific modulus and which is higher than that of normal wood. This may indicate a common origin of this property that may be not linked to structural features but to the loading history of these tissues. Reaction tissues are submitted to large bending moments because they are produced by tilted stems that they try to pull up to the vertical position. Thus, they work more than tissues of straight growing trees resisting mainly to the compression loads due to the weight of a tree crown. Intensive and repetitive loading of reaction wood tissues may lead to their fatigue and damage of the microstructure resulting in micro-cracks. Micro-cracks would dissipate more energy thus leading to higher damping coefficient. This phenomenon was

already suggested to explain higher damping of oven-dried specimens relative to air-dried ones. In this case, micro-cracks would not be caused by anisotropy of shrinkage of different cell wall layers but by a sort of fatigue of wood tissues due to the intensive loading history.

While the high damping coefficient of opposite wood is understandable because of its low specific modulus and the hypothesis of micro-cracks resulting from the mechanical fatigue, high damping coefficient of tension wood is not fully explained by this assumption. Higher specific modulus of tension wood should result in lower damping coefficient relative to the opposite wood. Also information that we have about the structural arrangement of wood fibres with G-layer (steep MFA angle) and its chemical composition (higher crystallinity, higher cellulose content and lower lignin and hemicelluloses content according to (Sugiyama *et al.* 1993; Fang *et al.* 2008)) let think that the damping coefficient of such tissues will be lower than that of normal wood. The fact that it does not correspond to our observation could be explained by the fact that the effect of mechanical fatigue is prevailing and dominates the difference that would issue from different specific modulus. Nevertheless, we have also keep in mind the diversity of the reaction wood structures and properties because the above mentioned arguments are valid only for the tension wood exhibiting G-fibres.

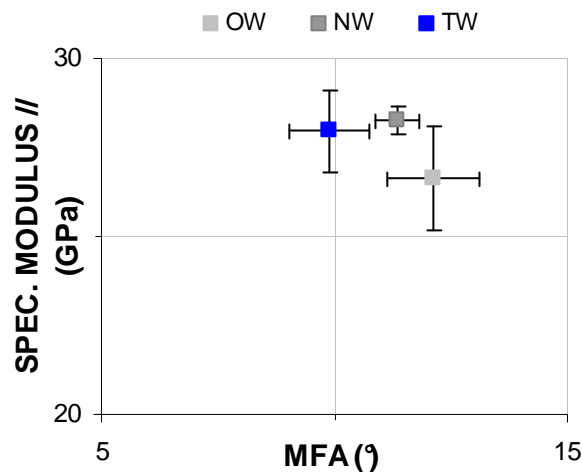


Figure A-50: Relationship between specific modulus along microfibrils and MFA in function of the wood type.

It is also interesting to note that specific modulus of the cell wall along microfibril is markedly lower in opposite wood compared to other wood types (Figure A-50). This indicates that some chemical changes or structural changes other than MFA have to occur in this tissue which definitely differs from normal wood.

8.2 Anatomical structure as a possible determinant of vibration properties

Percentage of different wood elements – fibres, vessels and radial and axial parenchyma – were measured on a part of the sample G1 (see §2.2 for details). The possible link between anatomical structure and vibration properties was investigated. Table A-4 summarises the correlation coefficients for relations between the percentage of wood tissues and mechanical properties. Basically, we can see that there is no correlation between mechanical properties and percentage of different wood tissues. Significant correlation between elastic modulus and percentage of radial parenchyma is likely due to the correlation between MFA and radial parenchyma. Once the effect of MFA accounted based on the theoretical equation (specific modulus //), no correlation can be observed with the percentage of radial parenchyma. It is interesting to note, however, that there is a strong relation between

the percentage of axial parenchyma and other anatomical elements (fibres and radial parenchyma).

Table A-4: Matrix of correlation coefficient between vibration properties and anatomical parameters

	<i>Elastic modulus</i>	<i>Specific modulus</i>	<i>Specific modulus//</i>	<i>Damping</i>	<i>Basic density</i>	<i>MFA</i>	<i>Fibres (%)</i>	<i>Radial par. (%)</i>
<i>Elastic modulus</i>	1							
<i>Specific modulus</i>	0.45	1						
<i>Specific modulus//</i>	0.30	0.95	1					
<i>Damping</i>	-0.37	-0.61	-0.55	1				
<i>Basic density</i>	0.87	-0.02	-0.19	-0.08	1			
<i>MFA</i>	-0.66	-0.55	-0.28	0.42	-0.45	1		
<i>Fibres (%)</i>	0.22	0.07	0.06	0.02	0.22	-0.04	1	
<i>Radial par. (%)</i>	-0.59	-0.32	-0.13	0.29	-0.56	0.66	-0.18	1
<i>Axial par. (%)</i>	0.23	0.16	0.03	-0.23	0.22	-0.45	-0.61	-0.66
<i>Vessels (%)</i>	0.15	0.09	0.10	0.01	0.08	-0.05	-0.21	0.35

Legend: Specific modulus //: specific modulus along microfibrils; Radial par.: percentage of radial parenchyma; Axial par.: percentage of axial parenchyma.

8.3 Conclusion

Analysis of the variability of measured parameters has confirmed that basic density explains the most of interspecific variability of the elastic modulus. Interspecific variability of the specific modulus is related to the MFA variability however this parameter is not always relevant when the intraspecific variability of the specific modulus is considered. Difference in specific modulus of tension and normal wood can be explained through the MFA variations while the specific modulus of the cell wall along microfibrils is significantly lower for opposite wood. Considering the wood type dependency on MFA, tension wood specimens exhibited lower MFA compared to opposite wood. Variability of the damping coefficient is only little explained by the variations in MFA. We have shown that if wood types are considered separately, tension wood and opposite wood exhibit similar damping coefficient regardless different MFA. Moreover, damping coefficient of both tissues reaction tissues is similar despite different specific modulus and higher than damping coefficient of normal wood. It was hypothesised that mechanical fatigue due to intensive loading of reaction tissues could explain the observed phenomenon. Definitely, opposite wood should not be confused with normal wood but considered as a sort of reaction wood along with tension wood as previously suggested by Clair *et al.* (2006). No significant relationship was found between mechanical properties and percentage of different wood tissues. This indicates that the origin of the variability of viscoelastic properties is not determined by anatomical structure. Consequently, we should search the parameters to explain the observed variability on different probably chemical level. Gain an insight into the properties and structure of opposite wood seems also essential to explain the observed intraspecific variability and understand its origin. Analysis of the structure/property relations will be continued in the part B of the manuscript dealing with creep properties.

B) LONGITUDINAL CREEP OF GREEN WOOD

1) Development of the creep device and testing procedure

In creep studies, the test pieces are usually loaded in bending because of the larger displacement developed in bending compared to tensile or compressive strains. Therefore, it is easier to obtain the required accuracy for investigating the creep behaviour. However, the interpretation of bending results is based on the assumption of identical behaviour of wood in compression and tension. This assumption is not necessarily satisfied in the case of specimens with tension wood occurrence. Moreover, to our best knowledge, no evidence exists on the fact that a loading (tensile) gradient has no effect on the creep response of polymers. That's all the more true for creep of wood sample. We decided then to perform tensile creep tests.

Conducting tensile creep tests on green wood in longitudinal direction is rather difficult because of the severe environment (humidity, temperature, test duration) and very low level of creep strain developed during tensile tests along fibres: 15-20 $\mu\text{m}/\text{m}$ during first 1000s and 10-20 $\mu\text{m}/\text{m}$ during the following 7h of the test if the sample remains in the linear domain. Consequently, the time necessary to solve all experimental problems such as an accurate conditioning, choice of transducers, choice of specimen's geometry and fixation in the creep device as well as development of the experimental procedure was quite long and only a small selection of specimens could be finally tested.

1.1 Tensile creep device

Creep tests were performed on a tensile device designed by Hunt (Hunt and Darlington 1978). Hunt's device was developed for conducting creep tests in the hygroscopic region so that many modifications had to be performed to enable testing of green wood.

For creep tests in general, accurate control of test conditions (humidity and temperature) is essential. Thus, the creep device was equipped with a water bath to enable the tests on green wood specimens (Figure B-1c). The temperature of the bath was controlled by a thermo-regulator with an accuracy of $\pm 0.1^\circ\text{C}$. Capacitive transducers previously used by Hunt for strain measurement could not work in water. We have tried to design a lever-arm system to ensure (and amplify) the strain signal transmission out of the bath. This approach was not successful because of unsatisfactory precision of the system. Finally, we decided to use a pair of strain gages glued with cyanoacrylate on each side of the specimen. The accuracy of strain gages is satisfying. 3-wires gages were used to correct changes in the lead wire electrical resistance with fluctuations of the room and bath temperatures. The risk of gage detachment was reduced by silicon coating which limited the disturbances of the gage output due to water currents. Nevertheless, detachment did occur during some tests, decreasing the number of valid creep tests.

Tensile loads were applied manually by means of weights coupled to the specimens through a lever-arm system. The applied load corresponded to an instantaneous elastic axial strain of about 500 $\mu\text{m}/\text{m}$; far below the limit of linearity generally estimated around 1500 - 1800 $\mu\text{m}/\text{m}$ for wood subjected to the tensile stress along the grain (Hunt 1988). Strain signal of both gages was recorded by a Wheatstone bridge. The frequency of data acquisition was of 10Hz during the first 1000s after the loading and reduced to 1Hz afterwards. Data obtained by both gages were averaged and smoothed to reduce the noise effects on the measurements.

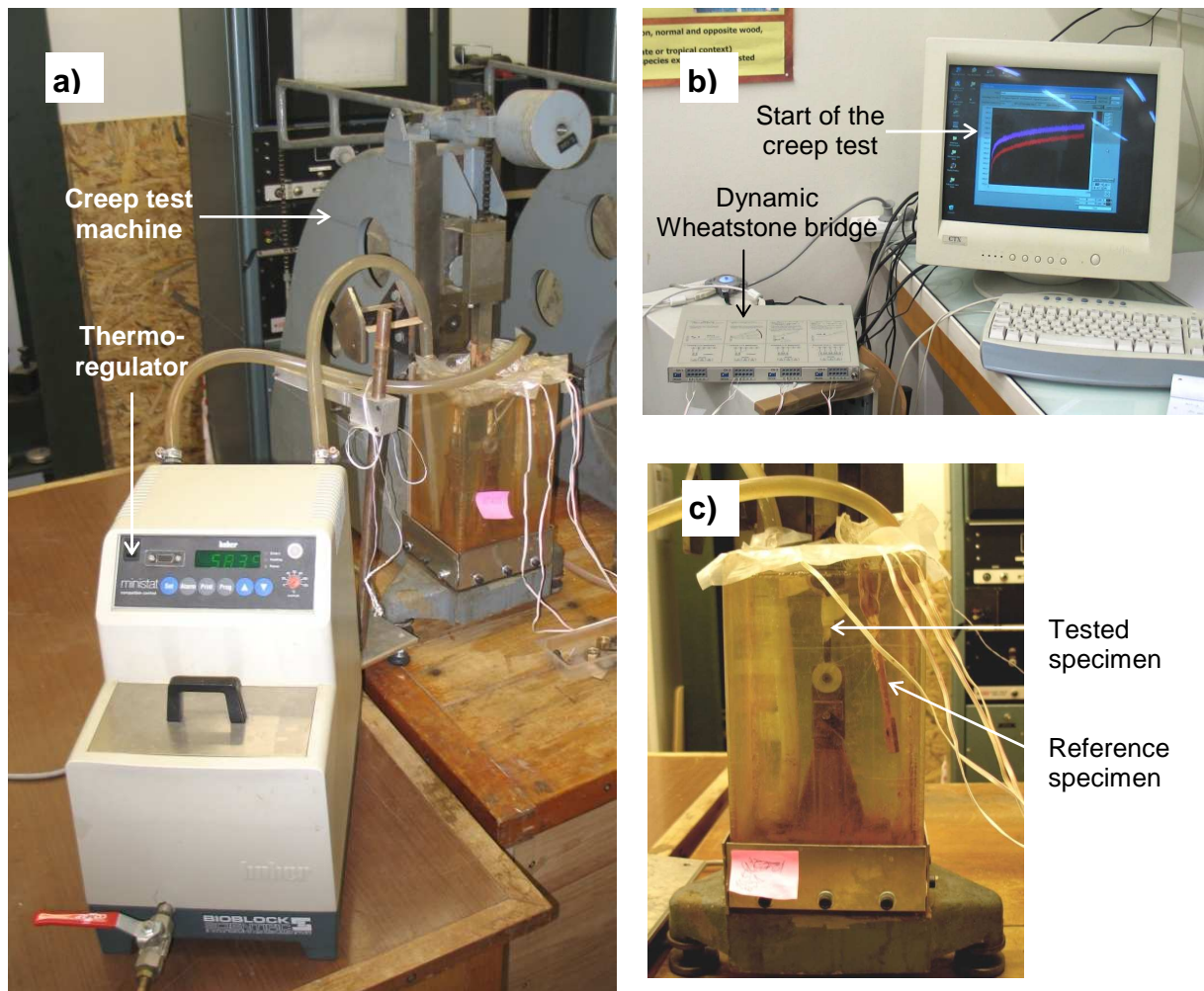


Figure B-1: Creep testing device. (a): Whole experimental equipment. (b): Recording of strain signals by Wheatstone bridge and transmission to the computer. (c): Detail of specimens in the thermo-regulated bath.

1.2 Creep specimens

Specimens previously measured by vibration method were used for the preparation of the creep specimens ($100 \times 6 \times 2 \text{ mm}^3$; L, R, T) so that both measurements are well matched. Because of the small width of the damping specimen, it was not possible to cut a whole creep specimen in one piece of wood. Thus, the damping specimen was shortened, bone-shaped (see Figure B-2) and equipped by additional heads. The removed part was used for the analysis of anatomical structure. The reduced width of the central part allowed us to decrease the applied load: because of the high rigidity of tropical species, it was difficult to ensure efficient transmission of axial loads without damaging the specimen.

Both ends of the bone-shaped specimen were provided by heads and fixed using MDI (methylene-diphenyl-diisocyanate) glue for green wood of the Japanese manufacture Daiichi Deiyako. During the gluing, specimen was hold in the fixture represented in Figure B-3 ensuring accurate position of the specimen and of the heads. The specimen was kept in the fixture for one hour to allow the glue to polymerise before moving to the drilling operation. It has been shown that free rotation of specimen heads enables the central part to distort and the resulting strain field is not affected by boundary load conditions. Hence, a 11mm hole was machined through the heads and a sphere-groove like joint made of brass was fixed in each hole. Further, additional clamps were used to improve the transmission of axial loads between the heads and tested specimen as shown in Figure B-2c.

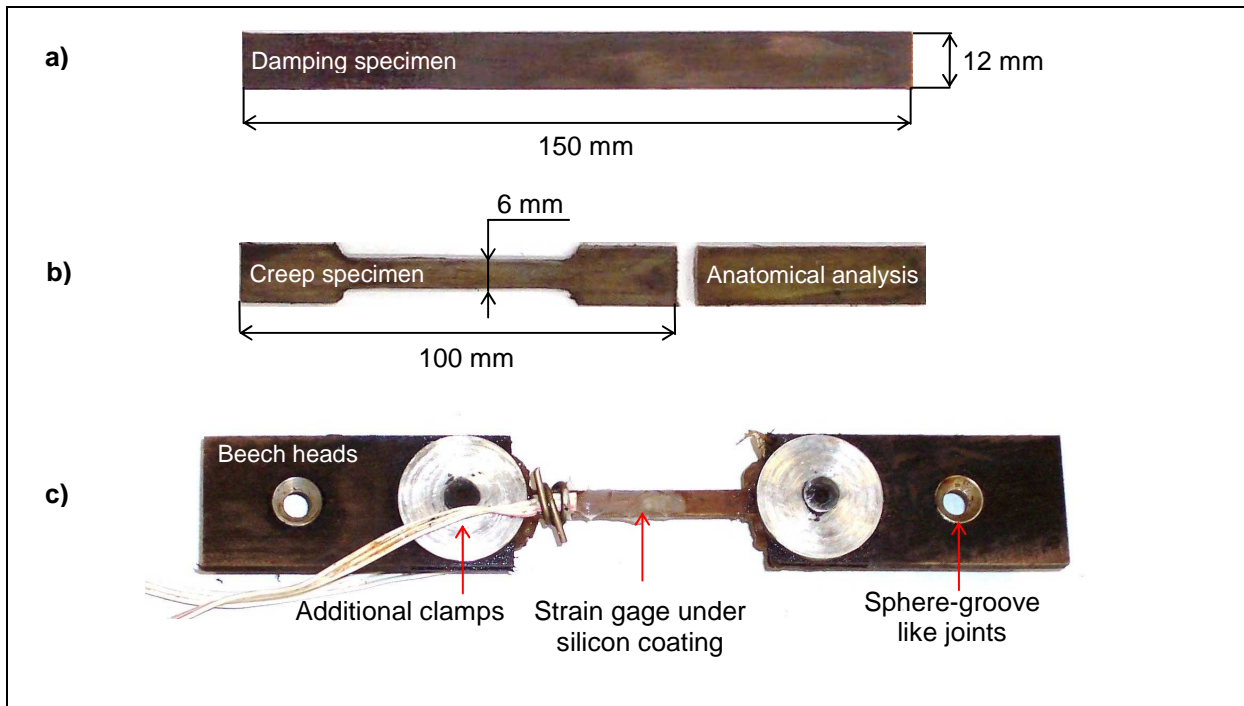


Figure B-2: Preparation and shape of the damping and tensile creep specimens. (a): Damping specimen used for the preparation of the creep specimen. (b): Creep specimen after machining. Remaining part was used for anatomical analysis. (c): Final instrumented creep specimen.

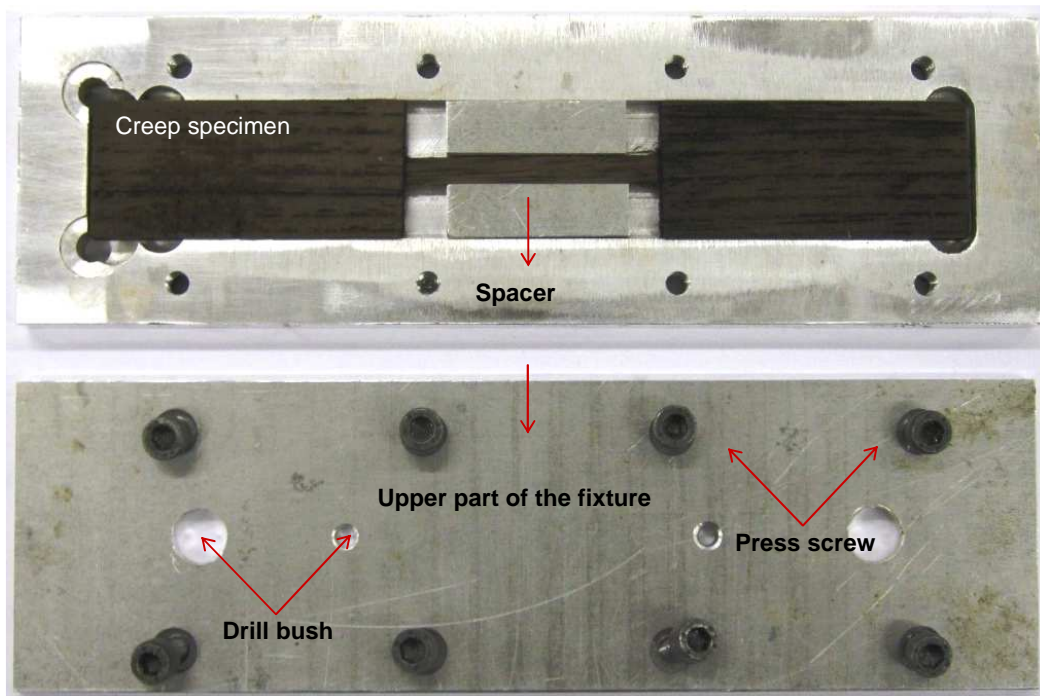


Figure B-3: Fixture used for accurate positioning of the specimen during gluing and drilling operations.

Finally, strain gages were glued on the specimen using cyanoacrylate glue (commercial name: Loctite) and covered by silicon. During the silicon hardening (at least 1-2 hours), the specimen was kept in a permanent bag wrapped in a piece of wet tissue because immediate immersion would increase the risk of gage detachment. Some tests with waterproof gages were also performed giving satisfying results but we decided not to use them because they are quite expensive. The creep behaviour of the cyanoacrylate glue was tested by Olsson *et al.* (2007). During creep tests on glass fibres, no strain was observed at 30°C and relative humidity varying from 30% to 80%. Furthermore, Hayashi *et al.* (1993) have performed tests of several glues used for strain gages and has found that cyanoacrylate

glue was stable at 20°C and 30% of RH but exhibited some variations at higher relative humidity (85%) or during random humidity fluctuations. Hence, precautions will be taken to account for the possible time-dependent drift of the gages.

1.3 Development of the experimental procedure

1.3.a Instantaneous deformation

It is always tricky to decide which point is to be considered as a starting point of the loading for creep tests. In the present study, we have considered as the onset of the test ($t_c = 0$) the point corresponding to the half of the loading time, *i.e.*, approximately 1s after the start of the loading (Figure B-4a). Points corresponding to $t_c < 3s$ (for time-temperature equivalency tests, we have taken 4s because the stabilisation at higher temperatures was longer) were not included in the further analysis because of the scattering in strain values due to oscillations resulting from manual loading (Figure B-4b). Thus, strain value at $t_c = 3s$, resp. 4s, was used to determine the instantaneous compliance J_i . The mean difference compared to the extrapolation of strain curve to 1s, typically used by Hunt to estimate the instantaneous compliance, is of $0.34 \pm 0.13\%$.

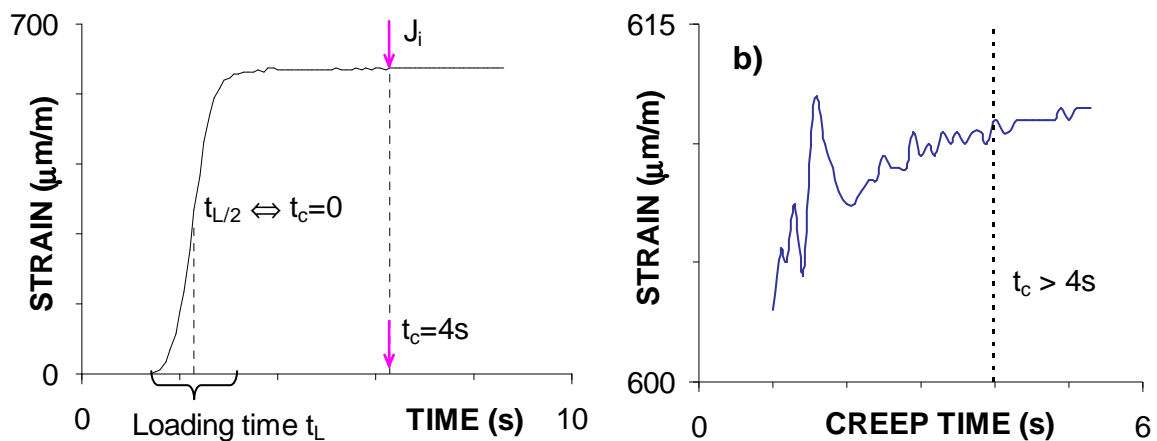


Figure B-4: (a) Determination of the instantaneous compliance and of the onset of the creep test. (b): Zoom on the very first seconds following the loading (unsmoothed data): example of the stabilisation of the creep signal. J_i : instantaneous compliance; t_c : testing time.

1.3.b Particular case of curved specimens

Some specimens exhibited more or less slight initial curvature before loading, which could be attributed to gradients of growth stress release. Bending resulting from initial straightening makes difficult the interpretation of strain values measured at very first moments after the loading: a relative difference up to 60% has been observed between strains measured on both sides of the specimen at 10s after loading. If attributed to the 'straightening' of the specimen, it represents an initial bowing of the order of 1mm that is highly possible. Similar problem was encountered also during the measurements of the additional time-dependent strain. In general, slight differences were observed between the values recorded by both strain gages. These differences were ascribed to the gradient of wood properties along the specimen thickness but they could also arise from a misalignment of the specimen with respect to the loading axis of the creep device. A criterion used to assess the effect of these two 'artefacts' on creep tests was to compute the average value of the developed strain. If the section was submitted on average to tensile stress and exhibited positive creep, the test was taken into account. In some cases, a negative creep was observed on one side while amplified positive creep was developed on the other side of the specimen. In that case, gage slippage was suspected. Except for one specimen used for investigation of the validity of the time-

temperature equivalency, where this effect appeared during the two last tests but the average creep value was positive, such specimens were not considered for further analysis.

1.3.c Duration of the procedure

Preliminary tests aiming to predict long-term creep behaviour consisted in stabilisation-creep-recovery cycles performed at 30°C; 45°C and 60°C. One cycle included a short stabilisation period at a given temperature (1h); a creep test lasting 24h; a recovery period at a given temperature (24h) followed by a recovery period at room temperature for following 48h. The whole test lasted 12 working days.

Two problems were encountered using this procedure: insufficient accuracy and problems with gage detachment. During the recovery period at room temperature the specimen was in general put away from the tensile device to enable another specimen to be tested. In that time, we had only one thermo-regulator to our disposal so that keeping the specimen in the testing device during the recovery period would yield the total duration of one complete cycle equal to 3 weeks. However removing of the specimen from the tensile device is arguable because the exact positioning of the specimen in the device differed between loadings thus increasing the experimental error (see 1.4.a).

Long duration of the complete procedure increased considerably the risk of gage detachment: it was unusual to keep the same pair of gages for all tests. Replacement of gages had similar impacts as removing the specimen from the device because we could slightly modify the position of gages.

Aiming to reduce the duration of the complete creep procedure, we decided to shorten the loading time. We have noticed that the shape of creep curve change around $t_c = 1000s$ ($\log t_c = 3$) so it was essential to go further. On the other hand, tests longer than 8h did not really bring more information considering the fact that we always represent creep results in respect of the log of the creep time. To accelerate the recovery, unloading of the specimen was followed by a short recovery period at a given temperature and heating to another temperature level. Details about the final procedure will be given in the chapter 3.

1.3.d Stability of gage output

We could observe a slight time-dependent drift of the gage output, likely increased by the use in non-standard conditions, *i.e.*, glued on wet support. Actually, some gages are waterproof but there is no gage designed to be glued on a wet surface. Such an application reduces the time of gages efficiency by increasing considerably the risk of gage detachment. To correct the drift of the gage output, becoming particularly important at high temperatures, we have used at first a reference gage (see Figure B-1). This method revealed to be inappropriate because the non-stressed specimen had a different drift compared to the loaded one. However, even gages submitted to the same loading conditions did not exhibit identical drift. This difference arose likely from the quality of the contact with the specimen and quality of the silicon protection. Finally, we have decided to use a stabilisation period prior to the loading and long enough to obtain a reliable extrapolation of the stabilised signal into the creep time period. Details about used ratio of the stabilisation and loading periods for each procedure are given in chapters 2 and 3.

Similar difficulties were encountered while testing the possibility to perform continuous creep tests at increasing temperature as was done for example by (Genevaux 1989). Such testing procedure is interesting because well-designed to obtain a lot of information. However, when we wanted to apply the testing procedure at continuously increasing temperature, there was a problem with thermal expansion of gages affecting their output during such a test. Strain gages are to follow the temperature expansion of measured

sample but this correction depends on the material tested. There are gages accounting for the thermal expansion of the wood but these are designed for dry wood in a given range of positive coefficient of thermal expansion. Heating of green wood results in a shortening of the specimen along longitudinal direction (Yokota and Tarkow 1962). Inherent thermal correction of gages is not appropriate to take this effect into account. Similarly to time-dependent drift, the temperature drift of gages was too variable between gages/specimens to allow reliable correction of the output. Thus, a procedure consisting of individual creep tests performed at a given temperature, after the thermal stabilisation of the gage, has been used. Moreover, the gage factor is dependent on the temperature however induced changes are negligible (0.08%/10°C) and were not considered.

1.4 Some verifications

1.4.a Repeatability

Uncertainty in the Young's modulus estimation at $t_c = 4s$ was of 0.76% if repeated loading of the specimen are considered without its removal of the test device (STD of 5 repetitions). When the specimen is put away or turned over, the incertitude increased up to 1.76% (STD of 16 repetitions). Repeatability of the creep strain was also tested during preliminary tests. Results are shown in Figure B-5. Between both tests, specimen was removed from the tensile device. Hence, we can notice a slight difference in instantaneous compliance (1.2%) however slope of both curves seems to be very close. This is evidenced in the second figure where the relative compliance is drawn. At the end of 5h creep test, difference between the amounts of relative creep is negligible (3.5%). Furthermore, results of linearity tests (§1.4.b) along with preliminary test in the aging procedure without prior application of heating treatment §2.3.a confirm this result.

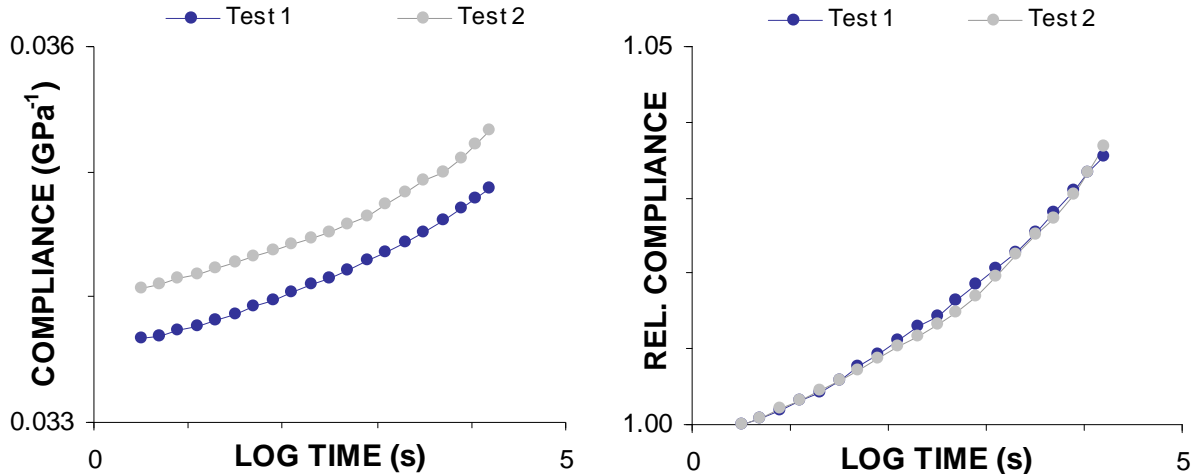


Figure B-5: Tests of repeatability. (a) Creep curves corresponding to the first and second creep test. (b) The same creep curves expressed in terms of relative creep.

1.4.b Tests of linearity and recovery

In this work, loading corresponding to the initial strain of 500µm/m was applied. Verification of linearity of the creep behaviour was tested up to 1000µm/m using successive loadings with increasing strain as depicted in Figure B-6a. Each strain step was equal to 250µm/m approximately and one creep test lasted 45 minutes. The same procedure was applied for the recovery tests. Obtained results are plotted Figure B-6b, time scale for recovery tests is reversed to enable easy comparison with corresponding creep tests. We can note that the recovery is complete; the same observation was done also during physical aging measurements (not shown).

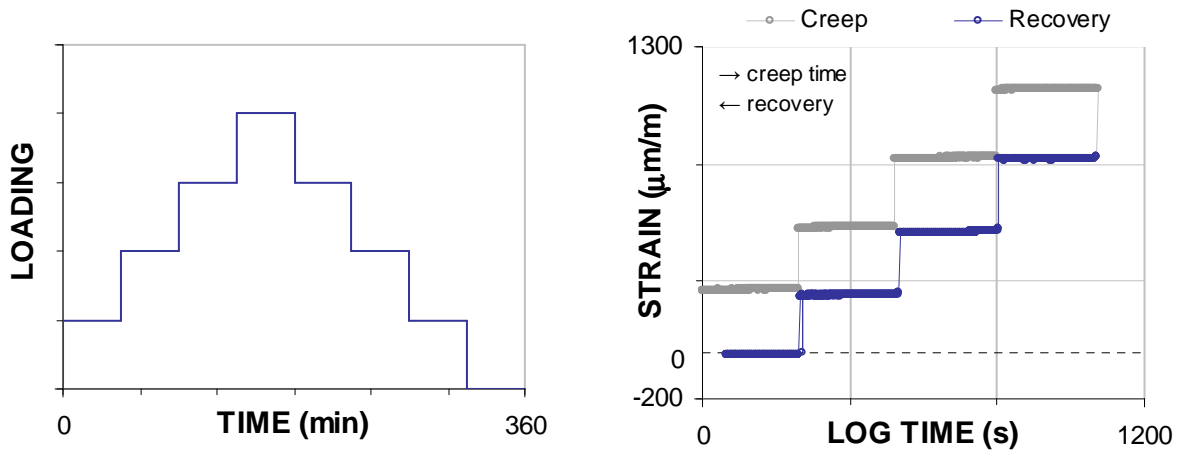


Figure B-6: Tests of linearity. (a) Schedule used for the linearity tests. (b) Obtained results from creep and recovery tests.

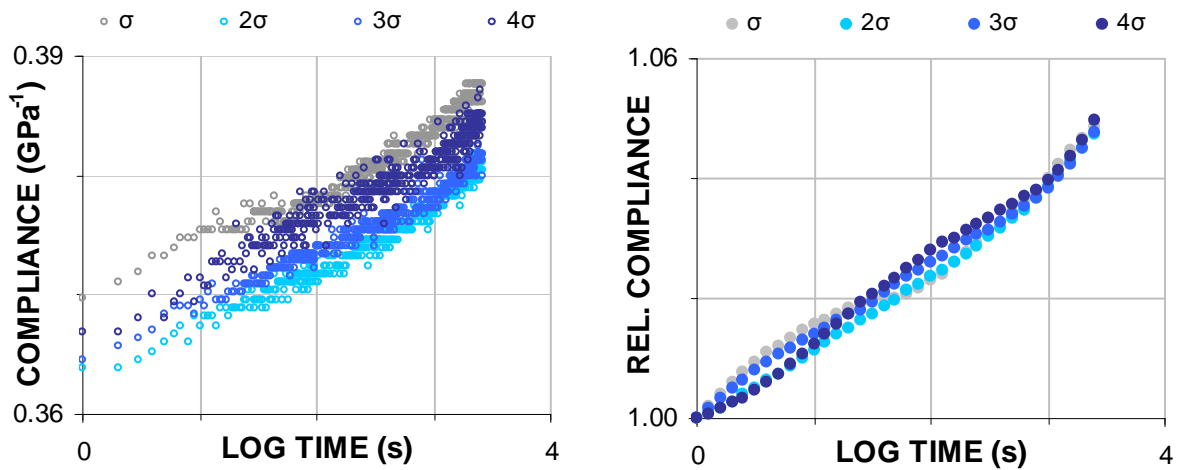


Figure B-7: Detail of creep tests performed at different stress level. (a) Raw compliance values. (b) Smoothed, interpolated and normalised compliance values.

Compliance curves obtained from successive loadings are displayed in Figure B-7. Figure B-7a represents raw experimental values. Slight differences observed between the instantaneous compliances are mainly due to small differences in the applied weights. In Figure B-7b, the same values but smoothed, interpolated and normalised by the applied stress are represented. All curves overlap in one single curve indicating that the limit of linearity has not been exceeded. Obtained results are in agreement with literature data stating the strain limit for non-linear behaviour of a softwood in tension around $1800 \mu\text{m/m}$ (Hunt 1989).

1.4.c Correction of the creep signal

Increase of temperature above approximately 35°C may trigger the release of residual growth strains (Yokota and Tarkow 1962). Moreover, we have noticed that gages, in particular at increased temperature, exhibit a slight time-dependent drift as explained in §1.3.d. Both, the release of locked-in strains along with the gage time-dependent drift overlap with the creep during the mechanical testing and make it difficult for the interpretation of the signal. To obtain clean data, we have used the stabilisation period long enough to allow a reliable extrapolation of the stabilisation signal to the following creep period as detailed in §3.2.b. An example of extrapolation is shown in Figure B-8a. For the typical ratio between the stabilisation and creep periods used during tests at different temperature levels, the extrapolation from $\log t = 4.73$ to $\log t = 4.93$ was used. Extrapolated signal was then used to

correct the creep recorded during the creep test as shown in Figure B-8b. Note the difference between the two time scales: at the onset of the creep test, the recovery time is equal to $\log t = 4.73$. Thus, the correction is close to zero for the first part of the test whereas it is quite huge for the last part. Depicted case corresponds to the stabilisation period at 60°C where the correction is the most important for a specimen exhibited large time-dependent drift. Note that such a correction is possible only under the assumption of viscoelastic linearity verified in the previous paragraph.

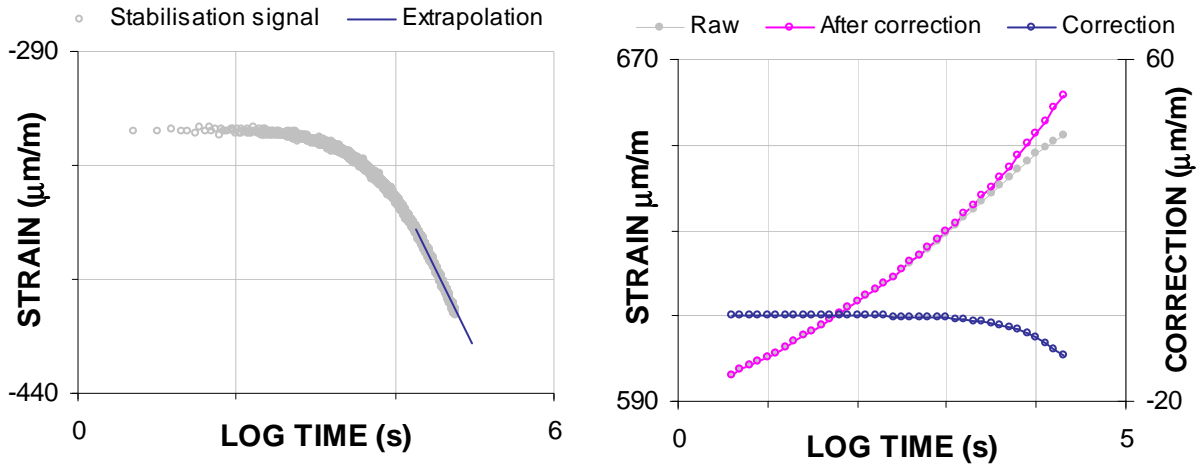


Figure B-8: Correction of the creep signal obtained during a test at increased temperature. (a) Extrapolation of the signal recorded during the stabilisation period. (b) Creep strain before and after the correction.

1.5 Data processing and analysis

For each tested specimen, following steps of analysis were performed:

1. First, strain values obtained by both gages were averaged and corrected by the extrapolation of the signal from previous recovery period (aging tests) or stabilisation period (time-temperature equivalency investigations) as explained in §1.4.c. Applied ratios of creep/recovery period as well as details on this procedure are given in the chapters 2)2 and 3 respectively. Compliance values were obtained from averaged and corrected strain values, section geometry and applied load.
2. Compliance values, further denoted by J , were smoothed by searching for the best-fitting second order local polynomial approximating J versus $\log t$. At the same time, values of J were interpolated to obtain a set of points equally spaced in a logarithmic time-scale. The interval between interpolated values $\log t = 0.1$ was used. At the same time, the slope corresponding to the derivate $dJ/d\log t$ was computed. The principle of interpolation is depicted in Figure B-9a. Criteria used for smoothing was a minimum of 20 points and a range $\Delta\log t = \pm 0.3$. The test duration was approximately 8h ($\log t = 4.5$). Very first values of J were also often disturbed by vibrations resulting from the manual loading (see Figure B-9 and also Figure B-4b). As the interpolation is not very reliable when one-sided, only values from $\log t = 0.5$ up to $\log t = 4.3$ was used for further analysis. An example of interpolated values and their correspondence with original experimental data is shown in Figure B-9b.
3. The interpolated values have been used to evaluate the real and imaginary part of the complex compliance $J^* = J' + iJ''$ using Alfrey's approximation (Alfrey 1948) as explained previously in 0-3.5.d:

$$J' \approx J(\log t); \quad (\text{Eq. B-1})$$

$$J'' \approx \frac{\pi}{2} \cdot \frac{1}{\ln(10)} \frac{dJ(\log t)}{d \log t}; \quad (\text{Eq. B-2})$$

where J' represents the real part and J'' the imaginary part of the complex compliance. Components of the complex compliance were further plotted in the approximated complex plane (ACP). The ACP was used to check for equivalency principles: time-aging time for the physical aging study and time-temperature for the long-term predictions. Further, rheological models applicable to wood are represented in the ACP by straight lines or circle portions so that the graphical representation of experimental data allows easy identification of a corresponding parametric model (Huet 1988). Thus, ACP is a very useful tool to decide about the mathematical form of the constitutive law without any preconceived idea about the physics of the studied phenomenon and the equations to use for the modelling.

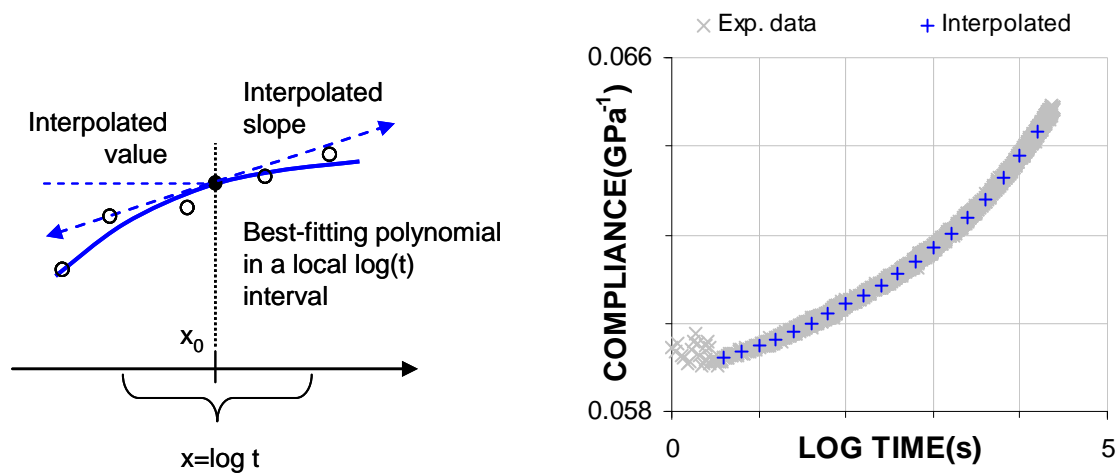


Figure B-9: (a) Principle of smoothing and interpolation by best-fitting local polynomial. (b) Examples of smoothed and interpolated procedure applied to specimen *Oa2*.

Further steps of data analysis will be detailed for each study separately in the following chapters.

2) Evidence and modelling of physical aging

Following results were published (Dlouhá *et al.* 2009) but slightly modified for their smooth integration to this manuscript.

2.1 Introduction

To produce biomechanical models valid over the whole life, the time-dependent behaviour of green wood needs to be predicted. The use of series of creep or relaxation tests at increasing temperature levels is the obvious way to identify such long-term rheological models, but several obstacles might produce difficulties. First, the complex polymeric composition produces overlapping of phenomena so that the observed mechanical response is not described easily by simple equivalence between time and temperature (Bardet and Gril 2002). Second, the recovery of locked-in strain due to the pre-stressing during wood formation at stem periphery is likely to occur during the tests at increasing temperature levels, and produce non-negligible perturbation of the viscoelastic data (Gril and Thibaut 1994).

Residual strains can be removed, or at least significantly recovered by heating above the glassy transition (T_g), typically 65°C for the *in-situ* saturated lignins of a hardwood (Kelley *et al.* 1987). However, when the wood is cooled below T_g after the heating, physical aging may occur: upon cooling below T_g , due to the low chain mobility the polymer cannot shrink fast enough to keep equilibrium volume, and the material properties undergo slow and gradual changes towards its new equilibrium state (Struik 1978). Consequently, the tests performed too shortly after the heating and subsequent cooling, may produce data poorly connected with the real behaviour of a never-heated green wood.

Physical aging has been already observed in wood. A number of arguments for its occurrence were given for wood in the hygroscopic range (Hunt and Gril 1996). The effects of a quench (rapid cooling) on wet wood properties was studied by Nakano (2005) who reported a temporary change in viscoelastic properties with a new equilibrium state definitely reached at the end of 10 hours. Free volume creation has been ascribed to the freezing of molecular chains of wood components, most likely lignin, during the quench. On the other hand, Ishimaru (2003) has investigated the effect of quenching rate on wood creep properties and observed that the effect of cooling had not completely disappeared after 40 days; but they have not examined the aging phenomenon in more details. In these studies, the wood was usually tested transversally to the fibres, in the radial (R) or tangential (T) direction, whereas for biomechanical consideration the behaviour in the longitudinal direction (L) is the most important.

The objective of this work is to verify the occurrence of physical aging in green wood, and, if possible, quantify it, based on tensile creep tests in L direction. In his pioneer study on physical aging of polymers, Struik proposed an experimental protocol to investigate the effect of aging time on small-strain creep properties after a quench, based on the “snapshot” assumption - testing time is very short relative to aging time. Assuming that aging changes by a negligible amount during each creep test, the creep response can be separated from the aging effect. Struik has also shown that in the case of simple polymers, creep curves for different aging times can be superimposed into a single master curve, and he proposed a simple mathematical description of the log time shift. We adopted Struik procedure, intending to verify the applicability of his descriptive model to green wood.

2.2 Material and methods

Wood samples of three tropical species *Oxandra asbeckii* (Pulle) R.E. Fries, *Licania alba* (Bernoulli) Cuatrec. and *Virola michelii* Heckel were used to investigate the aging phenomenon in green wood. Properties known at the moment of selection are summarised in Table B-1. Some specimens of tension wood were included in the study as well. Sample names are built as the initials of the species name with an index specifying the wood type (eg. Oa_N and Oa_T for *Oxandra asbeckii* normal and tension wood respectively).

Table B-1: Summary table of the specimen properties used for the aging study

Species	Basic density	Elastic modulus (GPa)	Specific modulus (GPa)	Damping
<i>Licania alba</i>	0.506	21.17	17.31	5.76E-03
<i>Licania alba</i>	0.506	20.40	16.68	5.99E-03
<i>Oxandra asbeckii</i>	0.850	20.54	15.84	5.31E-03
<i>Oxandra asbeckii</i>	0.850	16.18	12.47	6.94E-03
<i>Virola michelii</i>	0.450	10.75	4.27	6.93E-03

Legend: Data for basic density comes from CIRAD database, elastic modulus and damping were measured in green state, specific modulus stands for the ratio of elastic modulus and basic density.

After being heated at 80°C for 30 minutes to release all macroscopic residual strains and establish the thermodynamic equilibrium, the sample was quenched to 30°C and kept at 30±0.1°C. The quench was done by replacing the sample from the bath at 80°C to the water chamber of the testing device regulated at 30°C, the operation taking about 60 s. After that, a set of short-term creep tests was performed on the same specimen at various aging times t_a elapsed after the quench as shown in Figure B-10. It is important to distinguish aging time t_a , counted from the moment when the specimen was moved from the hot to the cold bath, and t_c , the creep time counted from the moment of each loading.

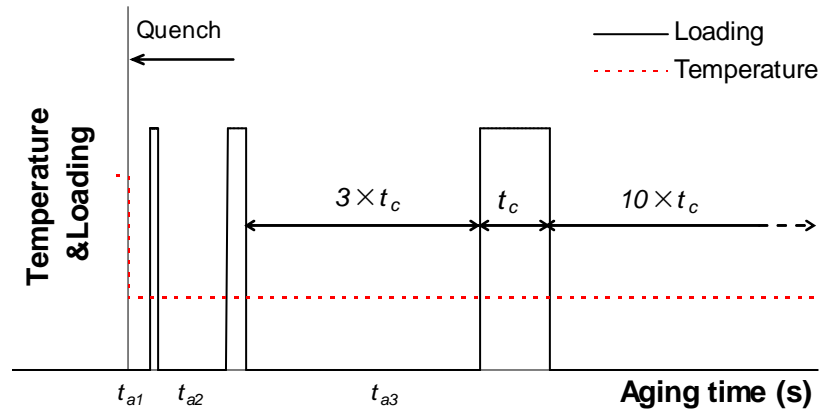


Figure B-10: Experimental procedure for investigating the aging time effect on small strain creep properties. a) Dashed line: temperature; solid line: load. t_a : aging time; t_c : creep time.

To separate the creep response from the aging effect, testing time t_c has to remain much shorter than t_a at the onset of the test. This is called the snapshot assumption because a test performed during such a short time ($t_c < 0.3 \times t_a$) will exhibit negligible effects of aging. Strain was measured during both creep and recovery periods. By extrapolation of the recovery curve in logarithmic time scale into the next creep period, the strain built up during each individual creep test could be singled out. The principle of this extrapolation is explained in §3.2.c. To obtain a reliable extrapolation, testing time has to be short relative to the previous ($3 \times t_c$) recovery period. We also need to have t_c short relative to the following recovery period ($10 \times t_c$). This condition takes into account the time necessary to complete the recovery of

previous loading so that at the end strain signal is quite stable and easy to extrapolate. In fact, corrections due to the extrapolation of recovery tests revealed to be negligible ($\sim 0.002\%$ for the longest creep test) so that the correction was not applied systematically. The total duration of the test procedure is 3.5 days.

2.3 Results and discussion

2.3.a Suitability of experimental procedure and evidence of aging phenomenon

The experimental procedure was first tested omitting the step of preliminary heating above T_g . In this case, curves corresponding to creep tests performed at different elapsed times after the onset of the test are superimposed into one single curve (Figure B-11a). This shows that the effect of loading history of the sample on a given creep test is negligible and we can use the proposed procedure to investigate the effect of aging time. Fig. 3b represents a set of creep tests performed on the same specimen after the quench. We can notice that higher creep strains were developed during the tests following the quench. The relative creep for the creep test performed at t_{a5} (Figure B-11a) amounted to $\sim 7.5\%$ against $\sim 12.2\%$ for the creep test (t_{a5}) in Figure B-11b. The shape of the creep curve corresponding to the first aging time (t_{a1}) was quite different from others. This effect was ascribed to the non achieved thermal equilibration of the specimen with the surroundings: in later tests, we have always applied the first loading at $\log t_{a1} > 2$, or 100 s after the quench.

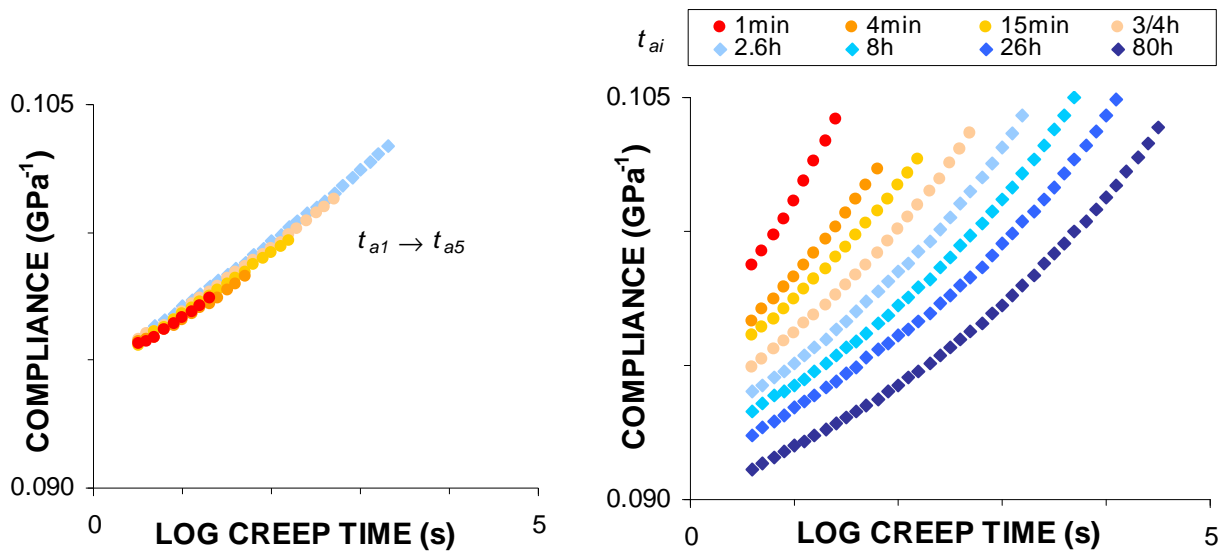


Figure B-11: Evidence of physical ageing occurrence in green wood (sample Vm_N). (a) Set of creep tests performed at different elapsed times t_1 - t_5 counting from the onset of the test without preliminary heating above T_g ; (b) Set of creep tests performed on the same sample at different aging times t_{a1} - t_{a8} following the quench

The gradual decrease of instantaneous compliance with increasing aging time as visible in Figure B-11b clearly confirms the occurrence of physical aging in green wood. The drop between successive creep curves does not reduce with increasing aging time. This suggests that the logarithmic aging rate remains approximately constant during the test; even at the end of the test period, 3.3 days after the quench, the specimen is far from a new equilibrium state. It definitely shows that the stabilisation period of our samples is much longer than expected considering Nakano's results transversally to the fibres. Figure B-12a shows a master curve obtained by shifting the curve for each aging time along the log time axis toward a reference curve corresponding to t_{a8} . The smoothness of the resulting master curve suggests that aging dependence of the creep response is rather uniform and tested material could be considered as rheologically simple. A commonly used method to describe

the aging behaviour is to display the shift factor a_{ta} versus the aging time t_a on double logarithmic scale. The slope yields the aging rate μ (Figure B-12b):

$$\mu = -d(\log a_{ta})/d(\log t_a). \quad (\text{Eq. B-3})$$

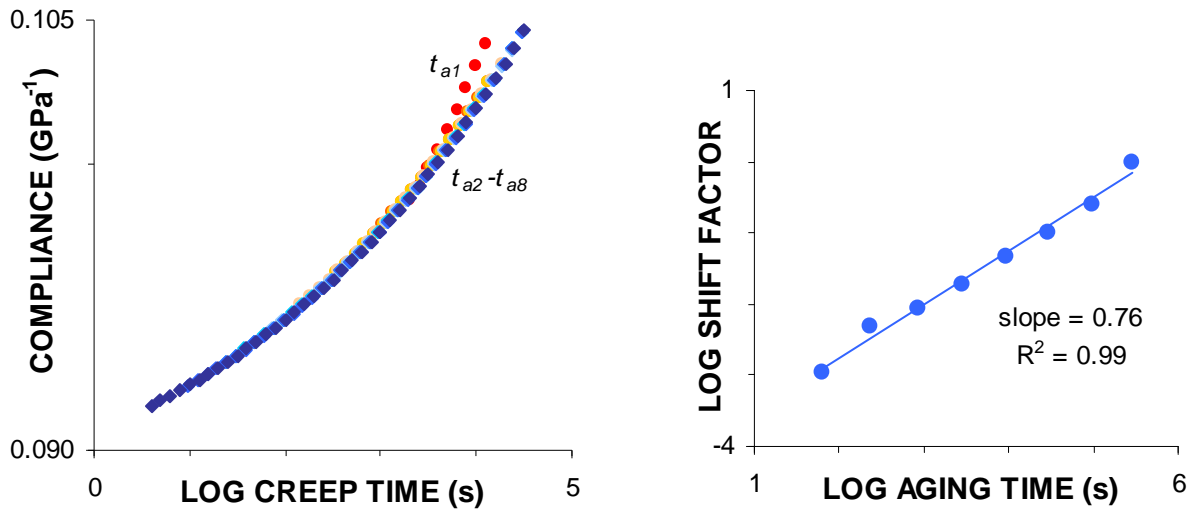


Figure B-12: Relationship between retardation and ageing time based on visual assessment (sample V_{MN}). (a) Master curve obtained by visual shifting of individual creep curves from Figure B-11b; (b) Double logarithmic plot of shift factors a_{ta} versus the aging time t_a .

2.3.b Identification of a rheological model

To improve the reliability of ageing quantification, a procedure based on rheological modelling was tried.

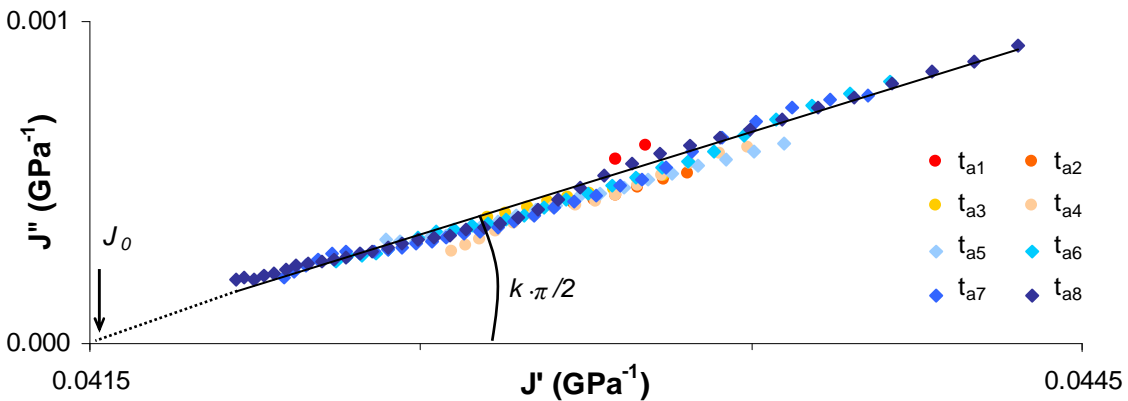


Figure B-13: Complex plot of a sequence of creep tests performed at different aging times t_a after the quench where J' is storage compliance and J'' loss compliance (sample Oa_N). For signification of J_0 and k see in the text.

In complex plot, the creep curves measured at various aging times are superimposed into one single straight line (Figure B-13). This means that the aging phenomenon in green wood can be described by a “parabolic Maxwell” model (Huet 1967) with an aging-dependent dashpot element. Creep behaviour of such a model obeys to the power law:

$$J(t_c) = J_0 [1 + (t_c / \tau)^k], \quad (\text{Eq. B-4})$$

where $J(t)$ is the creep compliance, J_0 the instantaneous compliance, τ the doubling time of the creep response and k the power parameter. The use of a power law has been often proposed to describe the creep response of wood (Huet 1988). This behaviour can be considered as the beginning of a 3 elements parabolic response as described above, for

durations considerably smaller than the characteristic time of the dashpot, so that the spring in parallel to the dashpot is subject to a negligible stress.

Estimates of J_0 and k can be obtained graphically as shown in Figure B-13 and have the same value for all aging times. Only τ depends on t_a , so that the creep compliance for any aging time can be written as:

$$J(t_c; t_a) = J_0 [1 + (t / \varpi(t_a))^k]. \quad (\text{Eq. B-5})$$

In this equation, the relation $\varpi(t_a)$ is not imposed. Assuming, in addition, the validity of aging rate uniformity claimed by Struik (Eq. B-3), we obtain:

$$\mu = - d (\log \varpi) / d (\log t_a) = - d (\log a_{ta}) / d (\log t_a), \quad (\text{Eq. B-6})$$

where μ is the aging shift rate where parameter a_{ta} represents the horizontal shift used in Struik's procedure to form a master curve from creep curves measured at different aging times.

Eq. B-6 yields:

$$\log \varpi(t_a) = \log[\tau_0] - \mu [\log(t_a) - \log(t_{a0})] \quad (\text{Eq. B-7})$$

where t_{a0} is the reference aging time and τ_0 the doubling time at t_{a0} . The combination of equations B-5 and B-7 allows to predict a whole data set like that of Figure B-14b, using 4 parameters only: J_0 , k , μ , τ_0 . As a reminder, Eq. B-5 is only valid for t_c values verifying the snapshot condition ($t_c \ll t_a$), so that the age of the specimen did not change significantly since it was loaded.

2.3.c Optimisation of model parameters

Model parameters were adjusted by least-square optimisation method using smoothed experimental data with regular step in log time scale ($\delta \log t_c = 0.1$). First, we have tested the suitability of the proposed description of aging behaviour deduced from the complex plot (Eq. B-5). Parameters J_0 , k and τ_i were adjusted omitting any presumption about the dependency of τ_i on aging times. This optimisation method will be called "fitting 1". Example of a master curve and adequacy between experimental and modelled creep curves is displayed in Figure B-14. As output of fitting 1, we have obtained a set of doubling times τ_i corresponding to different aging times t_{ai} at which were performed individual creep tests. Plotting the change in τ_i versus aging times t_{ai} in double logarithmic scale (Figure B-15.), we can assess the validity of the presumed aging rate uniformity. Excepting the sample Oa_T, the assumption of linearity is well satisfied.

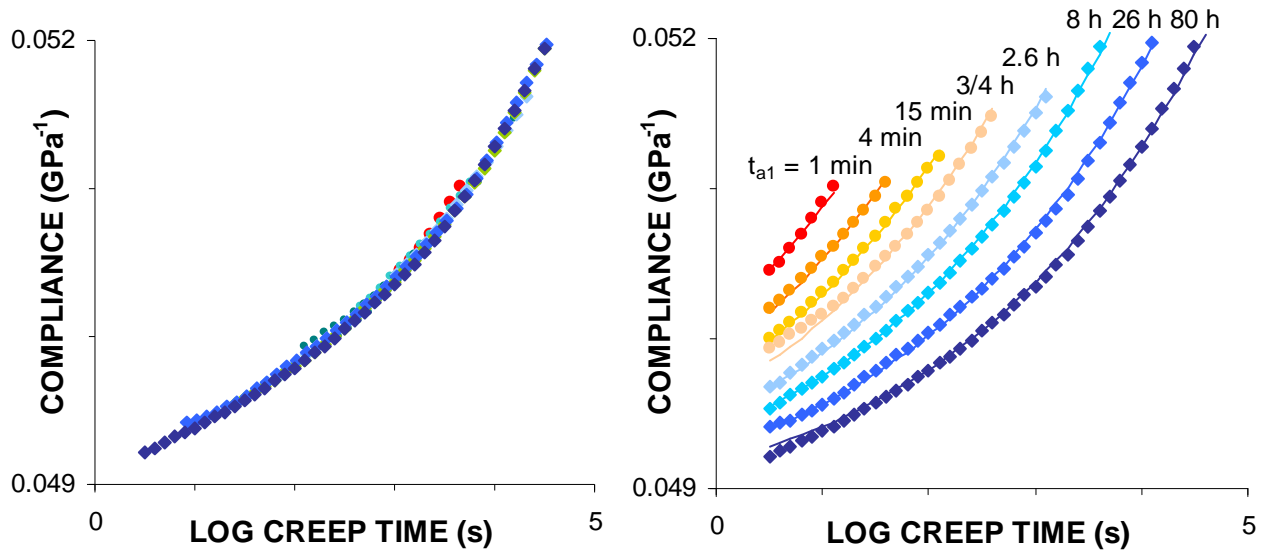


Figure B-14: Example of model fitting based on eq. B-5 for sample Oa_N : (a) Master curve produced by shifts resulting from optimisation without any presumed dependency between doubling and aging times. (b) Example of agreement between experimental (dots) and modelled creep curves (lines). Creep curve corresponding to the aging time $t_{a8} = 3.3$ days was taken as a reference.

Next, we have proceeded to the optimisation of model parameters J_0 , k , τ_0 and μ taking into account both Eqs. B-5 and B-7, referred to as “fitting 2”. An example of master curve using shift factors obtained by fitting 2 is shown in Figure B-16a. We can notice some discrepancies compared to the smooth master curve resulting from fitting 1 represented in Fig. Figure B-14a, however agreement between experimental and modelled creep curves based on parameters issued from fitting 2 remains very satisfactory (Figure B-16b).

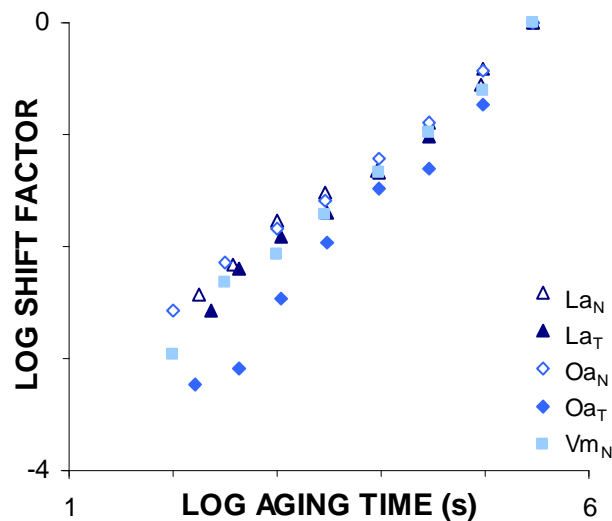


Figure B-15: Model fitting based on eq. B-5. Relationship between shift factors a_{ta} and aging times t_a in double logarithmic scale for different samples.

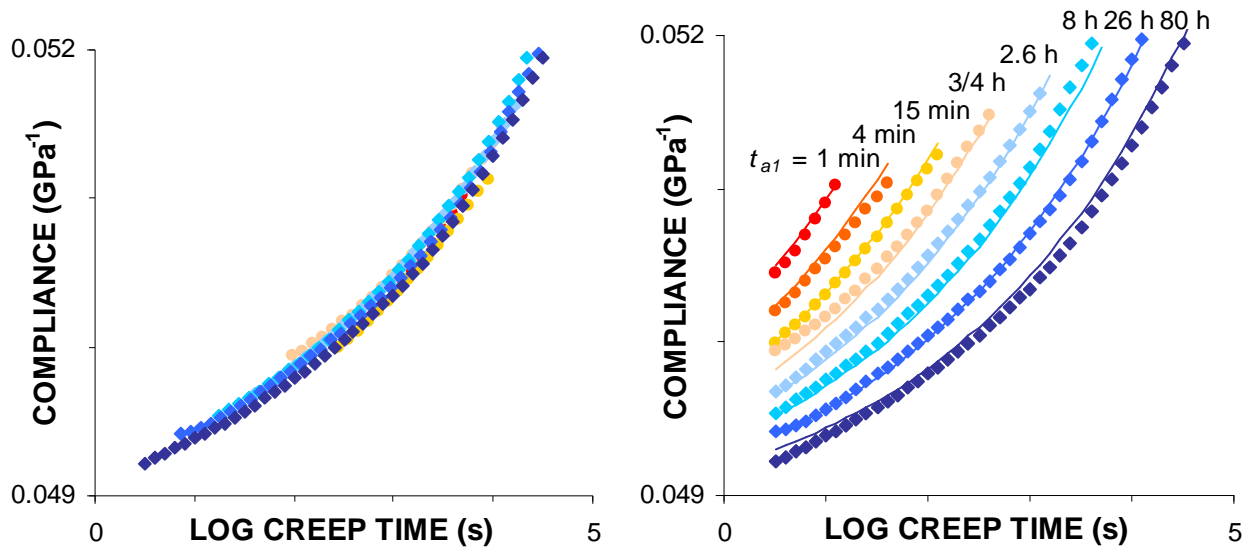


Figure B-16: Example of model fitting based on eq. B-5 and B-7 for sample Oa_N a) Master curve produced by shifts resulting from optimisation accounting for linear logarithmic dependency between doubling time and aging time. (b) Example of agreement between experimental and modelled creep curves issued from fitting 2. t_{a1} : aging time.

Table B-2 summarises parameters of the aging dependent model for all tested specimens adjusted by different methods and/or corresponding to different hypothesis about the doubling times dependency on aging times. Parameter values resulting from fitting methods 1 and 2 are very close. This indicates that the assumption of uniformity of aging rate (Eq. B-3) is valid and so we can reduce the number of model parameters without introducing an important error to the prediction of aging behaviour. It is also interesting to notice that the accuracy of visual fitting of the master curve is quite good (see values of μ by visual fitting and fitting 1). This study proved that complex plots are very useful to decide about the mathematical form of the behaviour law; however the accuracy of value of parameter k deduced from the graphical representation is not sufficient.

Table B-2: Adjusted parameters of aging time dependant model. Last line corresponds to results obtained for Nakano's data presented in §2.3.d. k : power exponent; J_0 : instantaneous compliance (GPa^{-1}); $\log \tau_0$: doubling time of the reference element and μ the aging rate.

	Vis.fitting	Complex plot		Fitting 1				Fitting 2			
	μ	k	J_0	μ^*	k	J_0	$\log \tau_0$	μ	k	J_0	$\log \tau_0$
La _N	0.70	0.21	0.035	0.71	0.17	0.041	11.7	0.72	0.18	0.041	11.4
La _T	0.79	0.12	0.027	0.79	0.14	0.033	12.4	0.80	0.14	0.033	12.4
Oa _N	0.77	0.21	0.042	0.73	0.19	0.048	10.8	0.75	0.19	0.048	10.7
Oa _T	0.98	0.14	0.037	0.97	0.13	0.033	14.2	0.97	0.13	0.033	13.8
Vm _N	0.77	0.14	0.087	0.80	0.14	0.086	9.5	0.80	0.14	0.086	9.3
Nakano				0.73	0.27		5.2	0.61	0.27		5.2

*value of μ for fitting 1 is deduced from the plot represented in Figure B-15.

Concerning the variability of instantaneous compliances between samples, it can be easily explained by the diversity of densities and Young's moduli of our sampling. On the other hand, parameters μ , k and τ_0 were very similar for all samples (excluding aging shift rate μ measured for the sample Oa_T) suggesting the common feature of aging phenomenon in green wood. Values of aging rate are consistent with bibliographic data. Struik has observed aging rate μ close to unity for amorphous polymers and $\mu \sim 0.75$ for rigid chain CAB

(cellulose acetate butyrate ester). Considering the partially crystalline and partially amorphous nature of wood, a lower aging rate can be explained by the slowing effect of rigid chains as proposed by Levita and Struik (1983).

2.3.d Application to the analysis of Nakano's data

Nakano studied *Picea jezoensis* (Carrhas), a Japanese softwood, loaded in bending in the R direction; although the wood was studied in the water saturated state, it had been previously kiln-dried so cannot be considered as green wood. The experimental procedure has been different from that suggested by Struik. While in our case aging times at which individual creep tests are performed are equidistant in logarithmic scale (step = 0.5), in Nakano's procedure the aging time step is not constant and tends to decrease for longer aging times ($\log t_{a_{n+1}} - \log t_{a_n}$: 0.78 – 0.48 – 0.3 – 0.37 – 0.22 – 0.27 – 0.19). Hence, it is difficult to deduce from the graphical representation of creep curves with respect of testing time if the material is close to its equilibrium state or not.

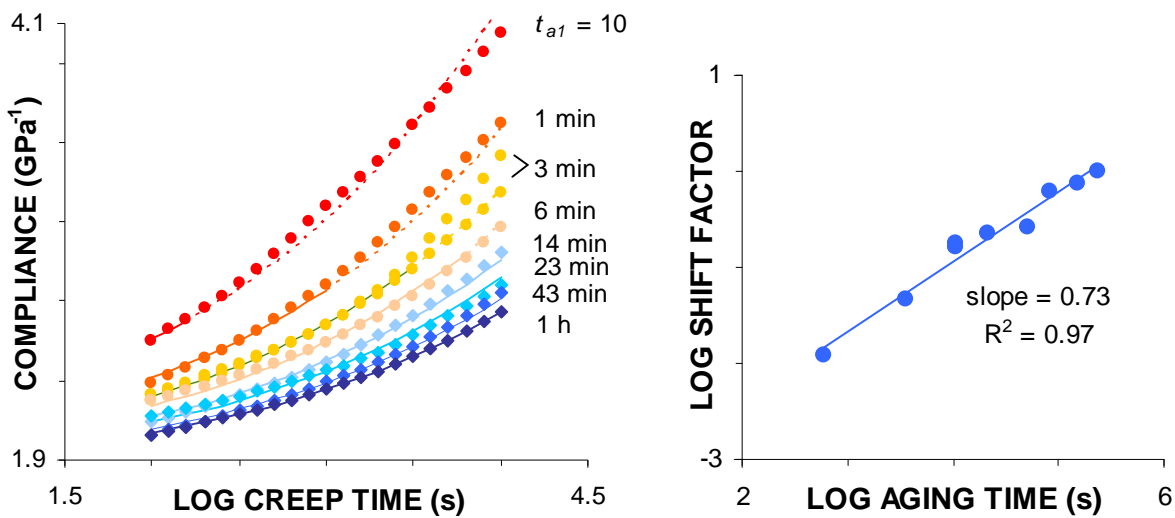


Figure B-17: Model fitting based on Eq. B-5 applied on Nakano's data: (a) Agreement between experimental and modelled creep curves for fitting 1. Solid lines represent the prediction for values of $t_c < t_a/3$; dashed lines correspond to modelled values not satisfying the snapshot condition $t_c > t_a/3$. (b) Relationship between shift factors a_{ia} and aging times t_a in double logarithmic scale.

To examine in more details Nakano's data, we have applied the optimisation method 1 – fitting without presumed linear logarithmic dependency of doubling times on aging times. As creep tests were not performed on the same sample, we have allowed J_0 to vary accounting for possible differences in instantaneous and delayed behaviour between samples. Only data fulfilling the snapshot condition ($t_c > t_a/3$) were used for the fitting. ACP of Nakano's data after the correction of J_0 are shown in the Appendix. Agreement between experimental and modelled creep curves is shown in Figure B-17a. Relation between shift factors and aging times is quite linear yielding aging rate equal to 0.73 (Figure B-17b) that is very close to our values for tropical hardwoods, loaded in longitudinal tension. It suggests that the dynamics of aging phenomenon is not dependant on the wood type or the loading direction.

2.3.e Discussion on the physical processes involved

According to Stamm and Loughborough (1935), the fibre saturation point (FSP), representing the maximum content of bound water, increases by 0.1% per 1°C decrease. This

estimate, deduced from sorption isotherms, is representative of phenomena occurring in the hygroscopic domain. However even in wet conditions, with the cellular cavities (lumens) filled with free water and the cell walls saturated with bound water, small moisture movements are likely to occur through the cell wall as a result of temperature changes.

The phenomenon stated by Stamm is qualitatively confirmed by the negative reversible thermal expansion observed in green wood and attributed to a moisture uptake during cooling (Yokota and Tarkow 1962). But the intensity of the phenomenon seems to be smaller. An expansion ratio of $-7.10^{-6}/^{\circ}\text{C}$ in the tangential direction can be evaluated for green wood from a previous study (Gril *et al.* 1993). Taking $+33.10^{-6}/^{\circ}\text{C}$ as the expansion ratio for dry wood (Kollmann and Côté 1968), the expansion resulting from the moisture uptake can be calculated as $-40.10^{-6}/^{\circ}\text{C}$. Assuming a typical expansion ratio of 0.3% per % moisture content, this would correspond to a moisture content increase of 0.7% for a 50°C temperature decrease, to be compared to the 5% predicted from FSP estimates.

Even by that small amount, the moisture uptake resulting from quenching is likely to influence the mechanical response. In the hygroscopic range, humidity variations, both adsorption and desorption, considerably accelerate the viscoelastic response, an phenomenon known as mechanosorptive effect (Grossman 1976) and described as a transient increase of molecular mobility (Back *et al.* 1983) of the hygroscopic matrix made of lignin, hemicelluloses and non-crystalline cellulose. However, at high humidity levels the contributions of mechanosorptive and stable-state creep are difficult to separate. Our data do not allow to distinguish that “hygrothermomechanical” process from the progressive return to equilibrium of temporary frozen molecular segments. The quenching provoked, for a number of reasons, an unstable molecular configuration of the matrix that is progressively recovered according to the identified kinetics.

The fact that Struik’s formalism seemed to be relevant to describe the physical aging of green wood, suggests that the pertinent level of description is that of a semi-crystalline polymer, where the heating above lignin glassy transition followed by a quench had induced a delayed return to a stable molecular configuration. The transient instability induced by the small moisture uptake does not necessarily contradict this interpretation as long as it only adds a reason for higher molecular mobility. However, if the variation in moisture content was the main cause for the change in behaviour with t_a , the remarkable superimposition of the creep curves in Figure B-13, resulting in a model where only τ varies with t_a , may not have been observed.

Higher levels of structural organisation should be also evoked to complement this molecular interpretation. In the longitudinal direction, because of the axial orientation and tubular shape of most cells, the cell-wall level is most appropriate. When a green wood specimen is isolated and heated, stress resulting from the cell growth process is easily recovered as soon as the temperature exceeds T_g , which was the case at 80°C . However, the condition of structural integrity limits the extent of recovery; a part of the locked-in strains and pre-stresses remain present locally, as their complete relaxation would require the destruction of the cell-wall structure. The local swelling anisotropy, and its incompatibility between layers, might interact with this initial pre-stressing resulting from cell-wall formation and be only partially released by the heating.

2.4 Conclusion

The effect of quench on creep that persists for a long time in green wood could be described as a physical aging process. The analysis of aging behaviour was performed in three steps. First, rough assessment of the validity of the aging rate uniformity was made by visual shifting of individual curves into a master curve. Second, complex plots were used to choose a rheological model and identify its parameters for each aging time t_a , without any

presumption about the influence of t_a . The model used, a parabolic Maxwell, describes the delayed compliance by a simple power law. Only the “doubling time” theoretically required to double the instantaneous response was affected by t_a (fitting 1). Based on results of this fitting, the validity of the assumption of the uniform aging rate was verified and introduced in the model in a third stage (fitting 2). The same approach was successfully applied on experimental data provided by Nakano. Model based on the linear dependency between doubling and aging times was considered satisfying for all studied samples suggesting common feature of the aging phenomena in wood. The transient adsorption process consecutive to the quench was considered as one of the possible causes of the higher molecular mobility observed.

3) Applicability of the time-temperature equivalency

Following results were published (Dlouhá *et al.* 2009) but slightly modified for their smooth integration to this manuscript.

3.1 Introduction

For long-term predictions of creep behaviour, accelerated experimental methods are in general used. One of them, used for static testing, is based on time-temperature equivalency stating that increasing the temperature is equivalent to stretching the real-time of the creep response. Based on a sequence of short-term creep tests performed at increasing temperature levels, the corresponding compliance curves are shifted along the log time axis to generate a creep master curve characteristic of the long-term behaviour of a given material. Previous works on the rheology of green wood, *i.e.*, that was never dried under the fibre saturation point, focused on the behaviour of wood across the grain (Bardet 2001; Placet *et al.* 2007) which is of a little relevance for tree mechanics modelling where properties along the fibres are predominant.

Viscous properties of wood are determined by the behaviour of the amorphous matrix made up of lignin and a variety of hemicelluloses. In the water-saturated state, such as the green condition, hemicelluloses are already softened at room temperature. Thus, softening of wood tissues, which occurs for quasi-static loading or at low frequencies in the vicinity of 70°C, was ascribed to the lignin glass transition (Kelley *et al.* 1987). Thermal activation of secondary relaxations occurring below the glass transition temperature is usually described by the Arrhenius law, where the characteristic time τ of the viscoelastic process is related to the absolute temperature T through an apparent activation energy W .

Salmén (1984) reported the applicability of the time-temperature equivalency in wood for temperatures above the lignin glass transition. He has also stated the validity of the Arrhenius law. This concept was also used by many authors to predict long-term behaviour of wood in the hygroscopic region (Le Govic *et al.* 1987; Genevaux 1989). However, these considerations relied mostly on the visual assessment of the master curve smoothness. While investigating the experimental data in the complex plot (McCrum 1967), Bardet (2001) reported some discrepancy of the time-temperature equivalency such as described by the Arrhenius law. Based on the same representation, Placet *et al.* (2007) has found that time-temperature equivalency could not be applied to the whole viscoelastic range but seems to be valid within each transition state.

In amorphous polymers like rubber, an effect of temperature on stress of pre-deformed specimen, usually called entropic (or rubber) elasticity, has been shown. This effect can be accounted for by multiplying the compliance by a correction factor dependent on the temperature. In particular in regions where the viscoelastic function is flat, the need of this factor was more important to obtain satisfactory matching of creep curves (Ferry 1980). In the case of wood, the applicability of such a correction is not straightforward because of its complex structure (Salmén 1984).

The aim of the present work was to check for the validity of above mentioned principles for wood and identify a generic rheological model applicable to wood specimens of different species, densities, nature and anatomical feature. According to the considered tree mechanics applications, we were interested in viscoelastic properties of green wood along the fibres. In this view, tensile creep tests in longitudinal direction in the temperature range 30-70°C were performed and obtained data discussed.

3.2 Material and methods

3.2.a Characteristics of selected specimens

Wood of four tropical species was selected for their contrasted Young's modulus and damping coefficient. Positioning of the selected specimens within Sample 1⁴ is shown in Figure B-18. The basic density was not available at the moment of the selection as specimens were green. Vibration properties measured in green state and structural parameters measured *a posteriori* are summarised in Table B-3. Following species were represented: *Dicorynia guyanensis* - *Dc*, *Lecythis persistens* - *Lp*, *Licania alba* - *La*, *Virola michelii* - *Vm*. Occurrence of tension wood is expected for two specimens (*Dg* and *La*). Specimen names are built as the initials of the species name followed by the specimen number. Altogether, ten specimens were tested.

Table B-3: Summary table of structural parameters measured *a posteriori* and mechanical properties measured by vibration method in green state.

Specimen	Basic density	MFA (°)	Young's modulus (GPa)	Specific modulus (GPa)	Damping coefficient
<i>Dg</i>	0.53	7.8	17.5	32.8	0.52%
<i>La</i>	0.74	10.3	24.0	32.4	0.73%
<i>Lp1</i>	0.68	20.0	15.7	23.0	0.77%
<i>Lp2</i>	0.68	11.3	15.8	23.3	0.76%
<i>Lp3</i>	0.68	9.7	13.8	20.3	1.00%
<i>Lp4</i>	0.75	13.2	17.4	23.2	0.90%
<i>Oa1</i>	0.86	14.6	20.5	23.8	0.73%
<i>Oa2</i>	0.84	13.2	19.8	23.6	0.80%
<i>Vm1</i>	0.43	20.8	8.6	20.0	1.18%
<i>Vm2</i>	0.45	21.8	9.8	21.7	1.04%

Legend: MFA: microfibril angle; Young's modulus was measured by vibration method in green state; specific modulus: ratio of Young's modulus and basic density.

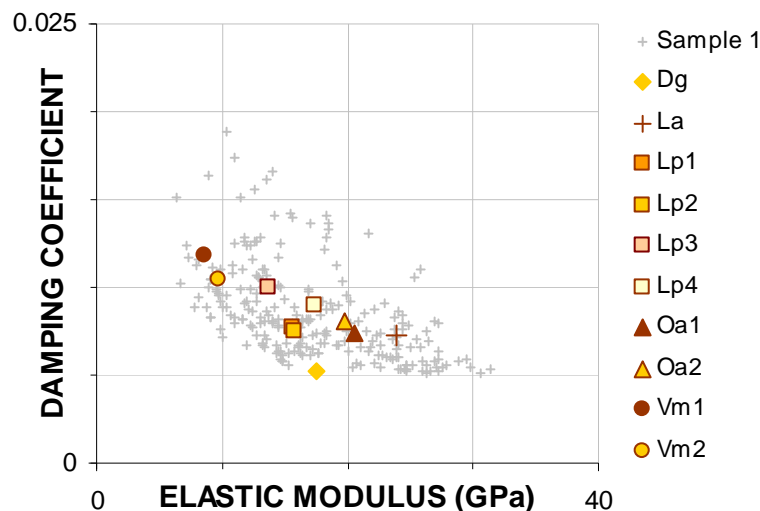


Figure B-18: Positioning of a selection of wood specimens used for the tests of time-temperature equivalency.

⁴ See chapter A) 2.2 for details

3.2.b Experimental procedure

Each specimen was submitted to stabilisation-creep-recovery cycles performed at isotherms between 30°C and 60°C as shown in the Figure B-19. Prior to the loading, each specimen was stabilised during 15h at a corresponding temperature. Afterwards, a constant load was applied during 8h, followed by a short recovery period and heating to the following temperature taking together approximately 1h. Thus one isotherm took 24h and the whole procedure holds in one week. Preliminary tests showed that a temperature step of 10°C gives an optimal overlapping of creep curves in the ACP plot.

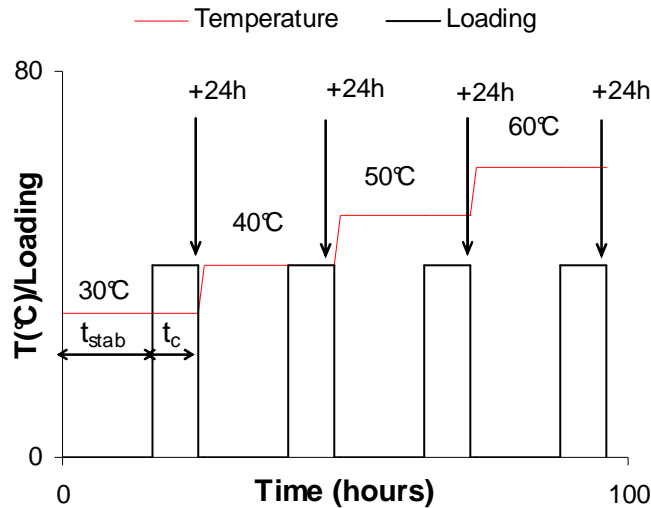


Figure B-19: Applied cycling schedule. t_{stab} : stabilisation time; t_c : creep time.

Considering thermal expansion coefficient of $-7.10^{-6}/^{\circ}\text{C}$ in the tangential direction evaluated for green wood from a previous study (Gril et al. 1993), the thermal dilation may induce the underestimation of the compliance of the order 0.04% that is negligible comparing with effects discussed later.

3.2.c Correction of strain data

During the stabilisation period prior to the loading cycle at a given temperature, the apparent strain is the result of different processes: recovery of preceding creep test, thermal stabilisation of the specimen (and of the gages themselves) and hygrothermal recovery of locked-in strains that can occur at elevated temperatures (Gril et al. 1993). To measure the creep strain developed during the following test, the stabilisation period has to be long “enough” to neglect the strain due to other processes. Another (faster) way is to correct strains arising from these other mechanisms by extrapolating them, in log time scale, using the strain measurements during the stabilisation period. Details about the extrapolation method are explained in §1.4.c. Note that the gages drift goes often in the direction opposite to the creep strain so that no correction would have resulted in an apparent decrease of the creep rate and thus misled the data interpretation.

3.3 Results and discussion

3.3.a Building of the master curve using log time shifts

Assuming the direct applicability of time-temperature equivalency, master curves were tentatively built from experimental data using shifts along the log time axis. Creep curves for each specimen were plotted as compliance versus log test time and shifted along the x-axis to build a master curve. Creep test performed at $T_0 = 30^{\circ}\text{C}$ was taken as a reference and

dimensionless shift factors, a_T , were numerically adjusted. The assumption that temperature affects only the kinetics of the creep response requires that the resulting curve is smooth.

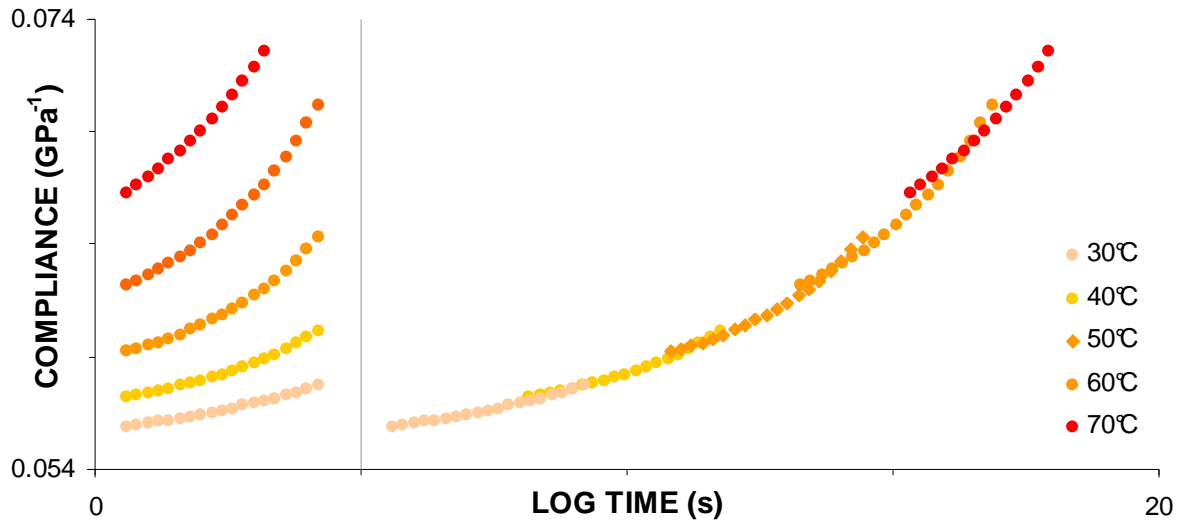


Figure B-20: Master curve obtained by shifting individual creep curves for the *Oa2* specimen along log time axis. Curve measured at 30°C is taken as a reference.

Figure B-20 shows a typical example of resulting master curve corresponding to experimental data obtained with *Oxandra asbeckii* specimen (*Oa2*, see below). Although the first three creep curves (30°-50°C) are quite well matched, overlapping of curves corresponding to the tests performed at higher temperatures is not complete. Nevertheless, log time shifts can be plotted against the reciprocal of temperature (Figure B-21a). The linear correlation between both parameters supports the applicability of time-temperature equivalency described by an Arrhenius law:

$$J(t;T) = J(t(T)/a_T;T_0), \quad (\text{Eq. B-8})$$

$$\log a_T = \frac{W_0}{\ln(10) \cdot R} \cdot \left(\frac{1}{T} - \frac{1}{T_0} \right), \quad (\text{Eq. B-9})$$

where a_T is the shift factor corresponding to the stretching of the real creep time with increasing temperature, W_0 the activation energy ($\text{J}\cdot\text{mol}^{-1}$), R the universal gas constant ($8.31 \text{ J}\cdot\text{mol}^{-1}\cdot\text{K}^{-1}$), T the temperature (K) and T_0 the reference temperature ($30^\circ\text{C} = 303.15 \text{ K}$ in this case). Activation energies derived from time shifts according to Eq. B-9 are given in Table B-4.

3.3.b Examination of experimental data in the complex plane

The representation in the ACP was then used for in depth analysis of the data. Obtained results will be illustrated on the *Oa2* specimen however ACP for each tested specimen is in the Appendix. Time-temperature equivalency requires that once plotted in the ACP, creep curves will form one single curve. However, when experimental data are drawn in the ACP, we can clearly observe discontinuities between the individual curves (

Figure B-22) that reflect the slope differences between poorly overlapping curve portions in Figure B-20. Individual creep curves are made up of linear segments with nearly the same slope but different J' -intercept for each of them so that final overlapping is poor. This obviously questions the validity of the assumption that only characteristic times are affected by temperature.

Let us assume that, similarly to rubber, the amorphous matrix of wood cell walls exhibits an entropic elasticity (Ferry 1980) whose effect can empirically be seen as a slight temperature dependency of the compliance J , denoted here as J - T effect. Suppose that $\lambda(T)$ is a multiplicative factor accounting for this effect:

$$J(t;T) = \lambda(T) \cdot J(t/a_T;T_0). \tag{Eq. B-10}$$

Such a temperature dependency of J will induce a homothetic transformation of creep curves in the ACP that could explain observed discontinuities between individual creep curves.

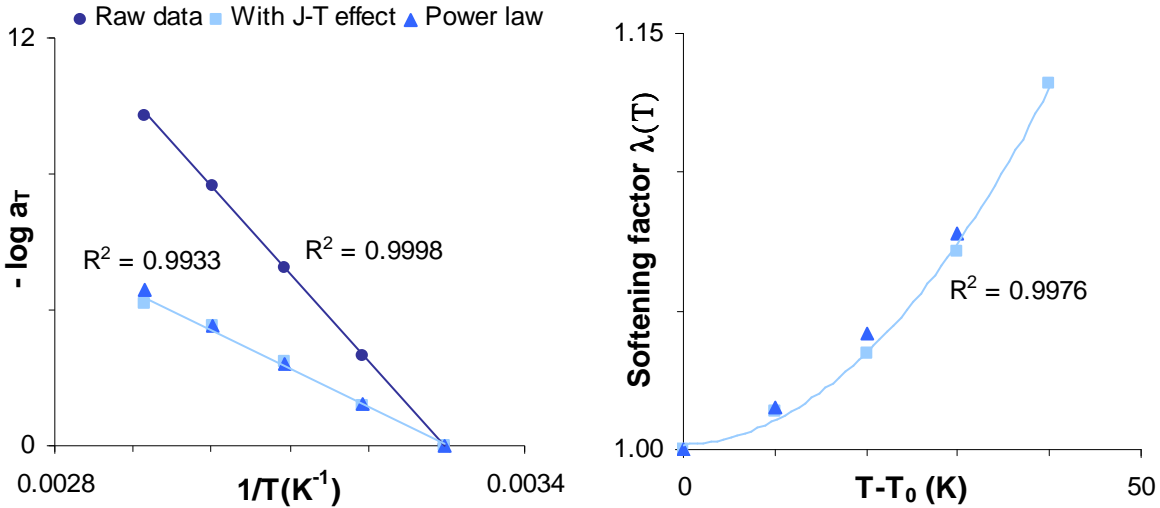


Figure B-21: (a) Temperature dependency of time shift factors issued from different optimisations and adequacy of an Arrhenius law (regression line). J - T effect: Experimental data corrected by the softening factor λ . Power law: Adjusted values of time shifts and softening factor based on Eqs. B-12-B-14. (b) Temperature dependency of the softening factor $\lambda(T)$ (*Oa2* specimen). The legend is the same as for Figure 5.

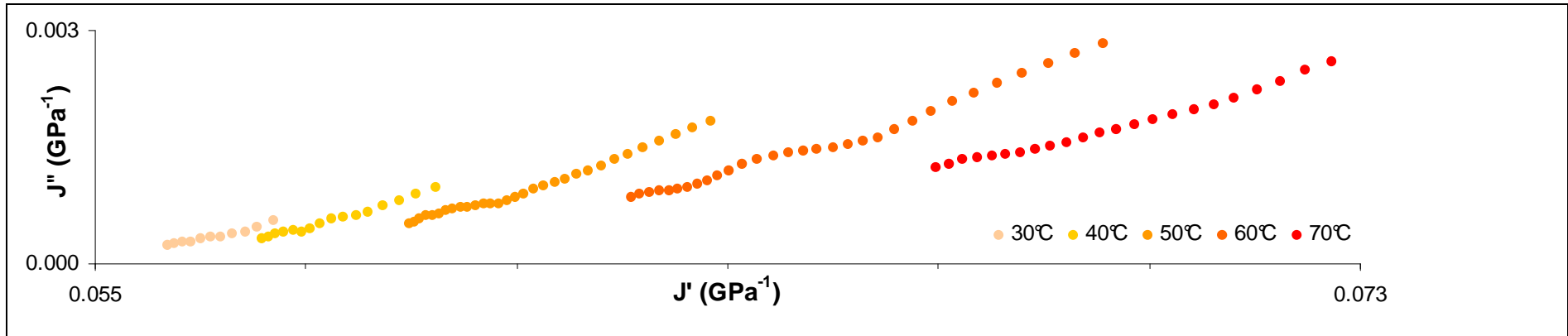


Figure B-22: Smoothed experimental data for the *Oa2* specimen plotted in the approximated complex plane (ACP) for different creep temperatures J' and J'' : Alfrey's approximations of storage and loss compliance respectively (Eqs. 1 and 2).

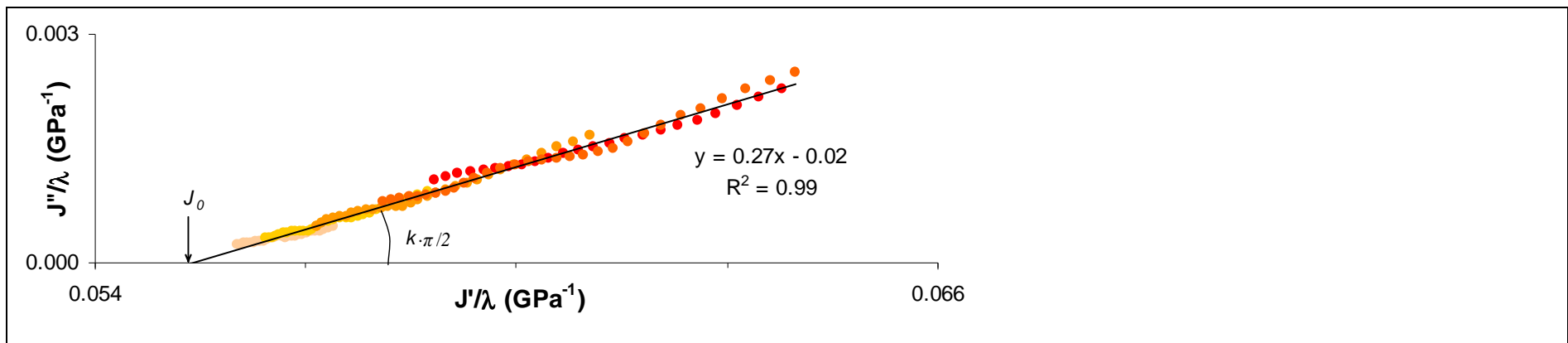


Figure B-23: ACP of

Figure B-22 corrected by the softening factor λ . J_0 : initial compliance, k : power exponent. J' and J'' : Alfrey's approximations of storage and loss compliance respectively (Eqs. 1 and 2).

Based on the assumption of the J - T effect, a two-steps procedure was applied on the experimental data. First, the temperature effect on the compliance was removed by performing a homothetic transformation of creep curves in the ACP. Multiplicative factors $\lambda(T)$ were adjusted in order to obtain a continuous curve, taking the test performed at 30°C as a reference. The resulting curve in the transformed ACP (*i.e.*, J''/λ versus J'/λ) was approximated by a polynomial of the second degree to allow for variations in the slope; however, a linear approximation was sufficient (Figure B-23). $\lambda(T)$ factors used for the correction were plotted with respect to temperature increase (Figure B-21b). An increase of temperature resulted in values of $\lambda(T)$ bigger than 1, meaning some kind of material softening. The relationship between both parameters in Figure B-21b was essentially linear, however polynomial of second degree was necessary for some specimens and finally used for all the specimens.

Once the condition of continuity between curves in the ACP has been satisfied, we apply the time-temperature equivalency. Data corrected for the J - T effect (J/λ) were used to construct the master curve. Plot of log time-shifts versus $1/T$ has showed again agreement with Arrhenius law to model thermal activation of green wood after correction (Figure B-21a). However, the slope of the regression line, proportional to the activation energy (denoted W_{J-T+} in Table B-4), was very different: omitting effect of the temperature on the compliance resulted in larger apparent time-temperature shift factors giving different kinetics of the creep response. Similar observation was made on polymethylmethacrylat (PMMA) by McCrum and Morris (1964) who stated temperature dependency of limiting modulus, analogous to our J_0 temperature dependency. Moreover, accounting for the J - T effect yields perfectly smooth master curve (Figure B-24). Thus, the assumption of temperature dependent compliance has been included in the rheological model.

3.3.c Identification of the rheological model

Based on the graphical representation of experimental data in the transformed ACP, close to a straight line, a “parabolic Maxwell” model (Huet 1988) was used to describe green wood creep as it was the case for physical aging. The behaviour of such an element is governed by a power law that can be written as:

$$J(t;T) = \lambda(T) \cdot J_0 \left[1 + \left(\frac{t}{\tau(T)} \right)^k \right], \quad (\text{Eq. B-11})$$

where $J(t;T)$ is the creep compliance, λ the multiplicative factor accounting for thermal softening of the compliance, J_0 the initial compliance, τ the doubling time and k the kinetic parameter (Figure B-23).

We used the same k for all the creep tests of a given specimen. This implies that the straight lines corresponding to individual tests in the ACP have the same slope. It can be seen from Figure B-23 that this assumption is rather well satisfied. On the contrary, parameters λ and τ are dependent on the temperature. The softening factor dependency on temperature is empirically modelled by a polynomial of the second degree (Figure B-21b) and evolution of τ is governed by the same Arrhenius law as Eq. B-9:

$$\lambda(T) = 1 + a_{1\lambda} \cdot (T - T_0) + a_{2\lambda} \cdot (T - T_0)^2, \quad (\text{Eq. B-12})$$

$$\ln \tau(T) = \ln \tau_0 + \frac{W}{R} \cdot \left(\frac{1}{T} - \frac{1}{T_0} \right), \quad (\text{Eq. B-13})$$

where T is temperature, T_0 the reference temperature and τ_0 the doubling time at T_0 with $a_T = \tau/\tau_0$. The model parameters (Eqs. B-11 - B-13) are directly identified on raw creep tests curves (

Figure B-22) and given in Table B-4.

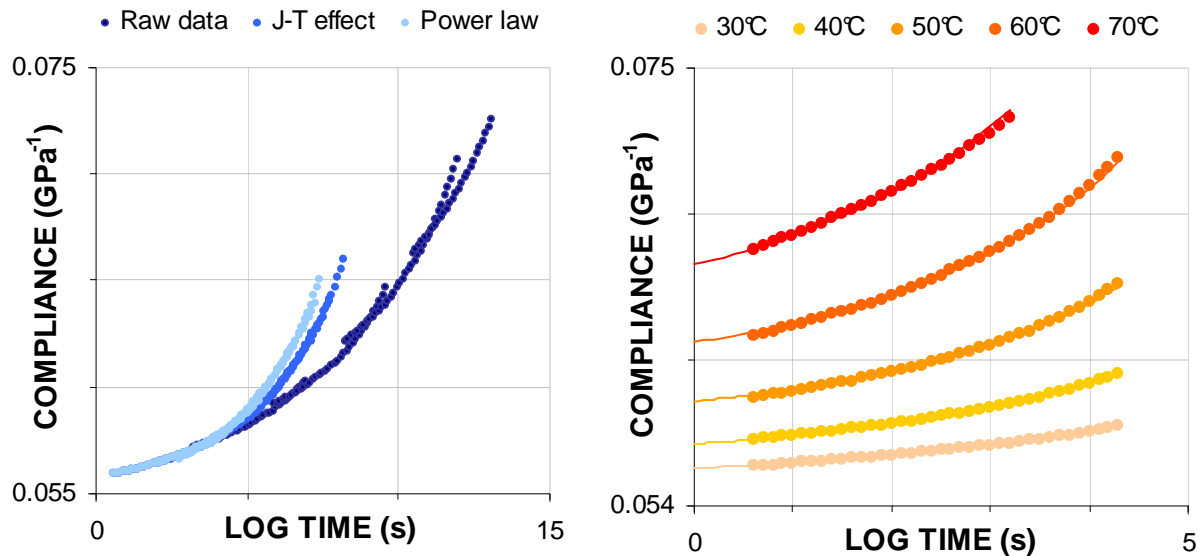


Figure B-24: (a) Master curves for the $Oa2$ specimen corresponding to different assumptions. Raw data: experimental d_{ata} from Figure B-20 shifted along the log time axis. $J-T$ effect: Experimental data corrected by softening factor λ . Power law: Modelled values based on Eqs. B-11 - B-13 accounting for the time-temperature dependency and softening factor λ . (b) Agreement between experimental data for the $Oa2$ specimen (markers) and the power law model (lines): power law $J-T$ effect and Arrhenius law (Eqs. B-11 - B-13).

3.3.d Variation of model parameters issued from different fitting methods

For some specimens the time-temperature shift factor for creep test performed at 70°C was not consistent with the Arrhenius law. This was ascribed to the vicinity of glass transition temperature for lignin (Salmén 1984) and corresponding creep curves were not used for further analysis. Also for specimens used during preliminary tests at many temperatures (see column “Extra T” in Table B-4 for details), only those done at “standard” temperatures (30-40-50-60°C) were used to enable comparison between specimens. However, note that including these data yields a negligible effect on the tuned parameter values for the rheological model. This confirmed the robustness of the proposed model.

Table B-4: Summary table of rheological parameters assuming different hypothesis

Specimen	W_0 $\text{kJ}\cdot\text{mol}^{-1}$	W_{J-T+} $\text{kJ}\cdot\text{mol}^{-1}$	Power law model parameters								Extra T
			J_0 (GPa ⁻¹)	k	$a_{1\lambda}$ ($\cdot 10^{-5}$)	$a_{2\lambda}$ ($\cdot 10^{-3}$)	λ_{60}	$\log \tau_0$ (s)	W $\text{kJ}\cdot\text{mol}^{-1}$	rms error (%)	
<i>La</i>	480	311	0.044	0.12	4.94	-0.14	1.04	15.5	322	0.09	55-65-70
<i>Oa1</i>	763	391	0.058	0.16	1.57	1.89	1.07	14.6	288	0.11	45
<i>Oa2</i>	487	237	0.055	0.18	5.15	1.05	1.08	12.1	228	0.07	70
<i>Dg</i>	628	355	0.053	0.07	0.48	0.97	1.03	23.0	367	0.07	
<i>Lp1</i>	561	254	0.064	0.13	3.80	0.85	1.06	14.8	275	0.07	55-70
<i>Lp2</i>	623	419	0.062	0.13	6.97	-0.51	1.05	16.3	385	0.14	70
<i>Lp3</i>	501	315	0.065	0.15	7.08	-0.18	1.06	13.7	335	0.21	
<i>Lp4</i>	513	327	0.051	0.11	7.32	-0.70	1.04	17.1	305	0.11	
<i>Vm1</i>	558	265	0.113	0.05	2.92	0.65	1.05	25.2	315	0.05	
<i>Vm2</i>	486	69	0.099	0.07	4.66	1.79	1.10	17.6	62	0.06	
ave	568	319	0.066	0.12	4.49	0.57	1.05	17.00	313		
std	91	62	0.022	0.04	2.34	0.92	0.02	4.11	48		
std%	16%	19%	33%	36%	52%	162%	2%	24%	15%		

Legend: W_0 : activation energy deduced from horizontal shifts of raw experimental data. W_{J-T+} : activation energy deduced from horizontal shifts of experimental data corrected by softening factor λ . Parameters of the power law (Eq. B-11): J_0 : initial compliance, k : power parameter, $a_{1\lambda}$, $a_{2\lambda}$: parameters of the polynomial temperature dependency of the softening factor λ (Eq. B-12), λ_{60} : softening factor for 60°C expressing the amplitude of the temperature effect on the compliance, W : activation energy, rms error: root mean square error between modelled and measured compliance values. *Extra T*: temperatures tested above the standard temperatures.

Table B-4 summarises the rheological parameters obtained by different methods developed before. W_0 is the activation energy derived from time shift factors used for the construction of the master curve from raw experimental data (only t - T effect). The second value of activation energy, W_{J-T+} , is obtained from the data corrected by the softening factor λ . The third set of data represents parameters of the rheological model governed by a power law with polynomial temperature dependency of the softening factor λ and Arrhenius law accounting for the time-temperature equivalency (Eqs. B-11 - B-13). Softening factor, λ_{60} , gives the magnitude of the temperature effect on the compliance at 60°C for comparison. Finally, the relevance of the model is assessed through the root mean square error (rms error) between modelled and measured compliance values.

The activation energy describes the magnitude of time-stretching effect of the temperature; higher values correspond to stronger temperature effect. From the comparison between W_0 and W_{J-T+} presented in Table B-4 we can see that including the J - T effect has reduced the apparent time-temperature effect. Consequently, corresponding master curves have different kinetics as illustrated in Figure B-24. Except for one specimen (*Vm2*), values of activation energy are similar for all the specimens, the average being of 545kJ/mol for W_0 and 319kJ/mol for W . Comparing with bibliographic data deduced from the $\tan\delta$ peak dependency on frequency, not affected by the presumed temperature effect on the compliance ($\tan\delta = J''/J'$), the assumption of thermal softening seems to give more consistent values of the activation energy (395kJ/mol for Salmén; 339kJ/mol for Kelley).

For the *Vm2* specimen, the raw value of the activation energy is consistent with others ($W_0 = 486\text{kJ/mol}$) if we do not take into consideration the transgression of the time-temperature equivalency, *i.e.*, discontinuity between creep curves observed in the ACP. However, once the J - T effect is considered to allow us to use of the time-temperature equivalency, very poor thermal activation is observed ($W_{J-T+} = 66\text{kJ/mol}$). Conversely, temperature effect on the compliance is larger than in other specimens ($\lambda_{60} = 1.1$ against the average of 1.05).

The rheological model showed a very good agreement with experimental values for all specimens as illustrated in Figure B-24b (see rms in Table B-4) in spite of contrasted values of J_0 resulting from the structural diversity of studied sample. Activation energy values are very close to W_{J-T+} and rather consistent between specimens (*i.e.*, standard deviation as low as 15%). This is quite interesting as it gives some idea on the physical meaning of this factor: it should not be much affected by structural parameters but rather by the chemistry. On the other hand, the variability of the kinetic parameter k and doubling times τ_0 , likely related to the structural diversity, was significant between specimens (around 30%).

Investigating the relationships between model parameters and structural properties, we can notice strong dependency of the power coefficient k and doubling time τ_0 on the wood basic density (Figure B-25). This correlation is positive in the case of the power coefficient and negative for the doubling time. At the same time, both parameters are significantly correlated one to another (Figure B-26a). This means that probably only one of mentioned correlations on basic density has some physical meaning. While a slight dependency of the softening coefficient at 60°C on the microfibril angle was observed (Figure B-26b), no significant dependency of kinetic parameters on microfibril angle has been noted. This opens perspectives on future work relying on the understanding of the physical meaning of the model parameters. Relation between the creep and structural parameters will be investigated further in §4.3.

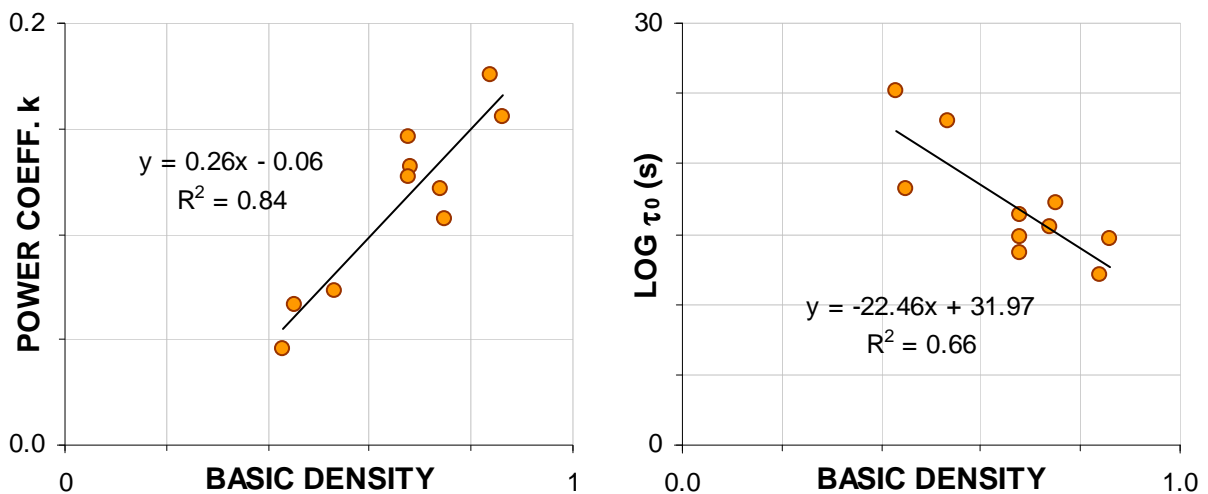


Figure B-25: (a) Relationship between the power coefficient and basic density. (b) Relationship between the log of doubling time τ_0 and basic density.

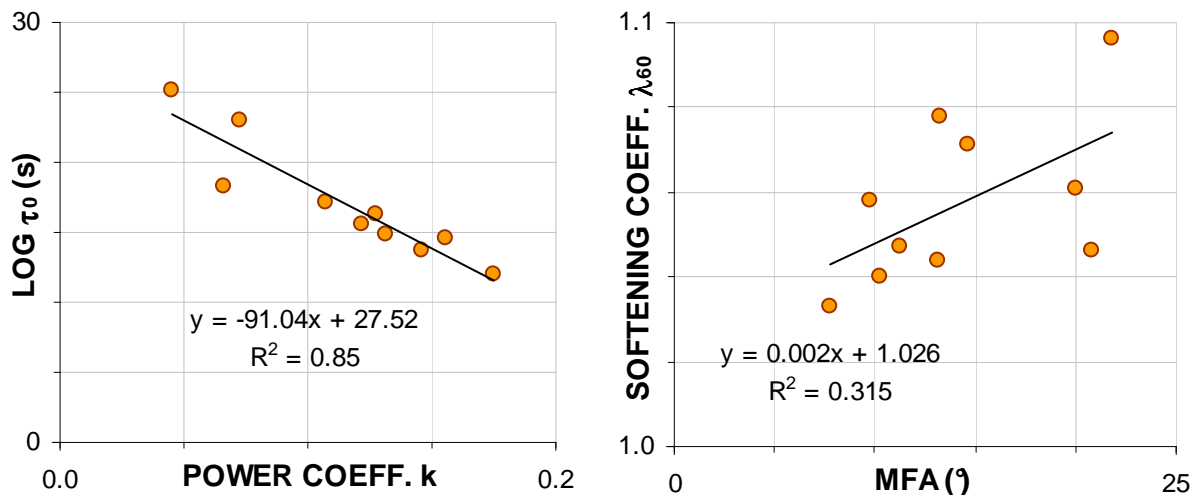


Figure B-26: (a) Relationship between the power coefficient and the log of doubling time τ_0 . (b) Relationship between the softening parameter λ_{60} and microfibril angle.

3.3.e Simplified predictions of the long-term creep based on reduced number of creep tests

As the characterisation of long-term creep behaviour is a time-consuming procedure, we wanted to see if some simplification of the experimental schedule was possible. The master curve obtained by horizontal shifting of the experimental data previously corrected by the softening factor (J - T effect, denoted further only master curve) was used as a reference. First tested hypothesis was to use only the creep test performed at 30°C. Figure B-27a shows the relationship between the creep observed after 8h and that predicted by the master curve at the end of 30 years. Excepting *V. michelii* specimens, there is a good relationship between both parameters. However if *V. michelii* specimens are considered, the correlation coefficient is markedly decreased ($R^2 = 0.32$).

Hence, we have tried to fit the parameters of the power law on the creep curve measured at 30°C and extrapolate the obtained curve into the desired period of prediction fixed to 30years. Figure B-27b shows an example of such an extrapolation obtained for *Oa2* specimen and compared to the master curve. For comparison, curve corresponding to the power law whose parameters were fitted on creep curves measured at four different temperatures (denoted as Power law) was also represented. Extrapolation of the creep curve measured at 30°C derives rapidly from the master curve yielding an average error of about 5.6 % (STD 29.3%) at the end of 30 years. Correspondence between this simplified prediction of the relative creep compliance and the master curve is not so bad (Figure B-28a).

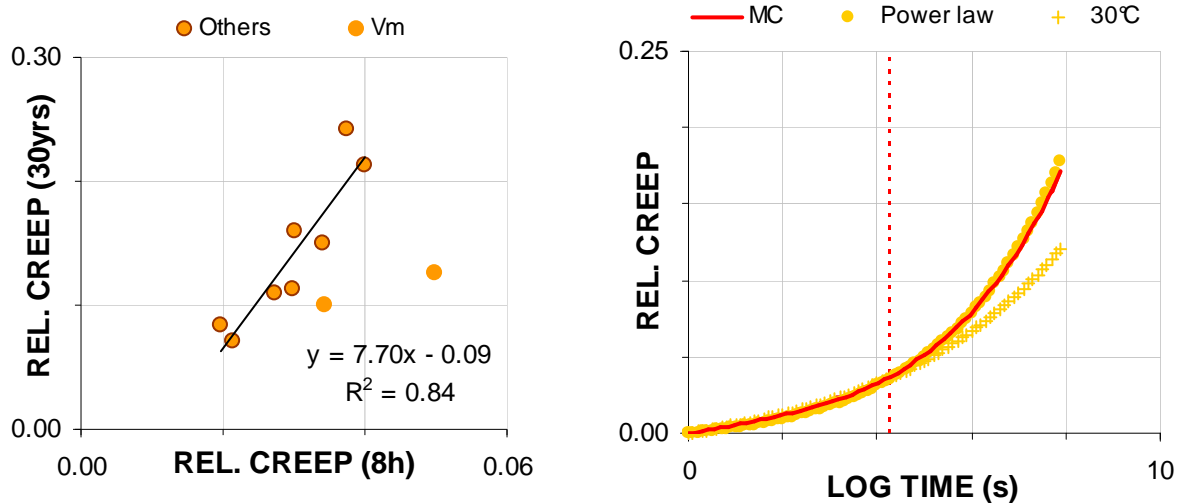


Figure B-27: (a) Relationship between the creep measured at the end of 8h and its prediction at the end of 30yrs. (b) Extrapolation of the creep curve measured at 30°C and compared to the master curve (MC) generated by horizontal shifting in the compliance – log time plots of the data previously corrected by softening factor λ and power law fitted on four temperature steps (power law). Dashed line represents the end of the test at 30°C. Specimen: *Oa2*.

A second approach was to take the creep curve measured at 50°C, using the mean values of activation energy and softening parameter λ at 50°C. The creep kinetics was expected to be better represented by the test at increased temperature. The obtained prediction is displayed in Figure B-28b. No significant improvement can be noticed. If the creep kinetic is slightly closer to that predicted by the complete power law, we add incertitude about the initial compliance because of the average values of activation energy and softening parameter. This method is even less suitable than simple extrapolation of the creep test performed at 30°C.

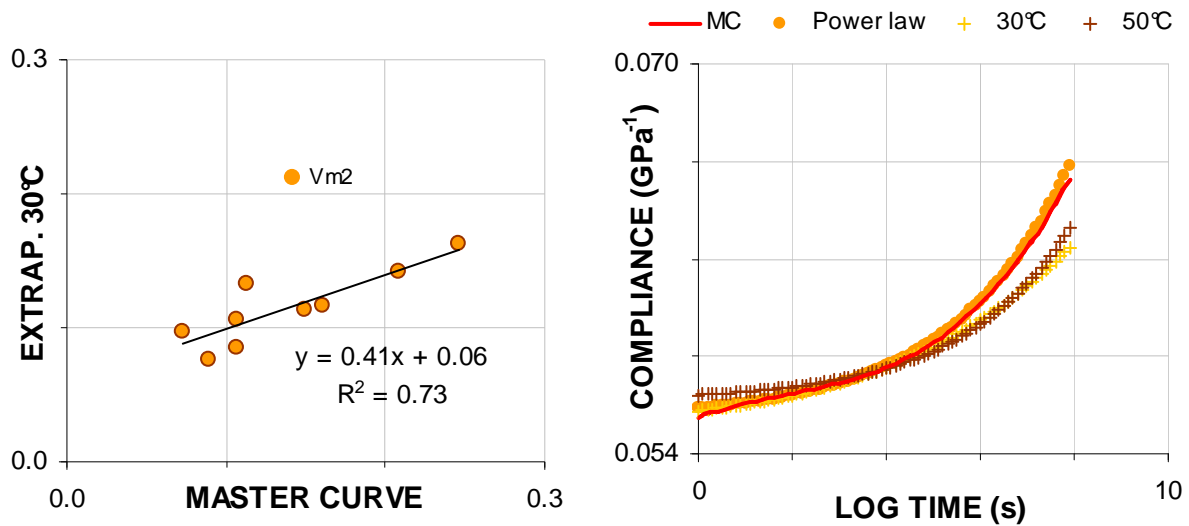


Figure B-28: (a) Correspondence between the creep prediction at the end of 30yrs period obtained by extrapolation of the power law fitted on creep data measured at 30°C and creep predicted by non parametric master curve. (b) Prediction of a long-term creep based on the creep test performed at 50°C. Specimen: *Oa2*.

Finally, we decided to base our prediction on two creep tests: one performed at 30°C and a second one at 50°C. In this way, values of activation energy and softening parameter can be obtained for each specimen. In the first simulation, only the activation energy was fitted and the mean value of λ_{50} was used. This result did not bring much improvement comparing to the prediction based only on the creep curve measured at 30°C (Figure B-29a). However, once the value of λ_{50} was adjusted, the simplified prediction became very close to the power law fitted on four temperature steps (Figure B-29b).

Correspondence between values of the relative compliance obtained from the master curve and that on predicted from two creep tests during a 30 years period is shown in Figure B-30b. Definitely we can say that under assumption that the proposed rheological model is valid, two creep tests performed at 30° and 50°C are sufficient to correctly predict the creep behaviour in the experimental window of 30 years. From the practical point of view, it allows to divide the needed experimental time by two. Average error of this simplified prediction relative to the power law is of 10.3% (STD = 8.6 %). Comparing to the master curve, the error of the prediction at the end of thirty years is of 13.3% (STD = 12.9%). Both *V. michelii* specimens are included in these considerations.

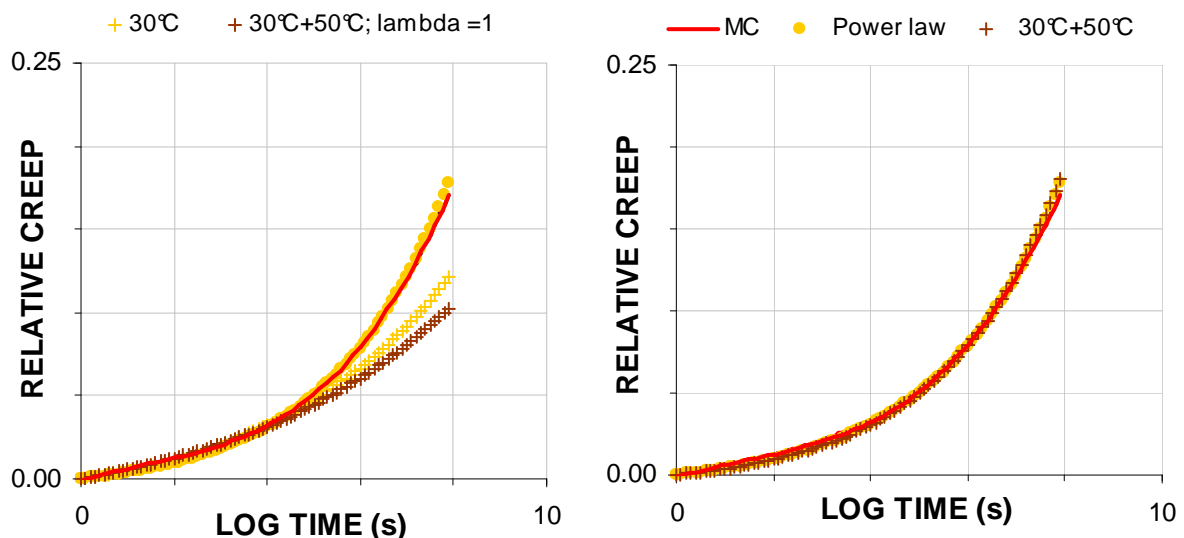


Figure B-29: Prediction of long-term creep based on creep tests performed at 30°C and 50°C. (a) Softening parameter λ is not considered. (b) Softening parameter is adjusted on experimental data. Specimen: *Oa2*. Legend of series symbols is common for both figures.

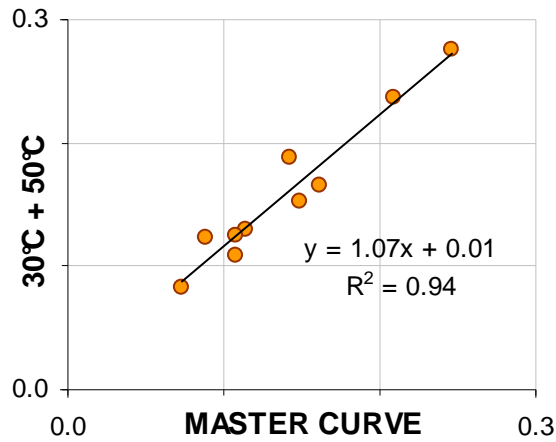


Figure B-30: Correspondence between the relative compliance at the end of 30 yrs given by the master curve and predicted using two creep tests performed at 30°C and 50°C.

3.4 Conclusion

Our work shows that time-temperature equivalency can be applied on green wood only if an additional temperature effect on the compliance, similar to entropic elasticity in rubber, is considered. It could be seen as some kind of material softening when the temperature increases. This means that temperature affects not only the kinetics but also the intensity of viscoelastic processes. Moreover, a rheological model governed by a power law accounting for this effect has shown its relevance to describe the delayed behaviour of a contrasted selection of tropical species. However, the meaning of this entropic elasticity and the way to model it in wood must be investigated deeper and questions have to be solved about the link between the model parameters and the structural features of wood material. First observations have outlined a poor relationship between the softening coefficient and microfibril angle. On the other hand, both kinetic parameters (k and τ_0) were strongly related to basic density and also correlated between them. Aiming to simplify the experimental procedure, predictions of the creep behaviour in the experimental window of 30 years based on one or two creep tests were assessed. If one creep test performed at 30°C or 50°C has not given satisfying results, two creep tests (30° + 50°C) were sufficient to predict accurately the creep behaviour in a given experimental window.

4) Relationship between structural parameters, vibration properties and creep properties

In this section, relations between creep data, vibration properties and structural parameters are investigated. Creep data of all specimens tested at 30°C are used. It includes specimens used for preliminary tests and specimens for which some measurement problem appeared during creep tests at higher temperatures. Measured parameters are summarised in Table B-5. There are mechanical properties from creep and vibration measurements along with basic density, microfibril angle and percentage of anatomical elements when these are available.

Specimen names are built as the initial of specie's name followed by a letter specifying the growing situation of a tree (S for straight growing tree, T for tilted tree), the tree number, a letter specifying the tree side and the number of the specimen. The tree side may indicate a possible difference between tension and opposite wood. However, as the occurrence of different wood tissues has been partially lost during the transport of logs (details in A-2.3), we did not want to denote specimens as tension wood as this one is not certain. Minimal and maximal values are also represented to illustrate the range of variability of the studied parameters. Altogether, 24 specimens from six different species were tested.

Table B-5: Summary table of mechanical properties and structural parameters of all specimens tested in creep at 30°C

<i>Specimen</i>	<i>Static modulus (GPa)</i>	<i>Rel. creep (8h)</i>	<i>Dynamic modulus (GPa)</i>	<i>Basic density</i>	<i>Specific modulus</i>	<i>Damping coefficient</i>	<i>MFA</i>	<i>Fibres (%)</i>	<i>Rad. par. (%)</i>	<i>Ax. par. (%)</i>
<i>Dg_S1_a1</i>	18.7	5.2	18.7	0.51	36.5	5.85E-03	7.9	59.6	11.6	26.5
<i>Dg_S1_a2</i>	17.7	2.0	18.7	0.53	35.1	5.24E-03	7.4			
<i>Eg_S1_a1</i>	23.6	8.5	22.6	0.72	31.6	6.18E-03	8.2	66.7	21.9	7.5
<i>Eg_S1_b1</i>	14.1	11.5	13.6	0.52	26.1	8.95E-03		63.1	21.5	11.0
<i>La_T1_a1</i>	28.4	1.9	27.6	0.82	33.8	8.40E-03	9.1	74.4	16.4	2.5
<i>La_T1_a2</i>	27.2	2.1	27.3	0.78	34.8	5.76E-03	10.2	72.7	14.9	8.0
<i>La_T1_a3</i>	25.7	4.3	26.2	0.77	34.1	6.46E-03	9.4	50.2	23.0	18.2
<i>La_T1_b1</i>	26.4	3.9	25.2	0.82	30.9	5.99E-03	8.7	75.0	19.0	0.0
<i>La_T1_b2</i>	23.8	3.1	23.5	0.74	31.7	7.28E-03	10.2	72.4	17.3	4.7
<i>La_T1_b3</i>	25.5	2.5	25.5	0.80	31.8	9.18E-03	9.8	73.7	12.9	6.7
<i>Lp_S1_a1</i>	15.7	2.7	15.1	0.68	22.2	7.70E-03	19.8	64.8	17.9	13.4
<i>Lp_S1_b1</i>	15.9	2.5	15.4	0.68	22.8	7.56E-03	12.0	66.0	17.8	12.7
<i>Lp_S1_b2</i>	13.6	3.7	13.3	0.68	19.6	1.00E-02	9.0	66.0	17.0	14.2
<i>Lp_S2_a1</i>	23.2	1.6	23.1	0.78	29.7	1.01E-02	8.7	70.5	11.5	15.0
<i>Lp_S2_b1</i>	19.4	2.8	19.0	0.75	25.4	8.96E-03	11.7	66.5	15.0	15.1
<i>Oa_T1_a1</i>	18.8	4.4	17.9	0.83	21.5	7.89E-03	13.6	62.0	18.8	14.5
<i>Oa_T1_a2</i>	19.0	3.4	18.5	0.84	22.1	8.01E-03	14.1	71.8	14.1	11.3
<i>Oa_T1_a3</i>	20.6	5.1	19.8	0.91	21.9	6.94E-03	12.9	70.2	14.7	11.8
<i>Oa_T1_a4</i>	19.5	1.9	18.5	0.86	21.5	7.34E-03	14.3			
<i>Oa_T1_b1</i>	21.9	5.2	21.4	0.77	27.7	7.53E-03	12.2	76.8	11.9	8.4
<i>Vm_S1_a1</i>	11.1	18.9	12.3	0.38	32.2	7.25E-03	11.8	67.9	27.6	0.0
<i>Vm_S1_a2</i>	10.7	15.6	11.4	0.45	25.5	6.93E-03	13.0	68.5	26.6	0.0
<i>Vm_S1_b1</i>	14.3	22.3	16.4	0.41	40.1	6.60E-03	12.0	70.0	23.8	0.0
<i>Vm_T1_a1</i>	8.5	10.2	8.2	0.37	22.0	1.01E-02	17.4	58.1	37.3	0.0
<i>Vm_T1_b1</i>	8.6	3.1	8.4	0.43	19.4	1.18E-02	20.5	54.8	38.9	0.0
<i>Vm_T1_b2</i>	9.4	4.8	9.1	0.45	20.1	1.04E-02	21.4	55.4	37.6	0.0
<i>min</i>	8.5	1.6	8.2	0.37	19.4	5.24E-03	7.4	50.2	11.5	0.0
<i>max</i>	28.4	22.3	27.6	0.91	40.1	1.18E-02	21.4	76.8	38.9	26.5

Legend: All mechanical properties are measured in green state. Rel. creep is the relative creep at the end of 8h lasting creep test performed at 30°C expressed in %. Specific modulus is calculated from dynamic modulus and basic density. MFA: microfibril angle. Rad. par.: percentage of radial parenchyma; Ax. par.: percentage of axial parenchyma.

4.1 Relation between creep and vibration data

Let us first assess relations between creep data and vibration measurements. Correspondence between Young's modulus measured by the vibration method and Young's modulus estimated from creep strain at 4s after the loading is represented in Figure B-31. We can observe a significant relationship between both measurements. The slope of the regression line is close to unity. Relation between the amount of relative creep at the end of 8h lasting creep test and damping coefficient is displayed in Figure B-31b. No dependency can be noted between both parameters.

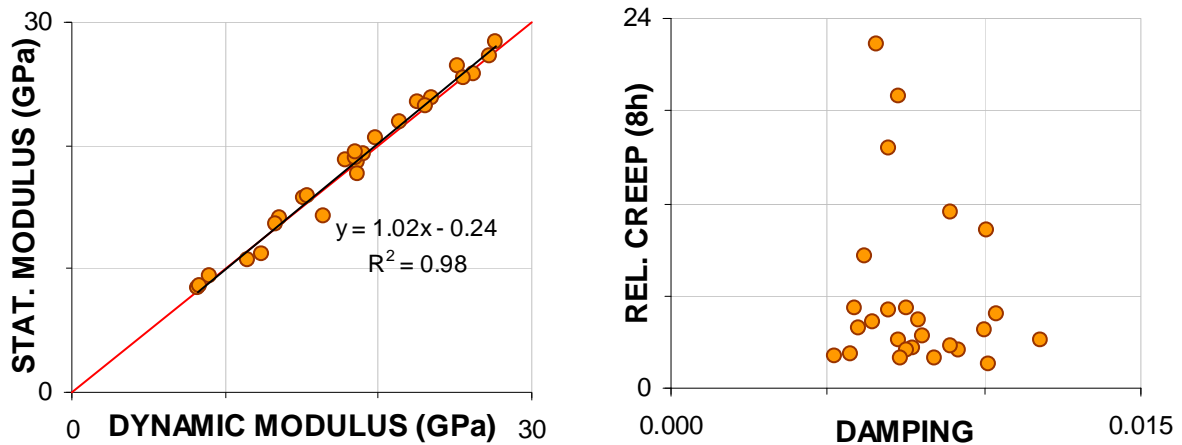


Figure B-31: Relationships between dynamic and static measurements. (a) Correspondence between Young's modulus measured by vibration method and Young's modulus estimated from the creep measurements. Red line represents the relation $y = x$. (b) Relationship between relative creep at the end of 8h and damping coefficient.

In conclusion we can say that elastic parameters obtained by static and vibration methods exhibit a strong linear dependency while the viscous parameters seem not to be related. This could be due to different observation time scales corresponding to both tests. The frequency of damping measurement ranges from 300 to 600 Hz whereas during the creep measurement the loading is quasi static. Wood is expected to exhibit several transitions depending on the frequency and/or temperature of investigation (for details see 0-3.5.c). Hence it is possible that the mechanism involved during the vibration measurement is different from the mechanism involved during the creep measurement.

ACP including vibration data

Let us now assume that the same mechanism is involved during dynamic and static measurements. Also the point obtained by vibration method should be positioned in ACP plot in the extrapolation of the curve representing the mechanism involved during the creep tests. As we have at our disposal estimates of damping coefficient measured by vibration method, we can easily obtain imaginary part of the complex compliance as follows:

$$J' \approx 1/E, \tag{Eq. B-14}$$

$$J'' = \tan \delta E, \tag{Eq. B-15}$$

where $\tan \delta$ is the damping coefficient and E the Young's modulus measured by vibration method. An example of ACP plot containing both static and dynamic measurements is shown in Figure B-32. Creep data displayed correspond to data after correction by softening factor λ (for details see §3.2.b). Creep curves form one single straight segment, a representation characteristic for a parabolic Maxwell model. If the same mechanism was involved during both tests, the point corresponding to vibration test should be positioned in the extrapolation

of the straight segment formed by creep curves. We can see that the point corresponding to the vibration measurement is positioned roughly in a good place but shifted to the left and its imaginary compliance is higher than expected if the same mechanism was involved. This indicates the possibility of two different mechanisms governing the viscoelastic behaviour at the acoustic time scale and quasi-static scale. The interpretation was not so straightforward for all specimens. In four cases, the point corresponding to the vibration measurement was shifted to the right side relative to the creep test performed at 30°C. This can be partly explained by the uncertainty of the compliance estimation that is represented for both measurements by the error bars (1.76% for the creep and 0.66% for the vibration measurements). The uncertainty of the imaginary compliance estimation ($2.96 + 0.66\%$, for details see A-3.2.b) is also plotted but so small that it is not visible. Another parameter affecting the comparison of creep and vibration results is that the creep measurement is local contrary to the vibration one. However, the imaginary part of the compliance was higher for all tested specimens supporting the idea about two different mechanisms. ACPs for all specimens containing also the vibration measurement are in the Appendix.

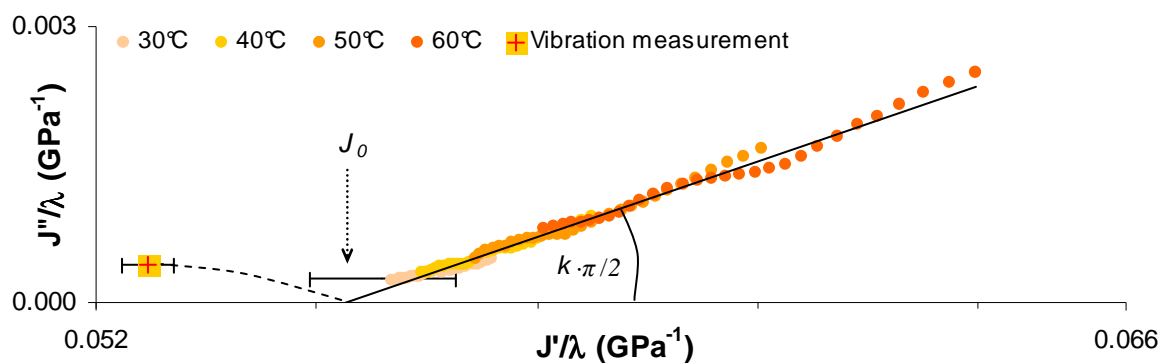


Figure B-32: Transformed ACP plot including the point corresponding to the vibration measurement. Dashed line represents presumed second rheological mechanism expressed during dynamic loading. Specimen: *Oa2*.

4.2 Variability of the creep response

Figure B-33 shows creep curves of all 26 specimens tested at 30°C. For most of them the amount of relative creep at the end of 8h is lower than 5%. However some particular behaviour is observed for some specimens reaching an amount of relative creep higher than 10%. Only two species exhibit this behaviour: *E. grandiflora* and *V. michelii*. Two of *V. michelii* specimens, however, have very similar behaviour comparing to other species. Note that it was the same species that exhibited a different thermal activation as detailed in §3.3.d. The absence of thermal activation was also observed for *E. grandiflora* specimens (not presented).

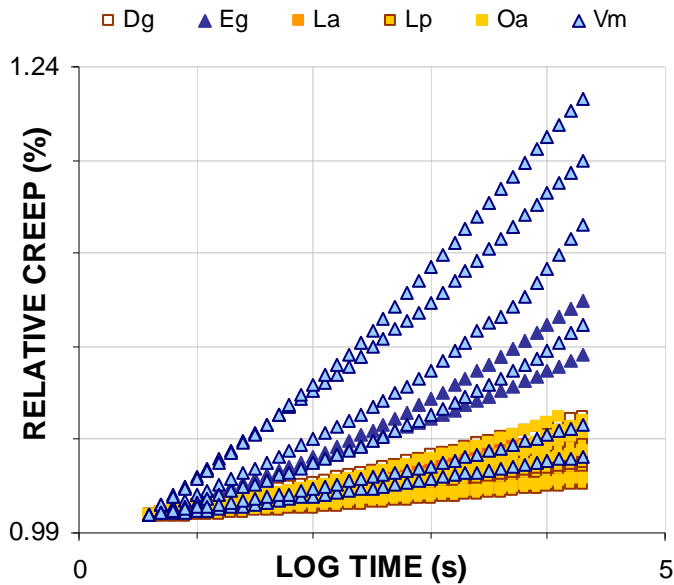


Figure B-33: Creep curves corresponding to all specimens tested at 30°C.

In the following chapter we will see, if the particular behaviour observed for some of specimens can be explained by their structure.

4.3 Structural determinants of viscoelastic behaviour

Structural parameters that we have at our disposal are the following: basic density, microfibril angle and percentage of different anatomical elements. In chapters A-6.3 and A-6.5, relations between vibration measurements and structural parameters have been discussed. Young's modulus was strongly related to the basic density as expected for a cellular solid and specific modulus was correlated with MFA. Previously reported empiric relation between damping coefficient and specific modulus was confirmed. On the other hand, damping coefficient was no related to MFA which was unexpected and no significant correlation was observed between vibration properties and percentage of different wood elements.

Table B-6 summarises correlation coefficients between the creep measurements and other parameters. Strong correlations are observed for elastic modulus while relative creep is not correlated with other parameters. The only parameter that seems to be correlated with the relative creep is the basic density. However, if we plot the values of relative creep in respect with basic density, we can note the correlation is due in particular to the presence of *V. michelii* specimens. On the other hand, no specimen with high basic density exhibits high relative creep.

Table B-6: Matrix of correlation coefficients relating mechanical properties obtained from creep tests and other parameters.

<i>n</i> = 26	Static modulus	Rel. creep (8h)
Static modulus	1	
Rel. creep (8h)	-0.48	1
Dynamic modulus	0.99	-0.41
Basic density	0.80	-0.65
Specific modulus	0.50	0.27
Damping coefficient	-0.45	-0.15
MFA	-0.66	0.05
Fibres (%)	0.51	-0.03
Rad. par. (%)	-0.71	0.39
Ax. par. (%)	0.29	-0.43

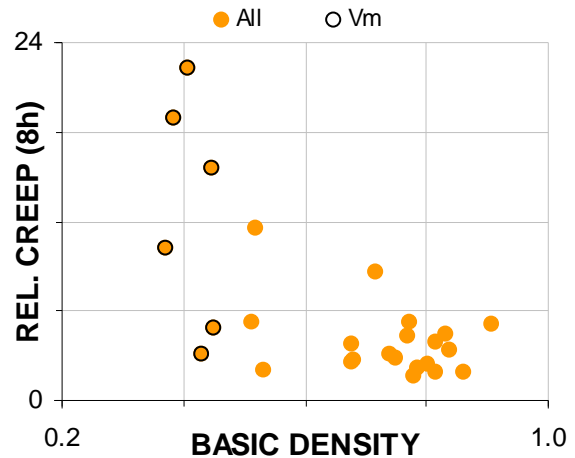


Figure B-34: Relationship between the amount of relative creep (%) and basic density.

According to some previous reports (El-Osta and Wellwood 1972; Kojima and Yamamoto 2004), the amount of tensile creep is expected to be positively correlated to the microfibril angle. On our sample, no correlation was observed (Figure B-35). This is probably due to the high diversity of our sample. Previous reports are characterised by a small number of species (3 for El-osta et al. and 1 for Kojima et al.). Further, they focused on softwoods with occurrence of compression wood. Thus implies great variation in MFA while other parameters as density vary less comparing to our sample. However, parallel to change in MFA compression wood is also characterised by increased lignin content that will affect the creep behaviour and that is not quantified in these studies. Another important difference is the regularity of the anatomical structure of softwoods comparing to hardwoods, in particular the tropical hardwoods. All these parameters can reduce the impact of MFA on the creep behaviour of our sample.

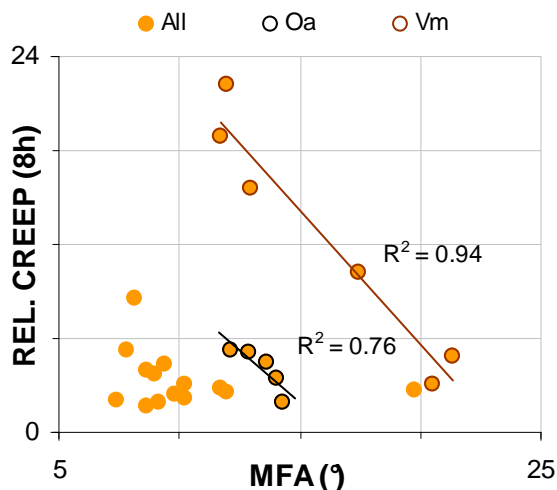


Figure B-35: Relation between relative creep and microfibril angle. Regression lines represent intraspecific correlations for *Oa* and *Vm* specimens.

While investigating intraspecific relationships between relative creep and microfibril angle, significant correlations can be often observed. However, these relationships are not always positive as shown in Figure B-35 and which was unexpected. This indicates that microfibril angle is probably linked to other parameters as for example chemical composition. However, we can not detail intraspecific relationships in the present study because of a reduced number of specimens by species that we have at our disposal.

4.4 Conclusion

Considering the absence of correlation between vibration data and creep data, it seems to be difficult to predict the long-term behaviour based on vibration measurements. The main difference between both viscoelastic parameters is the scale of the observation time. Thus, we have suggested that mechanism involved during vibration measurement is not the same as the rheological mechanism that determines the creep behaviour.

Investigating the variability of the creep response, we have seen that some of *V. michelii* and *E. grandiflora* specimens exhibited high amount of relative creep compared to other specimens. However, assessment of relationships between creep data and structural parameters has not brought any satisfying key to explain the observed variability. The effect of microfibril angle, reported in some previous studies as determinant for the creep behaviour, was not related to the relative creep in our sample. On the other hand, some significant intraspecific relationships were observed indicating that microfibril angle can be a good intraspecific indicator of the creep behaviour. However, because of the reduced number of tested specimens by species we could not progress in the intraspecific analysis. Studied parameters are not sufficient to explain the interspecific variability of the creep response indicating that creep response is dependent on many parameters.

5) Conclusion

The present chapter dealt with the creep behaviour of green wood in longitudinal direction. The aim was to investigate the possibility of the long-term prediction of the creep properties and explore its variability. During the set up of the experimental procedure, physical aging phenomenon typical of semi-crystalline polymers was evidenced in green wood from three tropical species. The assumption of uniform aging rate was verified by the construction of master curves from series of tensile creep tests in the fibre direction, performed at increasing time elapsed after a quench following heating above the glassy transition. The rheological response during periods of creep small enough to neglect the progress of aging was described by a parabolic Maxwell model, where only the characteristic time depends on the aging time. The model was able to describe results obtained by a previous author on softwood loaded transversally to the fibres. The possible role of a transient adsorption process consecutive to the quench was discussed.

Based on the results of aging study, continuous experimental procedure without any cooling period was suggested to test the validity of time-temperature equivalency principle. This principle is often used for long-term predictions of creep behaviour from short-term creep tests. The time scale considered in this study is the duration of a tree life. Aiming to predict the long-term behaviour of green wood, viscoelastic properties along fibres were investigated through a sequence of creep tests in the temperature range 30°- 70°C. The apparent validity of time-temperature equivalency was questioned by discrepancies evidenced in the approximated complex plane. This paradox was solved by assuming that the temperature not only accelerates the viscoelastic processes but also slightly increases their intensity. This softening effect of the temperature on the compliance, similar to rubber elasticity in amorphous polymers, was described by a 2nd degree polynomial. Time-temperature dependency fitted very well to the Arrhenius law up to 60°C. Based on the approximated complex plane, the power law was proposed for modelling creep behaviour in green wood. The method was successfully used for all specimens investigated. It is interesting to note that constitutive law used for the description of both, aging process and thermally activated creep, was the same. Simplified experimental procedure based on two creep tests instead of four was revealed as sufficient to obtain accurate prediction of the long-term creep.

On the other hand, very poor correlations were observed between vibration measurements and creep data. Wood is a complex polymer exhibiting multi transition behaviour. Thus, the mechanism governing the viscoelastic behaviour during vibrations at high frequencies is likely different from the mechanism prevailing during the creep tests. Investigating the variability of the creep response at the end of 8h lasting creep test at 30°C, we can clearly distinguish particular behaviour of some specimens exhibiting high amount of relative creep. Investigation of relationships between the creep data and structural parameters has not brought a satisfying answer to explain this variability. Even if some significant intraspecific relations were observed, we could not go further in the analysis because of the reduced number of specimens by species. If the rheological models used to describe creep behaviour seem to be valid despite the diversity of our sample, explaining the remaining variability based on structural parameters is not straightforward.

C) CONCLUSIONS AND PERSPECTIVES

1) Methodological advances

1.1 Storage of green specimens

While working on plant or other biological material, it is important to protect it against biological and physical degradations. The safest way is to perform the tests immediately after collection of plant material, *i.e.*, in the forest, but this involves the use of simple testing equipment able to work in such conditions, in general less precise, and it is possible only if the test is not too long. Thus, experimenter has often to compromise between measurements accuracy and storage time of the specimens that may lead to their degradation. For some tests as for example long-term creep it is not possible to work outside of the laboratory and so it is essential to know how long-term storage affects mechanical properties of the material.

The purpose of the study on storage conditions was to investigate the effect of applied storage procedure on mechanical properties of wood. Viscoelastic properties in the longitudinal direction of green specimens were compared with those of specimens in rehydrated state after storage in different conditions. First, long-term storage in water at low temperatures ($T = 4 \pm 0.1^\circ\text{C}$) was investigated. Vibration measurements were performed after 3, 8 and 12 months of storage. A very slight decrease was observed for both elastic modulus (-3.4%) and damping coefficient (-0.7%) after storage period of 12 months. Furthermore, the effect of 40 day soaking in 40% ethanol on vibration properties of saturated wood was investigated. Ethanol has not affected elastic modulus but has slightly increased the damping coefficient (6.2%). This effect was strictly proportional and considering the slight weight decrease of the specimens, it was attributed to residual ethanol content.

The effect of air drying (followed by a rewetting of the specimen) on elastic modulus and damping coefficient was also investigated. A slight decrease was observed for the elastic modulus (-5.8%) whereas the damping coefficient showed a significant increase (+15.9%). Agreement between values measured in green state and after rewetting is very good for the elastic modulus. By contrast, uncertainty of the green values estimated from the rehydrated ones is high for the damping coefficient (20%). Effect of air drying was linear for elastic modulus but non-linear for damping coefficient. Specimens with high damping coefficient were more affected by air drying than specimens with low damping coefficient.

Definitely, storage in water at low temperatures can be advised as the most appropriate way to preserve vibration properties of wood specimens in the green state. Effect of ethanol on vibration properties seems to be only transient but its use is questionable because of processes that may be involved in the transient state (Chang *et al.* 2008). Air drying can be used to preserve specimens against biological attacks when only elastic properties are required but is not appropriate for viscoelastic studies.

1.2 Correction of the creep signal obtained during tests at elevated temperature and suggested experimental procedure

During the creep tests performed at elevated temperature, the recovery of residual locked-in strains overlaps with the creep due to loading. Recovery of residual strains results in progressive shortening of the specimen in the longitudinal direction. Thus, the produced strain is of opposite sign compared to the creep strain. Addition of both signals may lead to an apparent stabilisation of the creep process, or worse a reverse process, and consequently mislead the choice of a rheological model. Thus, it is essential to separate the creep signal from the recovery signal.

Our first attempt to solve the overlapping problem was to release all residual strains by heating the specimen at 80°C during 30 minutes before the onset of creep tests. However, this procedure was inappropriate because the following cooling process was revealed to affect the creep properties in the long-term. Physical aging phenomenon was evidenced in green wood and results have clearly showed that the new thermodynamic equilibrium state has not been reached after several days. Consequently, heating of the specimen before the onset of creep tests was not a suitable way to obtain a clean creep signal.

Thus, a continuous experimental procedure was proposed to study the creep properties avoiding any cooling between consecutive tests. Each creep test was performed at a constant temperature. Prior to the loading, specimen was stabilised at a given temperature for 15 hours. Signal recorded during this period was extrapolated to the following creep test and used for the correction of the creep. As the stabilisation period was long enough relatively to the creep one, the extrapolation as a function of logarithm of time was reliable. Furthermore, this method allowed us to account for the possible time-dependant drift of strain gages that was not negligible for some tests performed at higher temperatures.

1.3 Simplified experimental procedure for satisfactory long-term predictions of the creep behaviour

Based on the graphical representation of the experimental data in the approximated complex plane (ACP), we have identified a corresponding rheological model whose behaviour was described by a power law. Parameters of the power law were adjusted in order to obtain the best fit with experimental data, satisfying at the same time the *TTE* and *J-T* assumptions (for details see §2.1). This power law will be further denoted as a complete power law because parameters were adjusted on the whole set of creep tests. The next step consisted in a search for the minimal number of creep tests needed to obtain a reasonable prediction of the long-term creep behaviour.

The first attempt was to consider the creep test performed at 30°C, fit the model parameters in order to obtain a good agreement with the creep curve and extrapolate the obtained power law to the prediction period fixed to 30 years. The kinetics of the creep behaviour was not well predicted by this extrapolation resulting in a highly variable quality of the creep prediction. Uncertainty in the relative creep predicted at the end of a 30-year period was of 30% considering the estimates given by the complete power law as a reference. Even less satisfying results were obtained from extrapolation of the power law with parameters fitted on the creep test performed at 50°C. While the kinetics of the creep process was slightly closer to the complete model, additional imprecision arose from an inaccurate estimation of the initial compliance. This was a consequence of the use of average values of activation energy and softening parameter.

Contrary to the predictions based on one single creep test, power law fitted on two creep tests (30°C and 50°C) has given satisfactory agreement with the complete power law. Prediction of the creep kinetics agreed well for all specimens investigated yielding an average error of $13.3 \pm 12.9\%$ considering the relative creep estimation at the end of 30 years. The use of two creep tests for long-term predictions offers the possibility to reduce the time needed for experiments by a factor of two.

2) Interpretation of creep data

Representation of the experimental data in the approximated complex plane (ACP) is useful for two reasons: to assess the validity of the equivalency principle and for the choice of a rheological model based on the graphical representation.

2.1 Assessment of physical hypothesis using ACP

Assumption of time-aging time or time-temperature equivalency (*TTE*) requires that once plotted in the ACP, all creep curves measured at different aging times/temperatures form one single curve. This is equivalent to say that horizontal shifts in the compliance – log time plot are sufficient to obtain a smooth master curve, *i.e.*, temperature or aging time are supposed to affect only the characteristic time. Assumed equivalency principle was verified for aging whereas for time-temperature, its direct application was questionable. Horizontal shifts were systematically observed between individual creep curves measured at different temperatures while plotted in the ACP. Thus, additional assumption of the temperature effect on the initial compliance (*J-T* effect) was proposed supposing that temperature not only accelerates the creep processes but slightly increases their intensity (cf the so-called entropic or rubber elasticity in polymer science).

2.2 Identification of a parametric rheological model

Creep curves measured at different aging times overlapped in the ACP in one single straight segment. Such a representation corresponds to a Maxwell model consisting of a spring assembled in series with a parabolic dashpot. The same type of model was identified for the thermally activated creep behaviour indicating that the effect of heating and cooling on the viscoelastic behaviour have similar, presumably molecular, origin. Furthermore, the model showed to be applicable on a different species and wood types. Viscoelastic properties of wood are often described by parabolic Zener model. In the parabolic Zener model, second spring is assembled in parallel with the parabolic dashpot. Thus, the creep of such model is reversible and solid exhibits a creep limit which is in agreement with the intuitive picture of structural limit of the creep in wood. It was thus suggested that identified Maxwell model is only the onset of a Zener one.

3) Structural determinants of viscoelastic properties

3.1 Relationships between vibration properties and structural parameters

Vibration measurements were performed on a large sample of 550 specimens of ten tropical species with basic densities ranging from 0.33 to 0.94. Species were selected in function of their growth strategy, and exhibited contrasted anatomical structures. Further, intraspecific variability of the sample was increased by the use of wood from both, straight growing and tilted trees. The main goal for taking a large variability of the sample was to assess the general validity of structure/property relations that are often based on mono-specific studies without consideration of reaction wood. Further, simple model predicting the cell wall properties from wood properties and microfibril angle was developed to investigate the role of microfibril angle (MFA) often believed to be the main determinant of cell wall properties.

Investigating the structure/property relationships, we have confirmed strong relation between the Young's modulus and basic density despite the high variability of the sample. Green density, however, was revealed to be affected by different saturation level of species so that its use for prediction of mechanical properties was questionable. Specific modulus was related to MFA but this parameter explained only 32% of the specific modulus variability. Large scatter of the specific modulus values was observed for low MFAs, probably due to the occurrence of tension wood. Damping coefficient has not exhibited a significant correlation with MFA which was unexpected. On the other hand, strong correlation was observed with the specific modulus. We have thus a sort of paradox: specific modulus is believed to be determined by MFA and damping coefficient by the specific modulus but damping coefficient

is not related to MFA. It clearly indicates that other parameters than MFA affect the specific modulus and damping coefficient.

The origin of variability of vibration properties was studied by splitting the sample in two groups representing the normal wood and tension + opposite wood respectively. Properties of tension + opposite wood represented considerably higher variability of vibration properties compared to normal wood. Proposed cell wall model fitted reasonably well to the normal wood properties but was unable to predict the properties of reaction woods because of its variability. Further, variability of properties in function of wood types (normal wood, tension wood, opposite wood) was investigated by species. The only systematic effect was lower MFA in tension wood compared to opposite wood. Moreover, opposite and tension wood exhibited the same damping coefficient despite different specific modulus and which was significantly higher than that of normal wood. It was suggested that it might be related to their intensive loading history leading to mechanical fatigue and formation of micro-cracks at the cell wall level. Micro-cracks would dissipate more energy leading to higher damping coefficient. The fact that damping coefficient is the same in tension as well as opposite wood would mean that the effect of mechanical fatigue is prevailing. Large scatter could be explained by the diversity of mechanical adaptations developed by trees to solve the problem of non-verticality of the stem or branch posture. This diversity makes impossible to predict vibration properties from MFA without considering the fine structure and chemical composition of both, opposite wood and tension wood. It is also interesting to note that opposite wood exhibited significantly lower specific modulus along microfibrils compared to tension wood and normal wood. This clearly indicates that some other changes have to occur likely at the chemical level or in the cell shape and which definitely differentiate opposite wood from normal wood.

3.2 Determinants of the creep behaviour

First, relation between vibration measurements and creep measurements were investigated. While Young's modulus obtained by static and vibration methods exhibit a strong linear relationship whose slope is close to the unity, viscous parameters (damping and relative creep at the end of 8h) seem not to be related. It was suggested that independency of both viscous parameters comes from different viscoelastic mechanisms involved during both measurements. Vibration measurement is performed at resonance frequencies ranging from 300 to 600 Hz at room temperature. Thus, the mechanism involved could be more affected by hemicelluloses. On the other hand, creep tests conducted at room temperature should be connected to the lignin behaviour. Based on our observations, it seems that relation between both mechanisms is not straightforward.

While plotting the twenty-six creep curves performed at 30°C in the same graph, we can note particular high relative creep for six of them, four *V. michelii* specimens and two *E. grandiflora* specimens. The others exhibited relative creep lower than 5% at the end of 8h. Investigating relations between the relative creep and structural parameters, significant relation was observed only with basic density. This observation ties up with observed basic density dependency of the kinetic parameter and doubling time of the power law used to describe the creep behaviour. However, when plotting the relative creep versus basic density we can see that the relation is strongly affected by occurrence of *V. michelii* samples exhibiting low basic density together with high relative creep for some of them. On the other hand, no contradictory case *i.e.* specimen with high density along with high relative creep was detected. This effect could be related with the relative contribution of fibres and middle lamella to the creep process. However, the relation between basic density and relative creep needs further investigations before drawing a conclusion about its relevance.

4) Viscoelastic properties of wood at different structural scales

While investigating relationships between structural parameters and viscoelastic properties, many questions arose about the structural determinants and the relevant scale level for viscoelastic considerations. In the following, a simplified representation of the hierarchical structure of wood material is given and the contribution of wood constituents to viscoelastic behaviour at different scale levels is discussed.

4.1 Simplified representation of the hierarchical wood structure

Hierarchical structure of wood at different scales can be pictures as shown in Figure C-1. At the tissue scale, wood can be represented as a parallel arrangement of vessels, fibres and axial parenchyma assembled in series with radial parenchyma. In the previous section we have seen that arrangement of anatomical elements has not shown significant correlation with vibration and creep properties. Let us so assume that mechanical properties in the longitudinal direction are governed mainly by the fibre fraction. Fibre fraction itself can be represented as a two-phase composite made up of fibres glued between them by the middle lamella. Middle lamella is a purely amorphous layer constituted mainly of lignin (80%), hemicelluloses and pectin while fibres contain the totality of crystalline cellulose. Crystalline cellulose is much stiffer than matrix components (lignin and hemicelluloses) and is generally assumed to be purely elastic. As a result, the percentage of fibres together with their structure and cell wall thickness are the main determinant of elastic properties of wood at the macroscopic scale. However, the properties of the amorphous middle lamella and bonds between the middle lamella and fibres may strongly affect the viscous behaviour. This could explain why the main characteristic parameters for wood stiffness *i.e* basic density and MFA which are directly related to the thickness and structure of the fibre wall, are not sufficient to explain the creep behaviour of what can be considered as a composite at the tissue scale.

Fibre cell walls exhibit themselves a multi-layer composite structure. Because the S2 layer stands for approximately 80% of the cell wall thickness, it is often assumed to control the strength of the entire fibre. Similarly to wood structure at the tissue level, an analogy can be drawn between the structure of the S2 layer and that of a unidirectional fibre-reinforced composite material, in which the cellulose microfibrils represent the fibre reinforcement and amorphous hemicelluloses and lignin represent the composite matrix. At macroscopic scale, creep process will have two components: creep in the matrix of fibres and in the middle lamella gluing the fibres together. Their relative contribution will depend on many factors such as ratio between the fibre and middle lamella stiffness, fibre length and zone of fibres overlapping, chemical composition of the middle lamella *etc.*

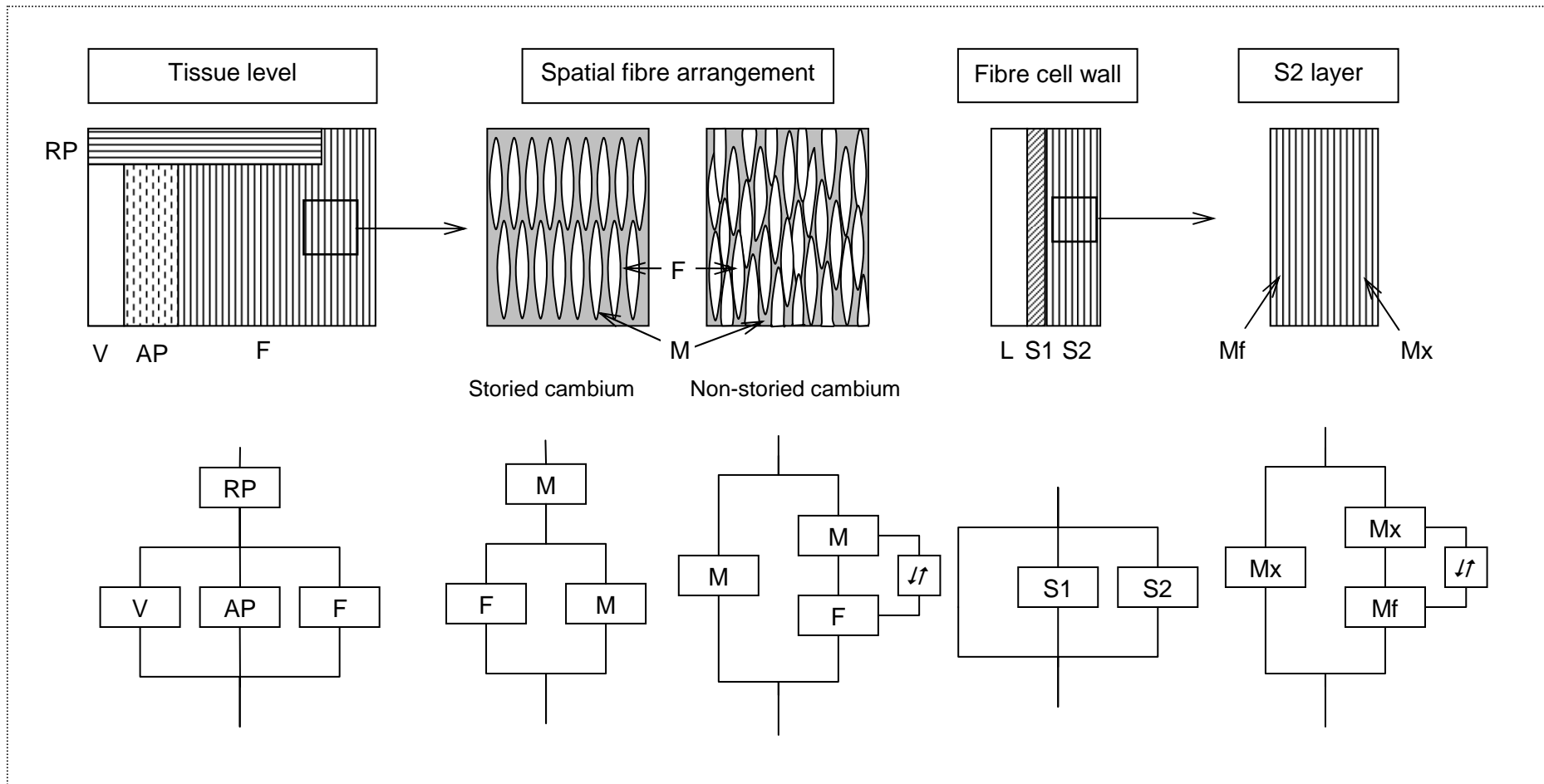


Figure C-1: Simplified representation of hierarchical wood structure. V: vessels; AP: axial parenchyma; F: fibres; RP: radial parenchyma; M: middle lamella; L: lumen; S1: S1 layer of the cell wall; S2: S2 layer of the cell wall; Mf: microfibrils; Mx: matrix; ↗: slippage.

4.2 Contribution of middle lamella and fibres at macroscopic scale

Olsson *et al.* (2007) have investigated the mechanosorptive creep rate in wood fibres investigated at constant humidity conditions and under cyclic humidity changes. Creep tests were conducted on single spruce fibres. Constant conditions corresponded to 80% relative humidity and 30°C leading to a moisture content of about 15.5%. For mechanosorptive creep, relative humidity was cycled between 80% and 30%. From plots of relative creep versus logarithm of time, they have determined a creep rate equal to $0.17 \pm 0.06 \text{ \%/log } t$ for the tests at constant humidity and to $0.28 \pm 0.08 \text{ \%/log } t$ for fibres subjected to humidity cycles. When equivalent calculus is applied based on our data, the obtained creep rate would be of $0.9 \pm 0.3 \text{ \%/log } t$ so nearly five times higher. Difference in moisture content of tested specimens can partially explain the observed difference. However, coupling of loading and humidity cycles is believed to accelerate the creep phenomenon and so should be at least comparable to the creep rate at higher moisture content. Nevertheless the creep rate of solid wood in green state remains approximately three times higher than the creep rate of fibres subjected to humidity cycles. A possible explanation of different creep rates observed for wood fibres and for solid wood could be the non negligible contribution of the middle lamella to the creep process. Similar conclusion has been drawn by Vincent (2006) based on results of thermally activated torsion tests performed on green poplar specimens.

Hunt and Gril (1994) have studied the possible contribution of slippage between fibres in the middle lamella in the case of air-dry spruce loaded in tension. The conclusion was that there is no doubt that some slippage should occur but the question of its quantitative contribution remained open. However, slippage in the middle lamella would be related with broken hydrogen bonds and thus probably partly irreversible, whereas during our experimentations no permanent deformation was observed. Furthermore, middle lamella is designed to ensure the role of a binder between fibres so that one could expect relatively high shear resistance. Relative contribution of slippage and viscous flow in the middle lamella will depend on many parameters. One of them is the fibre spatial arrangement. Basically, two patterns of fibres distribution exist in wood depending on the organisation of the cambium. As shown in Figure C-1, fibres can be organised in horizontal bands (storied cambium) or entangled (non-storied cambium). The creep process of the first pattern might be dominated by the viscous flow of the bands of middle lamella arranged in series with the fibres while the second type with tangled fibres would require important slippage between fibres to reach the same level of creep deformation.

4.3 Processes involved at the tree scale

Some creep experiments were also made at the tree scale level. Almeras *et al.* (2002) have studied the creep of 1-year old apricot tree branches. Tests were performed during the winter period when radial growth is stopped. Rate of decrease in the equivalent Young's modulus, determined from the digitalization of the branch deformation during 32 days, has ranged from 3.6 – 5.1 $\text{\%/log } t$ depending on the variety. This is more than three times higher than tensile creep rate measured on small specimens of solid wood in green state. However, in the creep process of a branch other parameters are involved. While the upper side of a branch is submitted to tensile stress, the lower side is submitted to compressive stress. Behaviour in tension and compression are not necessarily identical, in particular in creep tests because the linear viscoelasticity limit in compression is significantly lower than in tension (Hunt 1989). The level of applied stresses during the tests on the branch was relatively high so that tissues situated on the lower side could indeed pass over the linear viscoelasticity limit. One could also think about the occurrence of tension wood, probably present in its branches. We have some information about the elastic properties of tension and opposite tissues (Coutand *et al.* 2004) but not on their creep behaviour. In the present study, we have not quantified the

differences of the behaviour of both tissues however our sampling included all types of wood tissues (normal, opposite and tension) so that the difference in creep rate is contained in the SD of the mean estimation. This is, however, not sufficient to explain the observed difference. Moreover, some overestimation of the creep rate at the branch level could arise from the calculus of the Young's modulus including also the bark and pith that can represent a non-negligible part in the case of 1-year old branch. The reference for relative creep calculations might be higher because the creep process takes place in the wood part.

5) Perspectives

If some methodological progresses were made concerning the measurements of creep using time-temperature equivalency or storage of green specimens without damages, many questions remain unanswered. We have succeeded in modelling creep behaviour over several decades however a lot of work has to be done to understand the physical significance of the model parameters. Furthermore, the effect of temperature on the creep properties was not elucidated. Additional assumption of the temperature effect on the initial compliance similar to rubber elasticity in amorphous polymers (*J-T* effect) was suggested to allow the use of time-temperature equivalency. However some verifications of this assumption are needed and have not been done for the moment. Actually, it is necessary to check if the apparent acceleration of creep processes at long time scales resulting from the *J-T* effect corresponds to a reality or not. The verification is easy in principle but requires more time: to conduct a set of creep tests at different temperature levels with one additional test and much longer tests at intermediate temperature, for example at 45°C. This would allow us to check the validity of our prediction for the creep kinetics.

A lot of questions are still open in the field of understanding of the mechanisms involved in creep and physical ageing processes as well as its structural determinants. It seems that middle lamella plays an important role in the creep process but we do not know a lot about the creep properties of its constituents. Data about the mechanical properties of hemicelluloses and lignin are very scarce in the literature. However, if we want to relate the behaviour of middle lamella to the behaviour of its constituents, it would be nice to perform some experiments at a finer scale such as AFM⁵ measurements or nanoindentation as well as FTIR⁶ measurements to follow the bonds involved during the creep process.

Another interesting point is the independence of the creep and vibration viscoelastic parameters indicating the possibility of different mechanisms governing the behaviour at different observation time scales. To examine in greater detail this hypothesis, we could perform the vibration tests at different temperature in order to become closer to the observation times of the quasi-static measurements. Progress in the field of the rheological modelling is also needed to support this approach.

⁵ Atomic force microscopy

⁶ Fourier transform infrared spectroscopy

REFERENCES

- Akerholm, M. and L. Salmén (2003). "The oriented structure of lignin and its viscoelastic properties studied by static and dynamic FT-IR spectroscopy." *Holzforschung* 57(5): 459-465.
- Alfrey, T. (1948). *Mechanical behaviour of high polymers*. New York, Interscience publisher.
- Alméras, T. and M. Fournier (2009). "Biomechanical design and long-term stability of trees: Morphological and wood traits involved in the balance between weight increase and the gravitropic reaction." *Journal of Theoretical Biology* 256(3): 370-381.
- Almeras, T., J. Gril and E. Costes (2002). "Bending of apricot tree branches under the weight of axillary growth : test of a mechanical model with experimental data." *Trees - Structure and function* 16(1): 5-15.
- Almeras, T., J. Gril and H. Yamamoto (2005). "Modelling anisotropic maturation strains in wood in relation to fibre boundary conditions, microstructure and maturation kinetics." *Holzforschung* 59(3): 347-353.
- Altaner, C. M. and M. C. Jarvis (2008). "Modelling polymer interactions of the 'molecular Velcro' type in wood under mechanical stress." *Journal of Theoretical Biology* 253(3): 434-445.
- Alvarez-Clare, S. and K. Kitajima (2007). "Physical defence traits enhance seedling survival of neotropical tree species." *Functional Ecology* 21: 1044-1054.
- Archer, R. R. (1986). *Growth stresses and strains in trees*. Berlin/Heidelberg/New York, Springer Verlag.
- Back, E. L., L. Salmén and G. Richardson (1983). "Transient effects of moisture sorption on the strength properties of paper and wood-based materials." *Svensk papperstidning* 6 - 1983 - 86: 61-71.
- Bardet, S. (2001). *Comportement thermoviscoélastique transverse du bois humide*. Université de Montpellier 2. Montpellier, s.n.: 226 p.
- Bardet, S., J. Beauchêne and B. Thibaut (2003). "Influence of basic density and temperature on mechanical properties perpendicular to grain of ten wood tropical species." *Annals of forest science* 60(1): 49-59.
- Bardet, S. and J. Gril (2002). "Modelling the transverse viscoelasticity of green wood using a combination of two parabolic elements." *Comptes rendus mécanique* 330(8): 549-556.
- Bodig, J. and B. A. Jayne, Eds. (1982). *Mechanics of wood and wood composites*. New York, Van Nostrand Reinhold Company.
- Boiffin, J. (2008). *Variabilité de traits anatomiques, mécaniques et hydrauliques chez les juvéniles de vingt-deux espèces d'arbres de sous-bois en forêt tropicales humide*. Nancy, Université Henri Poincaré: 43 p.
- Bowling, A. J. and K. C. Vaughn (2008). "Immunocytochemical characterization of tension wood: Gelatinous fibers contain more than just cellulose." *American journal of botany* 95(6): 655-663.

- Brémaud, I. (2006). Diversité des bois utilisés ou utilisables en facture d'instruments de musique. Etude expérimentale des propriétés vibratoires en direction axiale de types de bois contrastés en majorité tropicaux. Relations à des déterminants de microstructure et de composition chimique secondaire. Université de Montpellier 2. Montpellier: 321 p.
- Brémaud, I., J. Dlouha, M.-F. Thévenon and J. Gril (2004). Vibrational properties, shrinkage and color of a selection of tropical woods with high extractives content. Proceedings of the Third international conference of the European society for wood mechanics, September 6th-8th, Vila Real, Portugal, 2004, Villa Real, Portugal, UTAD, Universidad de Tras-os-montes e Alto Douro.
- Brémaud, I., K. Minato, J. Gérard and B. Thibaut (2004). Effect of extractives on vibrational properties and shrinkage of African Padauk (*Pterocarpus soyauxii* Taub.). Proceedings of the Third international conference of the European society for wood mechanics, September 6th-8th, Vila Real, Portugal, 2004, Villa Real, Portugal, UTAD, Universidad de Tras-os-montes e Alto Douro.
- Burgert, I., A. Bernasconi and D. Eckstein (1999). "Evidence for the strength function of rays in living trees." *Holz als Roh- und Werkstoff* 57(5): 397-399.
- Butterfield, B. G., Ed. (1998). Microfibril angle in wood The proceedings of the IAWA/IUFRO International workshop on the significance of microfibril angle to wood quality. Chicago, International Association of Wood Anatomists.
- Cave, I. D. (1966). "Theory of X-ray measurement of microfibril angle in wood." *Forest products journal* 16(10): 37-42.
- Cave, I. D. (1969). "The longitudinal Young's modulus of *Pinus radiata*." *Wood science and technology* 3(1): 40-48.
- Chang, S.-S., B. Clair, J. Ruelle, J. Beauchene, F. Di Renzo, F. Quignard, G.-J. Zhao, H. Yamamoto and J. Gril (2009). "Mesoporosity as a new parameter for understanding tension stress generation in trees." *J. Exp. Bot.*: erp133.
- Chang, S., B. Clair, J. Gril, H. Yamamoto and F. Quignard (2008). "Deformation induced by ethanol substitution in normal and tension wood of chestnut (*Castanea sativa* Mill.) and simarouba (*Simarouba amara* Aubl.)." *Wood science and technology*.
- Chardin, A. and C. Sales (1983). Species developing a high level of growth stresses : a method to determine the distribution of longitudinal stresses and its application in French Guyana to the study of Wapa (*Eperua* sp.). Forest product research society, Norfolk (Virginia, U.S.A.) June 1983.
- Choong, E. T. and S. S. Achmadi (1991). "Effect of extractives on moisture sorption and shrinkage in tropical woods." *Wood and fiber science* 23(2): 185-196.
- Clair, B., T. Almeras and J. Sugiyama (2006). "Compression stress in opposite wood of angiosperms: observations in chestnut, mani and poplar." *Annals of forest science* 63(5): 507-510.
- Clair, B., J. Gril, F. Di Renzo, H. Yamamoto and F. Quignard (2008). "Characterization of a gel in the cell wall to elucidate the paradoxical shrinkage of tension wood." *Biomacromolecules* 9: 494-498.

- Clair, B., J. Ruelle, J. Beauchêne, M.-F. Prévost and M. Fournier Djimbi (2006). "Tension wood and opposite wood in 21 tropical rain forest species. 1. Occurrence and efficiency of the G-layer." *IAWA Journal* 27(3): 329-338.
- Clair, B., J. Ruelle and B. Thibaut (2003). "Relationship between growth stress, mechano-physical properties and proportion of fibre with gelatinous layer in Chestnut (*Castanea sativa* Mill.)." *Holzforschung* 57(2): 189-195.
- Cousins, W. J. (1976). "Elastic modulus of lignin as related to moisture content." *Wood science and technology* 10: 9-17.
- Cousins, W. J. (1978). "Young's modulus of hemicellulose as related to moisture content." *Wood science and technology* 12: 161-167.
- Coutand, C., G. Jeronimidis, B. Chanson and C. Loup (2004). "Comparison of mechanical properties of tension and opposite wood in *Populus*." *Wood science and technology* 38(1): 11-24.
- Dlouhá, J., T. Alméras, B. Clair, J. Gril and P. Horáček (2008). "Biomechanical performances of trees in the phase of active reorientation." *Acta Universitatis Agriculturae et Silviculturae Mendelianae Brunensis* 5: 39-45.
- Dlouhá, J., B. Clair, O. Arnould, P. Horáček and J. Gril (2009). "On the time-temperature equivalency in green wood: Characterisation of viscoelastic properties in longitudinal direction." *Holzforschung* 63(3): 327-333.
- Dlouhá, J., J. Gril, B. Clair and T. Alméras (2009). "Evidence and modelling of physical aging in green wood." *Rheologica Acta* 48(3): 333-342.
- Donaldson, L. (2008). "Microfibril angle: measurement, variation and relationship - a review." *IAWA Bulletin* 29: 345-386.
- El-Osta, M. L. M. and R. W. Wellwood (1972). "Short-term creep as related to cell-wall crystallinity." *Wood and fiber* 4(3): 204-211.
- El-Osta, M. L. M. and R. W. Wellwood (1972). "Short-term creep as related to microfibril angle." *Wood and fiber* 4(1): 26-32.
- Fang, C. H., D. Guibal, B. Clair, J. Gril, Y.-M. Liu and S.-Q. Liu (2008). "Relationships between growth stress and wood properties in poplar I-69 (*Populus deltoides* Bartr. cv. "Lux" ex I-69/55)." *Annals of forest science* 65: 307.
- Favrichon, V. (1994). "Classification of Guiana forest tree species into functional groups for a dynamic community matrix of vegetation." *Revue d'Ecologie* 49 (4): 379-403.
- Fengel, D. and G. Wegener (1984). *Wood. Chemistry, ultrastructure, reactions*. Berlin/New York, de Gruyter.
- Ferry, J. D. (1980). *Viscoelastic properties of polymers*. New York, John Willey.
- Fioravanti, M., N. Sodini and P. Navi (2006). Investigation of influence of hemicelluloses on time dependent behaviour of wood. Joint meeting of ESWM and COST Action E35, Florence - Italy.

- Fisher, J. B. and J. W. Stevenson (1981). "Occurrence of reaction wood in branches of dicotyledons and its role in tree architecture." *Botanical gazette* 142(1): 82-95.
- Fournier, M., B. Chanson, D. Guitard and B. Chanson (1991). "Mécanique de l'arbre sur pied : modélisation d'une structure en croissance soumise à des changements permanents et évolutifs. 1. Analyse des contraintes de support." *Annales des sciences forestières* 48: 513-525.
- Fournier, M., B. Chanson, B. Thibaut and D. Guitard (1991). "Mécanique de l'arbre sur pied : modélisation d'une structure en croissance soumise à des changements permanents et évolutifs. 2. Analyse tridimensionnelle des contraintes de maturation, cas du feuillu standard." *Annales des sciences forestières* 48: 527-546.
- Furuta, Y., M. Makinaga, H. Yano and H. Kajita (1997). "Thermal-softening properties of water swollen wood II - Anisotropic characteristics of thermal-softening properties." *Mokuzai Gakkaishi* 43(1): 16-23.
- Genevaux, J.-M. (1989). *Le fluage à température linéairement croissante : caractérisation des sources de viscoélasticité anisotrope du bois*. Institut National Polytechnique de Lorraine. Nancy, s.n.: 142 p. + annexes.
- Genevaux, J.-M. (1989). *Le fluage à température linéairement croissante: caractérisation des sources de viscoélasticité anisotrope du bois*. Institut polytechnique de Lorraine. Vandoeuvre les Nancy, s.n.: 198 p.
- Genevaux, J. M. and D. Guitard (1988). *Anisotropie du comportement différé : essai de fluage à température croissante d'un bois de peuplier*. Colloque scientifique européen 1988.
- Gibson, L. J. and M. F. Ashby (1997). *Cellular solids. Structure and properties*. Cambridge, Cambridge University Press.
- Gindl, W. (2002). "Comparing mechanical properties of normal and compression wood in Norway Spruce: the role of lignin in compression parallel to the grain." *Holzforschung* 56(4): 395-401.
- Gordon, J. E. (1978). *Structures or why things don't fall down*. Londres, Penguin Books.
- Gril, J. and M. Fournier (1993). *Contraintes d'élaboration du bois dans l'arbre : un modèle multicouche viscoélastique*. Actes du 11e congrès français de Mécanique, 6-10 septembre 1993, Lille - Villeneuve d'Ascq, Association Universitaire de mécanique/Groupe de concertation de mécanique.
- Gril, J. and D. Hunt (2002). *Analysing wood creep at constant moisture content using phase diagrams*. Proceedings of the First international conference of the European Society for wood mechanics, 19th-21st April, 2001 - Lausanne, Switzerland, Lausanne (Suisse), Ecole Polytechnique Fédérale de Lausanne.
- Gril, J., D. Hunt and B. Thibaut (2004). "Using wood creep data to discuss the contribution of cell-wall reinforcing material." *Comptes rendus biologie* 327(9-10): 881-888.
- Gril, J., F. Sassus, H. Yamamoto and D. Guitard (1999). *Maturation and drying strain of wood in longitudinal direction: a single-fibre mechanical model*. 3rd Workshop on Connection between silviculture and wood quality through modelling approaches and simulation softwares (IUFRO WP S5.01.04 "Biological Improvement of Wood

- Properties"), La Londe-Les Maures, September, 5-12, 1999, Nancy, ERQB-INRA Nancy.
- Gril, J. and B. Thibaut (1994). "Tree mechanics and wood mechanics : relating hygrothermal recovery of green wood to the maturation process." *Annales des sciences forestières* 51: 329-338.
- Gril, J., B. Thibaut, E. Berrada and G. Martin (1993). "Recouvrance hygrothermique du bois vert. I. Influence de la température. Cas du jujubier (*Ziziphus lotus* (L) Lam)." *Annales des sciences forestières* 50: 57-70.
- Grossman, P. U. A. (1976). "Requirements for a model that exhibits mechano-sorptive behaviour." *Wood science and technology* 10(3): 163-168.
- Grossman, P. U. A. and R. S. T. Kingston (1954). "Creep and stress relaxation in wood during bending." *Australian journal of applied science* 5(4): 403-417.
- Hamdan, S., W. Dwianto, T. Morooka and M. Norimoto (2000). "Softening characteristics of wet wood under quasi static loading." *Holzforschung* 54(5): 557-560.
- Hayashi, K., B. Felix and C. Le Govic (1993). "Wood viscoelastic compliance determination with special attention to measurement problems." *Materials and Structures* 26(6): 370-376.
- Hoffmeyer, P. (1990). Failure of wood as influenced by moisture and load duration. College of Environmental Science and Forestry Syracuse, New York, State University of New York. PhD: 122.
- Huet, C. (1967). "Représentation des modules et complaisances complexes dans les plans complexes arithmétique et logarithmique." *Cahiers du Groupe Français de Rhéologie* 5(1): 237-258.
- Huet, C. (1988). Some aspects of the termo-hygro-viscoelastic behaviour of wood. Colloque scientifique européen, 8 et 9 juin 1988, Bordeaux, Groupement scientifique Rhéologie du Bois.
- Huet, C. and P. Navi (1990). Multiparabolic multitransition model for thermo-viscoelastic behavior of wood. *Mechanics of wood and paper materials*. The winter annual meeting of the ASME - Dallas, Texas, nov. 25-30, 1990.
- Hunt, D. and J. Gril (1994). Possible contribution of fibre slippage to the longitudinal creep of wood. 4th COST 508 Wood Mechanics workshop, Espoo, Finland, 18-19.5.94, EC DGXII
- Hunt, D. G. (1988). Non-linearity in mechano-sorptive creep of softwood in compression and bending. Colloque scientifique européen, Bordeaux.
- Hunt, D. G. (1989). "Linearity and non-linearity in mechano-sorptive creep of softwood in compression and bending." *Wood science and technology* 23(4): 323-333.
- Hunt, D. G. (2004). "The prediction of long-time viscoelastic creep from short-time data." *Wood science and technology* 38(7): 479-492.

- Hunt, D. G. and M. W. Darlington (1978). "Accurate measurement of creep of nylon-6,6 at constant temperature and humidity." *Polymer* 19(8): 977-983.
- Hunt, D. G. and J. Gril (1996). "Evidence of a physical ageing phenomenon in wood." *Journal of materials science letters* 15: 80-82.
- Ishimaru, Y. (2003). Mechanical properties of wood in unstable states caused by changes in temperature and/or swelling. Proceedings of the Second international conference of the European society for wood mechanics. Stockholm, Sweden. May 25th - 28th 2003.
- Jones, R. M. (1975). *Mechanics of composite materials*. New York, McGraw Hill.
- Kelley, S. S., T. G. Rials and W. G. Glasser (1987). "Relaxation behaviour of the amorphous components of wood." *Journal of materials science* 22(2): 617-624.
- Kellogg, R. M. and F. F. Wangaard (1969). "Variation in The Cell-Wall Density of Wood." *Wood and fiber science* 1(3): 180-204.
- Kifetew, G., F. Thuvander, L. Berglund and H. Lindberg (1998). "The effect of drying on wood fracture surfaces from specimens loaded in wet condition." *Wood science and technology* 32(2): 83-94.
- Kojima, Y. and H. Yamamoto (2004). "Effect of microfibril angle on the longitudinal tensile creep behavior of wood." *Journal of wood science* 50(4): 301-306.
- Kollmann, F. F. P. and W. A. Côté, Jr. (1968). *Principles of wood science and technology vol. 1 Solid wood*. New York, Springer-Verlag.
- Kubler, H. (1987). "Growth stresses in trees and related wood properties." *Forest products abstracts* 10(3): 62-119.
- Le Govic, C. (1988). *Le comportement viscoélastique du bois en liaison avec sa constitution polymérique; Rapport bibliographique réalisé avec le concours financier du Ministère de la Recherche et de l'Enseignement Supérieur, CTBA - Centre Technique du Bois et de l'Ameublement: 40 p.*
- Le Govic, C., B. Felix, A. Hadj Hamou, F. Rouger and C. Huet (1987). *Mise en évidence d'une équivalence temps-température et modélisation du fluage du bois 1 Documents généraux - Thèmes 1 et 2. Actes du 2e colloque Sciences et Industries du Bois, Nancy, 22-24 avril 1987 - tome 1, Nancy, A.R.BO.LOR.*
- Le Govic, C., F. Rouger and B. Felix (1988). *Approche d'un modèle multitransitions paraboliques pour le fluage du bois. Colloque scientifique européen, Bordeaux.*
- Levita, G. and L. C. E. Struik (1983). "Physical ageing in rigid chain polymers." *Polymer* 24(8): 1071-1074.
- Matsunaga, M., K. Minato and F. Nakatsubo (1999). "Vibrational property changes of spruce wood by impregnation with water-soluble extractives of pernambuco (*Guilandina echinata* Spreng.)." *Journal of wood science* 45(6): 470-474.
- McCrum, N. G. (1992). "The interpretation of physical ageing in creep and DMTA from sequential ageing theory." *Plastics, rubber and composites processing and applications* 18: 181-191.

- McCrum, N. G. R., B.E. and Williams, G. (1967). Anelastic and dielectric effects in polymeric solids. London, Wiley.
- Nakano, T. (2005). "Effects of quenching on relaxation properties of wet wood." *Journal of wood science* 51(2): 112-117.
- Navi, P. and F. Heger (2005). *Comportement thermo-hydrromécanique du bois - Applications technologiques et dans les structures*. Lausanne, Presses Polytechniques et Universitaires Romandes.
- Norimoto, M. and J. Gril (1989). "Wood bending using microwave heating." *Journal of microwave power and electromagnetic energy* 24(4): 203-212.
- Norimoto, M., F. Tanaka, T. Ohogama, R. Ikimune and J. Gril (1986). "Specific dynamic Young's modulus and internal friction of wood in the longitudinal direction (traduction française)." *Wood research and technical notes* 22: 53-65.
- Nowick, A. S. and B. S. Berry (1972). *Anelastic relaxation in crystalline solids*. New York and London, Academic press.
- Obataya, E., M. Norimoto and J. Gril (1998). "The effects of adsorbed water on dynamic mechanical properties of wood." *Polymer* 39(14): 3059-3064.
- Obataya, E., T. Umezawa, F. Nakatsubo and M. Norimoto (1999). "The effects of water soluble extractives on the acoustic properties of reed (*Arundo donax* L.)." *Holzforschung* 53(1): 63-67.
- Okuyama, T., H. Yamamoto, M. Yoshida, Y. Hattori and R. R. Archer (1994). "Growth stresses in tension wood : role of microfibrils and lignification." *Annales des sciences forestières* 51(3): 291-300.
- Olsson, A.-M. and L. Salmén (1997). "The effect of lignin composition on the viscoelastic properties of wood." *Nordic pulp and paper research journal* 3: 140-144.
- Olsson, A.-M., L. Salmén, M. Eder and I. Burgert (2007). "Mechano-sorptive creep in wood fibres." *Wood science and technology* 41(1): 59-67.
- Ono, T. and M. Norimoto (1984). "On physical criteria for the selection of wood for soundboards of musical instruments." *Rheologica acta* 23: 652-656.
- Perré, P. and O. Aguiar (1999). "Fluage du bois "vert" à haute température (102°C) : expérimentation et modélisation à l'aide d'éléments de Kelvin thermo-activés." *Annals of forest science* 56: 403-416.
- Persson, K. (2000). *Micromechanical modelling of wood and fibre properties*. Lund University - Department of mechanics and materials. Lund (Suède), Lund University, Royal Institute of Technology, Division of structural mechanics: 223 p.
- Placet, V., J. Passard and P. Perré (2007). "Viscoelastic properties of green wood across the grain measured by harmonic tests in the range 0–95°C: Hardwood vs. softwood and normal wood vs. reaction wood." *Holzforschung* 61(5): 548-557.
- Plomion, C., G. Leprovost and A. Stokes (2001). "Wood formation in trees - Update on wood formation in trees." *Plant physiology* 127(4): 1513-1523.

- Poliszko, S. (1984). Anisotropy of dynamic wood viscoelasticity. *Rhéologie des matériaux anisotropes - Rheology of anisotropic materials*. CR 19e coll. GFR, Paris, nov 1984. Toulouse, Cépaduès-Editions: 453-480.
- Reiterer, A., I. Burgert, G. Sinn and S. Tschegg (2002). "The radial reinforcement of the wood structure and its implication on mechanical and fracture mechanical properties—A comparison between two tree species." *Journal of materials science* 37(5): 935-940.
- Ruelle, J., J. Beauchêne, A. Thibaut and B. Thibaut (2007). "Comparison of physical and mechanical properties of tension and opposite wood from ten tropical rainforest trees from different species." *Annals of forest Science* 64(5): 503-510.
- Ruelle, J., H. Yamamoto and B. Thibaut (2007). "Growth stresses and cellulose structural parameters in tension and normal wood from three tropical rainforest angiosperm species." *BioResources* 2(2): 235-251.
- Salmén, L. (1984). "Viscoelastic properties of in situ lignin under water-saturated conditions." *Journal of materials science* 19(9): 3090-3096.
- Salmén, L. (1988). Directional viscoelastic properties of wood. *Rheologica Acta*, Darmstadt (Allemagne), *Rheologica acta*.
- Salmén, L. (2004). "Micromechanical understanding of the cell-wall structure." *Comptes rendus biologie* 327: 873-880.
- Salmén, L. and I. Burgert (2009). "Cell wall features with regard to mechanical performance. A review COST Action E35 2004-2008: Wood machining - micromechanics and fracture." *Holzforschung* 63(2): 121-129.
- Salmén, L., A.-M. Olsson, M. Eder and I. Burgert (2006). Mechano-sorptive creep of single wood and pulp fibres. Joint meeting of ESWM and COST Action E35, Florence - Italy.
- Sassus, F. (1998). Déformation de maturation et propriétés du bois de tension chez le Hêtre et le Peuplier: mesures et modèles. L'Ecole Nationale du Génie Rural, des Eaux et Forêts. Montpellier: 150.
- Scurfield, G. (1973). "Reaction wood: its structure and function." *Science* 179: 647-655.
- Singleton, R., D. S. DeBell and B. L. Gartner (2003). "Effect of extraction on wood density of western hemlock (*Tsuga heterophylla* (Raf.) Sarg.)." *Wood and fiber science* 35(3): 363-369.
- Stamm, A. J. and W. K. Loughborough (1935). "Thermodynamics of the swelling of wood." *Journal of physical chemistry* 39: 121-132.
- Struik, L. C. E. (1978). Physical aging of amorphous polymers and other materials. Amsterdam, Elsevier Scientific Publishing Company.
- Sugiyama, K., T. Okuyama, H. Yamamoto and M. Yoshida (1993). "Generation process of growth stresses in cell walls: Relation between longitudinal released strain and chemical composition." *Wood science and technology* 27: 257-262.
- Thuvander, F., G. Kifetew and L. A. Berglund (2002). "Modeling of cell wall drying stresses in wood." *Wood science and technology* 36(3): 241-254.

- Timell, T. E. (1986). *Compression wood in Gymnosperms 3: Ecology of compression wood formation, silviculture and compression wood, mechanism of compression wood action, compression wood in the lumber and pulp and paper industries, compression wood induced by the basalm woolly aphid, opposite wood*. Berlin/Heidelberg/New York, Springer Verlag.
- Tomlins, P. E. (1996). "Comparison of different functions for modelling the creep and physical ageing effects in plastics." *Polymer* 37(17): 3907-3913.
- Tschoegl, N. W. (1997). "Time Dependence in Material Properties: An Overview." *Mechanics of time dependent materials* 1: 3-31.
- Vavrčík, H. and V. Gryc (2004). "Metodika výroby mikroskopických preparátů ze vzorků dřev." *Acta Universitatis Agriculturae et Silviculturae Mendelianae Brunensis* 2004, LII (4): 169–176.
- Vincent, P. (2006). *Comportement viscoélastique thermoactivé en torsion du bois de peuplier à l'état vert*. Montpellier, Université de Montpellier 2. PhD Thesis: 152.
- Vincent, P., S. Bardet, P. Tordjeman and J. Gril (2006). Analysis of viscoelastic properties of green poplar in torsion. International Conference on integrated approach to wood structure, behaviour and applications. Joint meeting of ESWM and Cost Action E35 - Florence - Italy May 15-17.
- White, J. R. (2006). "Polymer ageing: physics, chemistry or engineering? Time to reflect." *Comptes Rendus Chimie* 9(11-12): 1396-1408.
- Wilson, B. F. and R. R. Archer (1979). "Tree design : some biological solutions to mechanical problems." *Bioscience* 9(May 1979): 293-298.
- Winandy, J. E. and R. M. Rowell (2005). *Handbook of wood chemistry and wood composites*. Boca Raton, Fla., CRC Press.
- Xu, P. and H. Liu (2004). "Models of microfibril elastic modulus parallel to the cell axis." *Wood science and technology* 38(5): 363-374.
- Yamamoto, H., Y. Kojima, T. Okuyama, W. P. Abasolo and J. Gril (2002). "Origin of the biomechanical properties of wood related to the fine structure of the multi-layered cell wall." *Journal of biomechanical engineering* 124: 432-440.
- Yamamoto, H., T. Okuyama and M. Yoshida (1993). "Method of determining the mean microfibril angle of wood over a wide range by the improved Cave's method." *Mokuzai Gakkaishi* 39(4): 375-381.
- Yang, J. L. and R. Evans (2003). "Prediction of MOE of eucalypt wood from microfibril angle and density." *Holz als Roh und Werkstoff* 61: 449-452.
- Yano, H. (1994). "The changes in the acoustic properties of western red cedar due to methanol extraction." *Holzforschung* 48: 491-495.
- Yano, H., K. Kyou, Y. Furuta and H. Kajita (1995). "Acoustic properties of Brazilian rosewood used for guitar back plates." *Mokuzai Gakkaishi* 41(1): 17-24.

Yokota, T. and H. Tarkow (1962). "Changes in dimension on heating green wood." *Forest products journal* 43: 43-45.

Yoshida, M. and T. Okuyama (2002). "Techniques for measuring growth stress on the xylem surface using strain and dial gauges." *Holzforschung* 56(5): 461-467.

FIGURE LIST

Figure 0-1: (a) Honeycomb-like structure of wood at microscopic scale. (b) Multi-layered structure of the cell wall. From (Norimoto and Gril 1989).....	8
Figure 0-2: Distribution of main wood components in different layers of the cell wall according to Panshin and Zeuw [cited by (Navi and Heger 2005)]......	10
Figure 0-3: Maturation process and origin of growth stresses as pictured by (Plomion <i>et al.</i> 2001). As the newly developed wood cell (i) begins to differentiate (ii), the deposition of lignin and cellulose in the secondary cell wall tends to stretch the cell laterally and cause it to shrink longitudinally (black arrows). However, as the differentiating wood cell is attached to older wood (iii), it cannot deform completely, thereby setting up a mechanical stress in the cell wall (empty arrows). In normal wood (NW), this translates into a tensile stress, therefore, the wood in the outer surface of a tree (iv) is usually held in tension (+ and empty arrows). However, accumulation of peripheral maturation tensile stresses must be balanced by internal compression of the stem (- and full arrows).....	11
Figure 0-4: Left figure: Pre-stress and bending strength of tree trunks. (a) Tree bent by the wind without considering the field of pre-stresses due to the maturation process. Stress distribution across the trunk is linear and maximum tension and compression are equal. (b) Field of internal stresses resulting from the maturation process. The outside is in tension all around, the inside is in compression. (c) Pre-stressed tree in a strong wind. Compression stress is halved and this tree can bend twice as far as the one in (a). From Gordon (1978). Right figure: The positive effect of growth stresses on stem flexibility.....	12
Figure 0-5: Released longitudinal growth strain against mean MFA in S2 layer from (Sassus 1998)..	14
Figure 0-6: Schematic representation of delayed elastic deformation of a polymer chain: (a) original shape, (b) early stage of deformation, (c) final stages of elongation, (d) early stages of recovery, (e) recovered shape. (Bodig and Jayne 1982)	16
Figure 0-7: Plot of Young's modulus against temperature. T_g stands for the temperature of glassy transition and T_m for the melting pot.....	17
Figure 0-8: Storage modulus and loss peaks (damping) measured in spruce (—) and maple (---) at 10% moisture content by (Kelley <i>et al.</i> 1987).....	17
Figure 0-9: Theoretical creep curve representing two limiting compliances: C_g standing for the glassy compliance and C_r standing for the rubbery one.....	18
Figure 0-10: Creep data plotted as relative creep against log of time. From (Hunt 2004).....	19
Figure 0-11: Gressel's eight-year creep data for beech, compared with various method of prediction from short-term data: continuation of slope between 1-2 weeks is represented by the solid line and prediction based on the normalised logarithmic creep rate of the creep after 1 week by the dashed line. From (Hunt 2004).....	19
Figure 0-12: Representation of linear viscoelastic behaviour. Left: applied stress, right: resulting strain. From (Le Govic 1988).....	20
Figure 0-13: Compression and tension modulus of IM6-914 according to Vittecoq [cited in (Genevaux 1989)]......	21
Figure 0-14: Relative creep strains in compression, tension and bending. Moisture content of specimens was of ~11% for the figure (a) and 20% for the figure (b).....	22
Figure 0-15: (a) Damping coefficient as function of temperature for water saturated wood samples at 10 Hz. (b) Relative damping coefficient. From (Salmén 1984).	23
Figure 0-16: Softening temperature of wet wood at a stress frequency of 0.1 Hz against the methoxyl group content of the lignin. From (Olsson and Salmén 1997).....	24
Figure 0-17: Principle of the time-temperature equivalency as pictured by Tschoegl (1997). T stands for temperature, $\log a_T$ for shifts along the log time axis, τ for the characteristic time.....	25

Figure 0-18: Graphical representation of the hypothesis that the retardation spectra at T and T0 are displaced by $\ln a_T$ but are identical in shape (Alfrey 1948).	25
Figure 0-19: Idealized diagram showing effect of the temperature dependencies of limiting compliances denoted here as J_U and J_R on the creep compliance. (a) Plot of J_U and J_R against temperature. (b) Dependence of J^T and J^{T_0} on log time. AB and CD represent the measurable portions of the curve (i.e. for times between ca. 1 and 10^5 s). A'B' represents AB after reduction.	26
Figure 0-20: Hookean spring (left) and Newtonian dashpot (right).	28
Figure 0-21: The Maxwell model.	28
Figure 0-22: The Zener model.	29
Figure 0-23: Generalised Kelvin model.	29
Figure 0-24: Graphical adjustment of the numerical results of the multi-parabolic multi-transition model on the experimental creep results obtained in CTBA and results of dynamic tests at low temperature (Polizsko) and high temperature (Salmén). J stands for the compliance, W for the activation energy and p for the kinetic parameter. From (Huet and Navi 1990).	31
Figure 0-25: Representation of the Zener models containing Newtonian (half a circle) or parabolic (arc of circle) dashpot in the complex plane. Approximation of the parabolic model by a series of Kelvin models is also displayed. Axes account for both, representation of dynamic and static data.	32
Figure 0-26: Relation between MFA and density for plantation-grown <i>E. globulus</i> , <i>E. nitrens</i> and <i>E. regnans</i> between 15 and 33 years of age. From (Yang and Evans 2003).	33
Figure 0-27: The elastic modulus of the fibre wall of wood in the longitudinal direction as a function of fibril angle in the S2-wall as affected by different factors; cellulose content in the S2-wall and proportion of S2-wall compared to measurements by Cave (1969). Reference values: cellulose content in S2-wall 50%, proportion of S2-wall 79%. From (Salmén 2004).	34
Figure 0-28: Relation between density and elastic modulus on data issued from CIRAD database. Each point represents a mean value by species; altogether ~1000 species are represented.	35
Figure 0-29: (a) Relation between damping coefficient and specific modulus in double logarithmic scale. (b) Relation between damping coefficient and MFA.	36
Figure 0-30: Relation between specific modulus, damping coefficient and microfibril angle on a selection of three softwoods including compression wood. From (Brémaud 2006).	36
Figure 0-31: Relation between damping coefficient and specific modulus for compression wood (BC), intermediate wood (between BC and BN) and normal wood (BN); E: <i>Picea abies</i> ; PM: <i>Pinus pinaster</i> ; PS: <i>Pinus sylvestris</i> . From (Brémaud 2006)	37
Figure 0-32: (a) Relationship between total creep and microfibril angle as measured by (El-Osta and Wellwood 1972) at 0.03% strain level. (b) Same data when only mean values of total creep are considered.	38
Figure 0-33: Dependency between the adjusted viscosity parameter of Zener model and MFA. From (Kojima and Yamamoto 2004).	38
Figure 0-34: PCA plot after horizontal shift along E' axis. Specimen 34 was taken as a reference. From (Gril <i>et al.</i> 2004).	39
Figure 0-35: Creep of a single wood fibre and of a single pulp fibre, holocellulose. Fibres were tested at 30°C (strain adjusted at zero at one minute after loading). The first creep from 0 to 120 minutes occurred at constant humidity of 80%RH. The second phase from 120 to 615 minutes involved periods at 30 and 80%RH.	39
Figure A-1: Distribution and variability of specific gravities between species and growth strategy groups. For key see Table A-1.	42
Figure A-2: (a) Average value of released longitudinal growth strain for tilted and straight growing trees. (b) Gradient of growth strains for tilted and straight growing trees.	43

Figure A-3: Interspecific variability of gradients of growth strains. For the species names see Table A-1.	43
Figure A-4: Anatomical structure of studied species.....	45
Figure A-5: Repartition of the sample for different tests and treatments. G1 and G2: subgroups of sample 1; G2-R and G2-S: subgroups of sample G2; N: number of specimens; D: duration of the treatment.....	46
Figure A-6: Preparation of damping specimens from the log collected in the forest.....	47
Figure A-7: In-situ growth strain measurement. (a) Instrumentation by strain gages and recording of the strain signal by Wheatstone bridge. (b): Two grooves method and radial position marking.....	48
Figure A-8: Experimental device for vibration tests.....	48
Figure A-9: Comparison of damping results obtained by two different methods: Damping 1: half-band method; Damping 2: logarithmic decrement. Red line represents the relation $y = x$	49
Figure A-10: Measurement of the damping coefficient by logarithmic decrement.	50
Figure A-11: Simplified representation of a cell wall. LT stand for axes of global coordinate system and 12 for axes of a local coordinate system of the microfibril. θ denotes the microfibril angle.	53
Figure A-12: Prediction of the Young's modulus of the cell wall based on Eq. A-5.	54
Figure A-13: Saturation level of specimens in initial state and after different storage durations.	57
Figure A-14: Variations of Young modulus measured by vibration method in initial state (E_0) and after 3, 8 and 12 months of storage in water at low temperature ($4 \pm 0.1^\circ\text{C}$). Red line represents the relation $y = x$	57
Figure A-15: Variations of damping coefficient measured by vibration method after 3, 8 and 12 months of storage in water at low temperature ($4 \pm 0.1^\circ\text{C}$). Red line represents the relation $y = x$	58
Figure A-16: Effects of soaking in 40% ethanol and its residuals after washing in water on Young modulus. Red line represents the relation $y = x$	58
Figure A-17: Effects of soaking in 40% ethanol and its residuals after washing in water on damping coefficient. Red line represents the relation $y = x$	59
Figure A-18: Effect of air drying and resaturation on Young modulus. E_0 is the never-dry value. Red line represents the relation $y = x$	60
Figure A-19: Effect of air drying and resaturation on damping coefficient. Red line represents the relation $y = x$	60
Figure A-20: Effect of heating on Young modulus and damping coefficient.	61
Figure A-21: Difference between air drying and oven drying effects on Young modulus and damping coefficient. Red line represents the relation $y = x$	62
Figure A-22: Effect of moisture content on vibration properties. Lines represent experimental data reported by (Obataya <i>et al.</i> 1998) , squares our measurements.	62
Figure A-23: Double logarithmic relation between damping coefficient and specific modulus in green, rewetted and air dry state. Red line and equation in the box represent empirical equation proposed by Ono and Norimoto (1984).	63
Figure A-24: Relation between green and basic density. Red line represents the regression line on the entire sample and dashed line the theoretical relationship between both parameters. The gradient of colours represents the growth strategy going from the yellow heliophilic to the brown understorey species. The same key is used for all figures of chapter 6.	65
Figure A-25: Relationship between green density and basic density on specific mean values. See Figure A-24 for the caption.	65

Figure A-26: Correlation between MFA estimates accounting for Yamamoto correction for density and basic density. Red line represents the regression line on the entire sample.	65
Figure A-27: Correlation between MFA-Yam and basic density on average specific values.	66
Figure A-28: Correlation between MFA estimates and density on a selection of 22 tropical species (Boiffin 2008).	66
Figure A-29: Relationship between elastic modulus and green density. Red line represents the regression line on the entire sample. Red line represents the regression line on the entire sample....	67
Figure A-30: Basic density as a predictor of the green Young's modulus.	68
Figure A-31: Relation between the specific modulus and basic density.	69
Figure A-32: Relationship between the specific modulus and microfibril angle.	69
Figure A-33: Relationship between specific modulus and microfibril angle on mean specific values. .	70
Figure A-34: Relation between the approximation of the specific cell wall modulus along microfibrils and MFA.	70
Figure A-35: Relationship between damping coefficient and basic density.	71
Figure A-36: Relationship between damping coefficient and microfibril angle.	72
Figure A-37: Damping coefficient versus approximation of specific cell wall modulus along microfibrils.	73
Figure A-38: Relationship between damping coefficient and specific modulus.	74
Figure A-39: Correspondence between experimental and modelled values of specific modulus and damping coefficient.	75
Figure A-40: Prediction of the specific modulus for wood coming from (a) straight growing and (b) tilted trees.	76
Figure A-41: Prediction of the damping coefficient for wood coming from (a) straight growing and (b) tilted trees.	76
Figure A-42: Specific cell wall modulus and damping coefficient of the cell wall along microfibrils for wood coming from straight growing and tilted trees. Error bars represent the confidence interval for the mean estimation with 95% probability level.	77
Figure A-43: Variability of basic density in function of species and wood type.	78
Figure A-44: Variability of elastic modulus in function of species and wood type.	78
Figure A-45: Variability of specific modulus in function of species and wood type.	79
Figure A-46: Variability of microfibril angle in function of species and wood type.	79
Figure A-47: Variability of damping coefficient in function of species and wood type.	80
Figure A-48: (a) Relationship between damping coefficient and MFA depending on the wood type. Error bars represent the confidential interval for the probability level of 95%. (b) Relationship between damping coefficient and specific modulus in function of the wood type.	80
Figure A-49: Relationship between specific modulus along microfibrils and MFA in function of the wood type.	81
Figure B-1: Creep testing device. (a): Whole experimental equipment. (b): Recording of strain signals by Wheatstone bridge and transmission to the computer. (c): Detail of specimens in the thermo-regulated bath.	84
Figure B-2: Preparation and shape of the damping and tensile creep specimens. (a): Damping specimen used for the preparation of the creep specimen. (b): Creep specimen after machining. Remaining part was used for anatomical analysis. (c): Final instrumented creep specimen.	85

Figure B-3: Fixture used for accurate positioning of the specimen during gluing and drilling operations.	85
Figure B-4: (a) Determination of the instantaneous compliance and of the onset of the creep test. (b): Zoom on the very first seconds following the loading (unsmoothed data): example of the stabilisation of the creep signal. J_i : instantaneous compliance; t_c : testing time.	86
Figure B-5: Tests of repeatability. (a) Creep curves corresponding to the first and second creep test. (b) The same creep curves expressed in terms of relative creep.	88
Figure B-6: Tests of linearity. (a) Schedule used for the linearity tests. (b) Obtained results from creep and recovery tests.	89
Figure B-7: Detail of creep tests performed at different stress level. (a) Raw compliance values. (b) Smoothed, interpolated and normalised compliance values.	89
Figure B-8: Correction of the creep signal obtained during a test at increased temperature. (a) Extrapolation of the signal recorded during the stabilisation period. (b) Creep strain before and after the correction.	90
Figure B-9: (a) Principle of smoothing and interpolation by best-fitting local polynomial. (b) Examples of smoothed and interpolated procedure applied to specimen Oa2.	91
Figure B-10: Experimental procedure for investigating the aging time effect on small strain creep properties. a) Dashed line: temperature; solid line: load. t_a : aging time; t_c : creep time.	93
Figure B-11: Evidence of physical ageing occurrence in green wood (sample Vm _N). (a) Set of creep tests performed at different elapsed times t_1 - t_5 counting from the onset of the test without preliminary heating above T_g ; (b) Set of creep tests performed on the same sample at different aging times t_{a1} - t_{a8} following the quench.	94
Figure B-12: Relationship between retardation and ageing time based on visual assessment (sample Vm _N). (a) Master curve obtained by visual shifting of individual creep curves from Figure B-11b; (b) Double logarithmic plot of shift factors a_{ta} versus the aging time t_a	95
Figure B-13: Complex plot of a sequence of creep tests performed at different aging times t_a after the quench where J' is storage compliance and J'' loss compliance (sample Oa _N). For signification of J_0 and k see in the text.	95
Figure B-14: Example of model fitting based on eq. B-6 for sample Oa _N : (a) Master curve produced by shifts resulting from optimisation without any presumed dependency between doubling and aging times. (b) Example of agreement between experimental (dots) and modelled creep curves (lines). Creep curve corresponding to the aging time $t_{a8} = 3.3$ days was taken as a reference.	97
Figure B-15: Model fitting based on eq. B-6. Relationship between shift factors a_{ta} and aging times t_a in double logarithmic scale for different samples.	97
Figure B-16: Example of model fitting based on eq. B-6 and B-7 for sample Oa _N a) Master curve produced by shifts resulting from optimisation accounting for linear logarithmic dependency between doubling time and aging time. (b) Example of agreement between experimental and modelled creep curves issued from fitting 2. t_a : aging time.	98
Figure B-17: Model fitting based on Eq. B-6 applied on Nakano's data: (a) Agreement between experimental and modelled creep curves for fitting 1. Solid lines represent the prediction for values of $t_c < t_a/3$; dashed lines correspond to modelled values not satisfying the snapshot condition $t_c > t_a/3$. (b) Relationship between shift factors a_{ta} and aging times t_a in double logarithmic scale.	99
Figure B-18: Positioning of a selection of wood specimens used for the tests of time-temperature equivalency.	103
Figure B-19: Applied cycling schedule. t_{stab} : stabilisation time; t_c : creep time.	104
Figure B-20: Master curve obtained by shifting individual creep curves for the Oa2 specimen along log time axis. Curve measured at 30°C is taken as a reference.	105
Figure B-21: (a) Temperature dependency of time shift factors issued from different optimisations and adequacy of an Arrhenius law (regression line). J - T effect: Experimental data corrected by the	

softening factor λ . Power law: Adjusted values of time shifts and softening factor based on Eqs. B-12-B-14. (b) Temperature dependency of the softening factor $\lambda(T)$ (Oa2 specimen). The legend is the same as for Figure 5.....	106
Figure B-22: Smoothed experimental data for the Oa2 specimen plotted in the approximated complex plane (ACP) for different creep temperatures J and J' : Alfrey's approximations of storage and loss compliance respectively (Eqs. 1 and 2).....	107
Figure B-23: ACP of Figure B-22 corrected by the softening factor λ . J_0 : initial compliance, k : power exponent. J and J' : Alfrey's approximations of storage and loss compliance respectively (Eqs. 1 and 2).....	107
Figure B-24: (a) Master curves for the Oa2 specimen corresponding to different assumptions. Raw data: experimental d_{ata} from Figure B-20 shifted along the log time axis. J - T effect: Experimental data corrected by softening factor λ . Power law: Modelled values based on Eqs. B-12 - B-14 accounting for the time-temperature dependency and softening factor λ . (b) Agreement between experimental data for the Oa2 specimen (markers) and the power law model (lines): power law J - T effect and Arrhenius law (Eqs. B-12 - B-14).	109
Figure B-25: (a) Relationship between the power coefficient and basic density. (b) Relationship between the log of doubling time τ_0 and basic density.....	111
Figure B-26: (a) Relationship between the power coefficient and the log of doubling time τ_0 . (b) Relationship between the softening parameter λ_{60} and microfibril angle.....	112
Figure B-27: (a) Relationship between the creep measured at the end of 8h and its prediction at the end of 30yrs. (b) Extrapolation of the creep curve measured at 30°C and compared to the master curve (MC) generated by horizontal shifting in the compliance – log time plots of the data previously corrected by softening factor λ and power law fitted on four temperature steps (power law). Dashed line represents the end of the test at 30°C. Specimen: Oa2.....	112
Figure B-28: (a) Correspondence between the creep prediction at the end of 30yrs period obtained by extrapolation of the power law fitted on creep data measured at 30°C and creep predicted by non parametric master curve. (b) Prediction of a long-term creep based on the creep test performed at 50°C. Specimen: Oa2.....	113
Figure B-29: Prediction of long-term creep based on creep tests performed at 30°C and 50°C. (a) Softening parameter λ is not considered. (b) Softening parameter is adjusted on experimental data. Specimen: Oa2. Legend of series symbols is common for both figures.	114
Figure B-30: Correspondence between the relative compliance at the end of 30 yrs given by the master curve and predicted using two creep tests performed at 30°C and 50°C.	114
Figure B-31: Relationships between dynamic and static measurements. (a) Correspondence between Young's modulus measured by vibration method and Young's modulus estimated from the creep measurements. Red line represents the relation $y = x$. (b) Relationship between relative creep at the end of 8h and damping coefficient.	116
Figure B-32: Transformed ACP plot including the point corresponding to the vibration measurement. Dashed line represents presumed second rheological mechanism expressed during dynamic loading. Specimen: Oa2.....	117
Figure B-33: Creep curves corresponding to all specimens tested at 30°C.	118
Figure B-34: Relationship between the amount of relative creep (%) and basic density.....	119
Figure B-35: Relation between relative creep and microfibril angle. Regression lines represent intraspecific correlations for Oa and Vm specimens.	119
Figure C-1: Simplified representation of hierarchical wood structure. V: vessels; AP: axial parenchyma; F: fibres; RP: radial parenchyma; M: middle lamella; L: lumen; S1: S1 layer of the cell wall; S2: S2 layer of the cell wall; Mf: microfibrils; Mx: matrix; \downarrow : slippage.	128

TABLE LIST

Table A-1: Summary table of some basic information about studied species	45
Table A-2: Experimental standard deviations of vibration measurements in air dry conditions.....	50
Table A-3: Elements of the stiffness matrix used for testing of the simplified calculus of the elastic modulus along fibres	54
Table A-4: Matrix of correlation coefficient between vibration properties and anatomical parameters.	82
Table B-1: Summary table of the specimen properties used for the aging study	93
Table B-2: Adjusted parameters of aging time dependant model. Last line corresponds to results obtained for Nakano's data presented in §2.3.d. k : power exponent; J_0 : instantaneous compliance (GPa^{-1}); $\log \tau_0$: doubling time of the reference element and μ the aging rate.	98
Table B-3: Summary table of structural parameters measured <i>a posteriori</i> and mechanical properties measured by vibration method in green state.	103
Table B-4: Summary table of rheological parameters assuming different hypothesis	109
Table B-5: Summary table of mechanical properties and structural parameters of all specimens tested in creep at 30°C	115
Table B-6: Matrix of correlation coefficients relating mechanical properties obtained from creep tests and other parameters.	118
Table 0-1: Summary table of vibration properties and structural parameters by species	149

APPENDIX

Summary of the diversity of vibration properties and structural parameters by species

Table 0-1: Summary table of vibration properties and structural parameters by species.

Species	Basic density	SD	SD %	MFA	SD	SD %	E (GPa)	SD	SD %	Espec (GPa)	SD	SD %	Damping	SD	SD %
<i>Goupia glabra</i> Aubl.	0.71	0.04	5.4%	8.7	2.5	28.8%	17.9	2.8	15.7%	25.1	3.3	13.3%	1.04%	0.21%	20.2%
<i>Tachigali melinonii</i> (Harms) Barneby	0.51	0.11	22.0%	11.8	4.7	40.1%	14.4	3.8	26.3%	28.8	5.5	18.9%	1.14%	0.50%	43.9%
<i>Virola michelii</i> Heckel	0.42	0.09	22.4%	16.1	4.1	25.6%	9.7	2.9	30.3%	23.2	5.3	23.0%	0.98%	0.26%	27.1%
<i>Dicorynia guyanensis</i> Amsh.	0.58	0.08	13.0%	10.8	3.5	32.3%	14.2	2.4	17.2%	24.2	4.2	17.3%	0.88%	0.27%	31.0%
<i>Eperua grandiflora</i> (Aubl.) Benth.	0.63	0.04	6.4%	13.9	4.9	35.2%	16.2	2.6	16.0%	25.6	3.4	13.2%	0.90%	0.30%	33.5%
<i>Lecythis persistens</i> Sagot	0.73	0.11	15.5%	12.2	2.8	22.7%	18.2	4.5	24.8%	25.2	3.0	11.9%	0.85%	0.19%	22.7%
<i>Licania alba</i> (Bernoulli) Cuatrec.	0.86	0.04	4.1%	7.6	5.0	65.6%	25.1	4.3	17.2%	29.3	3.8	13.1%	0.74%	0.20%	26.7%
<i>Gustavia hexapetala</i> (Aubl.) J.E. Smith	0.66	0.06	8.9%	13.3	6.5	48.5%	13.4	3.8	28.1%	20.3	4.1	20.2%	1.31%	0.57%	43.7%
<i>Oxandra asbeckii</i> (Pulle) R.E. Fries	0.86	0.05	5.9%	9.6	4.6	47.7%	23.3	4.4	19.1%	27.6	3.2	11.6%	0.63%	0.40%	62.7%
<i>Pogonophora schomburgkiana</i> Miers ex Ben	0.81	0.03	3.2%	10.3	1.8	17.2%	22.0	1.6	7.1%	27.2	1.3	4.8%	1.25%	0.20%	15.8%

Legend: SD: standard deviation; MFA: microfibril angle; E: modulus measured by vibration in the green state; Espec.: specific modulus.

Creep curves for physical aging tests by specimen

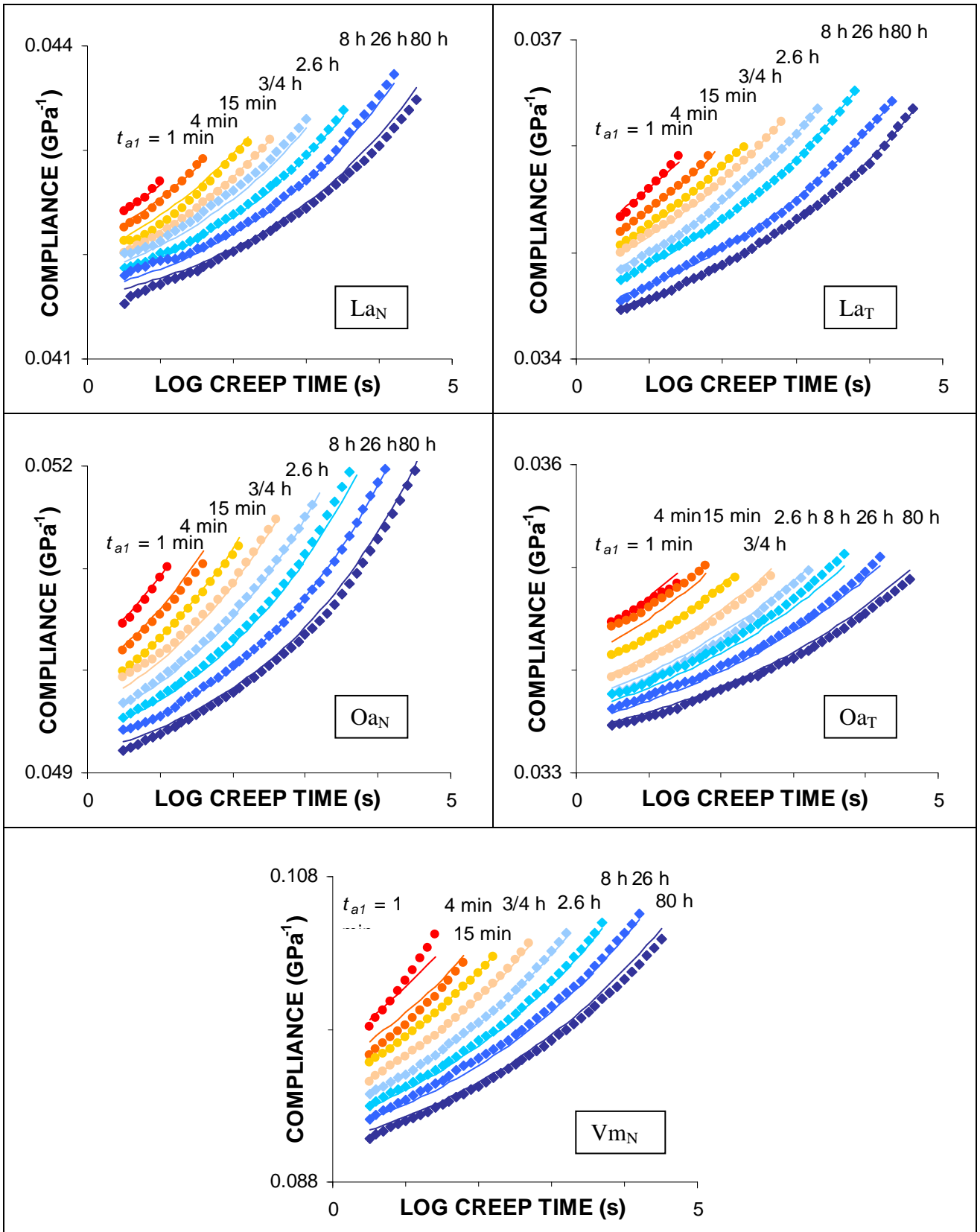


Figure 0-1: Adequacy between experimental and creep curves predicted by fitting 2 method during investigation of physical aging phenomena. Individual results by specimen.

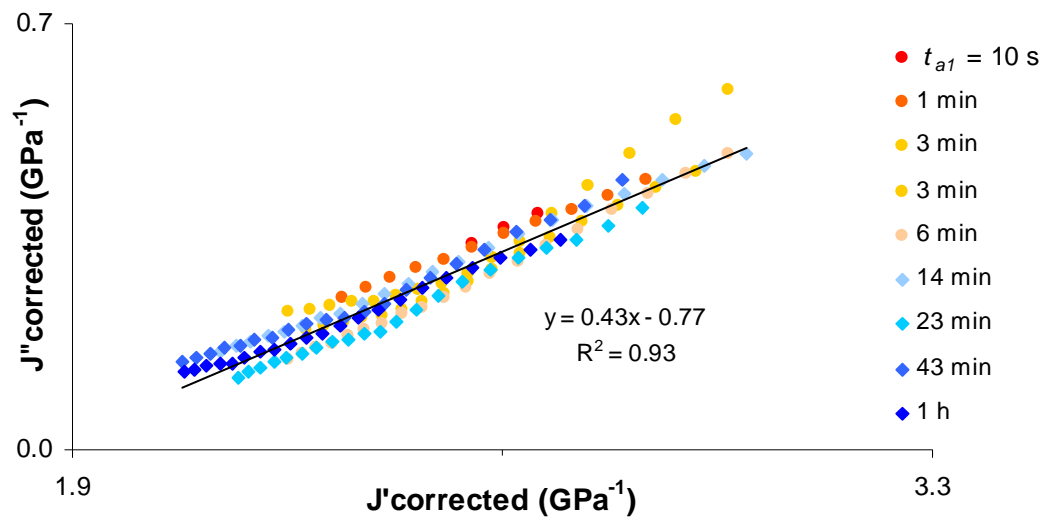
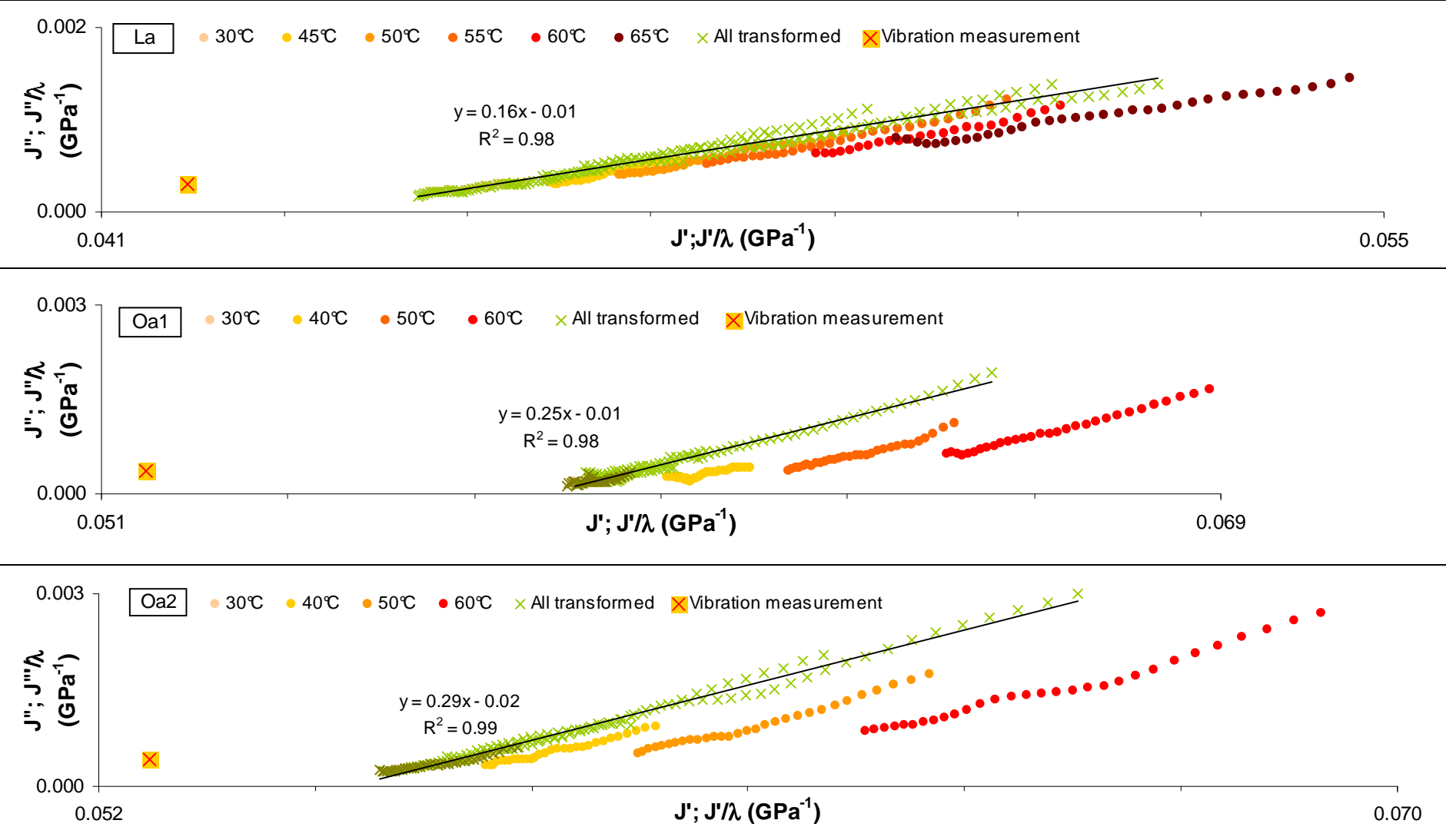
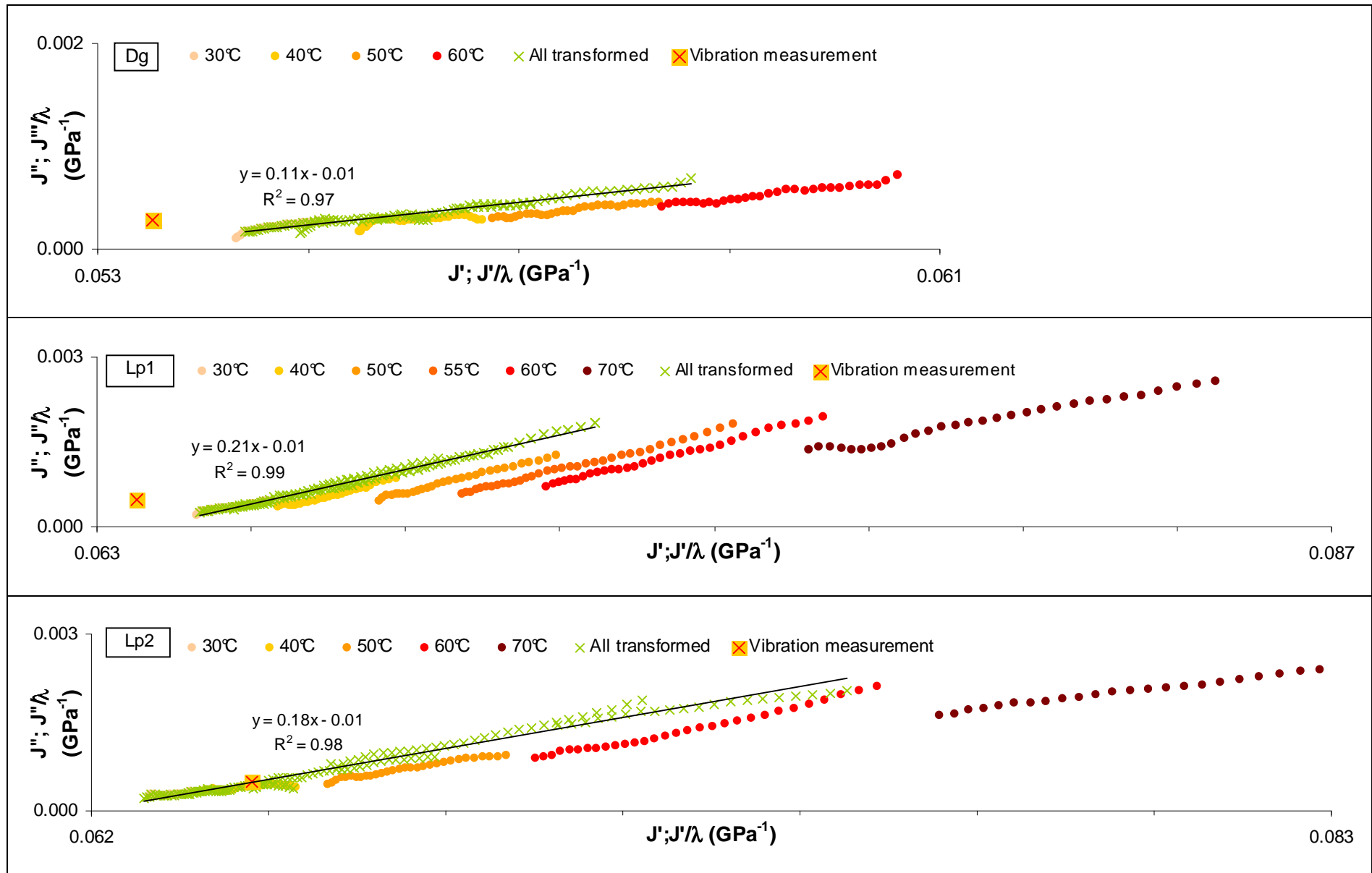
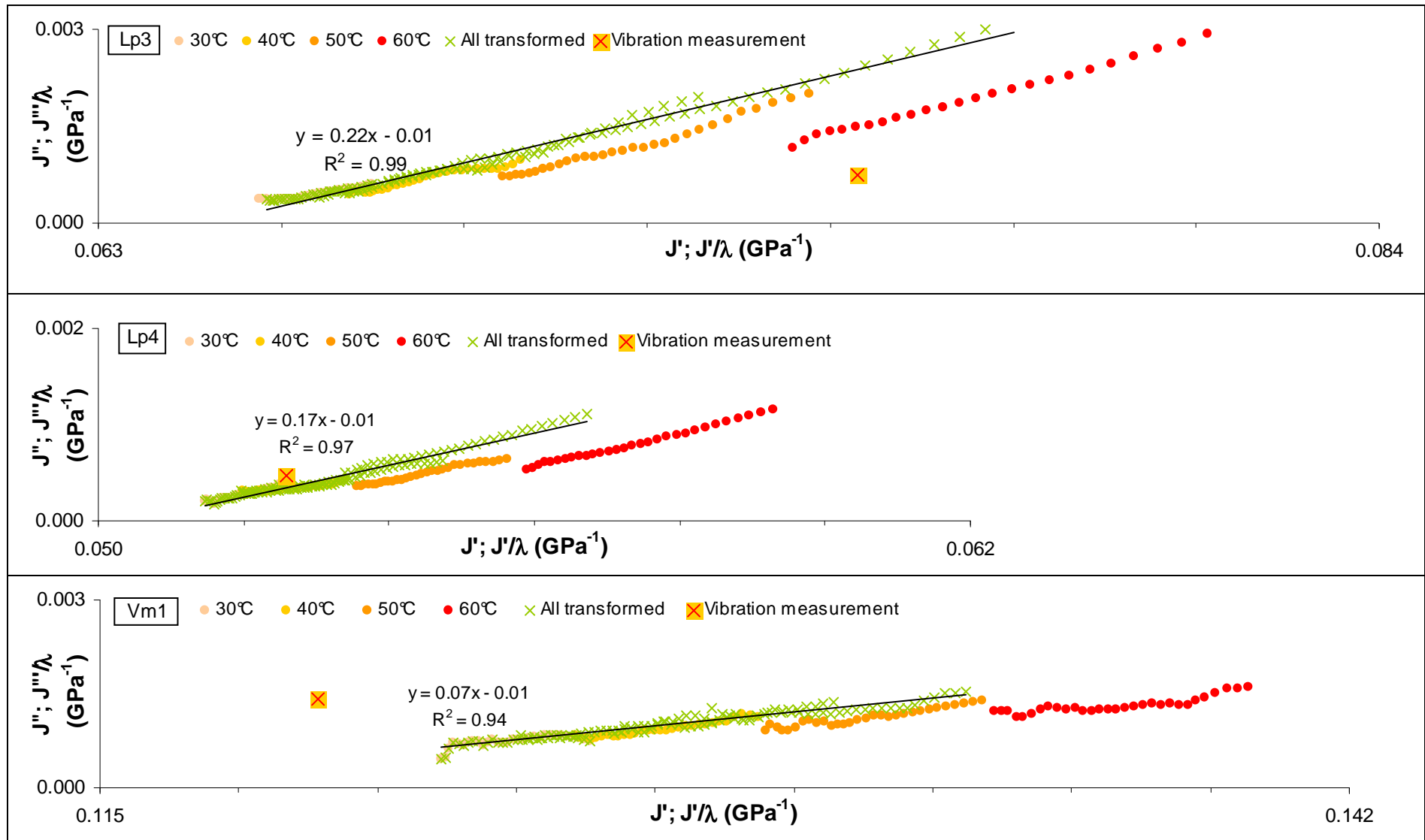


Figure 0-2: Nakano's data after correction of the compliance (tests performed on different specimens).

Approximated complex plane for individual specimens tested at different temperature levels including the vibration measurement







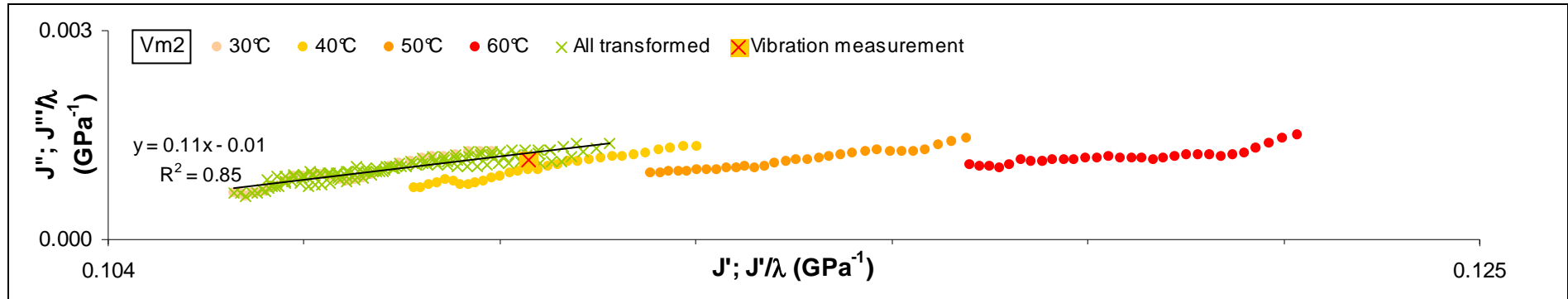


Figure 0-3: Approximated complex plane for each specimen.